Spectroscopy Surface Analysis of Paracetamol and Paracetamol and Excipient Systems

A thesis submitted to the University of Manchester
for the degree of Doctor of Philosophy in the
Faculty of Engineering and Physical Sciences

2011

Hamizah Mohd Zaki

School of Chemistry

Table of Contents

WORD COUNT: 51,742

Abbreviations

AFM	Atomic Force Microscopy
API	Active Pharmaceutical Ingredients
ATR-IR	Attenuated Total Reflection Infrared
BFDH	Bravais, Friedel, Donnay and Harker
BHT	Butylated Hydoxytoluene
CAE	Constant Analyser Energy
CED	Cohesive Energy Density
CSD	Cambridge Structural Database
DFT	Density Functional Theory
DSC	Differential Scanning Calorimetry
EO	Poly(ethylene oxide)
FWHM	Full Width Half Minimum
GCM	Group Contribution Method
IMFP	Inelastic Mean Free Path
NSAID	Nonsteroidal Anti Inflammatory Drugs
NIST	National Institute of Science and Technology
NMR	Nuclear magnetic Resonance
P188	Poloxamer188
P338	Poloxamer338
P407	Poloxamer407
PO	Poly(propylene oxide)
SEM	Scanning Electron Microscope
SXRD	Single Crystal X-ray Diffraction
UHV	Ultra High Vacuum
VB	Valence Band
XPS	X-ray Photoelectron Spectroscopy
XRD	X-ray Diffraction
PXRD	X-ray Powder Diffraction

List of Scientific Terms

E_B	Binding energy
E_K	Kinetic energy
ΔH	Enthalpy change
h	Planck constant (= 6.626×10^{-34} J s)
$h\nu$	Photon energy
T_g	Glass transition temperature
T_m	Melting temperature
φ_w	Work function
λ	IMFP *or* Wavelength
ν	Frequency
θ	Theta / Diffraction angle

List of Figures

List of Tables

Abstract

A detailed, fundamental understanding of the surface properties of molecular crystals and their interaction with adsorbing molecules (e.g. excipients) is important for tailoring the stability of formulations and the bioavailability of Active Pharmaceutical Ingredient (APIs). Few fundamental experimental studies with surface sensitive probes have been carried out for organic molecular crystals. X-ray photoelectron spectroscopy (XPS) is an established surface analysis method in the fields of adsorption, catalysis and surface chemistry of inorganic crystals. It has high surface sensitivity, probing approximately the top 1-3 nm of a crystal, and allows surface elemental analysis combined with the determination of the chemical state of the elements. To explore the possibilities and limitations of XPS for the surface characterisation of molecular crystal systems, investigation has been made on a range of paracetamol systems, three different poloxamers and blends of paracetamol with poloxamer 188.

It was found by investigations of a range of polycrystalline paracetamol forms that the C1s, N1s and O1s core level emissions from the amide group of paracetamol allow to quantify, for the first time, the influence of surface contamination and adsorbed species on the paracetamol XPS data. Results of quantitative XPS analyses must be critically evaluated taking the material and energy-specific escape depth of the photoelectron signals into account. Analysis of the polycrystalline powder samples, including two different polymorphs and various partially amorphous forms of paracetamol, indicated that the core-level shifts associated with varying intermolecular interactions do not perturb the local electronic structure variations in paracetamol enough to become detectable through chemical shifts in the core level photoemission spectra.

Subsequently, large, high quality single crystals of the monoclinic form I (with facet diameters between ~5 and ~10 mm) were obtained from different solvents (methanol, ethanol, acetone) to examine the influence of the crystallisation medium on the surface properties. Small spot XPS analysis was performed in several areas across facets to examine the possible influence of roughness and other lateral inhomogeneities. Careful curve-fitting of all results reveals only minor variations in the XPS data as a function of facet orientation, crystallisation medium or degree of crystallinity. Moreover, results indicate that any variations seen in XPS data very likely stem from low-level surface contamination, which is very difficult to avoid, even in a clean-room laboratory environment. In fact, the results indicate that the level of surface contamination depends significantly on the crystallisation apparatus cleanliness. Even minute concentrations of surface active components in the solutions, i.e. below the detection level of techniques for routine analytical methods, are likely to cause significant surface concentrations on crystal facets emersed from the solutions. The study thus highlights the paramount importance of microscopic surface cleanliness when assessing macroscopic facet-specific phenomena such as contact angles.

Finally, XPS was employed to analyse milled and physical mixtures of paracetamol with poloxamer 188 at different percent. At minimum mass percentages poloxamer 188 adsorbs on the paracetamol surfaces; in the presence of poloxamer 188 excess the conformation of adsorbed poloxamer on the paracetamol surface changes.

Studies of radiation damage on the poloxamer samples were performed both for several pure polxamers as well as for milled mixtures with paracetamol. They allowed the proposal of radiation-induced degradation mechanisms.

Declaration

This dissertation is the result of my own work, except where reference is made to other sources. No portion of the work referred to in the thesis has been submitted in support of an application for another degree or qualification of this or any other university or other institute of learning.

Hamizah Mohd Zaki
The University of Manchester

Copyright Statement

Acknowledgements

Firstly, I am heartily thankful to my supervisor, Dr Sven Schroeder, for his encouragement, guidance, pearls of wisdom and support from the initial to the final level, and especially for giving me the freedom to steer the project as I wished. Above all, he provided me with unflinching encouragement and support in various ways. His true intuition made him a constant oasis of ideas and his passion in science, inspired and enriched my growth as a student, a researcher and a scientist to be. I am indebted to him more than he knows. My deeply thanks to Beth for her willingness analysed my samples at any time. Many thanks from the bottom of my heart for both of you.

A special thanks goes to Prof Roger Davey for allowing me to use all his laboratory facilities at any time and for any purposes of my research. I gratefully thank all Roger's group members for helping me at any moment I needed. To Loris, I really appreciated and am thankful for your willingness and helpfulness during the experiments.

I also gratefully acknowledge the entire SMLS group members. I am much indebted to Joanna Steven, helpful and mindful roommate for her help, time and advice especially in the XPS analysis and experiments. Jo, I am very grateful in every possible way and hope to keep our collaboration in the future.

Millions of gratitude to Lorraine Onabanjo for her indispensable help dealing with administration and bureaucratic matters for my study. To John Walton, many thanks for his acceptance and concerns on the XPS applications. I do highly appreciate this as he realised my samples were high risks to the XPS operation. My humble thanks to my internal and external examiners, Karen William and Nick Bryan. No words for your kind and consideration.

Words fail to express my appreciation to my husband, Mohammad Noor Jalil, whose dedication, love and persistent confidence in me, has taken a load off my shoulders. To all my beloved children, Ahmad Luthfi, Ahmad Luqman and Aisyah Munirah, my special thanks to them. Thank you for their understanding, patience and tolerance along the PhD hurdle. My special thanks to 'Mak Cik Asma' for her willingness, help and forbearance. Last but not least, a humble, special mention to my parents for their inseparable support and prayers. My father, Hj. Mohd Zaki Abd Rauf and mother Hjh.Salmiah Mat Jelas who are always behind me and support me at any moment of my life with their love, sincerity and prayers. To all my siblings (Hj. Mohd Khairun Nizam, Hj. Mohd Farid, Hjh Siti Raudzah and laws) thanks for being supportive, helpful and caring. Also my endless thanks to my parents in law,Hj. Jalil Deraman and Hjh Tuminah Ikhsan for their courage, sincerity and prayers for my family.

Millions of thanks to Kementerian Pengajian Tinggi, Malaysia and Universiti Teknologi MARA for the PhD scholarship and allowances. Finally, I would like to thank everybody who was important to my PhD journey especially to Dr. Fauziah Nordin and family, Sue Husin, Norhayati Hazmi, and Erwina as well as my apology that I could not mention everyone personally.

CHAPTER 1: INTRODUCTION

1.1. Introduction

Market research by many global pharmaceutical companies and other reports indicate a significant growth in the pharmaceutical market, which was anticipated to grow by four to six percent in 2010[1]. Thus, there is a vital need for the enhancement of available commercial pharmaceutical products.

The purpose of the surface analysis of the active pharmaceutical ingredients (APIs) of a compound is mainly to enhance or improve the drug. Ninety percent of small molecule drugs are delivered to the human body in crystalline form[2]. Crystallinity confers better physical and chemical stability, forming a robust processing platform and storage conditions, resulting in a stable product which can be delivered safely to the patient. However, 90% of crystalline drugs have low solubility in water. Therefore the well controlled crystallisation of APIs is a vital operation in pharmaceutical manufacturing. The uncertainty of the pharmaceutical forms which may appear during the scaling-up of crystallisation from the laboratory to the manufacturing plant makes all pharmaceutical processes complicated. Of all drugs formulated, only 10% survive testing for safety and clinical efficacy to be available for commercial purposes.[2] Therefore, formulation must be optimized to ensure sufficient bioavailability and the efficacy of each drug in humans.

It is vital to understand the root behaviour of drugs, such as their morphology, the orientation of their molecules at the main crystal facets and their mechanisms of reaction. Single crystals of drug compounds may yield much information in the search for fundamental knowledge. They can be prepared so that the different facets can be examined by some analytical techniques such as X-ray photoelectron spectroscopy (XPS) and X-ray diffraction (XRD). An individual crystal has a number of facets or surfaces, each of which can exhibit different physical and chemical properties. These properties of the facets are important, as they transmit to the bulk material properties such as wettability, flowability and tabletability[3]. Therefore, knowledge of the surface structure at the atomic level is the first step towards understanding the physical and chemical properties of the crystal facet. In practice, the preparation of single crystals using solvents as the medium of nucleus growth may result in the distortion of the molecular structure and the inclusion of solvent in the crystal lattice, impairing the properties of the API

itself, which has led researchers to enhance the bioavailability, stability and other properties of APIs by introducing excipients into drug formulations. Excipients are by definition inert compounds, but ageing may result in their interaction with APIs by means of several possible mechanisms, including adsorption, complexation, chemical interaction, pH effects and eutectic formulation, resulting in drug products with desired or undesired properties. Therefore, it is important to explore and understand the mechanisms of the surface behaviour of drug molecules and their interactions when mixed with excipients.

1.2. Objectives

The objectives of the study are as below:

i) To prepare, characterise and analyse surface composition of different forms of paracetamol (untreated powder, treated powder and single crystal) by using X-ray Photoelectron Spectroscopy (XPS) advanced surface technique; complement with other techniques such as Differential Scanning Calorimetry (DSC), Attenuated Total Reflection- IR (ATR-IR) and X-ray Diffraction (XRD).

ii) To characterise surface composition three different types of Poloxamers; Poloxamer 188 (P188), Poloxamer 338 (P338) and Poloxamer 407 (P407) by using XPS.

iii) To determine the best ratio of paracetamol and poloxamer188 mixture composition for coating purposes using XPS surface technique.

1.3. Pharmaceutical Surfaces

The terms ‘surface’ and ‘interface’ are to some extent interchangeable, depending on the phases involved. The surface represents a discontinuation from the bulk, as in crystalline solids, where the surface involves termination of the crystal structure. Chemical sciences considered surface to include the first few atomic layers, and it is this small magnitude that causing problems with assessing and characterising the surface. Where two visible phases are concerned, it is normal to refer to a solid-liquid or solid-solid interface, while a solid-gas interface is commonly known as a surface. **Figure 1-1** summarizes the classifications of interfaces.

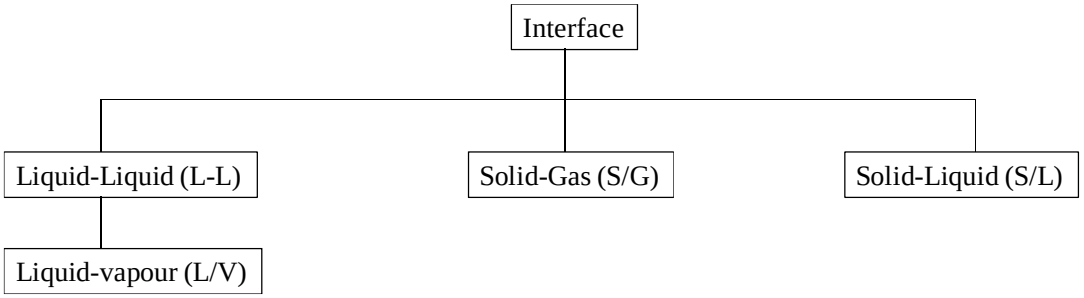

Figure 1-1: Classification of interfaces by phases

It is important to justify the focus of this study on the surface interactions of paracetamol, rather than its bulk properties. The surface properties of a pharmaceutical are not necessarily important at a biochemical level, as the substance will most likely be in solution when it has its clearest physiological and pharmacokinetic effects, especially the initial interaction of the product with the body. From the manufacturing perspective, however, the surface properties of pharmaceuticals impact upon the physical properties of formulations, such as their stability.

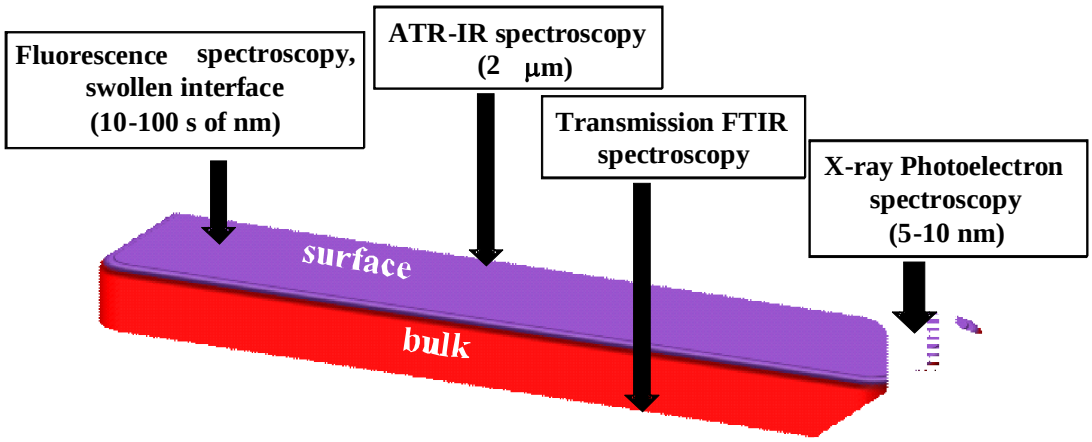

Figure 1-2 : Depth analysis of typical spectroscopic and physical methods used for surface characterisation

Many common techniques have been applied in surface analysis, ranging from simple to complicated instrument setup and methodology (**Figure 1-2**)[4]. For instance, attenuated total reflection infrared (ATR-IR) spectroscopy is a simple analytical technique which penetrates up to 2 µm below the surface, can be used to study surface

functional groups and is typically employed in the qualitative analysis of hydrogen bonding. However, such surface analysis is limited to a small region compared to the bulk material. The topmost atomic layer of a typical metal solid surface contains around 10^{15} atoms per cm^2 – a number both too large and too small. On the other hand, the number is smaller, for example, than the typical number of atoms (10^{23} atom per cm^3) involved in bulk chemical reactions in solutions, which means that surfaces present a challenge for even the most sensitive traditional analytical techniques. This makes changes in surface properties far too small to detect using conventional bulk sensitive techniques such as nuclear magnetic resonance (NMR). In order to detect impurities at the 1% level, techniques used in surface analysis must be sensitive to the presence of 10^{13} atoms. Therefore, specialized techniques are needed to study surface regions. Solid surfaces are exposed to airborne contamination in the form of particles, gases or hydrocarbons. Therefore, surface analysis with an ultra-high vacuum (UHV) system must be used to prepare the sample and to overcome any surface contamination by ensuring a clean and inert environment. **Figure 1-3** illustrates some surface-sensitive techniques, showing the incident and outgoing radiation beams[4].

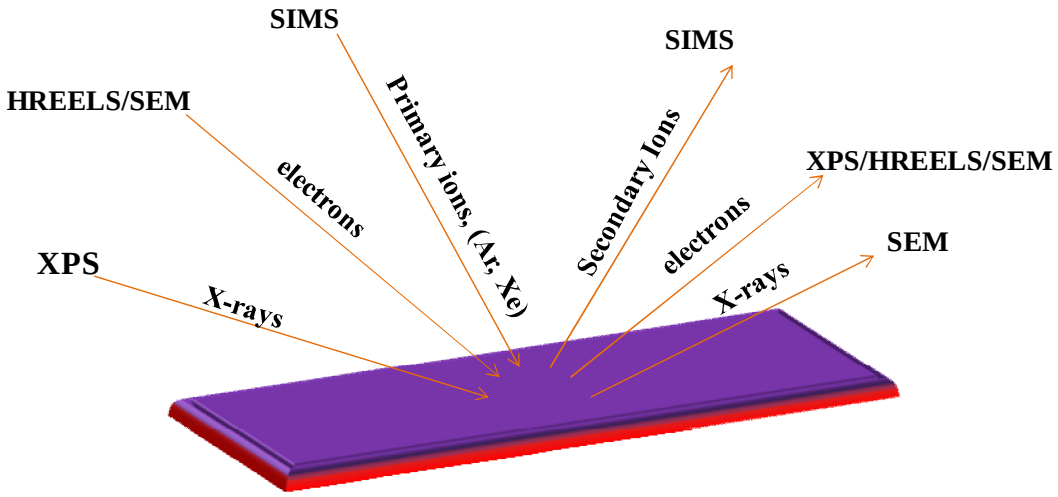

Figure 1-3: **Schematic of some surface characterization techniques using different types of radiation for incident and outgoing beams**

The surface analysis of pharmaceuticals serves a number of purposes. First, it plays a critical role in verifying composition and detecting contaminants that could interfere with the performance of the product. The composition of the outermost atomic layer of pharmaceuticals critically affects or determines properties such as chemical

activity, adhesion, wettability, electrostatic behaviour, bio-compatibility and many other aspects of processing enhancement.

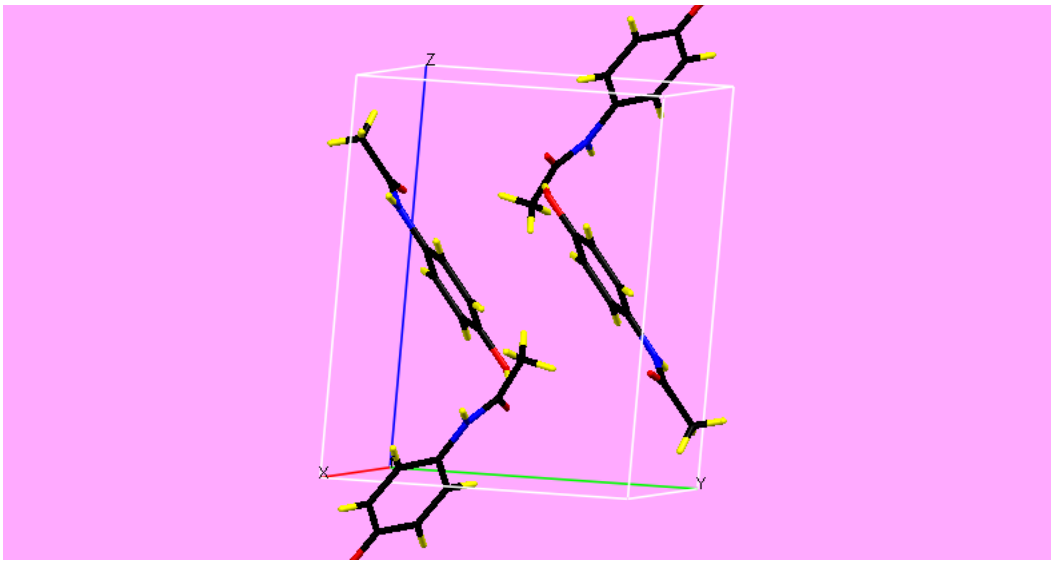

Figure 1-4: Paracetamol unit cell

In addition, contaminants, process residues, diffusion products and impurities are typically present at the surface of solid samples or at the interface of thin film structures; qualitative and quantitative studies of these are vital for the improvement of pharmaceutical products and processes. A typical metal solid surface, as noted above, has 10^{15} atoms per cm^2, which means that even slight contamination on the metal surface can influence the surface analysis. Because of the relative complexity of organic material surfaces, with exact positions of atoms usually unknown, the number of surface molecules per unit area can often only be estimated. In the case of paracteamol, the unit cell (CSD: HXACAN) contains a single molecule, with 4 molecules crossing the four unit cell faces (**Figure 1-4**). An estimate of the surface density of molecules can be carried out as follows.

The mass density of paracetamol is ρ = 1.263 g cm^{-3}. The molar mass, M, is 151.17 g mol^{-1}. The concentration of molecules in the crystal is therefore ρ / M = 8.35 × 10^{-3} mol cm^{-3}, and the number density is 5.031×10^{21} molecules cm^{-3}. Penetrating into the crystal normal to the (001) surface we encounter one (001) plane every interplanar spacing of 11.66 Å. For a cube with a volume of 1 cm^3 the top molecular layer on the (001) surface has a volume of $11.66\times10^{-10} \times 10^{-2} \times 10^{-2}$ m^3 = 11.66×10^{-7} cm^3. A cm^2 of

the (001) surface of a paracetamol crystal therefore exposes approximately 5.031×10^{21} × 11.66×10^{-7} molecules = 5.866×10^{14} molecules.

1.4. Paracetamol as an Active Pharmaceutical Ingredient (API)

Paracetamol, which was first prepared by Morse in 1878[5] and is also known as acetaminophen or N-acetyl-aminophenol, has been used as a drug since 1956 for its antipyretic and analgesic properties. The names paracetamol originate from its chemical name, para-acetylaminophenol. It can be prescribed as a single medication or combined with other pharmaceuticals and has been used for fever, headache and mild to medium pain[6]. Paracetamol was synthesised by Harmon Northrop Morse via the reduction of *p*-nitrophenol with tin in glacial acetic acid. The invention was sparked by the research on aspirin, obtained from the bark of the cinchona tree in the middle of the 19th century. When cinchona bark became scarce in 1880, the production of aspirin as an antipyretic was depleted and two alternative antipyretics, acetanilide and phenacetin, were invented in 1886 and 1887 respectively. The discovery of paracetamol was made accidently in the 1880s, when acetanilide was added to a patient's prescription, but it was largely ignored until 1946. Since acetanilide was found to be toxic at moderate usage levels, a less harmful alternative analgesic had to be found. Following a grant from the Institute for the Study of Analgesic and Sedative Drugs, New York City's Department of Health successfully reproduced paracetamol and sold it to McNeil Laboratories as a pain and fever reliever for children with the brand name Tylenol Children's Elixir[7]. Paracetamol is commonly administered in tablet form but exists in many forms, including liquids, capsules and suppositories. It has been accredited as an over-the-counter (OTC) drug since 1963[6] as it is safe and efficacious in therapeutic doses. Paracetamol is not categorised as a nonsteroidal anti-inflammatory drug (NSAID), like aspirin and ibuprofen, because it does not inhibit cyclooxygenases in the presence of peroxide and does not participate in the inflammatory response[8]. In addition to its antipyretic and analgesic uses, paracetamol is also used as an intermediate in the manufacture of azo dyes and photographic chemicals[9]. The maximum dose of paracetamol is 4 g/day[10] and 90 mg daily for children. The misuse of paracetamol will lead to hepatoxicity, which in severe cases will lead to acute liver failure[8].

Paracetamol is a derivative of aniline compounds[11]. The OH at the para position distinguishes the molecules from other acetanilide derivatives. Paracetamol is a weak

acid, pK_a = 9.70.[5] **Figure 1-5** shows the chemical structures of paracetamol, acetanilide and phenacetin.

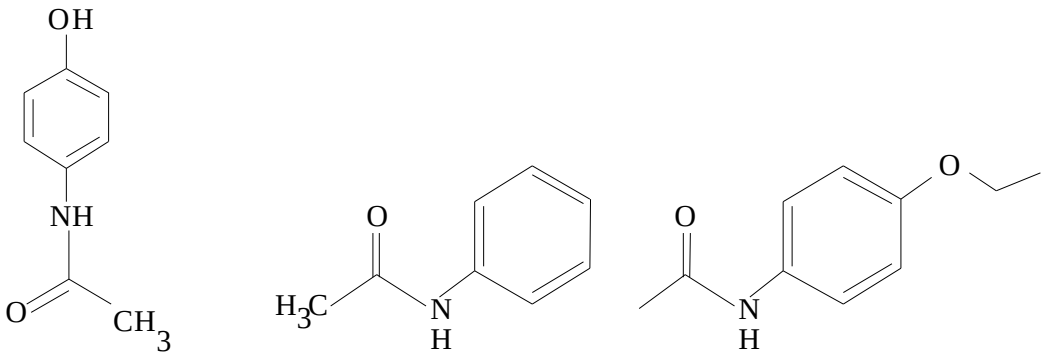

Figure 1-5: Structure of (a) paracetamol (b) acetanilide (c) phenacetin

Paracetamol can be synthesised in many ways: its industrial production can be by the classical route or the Hoechst-Celanese process, as illustrated in **Figure 1-6** below[12].

a) Classical route of paracetamol synthesis[12]

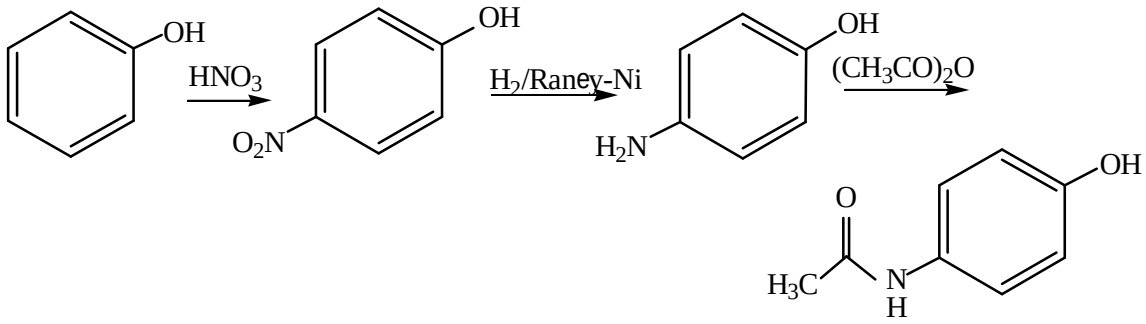

Paracetamol

b) Hoechst-Celanese process

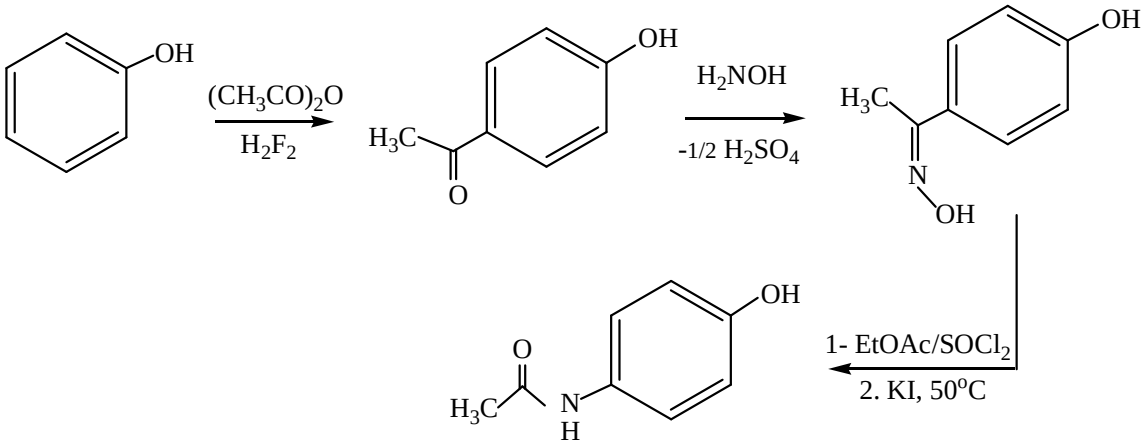

Figure 1-6: Synthesis of Paracetamol

Paracetamol polymorphs have been known for decades. The common commercial polymorph is form I, with a monoclinic crystal structure, which was first reported in 1976 by Haisa, who obtained it from aqueous solution, while the orthorhombic form II was obtained two years earlier, also by Haisa, by slow evaporation of an ethanol solution.[13, 14-16] Recently, an unstable crystal structure, form III, has been observed during fusion experiments and is reported to be so unstable that no crystals have been isolated to enable its structure or physicochemical properties to be determined[2, 17]. Form I, a monoclinic form, is commercially available and stable at ambient temperature and pressure[18]. Nevertheless, this polymorph is characterised by poor technological and biopharmaceutical properties, which include flowability, compactibility, wettability and dissolution rate. The lack of slip planes in the monoclinic form of paracetamol requires the addition of plasticisers or excipients as supporting materials for compaction of the drug. The existence of slip planes is a prerequisite for plastic deformation upon compaction[19]. Secondly, form II, which is orthorhombic, undergoes plastic deformation and is suitable for direct compression[18]. In addition to forms I and II, paracetamol can exist as a monohydrate crystal structure, but this is unstable with respect to loss of water and will dehydrate within five minutes on exposure to air, becoming the monoclinic form[20]. Paracetamol form III has a crystal structure which has not yet been determined, due to its high physical instability[18]. Solvates and hydrates of paracetamol are also reported in the literature[21]. **Table 1-1** summarises the physicochemical properties of the three polymorphs.

Table 1-1: Physicochemical properties of the three paracetamol polymorphs

Polymorph	Melting Point (°C)	Crystal Structure	Method of Preparation	Solubility in water (mg mL^{-1} at 20 °C)
I	168-172	Monoclinic	Recrystallisation	13.12
II	157-159	Orthorhombic	Recrystallisation / from the melt	13.28
III	120-130	n.a.	From the melt	n.a.

1.5. Excipients

Excipients are inactive pharmaceutical ingredients[22] added to the formulation of drugs to aid their manufacture, administration or absorption[23, 24]. Other concerns are for product differentiation, appearance enhancement, retention of quality and bioavailability in the body. All such excipients must be biocompatible, nontoxic and non-carcinogenic; they should not induce immunological or allergic responses and should not accumulate in the tissues or organs.[25] In the USA, the Food and Drug Administration (FDA) is the body which maintains a list of safe and established excipients and information on these[26]. The chosen excipients must have combined hydrophilic and hydrophobic properties. They should be system-specific, hydrosoluble and biocompatible, so that they can be cleared from the body by dissolution in physiological fluids[25]. The second requirement of any excipient is the support of the pharmacological agent. This component can be linked directly to the drug through the spacer group to increase the flexibility and mobility of the side residue, to minimize the steric hindrance of the neighbouring groups and therefore to facilitate the pharmacological action and the enzymatic cleavage of the active side residue.[25] After the cleavage of the side drug residue, the functional groups of the drugs such as amides or esters, promoted by enzymes such as esterase or lipases, are transformed into corresponding sodium salts which are readily soluble in the physiological fluids and cleared from the body through the normal urinary pathway[25].

However, excipients may have functional groups or contain impurities or residues, or they may undergo degradation which in turn leads to the decomposition of the drug formulation[6, 27]. These phenomena can initiate, propagate or prolong the participation of an excipient in chemical or physical interactions with the API. Three

phases of drug decomposition have been identified as the lag, acceleration and deceleration phases, as presented in **Figure 1-7**[26].

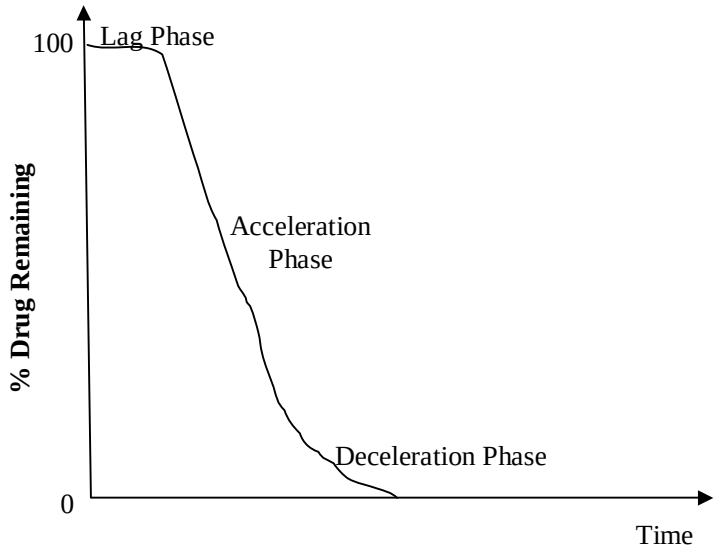

Figure 1-7 : Typical solid state decomposition curve

Understanding the molecular mechanisms of APIs and excipients is essential to comprehend the physical or chemical interaction between them. Physical mixtures must be studied to provide a comparison or benchmark for further investigation of the API and the excipients. In recent years, research has found that excipients can be adsorbed directly onto drug particles to produce powders with optimised physicochemical properties[28]. The interactions of drugs and excipients can be studied using solid dispersion techniques such as co-evaporation or co-precipitation, physical mixture or milling of the mixture[29, 30]. Milling is the classical micronization technique, but gives rise to disorder and defects on the crystal surface, which may influence the processing properties and the performance of a formulation[28]. The type of tumbling mill most commonly used in pharmacy is the ball mill. Several parameters are involved in the ball mill method, such as rotation speed, mill size, wet or dry milling and amount of material to be milled. Prolonged milling time may be detrimental to compound crystallinity and stability[26]. The improvement of drug and excipients processing has been reported by precipitation of drugs in the presence of excipients[28]. In this technique, drug particles are grown by association of molecules rather than breakage of crystal structure[28].

Changes in the morphology, habits and growth of specific faces during the crystallisation of drugs and excipients may be anticipated from the original drug crystal properties[28]. This phenomenon arises from the adsorption of excipient or drug onto one of the compounds. A study by atomic force microscopy (AFM) revealed that surfactants do not always form a homogenous layer at the interface[31].

Poloxamer 188, has been chosen excipient for its unique hydrophilic and hydrophobic properties. Poloxamers are block copolymers consisting of poly(ethylene oxide) (EO) and poly(propylene oxide) (PO). They form a class of amphiphilic surface active agents in aqueous solution but are also shown to form structures in the absence of solvents.[32] However, they have been found to have a greater ability to self-assemble in solution than in the absence of solvent[32]. Poloxamers are always used in the formulation of suppository drugs because of their gelling properties in the presence of body fluids.

1.6. X-ray Photoelectron Spectroscopy

A surface-sensitive technique is needed for the surface characterisation of single crystals. The analysis of solid surfaces by one of the soft X-ray techniques, XPS, is based on irradiation by an X-ray beam under UHV and the consequent emission of electrons, whose kinetic energy is then analysed. It is a surface-sensitive technique which is applied only at a solid-air interface. The resulting spectrum is plotted as a function of the binding energy, E_B, or kinetic energy, E_K of the photoemitted electron. Two basic analyses are normally performed: a wide survey analysis and a high resolution analysis on each selected element. The peaks in the spectra arise from electrons bound in atomic core levels (1s, 2s, 2p, etc). The E_B is influenced by the chemical environment of the element and thus provides information on the functional chemical groups in which it is incorporated. Through inelastic scattering of electrons in the solid the emission peaks are specific to outermost molecular or atomic layers, with electron emission arising from approximately 2 to 5 nm from the surface. The position and shape of the peaks give information on the bonds and thus on the chemical functions in which the elements is involved[33, 34].

1.7. Motivation: API/Excipient Interactions

Most pharmaceutical products are based on active ingredients which have organic properties such as insulation and which also tend to have high vapour pressure values. These characteristics make XPS a poor choice for studying pharmaceuticals. The only

study of paracetamol single crystal faces was by Heng,[35] who used a high vacuum XPS instrument (Kratos AXIS HSi), equipped with a charge neutraliser, with Mg K_α as the X-ray source. The analysis revealed that facet (001) was the most nitrogen-deficient face and correspondingly carbon-enriched. The (001) facet was also found to be the most polar, with water molecules detected at the surface, as indicated by an O 1s deconvoluted peak at 534.6 eV. The surface polarity of paracetamol facets was determined by XPS to decrease in the order (001) > (011) > (110) > (010) [35] .

The XPS technique is widely and efficiently used to determine a range of chemical compositions, the concentration of hydrocarbon contaminants, the atomic concentration present in samples, adsorbed layers on substrates, oxidation states and the reactivity of microorganisms to inorganic and organic compounds[33]. It has been used in the analysis of food, wood species surface and ageing analysis.[36] The ratios of elemental concentration or intensity (e.g. C/O or O/C) can be used as indicators of oxidation processes undergone by compounds or to characterise the surface of samples.[36] The shift of binding energy of each deconvoluted peak from the standard or reference value indicates the occurrence of oxidation, protonation or deprotonation in the core electrons of carbon, C 1s, oxygen, O 1s, or nitrogen, N 1s[34].

For example, XPS has been used in the determination of the heterogeneity of D-mannitol single crystal faces, by detecting the hydroxyl concentration on each of the chosen faces [37]. In another study, a poorly water-soluble drug, siramesine hydrochloride, was precipitated by the antisolvent method in various polymeric and surface active excipients. By using AlK_α X-ray sources at the elemental analysis depth of 100 Å, XPS was used to quantify the amount of excipient adsorbed to the surface of the drug particles[28]. The adsorbed excipients were detected by the increased O coverage compared with other elements such as N, F and Cl. Poloxamer 188 was one of the excipients used and was shown to be adsorbed inhomogeneously on the surface in thin layers and multilayers.

An XPS study of the adsorption of pyrrole, aniline, 3-pyrroline and pyrrolidine on the surface of silicon revealed that the bonding of pyrrole or aniline was through the cleavage of N-H bonds, leaving the benzene ring intact. The XPS study of pyrrole, aniline and their saturated analogues at a silicon surface has helped to establish some general trends for understanding the chemistry of organic amines at the (001) face of silicon

crystals[38]. The adsorption of a surfactant, sodium lauryl sulfate (SLS), onto drug crystals of Siramesine revealed that the SLS layer on the drug surface was 0.6 nm thick, with a patchy monolayer structure. It was assumed that monolayer coverage was about 30%.[28]

Extensive studies of biomedical materials have thus shown that the wide-scale use of XPS on pharmaceutical materials is feasible, and the popularity of recent reviews in pharmaceutical surface science show that such applied systems are of increasing interest to surface science workers. With advances in instrumentation it now appears that XPS could become a routinely used technique for fundamental study and formulation development. The present study uses XPS with the aid of surface structure techniques such as functional group spectroscopy (ATR-IR) and thermal analysis by differential scanning calorimetry (DSC) for the abovementioned purposes. In addition, the crystallinity and Miller Index of samples will be analysed by Powder X-ray Diffraction (PXRD) or Single crystal X-ray Diffraction. The fundamental analysis of a single crystal is compared with that of paracetamol powder. Milled and treated pure powder in an amorphous state are characterised in order to analyse the changes to paracetamol polymorphism using the XPS technique. The aromatic ring structure is revealed in XPS spectra as a shakeup satellite and the loss of aromaticity is anticipated to cause the loss of the shakeup peak. Previous studies have found that the adsorption of aromatic compounds by a silicon surface was accompanied by a loss of aromaticity[38].

1.8. Structure of the Thesis

This thesis is organised as follows.

Chapter 1, the present chapter, has discussed the motivation and background of the research, then presented a literature review of the techniques used in the studies, with a section on the main technique used, which is X-ray photoelectron spectroscopy.

Chapter 2 summarises the properties of paracetamol and the chosen excipients. It covers the theory and instrumental background of all the techniques used in the study. In addition, the interaction strength of three common drugs named as paracetamol, ibuprofen and aspirin with some choosen excipients have been calculated.

Chapter 3 discusses paracetamol crystallisation. It reports the study of single crystal preparations including a brief account of the techniques of crystallisation. The background study of crystallisation is also included.

Chapter 4 is about degradation of poloxamers. In addition, it draws attention to the importance of poloxamer degradation in the deep study of paracetamol-poloxamer interactions, concluding that the existence of a carbonyl peak in XPS analysis is an indication of degradation.

Chapter 5 is concerned with the analysis of paracetamol powder by XPS, supported by the XRD and ATR-IR techniques. The powdered paracetamol was treated by several mechanical techniques such as milling and grinding, by melting under an inert flow of nitrogen gas in a DSC chamber and by melting and abrupt cooling in liquid nitrogen.

Chapter 6 reports the quantitative analysis by XPS of single paracetamol crystals grown in three different solvents. The quantification of the crystals facets by XPS is explained.

Chapter 7 reports the interaction of physical mixtures of paracetamol and poloxamer 188, following the same structure as set out above for chapter 6.

Chapter 8 draws conclusions from the studies and offers suggestions for the enhancement of the existing research.

1.9. References

1. An exposition of everything that's Pharmaceutical industry: Pharmaceutical Market Trends 2010. (29 July 2010),

2. Narayan, V.; Aaron, S. C.; Michael, F. D., From form to function: Crystallization of active pharmaceutical ingredients. *AlChE J.* **2008,** 54, (7), 1682-1688.

3. Kiang, Y. H.; Shi, H. G.; Mathre, D. J.; Xu, W.; Zhang, D.; Panmai, S., Crystal structure and surface properties of an investigational drug--A case study. *Int. J.Pharm.* **2004,** 280, 17-26.

4. Stamm, M.; SpringerLink, *Polymer Surfaces and Interfaces [electronic resource] : Characterization, Modification and Applications*. Springer-Verlag: Berlin, Heidelberg, 2008; p digital.

5. Binev, I. G.; Vassileva-Boyadjieva, P.; Binev, Y. I., Experimental and ab initio MO studies on the IR spectra and structure of 4-hydroxyacetanilide (paracetamol), its oxyanion and dianion. *J.Mol. Struct.* **1998,** 447, 235-246.

6. Nair, R.; Nyamweya, N.; Gönen, S.; Martínez-Miranda, L. J.; Hoag, S. W., Influence of various drugs on the glass transition temperature of poly(vinylpyrrolidone): a thermodynamic and spectroscopic investigation. *Int. J. Pharm.* **2001,** 225, 83-96.

7. Friderichs, E.; Christoph, T.; Buschmann, H., *Analgesics and Antipyretics*. Wiley-VCH Verlag GmbH & Co. KGaA: 2000.

8. Dargan, P. I.; Jones, A. L., Management of paracetamol poisoning. *Trends Pharmacol. Sci.* **2003,** 24, 154-157.

9. Boerrigter, S. X. M.; Cuppen, H. M.; Ristic, R. I.; Sherwood, J. N.; Bennema, P.; Meekes, H., Explanation for the Supersaturation-Dependent Morphology of Monoclinic Paracetamol. *Cryst.Growth Des.* **2002,** 2, 357-361.

10. Paracetamol. http://www.medic8.com/medicines/Paracetamol.html

11. Behzadia, H.; Esrafilia, M. D.; Hadipour, N. L., A theoretical study of 17O, 14N and 2H nuclear quadrupole coupling tensors in the real crystalline structure of acetaminophen. *Chem.Phys.* **2007,** 333, 97-104.

12. Ullmann, F., *Ullmann's encyclopedia of industrial chemistry [electronic resource]*. John Wiley: [New York], 2005.

13. Naumov, D. Y.; Vasilchenko, M. A.; Howard, J. A. K., The Monoclinic Form of Acetaminophen at 150K. *Acta Crystallogr. C* **1998**, 653-655.

14. Moynihan, H. A.; O'Hare, I. P., Spectroscopic characterisation of the monoclinic and orthorhombic forms of paracetamol. *Int. J. Pharm.* **2002,** 247, 179-185.

15. Di Martino, P.; Guyot-Hermann, A. M.; Conflant, P.; Drache, M.; Guyot, J. C., A new pure paracetamol for direct compression: The orthorhombic form. *Int.J. Pharm.* **1996,** 128, 1-8.

16. Oswald, I. D. H.; Allan, D. R.; McGregor, P. A.; Motherwell, W. D. S.; Parsons, S.; Pulham, C. R., The formation of paracetamol (acetaminophen) adducts with hydrogen-bond acceptors. *Acta Crystallogr. B* **2002,** 58, 1057-1066.

17. Nichols, G.; Frampton, C. S., Physicochemical characterization of the orthorhombic polymorph of paracetamol crystallized from solution. *J. Pharm.Sci.* **1998,** 87, 684-693.

18. Giordano, F., Thermal behavior of paracetamol-polymeric excipients mixtures. *J Therm. Anal. Calorim.* **2002,** 68, 575-590.

19. Al-Zoubi, N.; Nikolakakis, I.; Malamataris, S., Crystallization conditions and formation of orthorhombic paracetamol from ethanolic solution. *J. Pharm. Pharmacol.* **2002,** 54, (3), 325-333.

20. Parkin, A.; Parsons, S.; Pulham, C. R., Paracetamol monohydrate at 150 K. *Acta Crystallogr. E* **2002,** 58, (12), o1345-o1347.

21. Bouhmaida, N., Charge density and electrostatic potential analyses in paracetamol. *Acta Crystallogr.B* **2009**, 363-374.

22. Excipients. *Chem. Eng. News* **2008,** 86, 25.

23. Lukyanov, A. N.; Torchilin, V. P., Micelles from lipid derivatives of water-soluble polymers as delivery systems for poorly soluble drugs. *Adv.Drug Deliver.Rev.* **2004**, 1273-1289.

24. Torchilin, V. P., Structure and design of polymeric surfactant-based drug delivery systems. *J.Control Release* **2001,** 73, 137-172.

25. Román, J. S.; Levenfeld, A. G. B., Polymeric drug delivery systems. *Adv. Mater.* **1995**, 203-208.

26. Gibson, M., *Pharmaceutical preformulation and formulation : a practical guide from candidate drug selection to commercial dosage form*. Interpharm/CRC: London, 2004; p xi, 596.

27. Patrick, C.; Martini, L. G., Drug-excipient interactions. *Pharm. Technol. Int.* **2001,** 13, 26-28+30.

28. Zimmermann, A.; Millqvist-Fureby, A.; Elema, M. R.; Hansen, T.; Müllertz, A.; Hovgaard, L., Adsorption of pharmaceutical excipients onto microcrystals of siramesine hydrochloride: Effects on physicochemical properties. *Eur. J.Pharm. Biopharm.* **2009,** 71, 109-116.

29. Pignatello, R.; Ferro, M.; Puglisi, G., Preparation of solid dispersions of nonsteroidal anti-inflammatory drugs with acrylic polymers and studies on mechanisms of drug-polymer interactions. *AAPS PharmSciTech* **2002,** 3, (2), 35-45.

30. de Villiers, M. M.; Wurster, D. E.; Van der Watt, J. G.; Ketkar, A., X-ray powder diffraction determination of the relative amount of crystalline acetaminophen in solid dispersions with polyvinylpyrrolidone. *Int.J. Pharm.* **1998,** 163, 219-224.

31. Santander-Ortega, M. J.; Jodar-Reyes, A. B.; Csaba, N.; Bastos-Gonzalez, D.; Ortega-Vinuesa, J. L., Colloidal stability of Pluronic F68-coated PLGA nanoparticles: A variety of stabilisation mechanisms. *J.Colloid Interf. Sci.* **2006**, 522-529.

32. Alexandridis, P., A record nine different phases (four cubic, two hexagonal, and one lamellar lyotropic liquid crystalline and two micellar solutions) in a ternary isothermal system of an amphiphilic block copolymer and selective solvents (water and oil). *Langmuir* **1998,** 14, 2627-2638.

33. Aguié-Béghin, V., Structure and chemical composition of layers adsorbed at interfaces with champagne. *J.Agr. Food Chem.* **2009,** 57, 10399-10407.

34. Mozes, N., On the relations between the elemental surface composition of yeasts and bacteria and their charge and hydrophobicity. *Biochim. Biophys. Acta Biomembr.* **1988,** 945, 324-334.

35. Heng, J. Y. Y.; Bismarck, A.; Lee, A. F.; Wilson, K.; Williams, D. R., Anisotropic surface energetics and Wettability of macroscopic form I paracetamol crystals. *Langmuir* **2006,** 22, 2760-2769.

36. Popescu, C.-M.; Tibirna, C.-M.; Vasile, C., XPS characterization of naturally aged wood. *Appl.Surf. Sci*. **2009,** 256, 1355-1360.

37. Hinderb, S. J.; Wattsb, J. F.; Dilworthc, S. E.; Williams, D. R.; Heng, J. Y. Y., Determination of surface heterogeneity of d-mannitol by sessile drop contact angle and finite concentration inverse gas chromatography. *Int. J. Pharm.* **2010,** 387, 79-86.

38. Cao, X.; Coulter, S. K.; Ellison, M. D.; Liu, H.; Liu, J.; Hamers, R. J., Bonding of Nitrogen-Containing Organic Molecules to the Silicon(001) Surface: The Role of Aromaticity *J. Phys. Chem. B* **2001,** 105, 3759-3768.

CHAPTER 2: MATERIALS, METHOD AND TECHNIQUES

2.1. Introduction

In order to understand the molecular mechanisms by which pharmaceutical compounds interact in multiphase and multicomponent mixtures, the single crystal form of the drug must be prepared, as the known crystallography gives a deeper understanding of the drug's molecular interactions than the powdered form, which will not replicate the real conditions of the molecules' behaviour.

Some compounds can be arranged in more than one crystal structure arrangement, a phenomenon called crystal polymorphism, which can result from differences in crystal packing, conformers and properties. The conformers will crystallise in ways which are favourable to the minimising of the surface free energy, while the surface energy is influenced by intermolecular forces such as van de Waals, dipole-dipole and hydrogen bonding forces, which differ in strength according to crystal orientation. At different conformations and different angles of molecular rotation, the flexibility and stability of the molecules are affected[1].

The crystallisation process is best understood as proceeding by stages. It starts with the aggregation of asymmetric molecules forming a small network known as a unit cell at the pre-nucleation stage. These nuclei will then aggregate and grow into larger networks to form mature crystals[1]. The unit cells are arranged like a line of networks in three dimensions. The intersection of the lines, known as the lattice point (lattice site), has the same environment in the same direction. The summation of the intermolecular interactions and those between central molecules and the surrounding molecules yields the lattice energy, E_{latt}[2]. The distortion of crystal arrangement forms Bravais lattices of the crystal[14]. Bravais lattices can be illustrated as crystal unit cells. The growth of crystals is the result attachment of solute molecules at the crystal facets.

Crystallisation is the process of formation of solid crystals from a homogenous solution[3]. The crystallisation process involves two basic steps, which are nucleation and crystal growth. Nucleation is the process where a solute disperses in the solvent and creates nuclei, clusters or embryos. Before crystals can develop, a number of solid bodies in the form of seeds, embryos or nuclei must exist in the solution as the centres of

crystallisation. The nucleation process can be induced spontaneously or artificially[4]. Nucleation can be divided into primary and secondary types, and further classified as homogeneous or heterogeneous. Homogeneous nucleation occurs without the influence of foreign particles, while heterogeneous nucleation involves foreign particles[5]. Secondary nucleation is that induced by other crystals existing in the solution. Nuclei can be stabilised by controlling the operating conditions such as the supersaturation temperature. Environmental conditions such as vibration and humidity, solution solubility and mass will create good nuclei. Any unstable clusters will be redissolved in the solvent, while stability is reached when the cluster exceeds a specific size, forming a critical nucleus[5]. Critical nuclei are thus those formed by clusters of the minimum size required to become crystals[5]. Physically, the phenomenon occurs when the solution becomes supersaturated, which depends on solubility. In the so-called labile zone of supersaturation, spontaneous nucleation will be feasible, while the metastable zone is where spontaneous crystallization is improbable but possible with the help of a seed (**Figure 2-1**). Finally, in undersaturated solutions, any crystal will be redissolved and nucleation will be impossible[5].

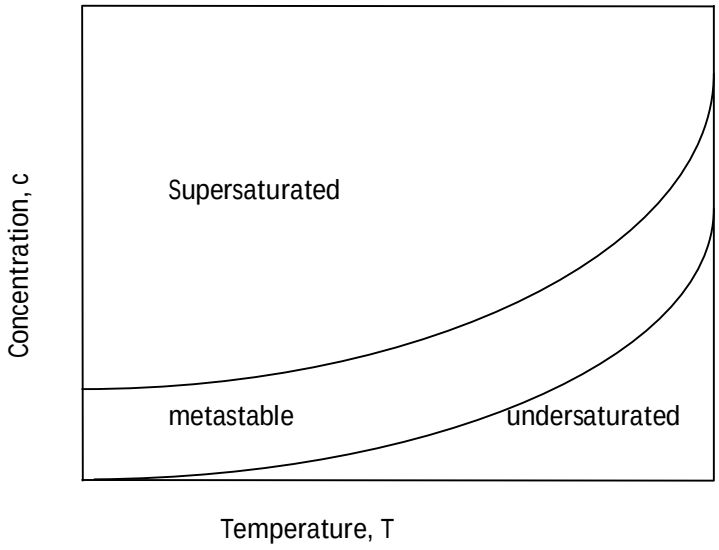

Figure 2-1: Nucleation Zones of Crystallisation

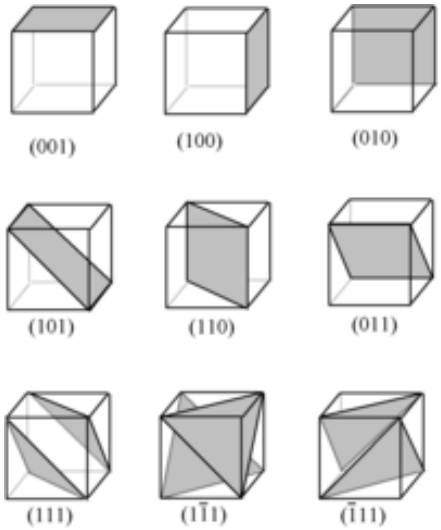

Figure 2-2: Examples of plane direction according to the Miller Indices System

In order to relate a surface to the crystal structure, the system of Miller indices was introduced (**Figure 2-2**). This is a notation used to describe lattice planes and directions in a crystal. It defines the orientation of the surface in relation to the crystallographic unit cell. The direction of the crystal plane is represented by three integers, obtained from the intersections of the face with the three crystallographic axes: x, y and z. In the Bravais-Miller indices system a crystal plane direction will be written as (*hkl*), as shown in **Figure 2-2**[5].

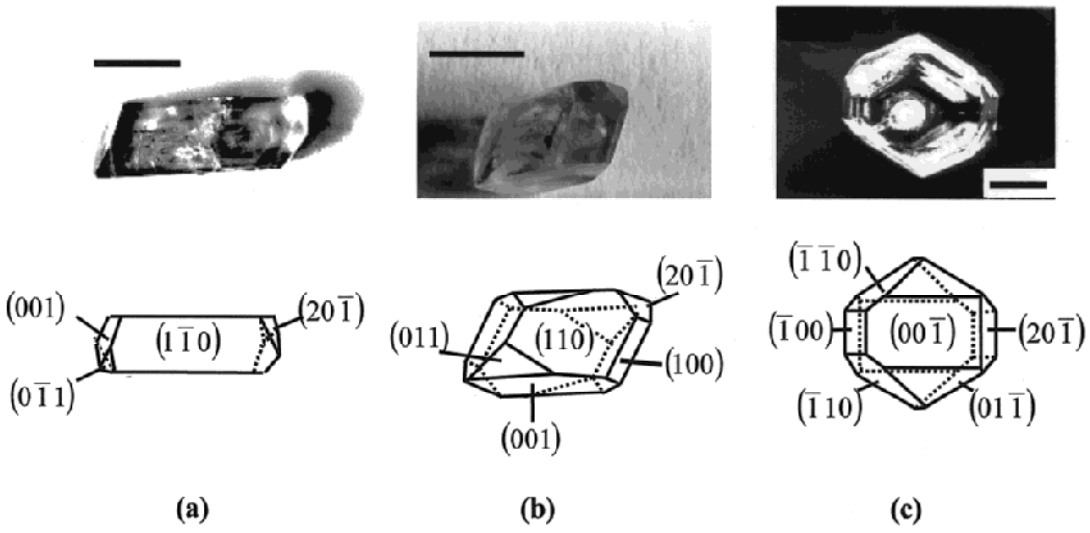

Figure 2-3: Macromorphology of paracetamol crystals grown at (a) low, (b) medium and (c) high supersaturation all images shows habits and the forms of the paracetamol crystals

Figure 2-3 shows the differing morphology of paracetamol single crystals grown in solutions at different levels of saturation. The macromorphology of a crystal will depend on the relative growth rates of the different crystallographic faces[6]. The crystal will exhibit differences in growth at its various facets, under the influence of external parameters such as supersaturated conditions and impurities, and of internal parameters such as crystal structure, bonds and crystal defects[6, 7]. Crystal facets appear because some crystal surfaces grow more slowly than others. Over time, these unit cells are interconnected to form a structure or pattern. The general rule for the mechanism of face formation is that the slower a face grows, the larger its relative size on the crystal[6]. The formation of a face depends mainly on the nature of the molecular incorporation and binding at different crystal faces, the density of active growth sites, layer by layer of the crystal growth, and the environmental conditions[6] (**Figure 2-4**) . The anisotropic properties of organic compounds result in a crystal with distinct facets of differing surface areas and orientations. Each crystal facet forms an angle with another facet. Faces with high molecular densities are more energetically stable and grow more slowly than ones with low molecular densities. Only strong chemical bonds can build a crystal structure. The effective time during which strong bonds build the crystal structure is known as the periodic bond chain vector. The large amount of energy which is released when strong bonds form is known as the attachment energy[8], defined as the energy released when a mole of molecules attaches onto a given crystal face[6, 9]. A high attachment energy indicates a rapid growth of the face, because the growth rate of a surface is proportional to its attachment energy[6]. Such a rapidly growing face tends to be offset by slower growing faces[9]. Thus, the largest crystal facet, which has the most important morphology, is grown with the lowest attachment energy[2]. On this basis the morphologies of compound faces can be anticipated.

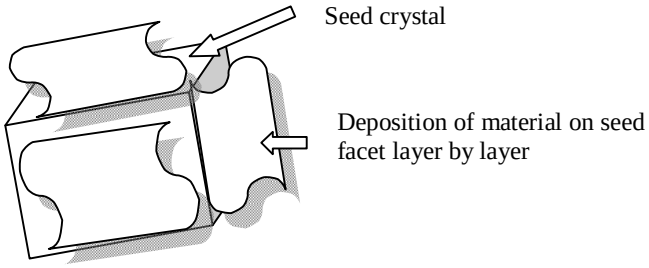

Figure 2-4: Illustration diagram of the seed growth by deposition of material on seed surface.

The three principal theories concerning crystal facet mechanisms which allow the morphology prediction of crystal indexes began with the study of crystal lattice geometry by Bravais (1866), whose ideas were modified by Friedel (1907) and finally by Donnay and Harker (1937). The resulting BFDH model states that the most energetically stable and slowest growing faces are the ones with the highest density of material and the largest spacing between the adjacent layers of molecules. The concept was expanded for better understanding by Wells (1946). The same concept as that of the BFDH model, but with a different approach, was developed from the intermolecular interaction approach of Hartman and Perdok, based on attachment energy, E_{att}, and energy calculations[6, 10].

Crystal faces may be divided into three classes: flat or F-faces, stepped or S-faces and kinked or K-faces. F-faces are the most important, followed by S- and K-faces. K-faces occur rarely or not at all, due to their fast growth and high attachment energy, while F-faces comprise the largest group in crystal morphology[11].

Paracetamol crystal morphology is known to depend strongly on the supersaturation of the solution. Crystal facet analysis has revealed a dead zone for faces[12] and beyond this a relatively rapid increase in crystal growth rate[13]. Studies have also revealed that the fastest paracetamol crystal facet growth was at (100) and that the facet disappeared quickly from the crystal habit[6, 13]. Moreover, analysis of the crystal surface by interference contrast micrography concluded that the ((201), (011), (100) and (001) faces all grew with a spiral growth mechanism in the presence of screw and mixed dislocation crystal sources[6, 13, 14],whereas for the (110) faces, relatively few well separated dislocation sources were observed[13].

In the theoretical study of crystal faces, the energy of interaction between the growth units is calculated using molecular mechanics. A computerised calculation known as the

force field technique takes account of energy values and the charges on molecules. Different force field models may use different expressions and numerical constants to calculate the energy term. The most common force field model is the Dreiding model, which is based on experimentally observed geometries and has been shown to work well on most organic crystals taken from the Cambridge Structural Database (CSD). Compound charges used in the Dreiding model are derived from the molecular electrostatic potential (ESP). Alternatively, the Compass force field model has its own charge set, based on *ab initio* calculations, while the DMA force field model treats crystal molecules as rigid bodies, as it contains no intramolecular calculations[13]. The abovementioned models were used as attachment energy models for the calculation of flat faces. The flat faces were determined by crystallography and analysed by connected net analysis. They were confirmed by the existence of connected nets on the crystal graph[13].

2.2. Paracetamol

Paracetamol is a very common API, known as acetaminophen in the United States, Canada, Hong Kong, Iran, Colombia and other Latin American countries. It is also known as p-hydroxyacetanilide and was launched as a drug in 1956[15]. Its solid forms include tablets, suppositories and capsules, while liquid paracetamol is commercially available as suspensions and solutions[16]. It is widely available as an Over the Counter (OTC) drug.

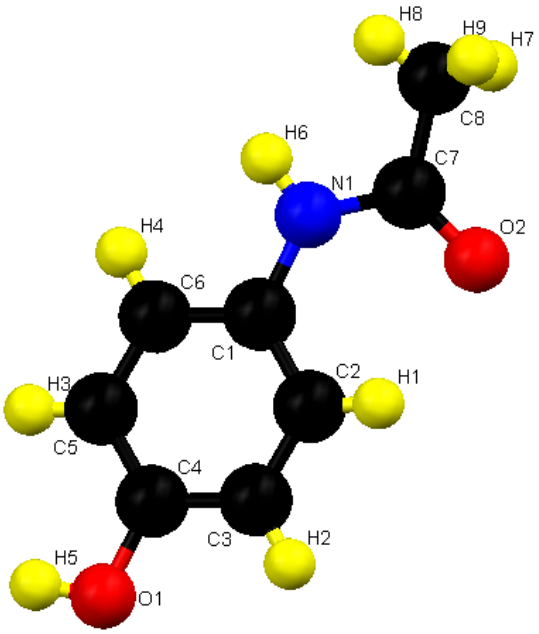

Figure 2-5: Paracetamol structure (C: Carbon, H: Hydrogen, O: Oxygen, N: Nitrogen). (Source: Mercury Software)

The molecular structure of paracetamol **(Figure 2-5)** comprises two main active groups, hydroxide (OH) and amide (N-C=O), attached to an aromatic ring. The study of single paracetamol crystals has proved that the symmetry and the arrangement of the ions are manifested by the anisotropy of the crystal structure. The paracetamol molecules possess several potential centres at which the reaction can be initiated. Four places in the structure have been identified: the benzene ring, OH, NH and CO (C=O). These are the basic fragments for the formation of hydrogen bonds, providing the structure of the paracetamol lattice[17]. The surface structure of paracetamol carries high negative charges which remain undetermined and unexplained. The lone pair electrons of nitrogen and oxygen atoms are good electron donors, giving paracetamol useful chemical and electrical properties. This structure can be characterised using highly surface sensitive methods to determine the surface composition, binding energy and elemental analysis.

A characteristic of paracetamol crystals is that they undergo severe cracking and fracture because of the highly brittle nature of the material. This fracture behaviour of paracetamol can be explained on the basis of the molecular packing and attachment energies in the crystal structure[18]. The study of crystals relies on five concepts: atomic position, symmetry, asymmetric unit, unit cell and space group [9]. The crystal structure of

paracetamol has been studied by many researchers[19, 20]. Given the physical differences in crystal structure between paracetamol forms I and II, they can be differentiated in terms of their crystal packing architectures: form I has a zigzag crystal pattern, while form II has a more planar arrangement, as shown in **Figures 2-6 and 2-7**[16] .

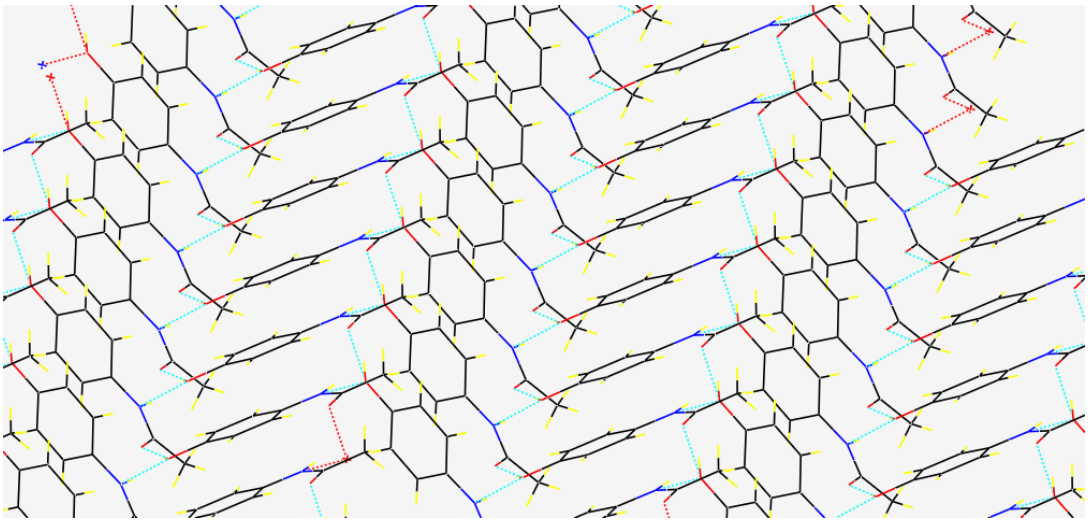

Figure 2-6: Crystal packing architecture of form I paracetamol.
(black: C, red: O, yellow: H, blue; N, light blue; hydrogen bond)

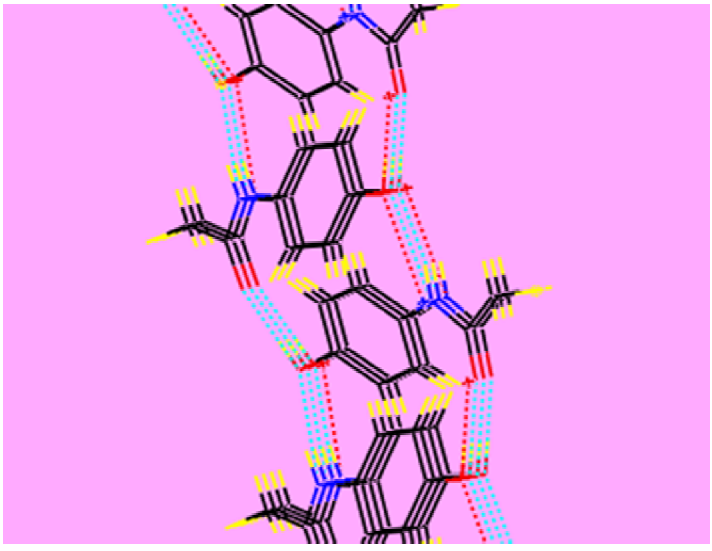

Figure 2-7: Crystal packing architecture of form II paracetamol
(black: C, red: O, yellow: H, blue: N, light blue: hydrogen bond)

The crystal structure of paracetamol is determined by hydrogen bonding,[15] which plays a significant role in paracetamol morphology[21]. Potential electron donors in the structure are detected as lone pairs of electrons of oxygen and nitrogen in the aromatic ring[22]. Each crystalline paracetamol molecule is linked to four neighbouring ones via O-H...O and N-H...O hydrogen bonds. It has been proven by the application of density functional theory (DFT) that O=CNH makes a vital contribution to the crystalline paracetamol hydrogen bonding interactions[21].

Many techniques of paracetamol crystallization, including slow evaporation, solvent diffusion and slow crystallization, have been reported in various studies including investigations of macromorphology, micromorphology, computational and theoretical morphology, identifying oxyanions and dioxane within the molecules and studying interactions with excipients. In another line of enquiry, powdered monoclinic paracetamol[23] has been extensively studied mechanistically with regard to its poor compaction properties during the process of tableting [23, 24].

Single crystals of form I have been successfully prepared by slow evaporation crystallization using several solvents including methanol, ethanol and acetone[6, 18, 25-27]. Form I can also be prepared by slow cooling of a saturated ethanol solution[6]. It has further been reported that form I single crystals can be grown from the vapour by sublimation in vacuo on a temperature gradient[6]. The crystals harvested from the mother liquor were dried using a clean soft tissue[18].

Form II single crystals can be prepared from melted paracetamol powder, followed by slow cooling crystallization.[28, 29] Alternatively, form II can be crystallized by slow evaporation from an ethanol solution or produced by the milling of polycrystalline paracetamol[28]. Form II has high yields at low temperature but is readily transformed into form I as the temperature increases.[25] Form II is spontaneously converted to form I at 70 °C,[30] so precautions must be taken during the preparation of pure form II in order to avoid producing a mixture of form I and form II crystals.[28]

Forms I and II of paracetamol can be distinguished by the melting temperature in DSC analysis: form I will melt between 168 and 171 °C, form II at around 157 to 159 °C[30-32] .It has been reported that the thermodynamic stability of form I is caused by entropy rather than lower energy packing.[30]

It has also been shown that the packing arrangement of form I has more degrees of freedom in the vibrational motions related to the crystal lattice, intramolecular and intermolecular interactions[30]. The monoclinic crystal system of paracetamol form I has the space group $P2_1/n$[28]. Form II, the orthorhombic crystal structure, is assigned to the space group Pbca[28]. Thus, form II and form I paracetamol can be distinguished by using powder XRD (PXRD). In order to prevent form II from being converted to form I, it is important for crystallization to occur at low temperature and for the crystals to be harvested within one hour of the onset of nucleation.[28]

Forms I and II can also be distinguished by using vibrational spectroscopy. The two forms can be identified in the IR region of 1260-1225 cm^{-1}[33]. The spectrum of the monoclinic form I has three relatively strong absorptions of approximately equal intensity at 1260, 1244 and 1227 cm^{-1}, while for the orthorhombic form II only two absorptions were observed: a strong one at 1240 cm^{-1} and one of medium strength at 1218 cm^{-1}[33]. A mixture of the two forms can thus be detected by the existence of two absorption peaks, at 1227 cm^{-1} and 1240 cm^{-1}, the former being characteristic of form I and the latter of form II.[33] Structural and vibrational calculations have been carried out on paracetamol in a DFT approximation using hybrid (B3LYP) potentials[34]. IR characterisation in combination with these theoretical studies revealed the intermolecular hydrogen bonds formed by the O-H…O and N-H…O groups.[34]

The molecular structure of paracetamol crystals can be briefly affected by the crystallisation environment[35]. Some of the solvent used during crystallization is reported to be trapped as an impurity in the crystal lattice or to be present as a solvent inclusion in the crystal. The choice of solvent will determine the solubility of the solute and the quality of the saturated solution prepared for crystallization. The solvent also influences the kinetics of nucleation, crystal growth, crystal shape, crystal size distribution and degree of agglomeration, which decreases with increasing solvent polarity.[36] The interaction of solute and solvent during crystallization will affect the properties of the final crystal. The inclusion of solvent on the crystal surface has been predicted by theoretical studies[6]. Such inclusion of solvents and impurities affects the crystal habit by influencing the growth kinetics and growth process.[6]

Paracetamol is more soluble in ethanol than in water and has low solubility in nonpolar solvents[6]. In the crystallization of paracetamol from ethanol solution, the paracetamol molecules and ethanol are reported to interact by hydrogen bonding, with

ethanol acting as hydrogen bond donor. In contrast, in the crystallisation of paracetamol from a saturated acetone solution, there is a dipole-dipole interaction between paracetamol and acetone[37]. The presence of impurities has the potential to modify the solubility of the primary solute and affect the crystallization process[15]. Impurities such as excipients, solvent or contamination can block the adsorption of solute molecules and induce morphological changes. They can also dock onto the surface and become incorporated into the crystal lattice, disrupting the emerging nucleus and thus inhibiting the nucleation process[15].

Amorphous paracetamol can be prepared by melting paracetamol powder and quench cooling in liquid nitrogen[32, 38]. The amorphous paracetamol will partially recrystallize immediately after quench cooling and in a recent experiment it was reported that the entire crystallization process was completed in 14 days, even though the material was being stored well below the glass transition temperature, T_g[31]. Amorphous paracetamol can also be prepared by a heating and cooling programme in a hermetic DSC pan[31].

DFT studies have shown that in an aqueous ethanol medium, the phenolic -OH group of paracetamol partially ionizes reversibly into the corresponding phenolate ion (conjugate base, CB) and hydroxonium ion, H_3O^+ [22] .The DFT calculation reveals the delocalization of the negative charge of the phenolate ion into the ring during ionization. This delocalization does not spread to the N atom, as is evident from the length increase in C_6-N- (**Figure 2-8**) upon ionization. The DFT calculation also shows that the N-C_{15} bond length decreases, while the C_{15}-O_{16} bond length increases, in the transformation from paracetamol to CB during ionization in ethanol[22].

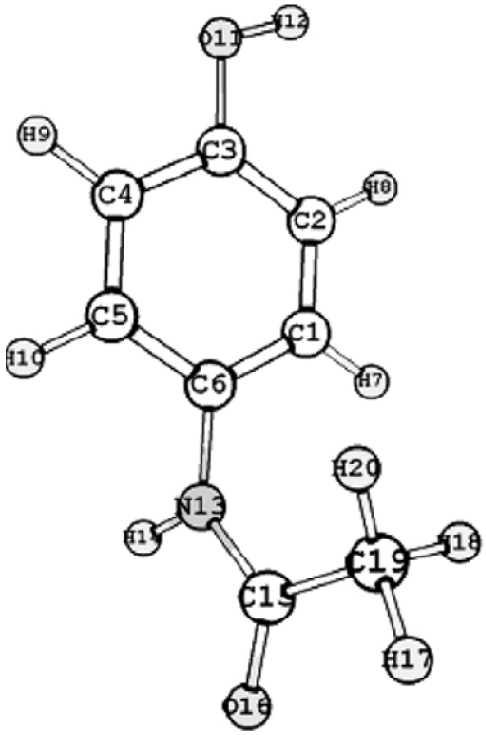

Figure 2-8: DFT optimized structure of paracetamol. H: Hydrogen, C: Carbon, N: Nitrogen, O: Oxygen.[22]

It has been suggested that the most polar face of paracetamol is the (001) face[26, 27]. Form I single crystals grown in ethanol (industrial methylated spirit) had a prismatic to platy habit that was elongated in the direction of the c-axis but parallel to the (101) face,[28] while form II consisted of prisms that were elongated along the c-axis. The cleavage face of paracetamol is (010).[39] Single crystals with columnar habit had major faces at (110), while tablet-like crystals had major (001) faces.[18] Single crystal paracetamol is reported to have a pinacoid open form. A mature single crystal (grown for a longer time) grown in ethanol shows the development of pinacoids (10-1) and (101) and of prisms (011) and (110) as the dominant forms, whereas the immature crystals have pinacoids (001) and prisms (111), which are the fastest growing faces[28]. An increase in saturation of the crystallization solution yielded crystals of a flat, tabular morphology, where the (001) faces were morphologically most important and dominated the habit[6]. The fastest growing face in a highly saturated solution was at (110) [6]. The (110) growth sectors were characterized by a much larger density of solvent inclusions than observed in any of the other sectors[6]. It was observed that in a supersaturated solution the hillock morphology growth on the crystal surface would lead to the capture of solvent in the crystal

micromorphology[6]. Face (010) has been reported as being the preferred cleavage plane of paracetamol, as the attachment energy is the lowest at this face[26].

The morphology of paracetamol forms I and II has been established using the Bravais, Friedel, Donnay and Harker (BFDH) algorithm on the Mercury program version 2.3 and the attachment energy model. The morphology of form I predicted in this way was in agreement with the experimental results but in poor agreement with that of form II.[28] The morphology of paracetamol has also been predicted using the Dreiding II and Momany force field programs,[6] while the paracetamol crystal habit has been calculated using the HABIT95 program,[6] which considers both the structure of the material and the nature of the intermolecular force fields in the crystal. It may be as a result of the technique of melting and abrupt cooling in liquid nitrogen that the form II crystal solution did not achieve a dynamic equilibrium during the crystallisation process. In contrast, the BFDH modelling assumed that the crystal solution had achieved dynamic equilibrium.[6] It was shown that form II was not converted to form I by grinding, nor by compression.[28, 33] X-ray topography experimentally indicates their presence at certain faces of the crystal[6]. Paracetamol molecules are polar, with the charge distribution shown in **Figure 2-9**[40].

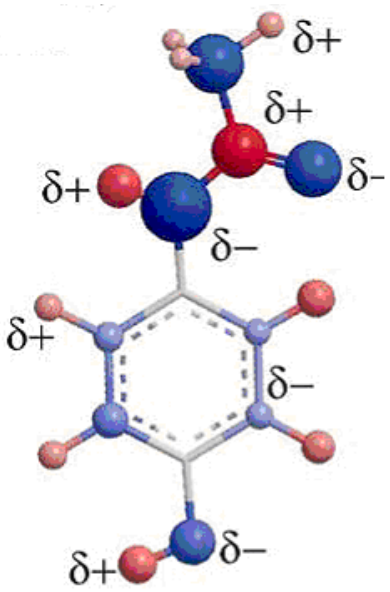

Figure 2-9: The distribution of partial charge of Paracetamol by MOPAC.

In the present study, the molecular structure of paracetamol was compared with that of acetanilide and found to differ only by the OH group in the para position. The paracetamol benzene ring is practically flat, with deviations of C atoms from the common plane not exceeding 0.007 Å. The flat benzene ring forms dihedral angles with the acetamido and hydroxyl groups at 20.5° and 17.2° respecively[20]. The large electronegative value of O and H, the hydroxyl (O-H) group at para position was expected to form a covalent bond[41]. The amide (N-C=O) group in paracetamol is very sensitive to the hydrogen bond environment[19]. The trans position between hydroxyl and amide groups is the most thermodynamically stable[42]. Single crystal paracetamol molecules were found to be rigid at a variety of temperatures. Atoms and molecules in crystals are not immobile but move with changes of temperature or pressure. Therefore, atomic displacement parameters (ADPs) are usually taken as a measure of the thermal motion of atoms[9]. The rigidity of the methyl group in the crystal structure affects the crystal facet concentrations and the methyl group gives static disorder to the crystal molecules. However, the shorter C-H methyl group bond showed liberation due to the high thermal vibration detected by neutron diffraction analysis[43, 44].

2.3. Excipients

An excipient is an inert compound in a formulation with an API. Most drugs are not easy to administer or easily absorbed by the human body[45] because of their physicochemical properties, so have to be dissolved or mixed with inert components that overcome these barriers to use, which is the function of excipients. Nonionic polymers are widely used in the formulation of pharmaceuticals because of their compatibility, high stability,low toxicity and good suspending and steric stabilising effects, especially on suspension solutions[46, 47]. Non-ionic molecules comprise both polar and non-polar segments, possessing a wide range of interfacial activity and versatile functions as wetting agents, emulsifiers, solubilisers, ocular permeability enhancers and in some cases as inhibitors[46].

For example, many pharmaceutical compounds have few slip planes[48]. At the slip plane lines, the crystal arrangement has mobility during the process of drug compaction or tableting. Drugs with fewer slip planes have less mobility and therefore difficulties may affect the compaction process. During compaction, the drug particles will be rearranged, allowing elastic deformation and volume reduction, while at the yield point, plastic deformation of the drug will occur. Plasticity of drugs will lead to the formation of interparticular bonds and enhance the coherent strength of tablets. However, some drugs

are very elastic and resist plastic deformation. Such elasticity has to be avoided, because it will lead to lamination of the drug and mechanical instability of the tablets. Excipients are needed to enhance the plasticity of drugs[6, 18, 48-50] and to maintain their reactivity and stability. However, the proportion of excipients in any formulation must be minimal for safety reasons[49]. The traditional techniques used in the characterisation of drugs and excipients are DSC, ATR-IR, XRD and Raman spectroscopy, which determine the functionality, crystalline structure and thermal behaviour of mixtures[51, 52].

2.3.1. Interactions between paracetamol and excipients

The molecular mechanisms of drug-excipient interactions can be studied by calculating the miscibility of drugs and selected excipients, in order to enhance the bioavailability and solubility of the blend. Miscibility may be facilitated scientifically, based on the selection of polymeric partners for given pharmaceutical substances[53]. The degree and type of interaction will contribute to the overall free energy of mixing. Two methods were considered in the calculation of drug-polymer miscibility: measuring solubility and the depression of the melting point respectively.

Solubility is a parameter used to describe the cohesive forces within materials; it has been used to describe the physical properties of a material and to predict interactions between materials[54]. The units of solubility are $(J/m^3)^{1/2}$, $MPa^{1/2}$ [55] or $(cal/cm^3)^{1/2}$, where 1 $(cal/cm^3)^{1/2}$ is equivalent to 2.0421 $MPa^{1/2}$. Knowing the solubility values for different excipients allows the prediction of the magnitude of interactions between the components of formulations as well as the stability of a product. Solubility can be evaluated and predicted by four methods[54]: measuring the solubility of test materials in solvents of known solubility parameters; measuring refractive index values using inverse gas chromatography; using heat of evaporation data (not suitable for polymers); and the group contribution method (GCM).

Measuring differences in solubility parameters between drugs and excipients has been advocated as a method to predict miscibility in pharmaceutical systems. Compounds with similar solubility are likely to be miscible. The solubility difference between two compounds is designated $\Delta\delta$; pairings with $\Delta\delta < 7.0$ $Mpa^{1/2}$ are likely to be miscible, while those where $\Delta\delta > 10.0$ will be immiscible[56,54, 57].

2.3.2. Solubility parameter calculations

The energy required to separate the constituent atoms and molecules of a material to an infinite distance is known as its cohesive energy and can be considered a direct measurement of the attraction that the atoms or molecules have for one another. It is the net effect of all the interatomic or molecular interactions, including van der Waals interactions, covalent bonds, hydrogen bonds, electrostatic interactions, induced dipole and permanent dipole interactions[58].

The cohesive energy is commonly quantified by solubility parameters, whose values for different pharmaceutical compounds allow the prediction of the magnitude of interactions between the components of a formulation as well as the stability of a product. The solubility parameter was first developed by Hildebrand and co-workers[58, 59]. The Hildebrand solubility parameter, δ, is restricted to non-polar systems and is related to the cohesive energy density (CED), which in turn relates the free energy of vaporisation, ΔE, with molar volume, V_m, by the following equation[58-61]:

$$\delta = (CED)^{1/2} = \left[\frac{\Delta \mathrm{H\ RT}}{V_m}\right]^{1/2} = \left[\frac{\Delta E}{V_m}\right]^{1/2}$$

Equation 2-1

Where ΔH is the enthalpy of vaporization, R is the gas constant and T is the absolute temperature. The Hildebrand parameter was extended by Hansen to polar and hydrogen bonding systems. The Hansen parameter assumes that cohesive energy can be considered to be the sum of contributions from dispersive interaction (E_d), polar interactions (E_p) and hydrogen bonding interaction (E_h) by the following relation[58]:

$$-E_{coh} = -E_d - E_p - E_h$$

Equation 2-2

From the above equation Hansen derived the total solubility, δ_T, as given by the following equation[55]:

$$\delta_T = \delta_d^2 + \delta_p^2 + \delta_h^2$$

Equation 2-3

Where δ_d is the partial solubility of the intermolecular dispersive force, δ_p is the partial solubility of the intermolecular polar force and δ_h is the partial solubility of the intermolecular hydrogen bond force[59].

δ_{drug} has been calculated by the group contribution method (GCM), which is used widely in the pharmaceutical industry[62]. The GCM approach, which is a development of the theories of Hildebrand and Hansen, is based on the assumption that the total intermolecular interactions among the molecules of a liquid are given by the linear sum of the contributions of the various chemical moieties within the molecules. The Hildebrand and Hansen solubility parameters are related by the following equation[61, 62]:

$$\delta^2 = \delta_d^2 + \delta_p^2 + \delta_h^2 \qquad \textbf{Equation 2-4}$$

Where subscripts *d*, *p* and *h* refer to dispersion forces, polar forces and hydrogen bonding respectively.

$$\delta_\delta = \frac{\sum F_{di}}{V} \qquad \textbf{Equation 2-5}$$

$$\delta_P = \frac{\left(\sum F_{PI}^2\right)^{1/2}}{V} \qquad \textbf{Equation 2-6}$$

$$\delta_h = \frac{\left(\sum E_{hi}\right)^{1/2}}{(V)^{1/2}} \qquad \textbf{Equation 2-7}$$

F_{di}, F_{pi} and E_{hi} refer to the contributions of various chemical moieties and the value obtained from the Hoftyzer-Van Krevelen method, while the value of F can be obtained by the Fedors method[62]. **Table 2-1** shows the Paracetamol GCM value of all the F_{pi}, F_{hb} and V_m as referred from the Hoftyzer-Van Krevelen table. From **Table 2-1** the solubility parameters of paracetamol were estimated. **Table 2-2** shows the solubility parameters estimated for all the chosen compounds [54].

$$\delta_\delta = \frac{\sum F_{di}}{V} \qquad \delta_P = \frac{\left(\sum F_{pi}^2\right)^{1/2}}{V} \qquad \delta_h = \frac{\left(\sum E_{hi}\right)^{1/2}}{(V)^{1/2}}$$

$$\delta_d^{Paracetamol} = 21.93\,\mathrm{J}^{1/2}/\mathrm{cm}^{3/2} \quad \delta_{pi}^{Paracetamol} = 6.71\,\mathrm{J}^{1/2}/\mathrm{cm}^{3/2} \quad \delta_{hb}^{Paracetamol} = 16.02\,\mathrm{J}^{1/2}/\mathrm{cm}^{3/2}$$

Table 2-1: Estimated values of F_{pi}, F_{hb} and V_m for paracetamol functional groups

Group	F_{pi}	F_{hb}	V_m
CH_3	0	0	33.5
NH	$(210)^2 = 44100$	3100	4.5
C=	0	0	-5.5
O	$(400)^2 = 160000$	3000	3.8
OH (at adjacent C atom)	$(500)^2 = 250000$	20000	13.0
Phenylene	$(110)^2 = 12100$	0	52.4
Σ	466200	26100	101.7

Table 2-2: Calculated solubility for Paracetamol, Ibuprofen, Aspirin and potential excipients

Compounds	δ_d	δ_p	δ_{hb}	δ_T
Paracetamol	21.93	6.71	16.02	27.97
Poloxamer 188	17.71	13.42	9.56	24.19
Poloxamer 338	17.70	13.39	9.49	24.14
Poloxamer 407	17.58	12.95	9.35	23.75
PVP	17.96	10.30	5.88	21.52
Ibuprofen	17.85	2.22	7.15	19.36
Aspirin	21.70	10.53	11.02	26.52

2.3.3. Interaction Parameter and Strength of Interaction

In a binary system involving two materials, A and B, there are two types of interaction:

i) Inter (A-A) or (B-B), known as cohesive interactions

ii) Intra (A-B), known as adhesive interactions.

Based on the Leonard-Jones pair potential function, Rowe relates the strength of interaction (σ in MPa) to the solubility parameters (δ) of two surfaces[63]:

$^{BB}\sigma = 0.25\ ^{B}\delta^2 \qquad ^{AA}\sigma = 0.25\ ^{A}\delta^2 \qquad ^{AB}\sigma = 0.25\ \phi^{A}\delta^{B}\delta$ **Equation 2-8**

Where ϕ^{AB}, the interaction parameter, is defined by the harmonic mean equation proposed by Wu[63]:

$$\phi^{AB} = 2.\left[\frac{{}^{A}x_d.{}^{B}x_d}{{}^{A}x_d.g_1+{}^{B}x_d.g_2}+\frac{{}^{A}x_p.{}^{B}x_p}{{}^{A}x_p.g_1+{}^{B}x_p g_2}\right] \qquad \textbf{Equation 2-9}$$

Quantities x_d and x_p are the fractional non-polarity and polarity respectively ($x_d + x_p = 1$) for each material, defined by the expressions

$$x_d = \left(\frac{\delta_d}{\delta}\right)^2 = \frac{\gamma_d}{\gamma} \quad \text{and} \quad x_p = 1 - \left(\frac{\delta_d}{\delta}\right)^2 = \frac{\gamma_p}{\gamma} \qquad \textbf{Equation 2-10}$$

Where δ_d is the dispersion or non-polar component of the Hansen three-dimensional solubility parameters. The parameters g_1 and g_2 can also be defined in terms of the solubility of the materials:

$$g_1 = \frac{A_\gamma}{B_\gamma} = \frac{{}^{A}\delta^2.{}^{A}\delta^{1/3}}{K} = \frac{K}{{}^{B}\delta^2.{}^{B}V^{1/3}} = \frac{{}^{A}\delta^2.{}^{A}V^{1/3}}{{}^{B}\delta^2.{}^{B}V^{1/3}} \qquad \textbf{Equation 2-11}$$

$$\mathbf{g_2} = \frac{1}{g_1} = \frac{{}^{B}\delta^2.{}^{B}V^{1/3}}{{}^{A}\delta^2.{}^{A}V^{1/3}} \qquad \textbf{Equation 2-12}$$

Where K is the constant and V is the molar volume of the material, i.e. its molecular weight divided by its density, assuming that the materials are supercooled liquids or amorphous polymers. **Table 2-3** reveals the calculated value of selected API (paracetamol, ibuprofen and aspirin) with 4 chosen excipients. All the values were calculated as formula above explained.

Table 2-3: Interaction parameters and strength calculated of interactions of Paracetamol, Ibuprofen and Aspirin and potential excipients

	Paracetamol-P188	**Paracetamol-P338**	**Paracetamol-P427**	**Paracetamol-PVP**
Interaction parameter (ϕ)	0.58	0.49	0.53	**0.91**
Strength of interactions (σ)	98.82	83.34	87.30	**137.40**
	Ibuprofen-P188	**Ibuprofen-P338**	**Ibuprofen-P427**	**Ibuprofen-PVP**
Interaction parameter (ϕ)	0.36	0.31	0.33	**0.95**
Strength of interactions (σ)	42.15	36.09	37.99	**98.95**
	Aspirin-P188	**Aspirin-P338**	**Aspirin-P427**	**Aspirin-PVP**
Interaction parameter (ϕ)	0.57	0.48	0.52	**0.93**
Strength of interactions (σ)	**91.65**	**77.42**	**81.10**	**132.69**

Table 2-3 shows that paracetamol, ibuprofen and aspirin have strongest interaction with PVP but least interaction with P338. PVP reveals the strongest interaction with paracetamol. The interaction of ibuprofen and all the excipients reveals the least. It also estimated that P188 shows the strongest interaction for the entire API with the strongest interaction with paracetamol. Therefore, from the above calculation the justification for the API and excipients chosen for the study was made.

2.3.4. Poloxamer

Poloxamers are nonionictriblock copolymers, commercially known as Pluronic (BASF), Poloxamer (ICI)[64] or Synperonic. They were developed and first marketed by the BASF Corporation and differ from other polymeric surfactants in having both a hydrophobic and a hydrophilic end. The chemical structure of the polymer is shown in **Figure 2-11** [65]. The hydrophobic polymer, polypropylene oxide is flanked by polyethylene oxide, which has the hydrophilic character that makes poloxamers non-ionic surfactants[66]. The EO and PO segments are joined by ether bonds[67]. The range of block numbers can be tailored

with the molecular weight[64]. The hydrophilic part maintains the polymer's solubility in water, while the hydrophobic part provides associative behaviour in water.

By popular convention, poloxamer P188, for example, indicates the prill form of the compound (designated by the initial P), while 18 (the first two digits) multiplied by 100 gives the molecular mass of the PO and 8 (the last digit) multiplied by 10 denotes the percentage of EO. A prill is a dry sphere of solid formed by cooling the molten form. It is a solid at room temperature and a low viscosity liquid when melted. All forms of poloxamer can been differentiated by the ratio of EO to PO, marked as *n* and *m* in **Figure 2-10**. This ratio will affect the physical surface-active properties. It also corresponds to physicochemical characteristics such as the melting point, cloud point and hydrophilic-lipophilic balance. The phase (liquid, flake or prill) is indicated by L, F or P in the names of the different forms shown in the Pluronic grid (**Figure 2-10**), which is based on a mapping of the percentage of hydrophile as a function of the hydrophobe molecular weight.

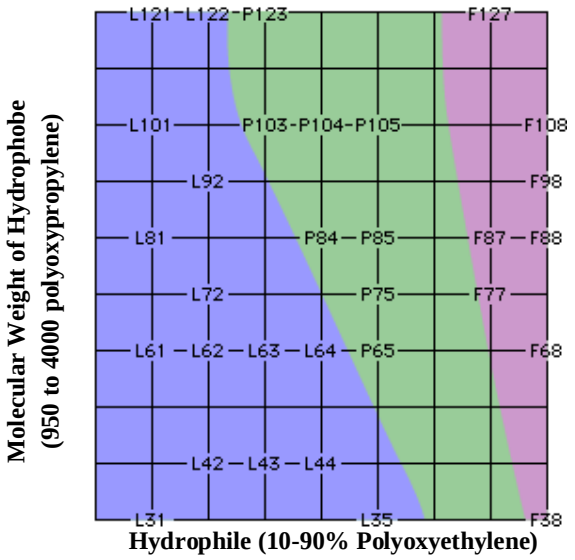

Figure 2-10: Pluronic Grid presented the percent of Polyoxyethylene and Polyoxypropylene and physical forms exist for Poloxamers. (L = liquid, P = prill, F = flake).

In the Pluronic grid **(Figure 2-10)**, the nomenclature is given by multiplying the PO axis by 300 and giving the molecular mass of PO. Multiplying the last number by 10 gives the percentage of EO. For instance, F68 is the flake form of the poloxamer containing PO of molecular weight 1800 and 80% EO. **Table 2-4** gives examples of poloxamer *m* and *n* values with the molecular weights and phases as appropriate.

According to the hydrophile-lipophile balance (HLB) system designed for categorizing non-ionic surfactants, the higher the portion of *n* (the hydrophilic part) in the Poloxamer structural formula, the higher the HLB value of the poloxamer and the more soluble it is in aqueous solution[46].

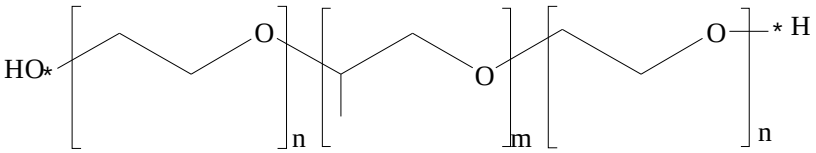

Figure 2-11: Chemical structure of Poloxamer

Table 2-4: Examples of some poloxamers properties indicated by their names

Poloxamer Name	Physical form	m	n	Molecular weight
L124	Liquid	12	20	**2090-2360**
P338	Solid	141	44	**12700-17400**
P188	Solid	80	27	**7680-9510**
P407	Solid	101	56	**9840-14600**
P237	Solid	64	37	**6840-8830**

Higher values of EO segments, (*n* segment as in **Figure 2-11**), indicate that poloxamer compounds can be dissolved in water at room temperature. As the temperature increases, water becomes a progressively poorer solvent for the PO segment, (*m* segment in **Figure 2-11**), leading to micelle formation and the creation of a gel phase. The two identity characteristics of poloxamers are known to be thermoreversible, which means that at low temperatures a solution is formed, while at higher temperatures a gel phase occurs. Rheological and diffusion studies indicate that the two phases occur because at low temperature and concentrations below 12.5%, the micelles are well separated and the poloxamer system displays Newtonian behaviour. However, at concentrations higher than 12.5% and high temperatures, the micelle volume fraction approaches close packing[68].

Studies of physical mixtures of paracetamol and poloxamer P188 are not common. However, the interaction through hydrogen bonds of ibuprofen and poloxamer

has been proposed by several studies[69]. Poloxamer conformation has been known with the PO block acting as anchor, while the EO block acts as a 'brush' at the surface of the mixture particles[70]. Poloxamers have demonstrated effective steric stabilisation, thought to arise from anchoring of the hydrophobic PO chain to the particle surface and subsequent stabilisation by the protruding EO chains. The capacity of charge reduction by poloxamers has also been shown to be greater than for other polymers[71].

Poloxamers are widely used as wetting and solubilising agents and surface adsorption excipients[72]. Their amphiphilic structure makes them useful in pharmaceutical applications, where they can be used to increase the water solubility of hydrophobic, oily substances as well as modelling systems in drug delivery applications. Their tendency to aggregate into micelles also makes poloxamers appealing candidates for the encapsulation and delivery of hydrophobic drugs[67]. In biomedical applications, poloxamers are applied as modifiers in drug delivery, in situ generated implants, gene expression, modelling membranes, including solubilisation of the membrane, alteration of membrane rigidity and soft tissue injury treatment[73]. Additionally, poloxamers are popular because of their incorporation in creams and aqueous suspensions as dispersion stabilisers and flocculants. They are also used as surface modifiers in organic distribution of colloidal particles. Poloxamers are also popular as surface active agents in ophthalmic delivery systems because they are less toxic, less homolytic and less irritating to the ocular surface and because they tend to maintain near physiological pH values when in solution[46]. Poloxamer188 was used as an emulsifier in Lipomul® IV, a product that was given to patients unable to ingest food taken orally, and to emulsify a volatile anaesthetic, methoxyflurane. Poloxamer188 was found to be effective in dogs in preventing the formation of fat emboli in prolonged cardiopulmonary bypass[65].

Several techniques have been employed to study poloxamers, including viscometry, light scattering, nuclear magnetic resonance (NMR), phase diagram determination, gelation mechanism, UV-VIS absorption, surface tension, electron spin resonance (ESR), small angle neutron scattering, fluorescence, Raman spectroscopy and ATR spectroscopy[64]. The adsorption of poloxamers on a hydrophobic surface was examined by AFM, and in situ experiments by surface plasmon resonance (SPR) spectroscopy revealed the brush conformation of poloxamer adsorbed on a gold surface[66]. The study also showed that the amount of poloxamer adsorbed reached a maximum near the critical micelle concentration and that the process was only partially reversible.

2.4. X-ray Photoelectron Spectroscopy (XPS)

X-rays are a form of electromagnetic radiation whose wavelength is from 10 to 0.01 nm, with energies from 120 eV to 120 keV. They may be soft or hard. Soft X-rays are those with wavelengths ranging from 0.12 to 3 keV, while those of hard X-rays range from 3 to 120 keV, the latter having greater penetrative ability.

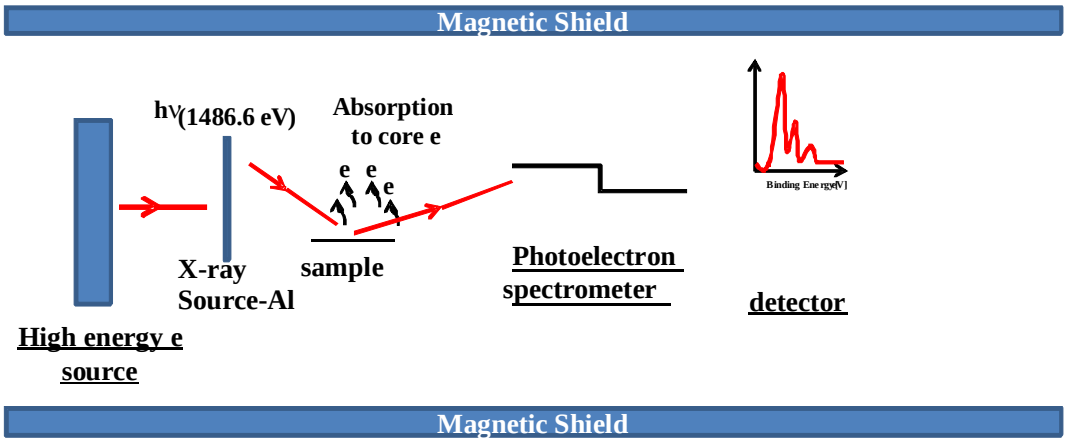

Figure 2-12: Schematic diagram of X-ray photoelectron spectrometer.

XPS works by irradiating a sample with a quantity of photons given by Equation 8 below, to produce large numbers of photoelectrons, then comparing the kinetic energy with the initial energy of the photons. **Figure 2-12** is the schematic diagram of an experimental XPS unit[74]. The absorption of high energy photons causes the ejection of electrons from tightly bound core levels or from more weakly bound valence levels. Each element produces a characteristic set of XPS peaks at characteristic binding energies. These E_B values directly identify each element present in or on the surface of the material being analysed. These characteristic peaks correspond to the electrons within the atoms. The number of electrons detected in each of the characteristic peaks is directly related to the amount of the element within the area (volume) irradiated.

The magnitude of electron attraction towards the nucleus is the atom binding energy and the quantity of energy that the particle loses in transit from the sample to the analyser is known as the work function. The kinetic energy difference is stated as **Equation 2-13**. The work function is consistent for each sample in a specific XPS analyser. However, in XPS survey analysis, every atom has its own range of binding energies used for element recognition. A subset of elemental analysis is high resolution

analysis. The different types of chemical bond will affect the appropriate E_B, creating a 'chemical shift' which affects high resolution analysis. For instance, the C 1s E_B for the methyl environment is at 284.7 to 285 eV, while N-C=O has a higher E_B of 288 to 289 eV. The energy of the photon is

$$E = h\nu \qquad \textbf{Equation 2-13}$$

where h is the Planck constant (6.62×10^{-34} J/s) and ν is the frequency. The kinetic energy, E_K, of the excited electron is related to the atom binding energy, E_B, by the following equation:

$$E_k = h\nu - E_B \qquad \textbf{Equation 2-14}$$

The photon energy, *hν*, probes the sample with energy E_i. The photon emissions to the sample surface will ionise the sample to E_f. Therefore, the energy equation can be written as:

$$E_i + h\nu = E_f + E_k \qquad \textbf{Equation 2-15}$$

2.4.1. Instrumentation

The basic layout of an XPS machine is as presented in **Figure 2-12**. Throughout the studies, the X-ray source is an X-ray tube. Commonly, the anode is made from aluminium (Al) or magnesium, at 1486.7 eV and 1253 eV respectively. In this study, Al was preferred, because monochromatic AlK_α X-radiation could be used to improve spectral resolution[74]. A high sensitivity instrument such as an XPS must be operated under ultrahigh vacuum, i.e. at a pressure of 10^{-6} to 10^{-9} Pa, in order to reduce the amount of noise in the spectrum and to avoid any surface contamination by residual gas which would alter the surface composition. In addition, to count the number of electrons at each value of kinetic energy with the minimum of error, XPS must be performed under UHV conditions, as this will help to prevent accumulation of gaseous contaminants onto the sample surface and reduce photoelectron-gas collisions, which are typically understood in terms of the inelastic free mean path (IMFP) concept. UHV is defined as $< 10^{-8}$ mbar. The minimum pressure needed for the photons to reach the sample surface and reduce collisions with gas molecules is 10^{-5} mbar. The relation of kinetic theory of gases and the

rate, r, of gaseous molecules arriving at the surface (assuming they stick and are incorporated) is:

$r = 3.51 \times 10^{22} P / (TM)^{½}$ **Equation 2-16**

Where P is the pressure in torr, T is the temperature in K and M is the molecular weight of the gas, where 1 Torr = 1.33 mbar. For example, for N_2, where M is 28, P is 1 Torr and T is 298 K, the rate will be 3.88×10^{20} molecules cm^{-1} s^{-1}. Assuming a monolayer ~ $2x10^{15}$ atom cm^{-2} (a typical number of atoms at the surface is $1x10^{15}$ cm^{-2}), the time needed for N_2 coverage is 2.6×10^{-6} s at 1 Torr, 2.6 s at 10^{-6}Torr and 44 minutes at 10^{-9}Torr. In order for relatively low contamination within the timescale of an experiment, the pressure should ideally be lower than 10^{-9} Torr. The UHV is obtained by means of several pumps, viz. diffusional, ion, mechanical, adsorption and turbomolecular pumps, each of which operates at a different pressure, as listed in **Table 2-5.**

Table 2-5: Vacuum stage and type of pump used to required pressure (Pa)

Vacuum Stage	Pressure (Pa)	Types of Pumps needed
Low vacuum	10^{2}	
Medium vacuum	10^{-1}	Diffusion Pump
High vacuum	10^{-4}	TurbomolecularPump
Ultra high vacuum	10^{-8}	Ion Pump
	10^{-11}	Titanium SublimationPump

Monochromators of various types are used in XPS for electron focusing. A magnetic monochromator allows double focusing. The first XPS instrument using the monochromatic principle was developed by Siegbahn's team[74]. Serial XPS spectrometers commonly use electrostatic monochromators, which are small and can increase the electron intensity. Their use is necessary to narrow the XPS peaks.

In order to resolve 1000 eV electrons to ± 0.5 eV, an analyser would be required with a slit plate width of 1 mm and radius of 1.2 metres. Therefore, it is convenient to retard the incoming electrons so that they have lower energy when passing through the analyser. A lens system is needed to focus the electron energy of the sample to increase the throughput. Focused electrons are then passed through the main part of the XPS equipment, the hemispherical analyser. Generally, there are two modes of hemispherical analyser, one known as fixed analyser transmission (FAT) or constant analyser energy

(CAE) and the other as fixed retard ratio (FRR) or constant retard ratio (CRR). In CAE mode the pass energy of the analyser is held at a constant value and it is entirely the job of the transfer lens system to retard the given kinetic energy channel to the range accepted by the analyser. The CAE mode is commonly used in XPS instruments. The higher the pass energy applied, the lower the peak resolution.

The parameters at which the XPS analysis is set will affect the spectrum produced. The full width half minimum (FWHM) of the spectrum is affected by the analyser diameter, pass energy and the spread of energies in the X-ray source. The consideration of localised charging may broaden the XPS lines. Therefore, the charge neutralisation setting is vital in XPS experiments.

2.4.2. Quantification of Surface Atomic Composition

Background Subtraction

Inelastic collisions of the electrons emitted on the sample surface may alter the number of electrons recorded by the detector. The energy loss processes will result in some modification to the spectrum background. There are three types of XPS background subtraction: linear, Shirley and Tougaard. The Tougaard background is the most complicated because it removes all the inelastic processes, while linear background is the simplest. Shirley background subtraction assumes that each unscattered electron is associated with a flat background of losses; the background intensity at a point is proportional to the intensity of the total peak area (above background at any point)[75]. Due to the shape of the most of the spectra of paracetamol and of paracetamol and excipient mixtures, the Shirley background was chosen to be used in all the XPS analyses.

Relative Sensitivity Factor

In XPS the detected photoelectron current is linearly related to the detected atom density. Mathematically, the idealisation of the sample intensity is difficult; the XPS data are quoted in terms of atom fractions. Therefore, the relative sensitivity factor (RSF) is used, where one elemental peak is taken as the standard to which other peaks are referred. In polymer analysis the standard is commonly C1s.

Sample charging

Electrons at the sample surface will be lost during photon bombardment. On a metal surface, the loss of electrons is compensated by the grounding abilities of the metal itself: new electrons move to the surface continuously to compensate the electron loss at the surface region. However, for organic or insulating samples, the rate of photo-electron loss is greater than the electron replacement from within the specimen, which leads to the creation of a positive surface potential. Electrons from the bulk of the sample cannot compensate for this loss and this reduces the field at the surface. As a result, the peaks will shift due to the reduced kinetic energy of the ejected electrons (**Figure 2-13**). Therefore, some adjustment has to be made during the experiment and to the XPS spectrum. A 'flood gun' of low energy electrons (0-5 eV) can be utilised to supply more electrons to the sample surface. Furthermore, the correction of lines with reference to adventitious C is needed before any fitting of the organic spectrum.

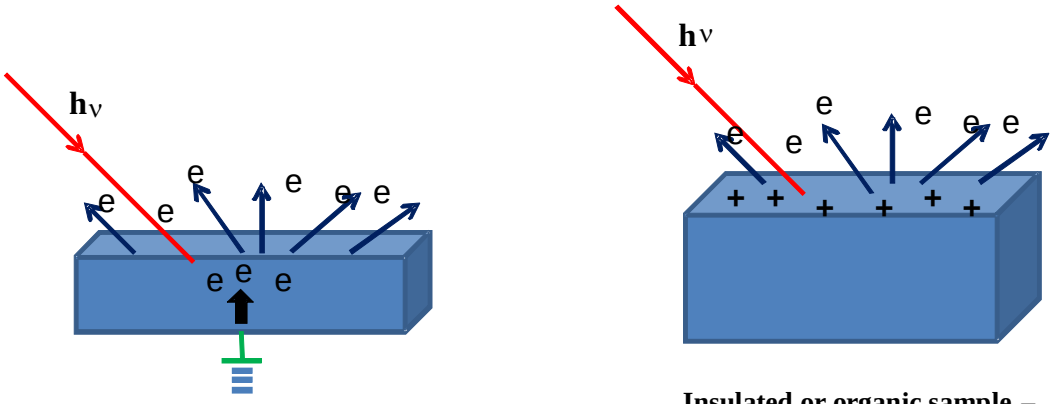

Figure 2-13: Schematic illustration of electrons at a conducting and an insulating surface during photoemission

XPS Spectra

There are two types of XPS spectra, viz. survey spectra and high resolution XPS spectra, which are distinguished by the pass energy utilised during the analysis. Survey spectra are generated by scanning over the whole available energy range, which requires higher pass energy to increase analysis sensitivity, while high resolution analysis is obtained from lower pass energy during XPS analysis. The spectra are detailed enough to allow

peaks to be deconvoluted as differences in the chemical environment of an atom and observed as shifts in E_B.

Binding Energy

Using XPS, chemical shift is detected from the value of E_B. The exact value of the binding energy of the core electrons of a given element depends on their atomic surroundings. The energy of an electron in a tightly bound core state is determined by the attractive potential of the nuclei and the Coulomb interaction of the repulsive core with all the other electrons. A change in the chemical environment of a particular atom involves a spatial rearrangement of the valence charges of this particular atom and a different potential created by the nuclear and electronic charges on all the atoms in the compound. This mechanism, called chemical shift, involves charge transfer to or from the core ionised atom. The second factor involves the electric field caused by the effective charges of the surrounding atoms[76].

The transfer of charge to an atom and neighbouring electronegativity will lead to shifts in the core level E_B of an atom, which can be used to distinguish between different functional groups and oxidation states. Reducing the electron density of the system and the formation of a cation environment leads to the shifting of E_B to a higher value, whereas the addition of electrons and anion formation in the system will lower the E_B. In other words, the value of E_B rises in proportion to the positive state of element oxidation in the compound, while in a negative oxidation state, the shift is towards smaller E_B values (negative shift)[74]. This is based on the increasingly electronegative pull of neighbouring electron density away from the element of interest. As a result, the element holds onto its remaining electrons more tightly, making it harder to remove an electron and thus increasing the E_B. Chemical shift can also be perceived by the changes in nuclear shielding, including core hole relaxation, where the electrons move closer to the hole in order to shield it from the positive nucleus.

Shake Up

When a core electron is photoejected, the Coulombic potential of the outer shell electrons is suddenly altered. The immediate change may induce the shake-up transition of a valence electron to a higher, previously unoccupied orbital. Shake-up peaks always appear at high E_B values[77]. The existence of shake up makes the kinetic energy decrease, distinguishing this from other molecules in which shake up do not occur. A weak shake-

up line is typical of aromatic carbon and conjugated systems. The relative area of the different components of XPS lines reflects the relative concentration of the corresponding atoms[78, 79].

$$E_{B\ shake\ up} = E_B + \Delta E \qquad \textbf{Equation 2-17}$$

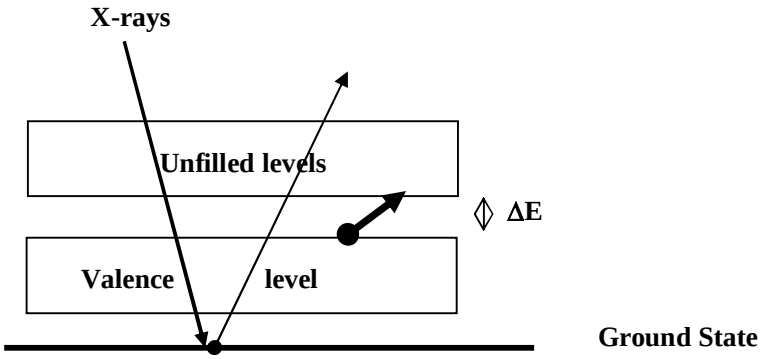

Figure 2-14: Schematic illustration of the effect of shake up electron excitation on an XPS spectrum

Figure 2-14 shows the shakeup phenomenon and the relationship is translated as **Equation 2-17.**

Valance band

The variation in the number of valence bands (VB) in samples is attributed to changes in the conformational structure of the molecules[80]. It provides information about the electrons contributing to the chemical bonding, as they are involved in delocalised or bonding orbitals. VB spectra with specific patterns indicate different chemical states.

Inelastic Mean Free Path

IMFP and attenuation lengths are two important parameters in XPS and quantitative surface analysis[81]. IMFP can be obtained from theory and certain types of experiment, whereas attenuated length (AL) is obtained from overlayer film experiments and by the use of a model which ignores electron scattering effects[82]. The IMFP begins when X-rays penetrate the sample surface to a depth of twice the mean free path and produce electron emissions **(Figure 2-15).** The electrons emitted with a certain kinetic energy, E_K, will travel an appropriate distance before reaching the sample surface. In XPS, the kinetic energy of such electrons is interpreted as indicating the chemical state of the atom. The

average distance covered by an electron between two inelastic shocks is called the mean free path, λ. The inelastic shock distance will vary from larger to smaller values. Any electron which undergoes a shock will experience random energy changes, meaning the loss of energy, so that the detected energy, E, will be lower than the initially emitted energy, E_o. Those electrons having reached the surface without any inelastic interaction will contribute to the background spectrum peak, while those which leave the material without inelastic shock or energy loss will form an XPS peak **(Figure 2-15).**

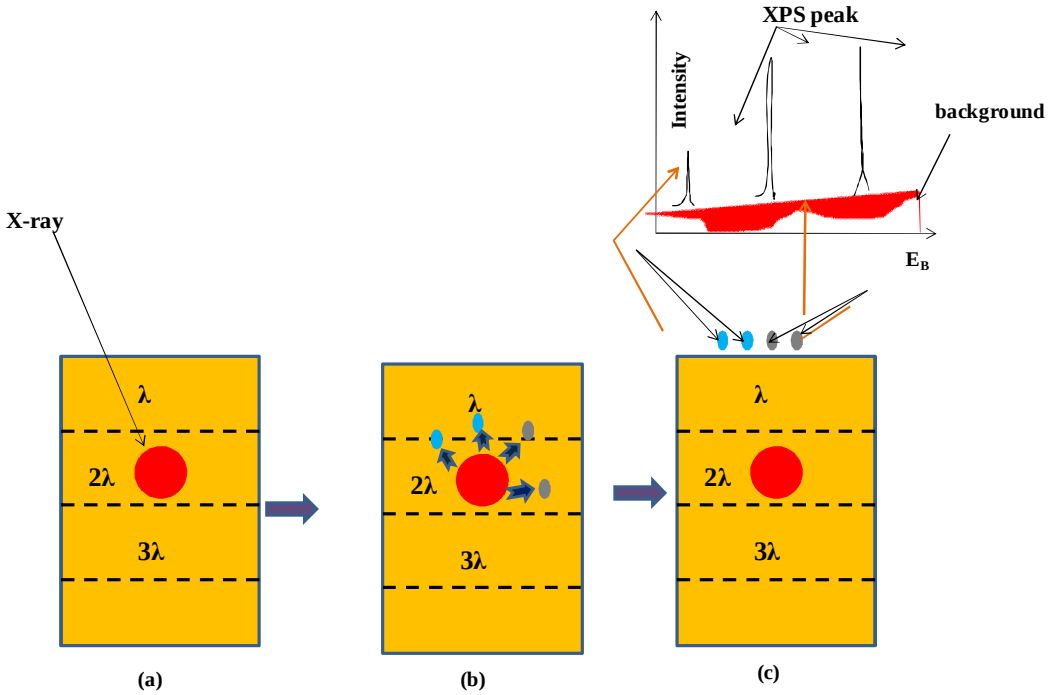

Figure 2-15: IMFP mechanism in XPS. (a) X-ray photoelectron emission of the atom at depth 2λ. (b) X-ray causes emission of 4 electrons: 2 (blue) will reach the surface without losing energy, while 2 (grey) undergo inelastic collision with other particles and lose energy. (c) The blue electrons form the XPS peak and the grey electrons the background peak in the XPS spectrum.

The IMFP depends upon two main factors, which are the kinetic energy, E_K, of the electron and the nature of the solid. Most organic solids have very similar IMFP energy relationships. Therefore, the nature of the solid is needed to recognise the behaviour of the chosen organic solid. The IMFP value is important in the calculation of layer thickness. **Figure 2-16** illustrates layers of two compounds: compound B is a substrate on which compound A is layered at thickness t. The XPS emission intensity without A is I_o, while the emission intensity with A has changed to I. Therefore, the thickness of layer A, t, can be calculated from the **Equation 2-18**.

$I = I_o (-t/\lambda)$ **Equation 2-18**

Where t = layer thickness, I = intensity with two layers, I_o=intensity without layer A, λ = IMFP.

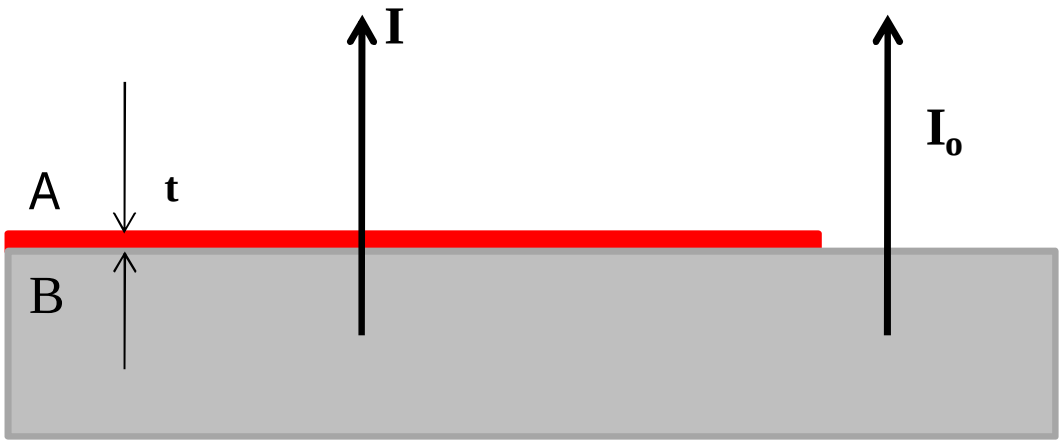

Figure 2-16: Illustration for the effect of XPS emission intensity on two compounds, A and B

Several researchers have made extensive attempts to calculate the IMFP,λ, value for organic and inorganic compounds[83, 84] by plotting the IMFP graph of kinetic energy (E_K) as a function of IMFP depth. Two methods can be used to calculate the IMFP: experimental determination and theoretical prediction. Recently, IMFP values have been provided by the National Institute of Science and Technology (NIST). There is a simple equation for IMFP estimation, as follows:[84]

$$\lambda_d = \frac{49}{E_K^2} + 0.11\sqrt{E_K} \quad \textbf{Equation 2-19}$$

This gives the IMFP, λ, value in mgm^{-2}, therefore to convert the value to nm the following equation is implemented:[84]

$\lambda_d = \lambda_n / \rho$ **Equation 2-20**

From **Equations 2-19 and 2-20**, the C 1s, O 1s and N 1s IMFP values can be estimated, as listed in **Table 2-6**.

Table 2-6: Elements, C, O and N approximation data of E_B, E_K and estimation value IMFP for Paracetamol.

Orbital	Binding Energy (E_B)	Kinetic Energy (E_K)	IMFP (nm)
C 1s	~ 280 eV	~ 1207 eV	**4.83**
N 1s	~ 400 eV	~ 1090 eV	**4.59**
O 1s	~ 530 eV	~ 960 eV	**4.30**

The formula for estimating the thickness of a surface layer using the ratio of intensities from the layer and substrate is as follows[85]:

$$\ln \left[\frac{I_{layer}}{I_{subst.}} + 1\right] = \frac{t}{\lambda \cdot \sin\theta} \qquad \textbf{Equation 2-21}$$

Where I_{layer} is the intensity of the peak arising from the surface layer, $I_{subst.}$ is the intensity of the peak arising from the substrate, t is the thickness of the surface layer, λ is the IMFP of electrons in the surface layer and θ is the angle at which the electrons exit the surface.

2.4.3. Method

The samples were analysed using a Kratos Axis Ultra [86] XPS instrument with a monochromated AlK_α source, a hemispherical analyzer with a hybrid (electrostatic and magnetic) lens system, charge neutralization by filament-generated, magnetically channelled low-energy electrons and a delay line detector (DLD). Throughout the study, two types of tapes used for samples mounting; double-sided adhesive carbon disks and double-sided tape. Only samples named Poloxamers and EtSingle used double sided tapes while others of XPS samples measurements used double-sided adhesive carbon disk (12 mm diameter double-sided carbon disks were cut into half for samples mounting). Samples were spread over double-sided tape for the XPS analysis, and care was taken to ensure that powdered samples particles completely covered the tape.

The analysis was conducted at a pressure below 10^{-8} mbar (UHV) with X-ray operating source power of 180 W (15 kV and 12mA). The instrument was operated in CAE mode. The CAE survey scans were conducted at an energy level of 80 eV and high resolution scans at 20 eV of photoemission from individual core levels. Surveys were measured in steps of 0.5 eV and 300 ms dwell time per data point.

C 1s high resolution spectra were measured at 0.1 eV steps and 300 ms dwell time per data point. O 1s dwell time was 400 ms per data point. Radiation-damaged samples were analysed by repeating the sample scans. The intensity/ energy response was calibrated with clean gold, silver and copper surfaces in accordance with the National Physical laboratory (NPL) procedure, an absolute reference obtained from the gold spectrum and compared with a clean gold surface to obtain the transmission function and appended to the data file[86]. Surveys were measured from 1100 to -5 eV with 0.5 eV steps and 300 ms dwell time. High resolution spectra were measured around the area of interest, with 0.1 eV steps and 300 ms dwell time per data point for C1s, 400 ms for O1s, and 500 ms for N1s spectra. Repeats were carried out to check for radiation damage. XPS data were analysed using the Casa XPS software.

A Shirley background was used in all curve fitting due to the. The binding energy scale was referenced to adventitious carbon hydrocarbon contamination at 285 eV, at which a separate peak was clearly visible. A lineshape GL(30) (70 % Gaussian, 30 % Lorentzian using the Gaussian/Lorentzian product form) was employed for C 1s spectra. For the O 1s spectra, an exponential tail GL (55) was used, as there appeared to be some asymmetry towards higher binding energy. Samples naturally containing C-C environments were referenced to adventitious hydrocarbon contamination at 285 eV. Samples without C-C environments were referenced to the lowest E_B photoemission; those paracetamol samples containing aromatic ring were referenced to C=C at 284.7 eV. Chemical environments/functional groups with position different ± 0.5 eV, two peaks were used to represent both environments for clarity and eased of discussion.

Figure 2-17: An example of an XPS instrument, a Kratos Axis Ultra at The University of Manchester, showing the X-ray source and monochromator (centre), electron analyser (top), loading chamber (left) and vacuum/pressure controls (right).

2.5. X-ray Diffraction

In 1913, English physicists WH and WL Bragg developed a theory to explain why the cleavage faces of crystals appear to reflect X-ray beams at a certain angle of incidence, known as theta (θ). In XRD, the basic variables are the distance, d, between atomic layers in a crystal bombarded by the incident X-ray beam of wavelength, λ, multiplied by an integer, n. XRD is a non-destructive technique utilised to define the geometry and structure of crystalline materials. The diffraction of incident X-rays is based on the elastic scattering of the electron clouds in an atom of the material. An electron in an alternating electromagnetic field will oscillate with the same frequency as the field. When an X-ray beam hits an atom, the electrons around the atom start to oscillate with the same frequency as the incoming beam. In almost all directions, the interference will be destructive, because the combining waves are out of phase, so there will be no resultant energy leaving the solid sample. However, the atoms in crystals are arranged in regular patterns and in a very few directions there will be constructive interference: the waves will be in phase and a well defined X-ray beam will leave the sample in these directions.

The X-ray diffraction principle starts with the incident beam at parallel atomic planes, separated by the interplanar distance, d. In **Figure 2-18** below, the incident X-ray

beams are coming from the left and reflecting from the planes. The beam will be diffracted by an angle θ from the plane.

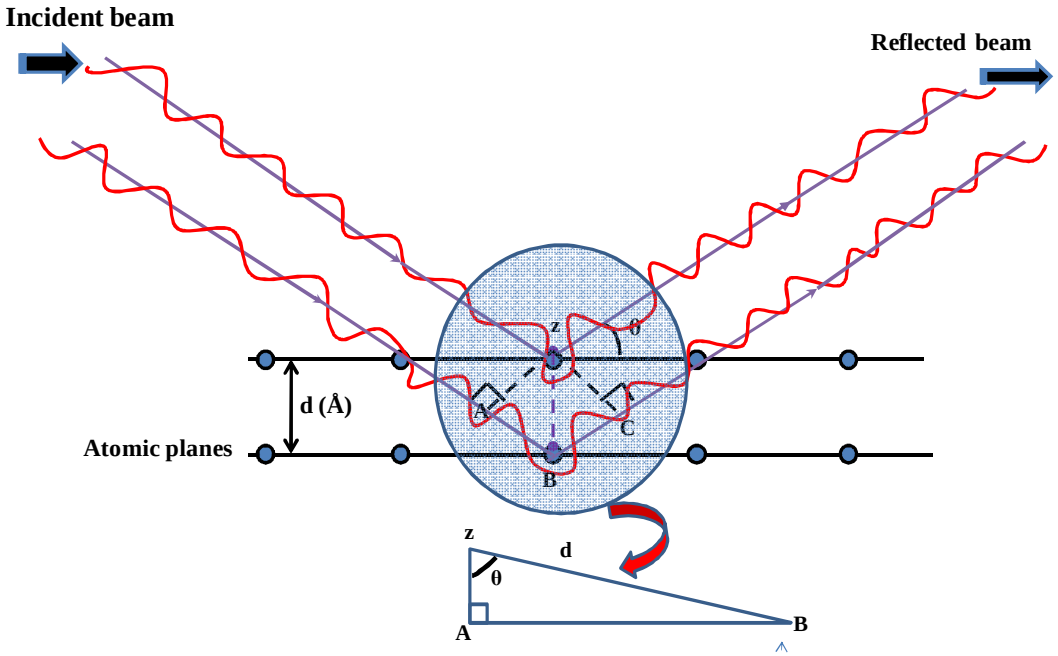

Figure 2-18: Schematic diagram of X-ray diffraction between planes in XRD

Figure 2-18 shows the relation of the reflected plane, the interplanar plane distance, d and θ in Bragg's Law[87]. Trigonometry is used to relate d and θ at the distance AB + BC. The distance AB is opposite θ thus[88]

$$AB = d\sin\theta \qquad \textbf{Equation 2-22}$$

$$n\lambda = 2AB \qquad \textbf{Equation 2-23}$$

Substituting **Equation 2-22** in **Equation 2-23** we obtain

$$n\lambda = 2d\sin\theta \qquad \textbf{Equation 2-24}$$

Where n is an integer, λ is wavelength, d is the interplanar spacing in Å, θ is the diffraction angle in degrees. For the general case for plane *hkl*, **Equation 2-24**, which is known as Bragg's Law, can be rewritten as **Equation 2-25**:

$$\lambda = 2d_{hkl}\sin\theta_{hkl} \qquad \textbf{Equation 2-25}$$

Instrumentation

An X-ray diffractometer consists of three main elements: an X-ray tube, a sample and an X-ray detector (**Figure 2-19**). First, the X-rays are generated by the bombardment of electrons from the tungsten filament of a cathode tube on a metal target acting as anode. Different metal targets will be characterised by specific wavelengths. Some common metal targets are Cu, Fe, Mo and Cr, with Cu being the most common target material for single crystal diffraction; in this case, the value of K_α is 1.5406 Å. At sufficient electron energy to dislodge inner shell electrons of the target material, characteristic X-ray spectra are produced. These have several components, the most common being K_α and K_β. The high intensity K_α consists in part of $K_{\alpha1}$ and $K_{\alpha2}$, where $K_{\alpha1}$ has a slightly shorter wavelength and twice the intensity of $K_{\alpha2}$. Because the wavelengths characteristic of $K_{\alpha1}$ and $K_{\alpha2}$ are close, the average of the two intensities is used in the XRD patterns. This X-ray generating mechanism occurs in a device known as a scintillating tube. The X-rays are then collimated and directed onto the sample by slits. As the sample and detector are rotated, the intensity of the reflected X-rays is recorded. When the geometry of the incident X-rays colliding with the sample satisfies the Bragg equation, constructive interference occurs and there is a peak in intensity. The detector records and processes this X-ray signal and converts it to a count rate, which is then output to a device such as a computer monitor.

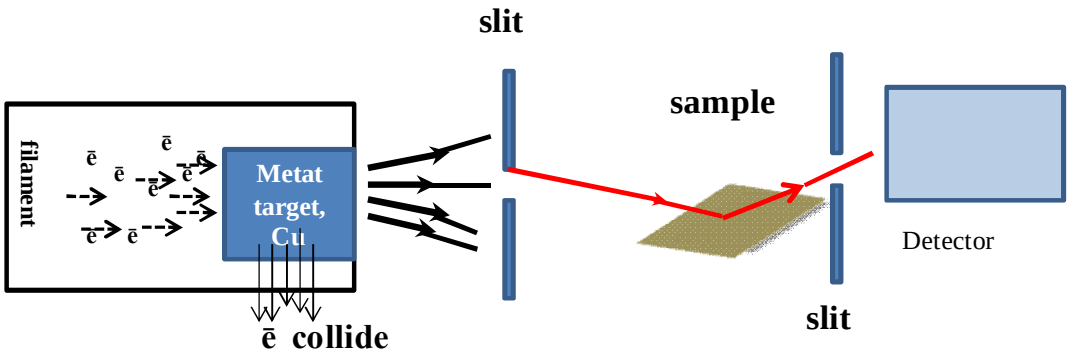

Figure 2-19: Schematic diagram of an X-ray diffractometer

2.6. Prediction of Crystal Morphology

Crystal morphologies were predicted using the Material Studio Simulation package from Accelrys[89].

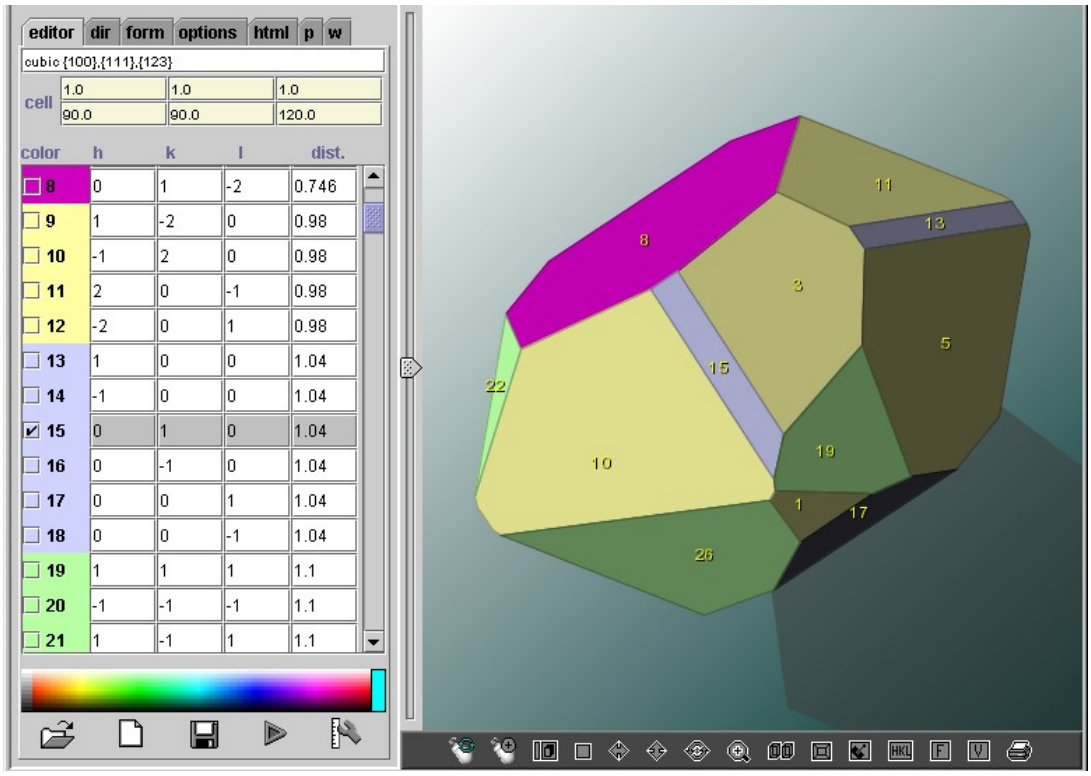

Figure 2-20: BFDH calculations adapted from Material Studio for the prediction of crystal facet indexing and number 15 facet has been predicted as (010) facet (shown from √ sign).

The package incorporates three methods for crystal morphology prediction from crystal structure data, which were in this work obtained in CIF format from the Cambridge Structural Database (CSD). The three methods are[89]

1. The Bravais-Friedel Donnay-Harker (BFDH) method, which uses the crystal lattice and symmetry to generate a list of possible growth faces and their relative growth rates [90, 91]. Faces with lowest attachment energy are the slowest growing and therefore have the most morphological importance. The attachment energy is the energy released on attachment of a growth slice to a growing crystal surface. The attachment energy is calculated by combining the Donnay-Harker rules, which identify the (h k l) indices of likely growth planes, with the Bravais-Friedel rules, which deduce relative growth rates by assigned center-to-face distance of each

face. The combined information is then used to construct the morphology with a Wulff construction.

2. The growth morphology method, which assumes that the growth rate of a crystal face is proportional to its attachment energy (the energy released on attachment of a growth slice to a growing crystal surface)[2, 92]
3. The equilibrium morphology of a crystal, which is determined by the minimum of the surface energies for all relevant crystal faces at zero Kelvin [93].

Using these methods, the relationship of external morphology and internal crystal structure allows the prediction of crystal shape, the development of tailor-made additives and the control of solvent and impurities effects. It can be rationalised with Material Visualiser which provides all of the graphical tools for constructing models of molecules, crystalline materials, surfaces, polymers and mesoscalestrutures. The integrated model building and editing tools can be manipulated, view and analysed in an asymmetric unit or structures of crystallisation solids [89].

These methods are suitable for organic molecule system under the assumption that the surface is a perfect termination of the bulk structure and that no surface relaxation takes place. Surface relaxation is not significant for organic materials. The latter restriction is important for crystal structures that do not have a centre of inversion. Finally, the equilibrium morphology method calculates the surface energy using a predefined finite and fixed slab thickness at a temperature of 0 K. It is assumes the surface energy is an average between the surfaces with Miller indices {h k l} and {-h –k l}. The most features of Material Studio stimulation is the predicted morphology is related to experiment, enabling indexing of experiment data [89]. Therefore, Material Studio Stimulation is suitable for the big crystal facets indexing due to the instruments restriction by XRD goniometer or optical microscope.

2.7. Attenuated Total Reflection Infrared (ATR-IR)

Infrared (IR) spectroscopy is a popular quantitative technique to measure the vibration frequency and mode of the molecules vibration. The vibrational frequencies of a molecule are characteristic of the bonds between its constituent atoms and correspond to certain frequencies of infrared light. The IR technique uses light radiation from 4000 to 400 cm^{-1}, known as mid-infrared. In pharmaceutical analysis, IR is used to assess purity via the existence of moisture on the surface and to determine functional groups in

conjunction with the molecular bonds. IR is a popular technique for hydrogen bond determination.

ATR-IR spectroscopy, invented in the 1960s, is an enhancement of IR which uses the reflection of an IR beam to determine molecular vibration. Three popular types of reflection IR are internal reflection spectroscopy (ATR), external reflection spectroscopy, otherwise called specular reflection and typically used for smooth surfaces, and a combination of internal and external reflection spectroscopy, known as diffuse reflection spectroscopy (DRIFT), which is useful for rough surfaces. It is a versatile and non-destructive technique of sample analysis and can be used to analyse a variety of materials, including powder, rubber, thin film, pharmaceuticals and even liquid samples. The concept is based on the total reflection of the IR beam when it comes into contact with the sample (**Figure 2-21**). The beam is directed onto an optically dense crystal with a high refractive index at a certain angle to obtain reflection. The sample is clamped above the crystal, so that when the beam reflects through the crystal it penetrates the sample to a finite depth along the top surface of the crystal via evanescent waves. An evanescent wave is produced each time the infrared beam is reflected from the inside surface of the crystal. These evanescent waves penetrate the sample at each reflection point at a distance z. The altered (attenuated) energy from each evanescent wave is passed back to the IR beam, which exits the opposite end of the crystal and is directed to the detector of the IR spectrometer. The detector records the attenuated beam as an interferogram signal, which can be used to generate the IR spectrum. The crystals used are varieties which may affect the spectral range of the analysis and the depth of the penetration. Typically, the crystals used are zinc selenide (ZnSe), Germanium (Ge), silicone (Si) and diamond.

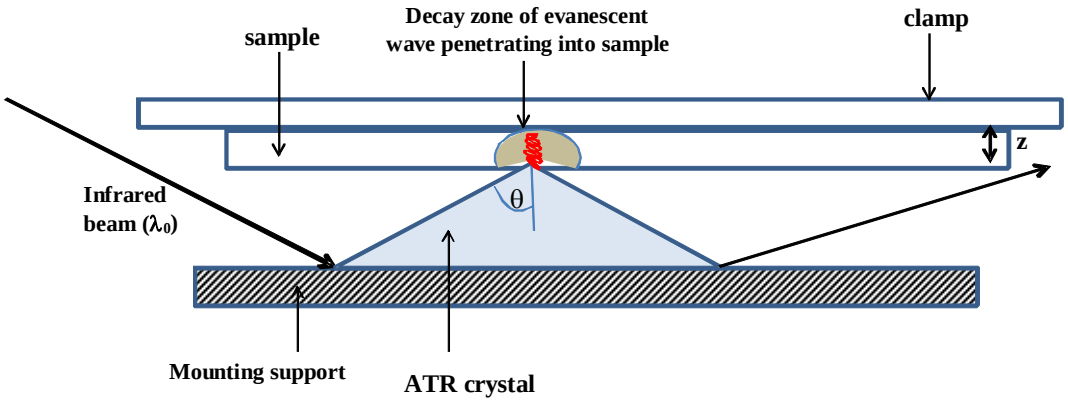

Figure 2-21: Schematic Diagram of Attenuated Total Reflection Infrared (ATR-IR) Spectroscopy functions.

2.8. Differential Scanning Calorimetry (DSC)

Differential Scanning Calorimetry (DSC) is a technique developed by Watson and O'Neill in 1960 and commercially introduced in 1963. The instrument illustrated in **Figure 2-22** below measures energy directly and allows precise measurements of heat capacity. DSC works by measuring the difference in heat energy absorbed and released by a sample, as compared to an inert reference (empty pan), when both are heated, cooled or held at a controlled temperature. The temperature of the sample pan increases linearly as a function of time, while the reference pan should have a well-defined heat capacity over the range of temperature scanned. For example, as a solid sample reaches its melting temperature, T_m, and changes to a liquid, it will require more heat flowing to it to increase its temperature at the same rate as the reference. The absorption of heat by the sample indicates the endothermic phase transition from solid to liquid. However, at the crystallisation temperature, T_c, for instance, less heat is needed to raise the sample temperature, as the process is exothermic. At more subtle phase changes, DSC can be applied to observe the glass transition temperature, T_g, of a polymer sample. DSC is widely used in research and industrial settings as a quality control instrument due to its applicability in evaluating sample purity and for the determination of polymer curing.

The DSC analysis is depicted in a graph of heat flux as a function of time or temperature. The DSC instrument will interpret exothermic reactions by producing positive or negative peaks, depending on the manufacturing technology. For a specific mass undergoing an endothermic or exothermic process, the enthalpy transition can be

calculated and related to the wider thermodynamic determination. The enthalpy of transition, ΔH, can be expressed by the integral of the curve, given by the **Equation 2-26**.

$$\Delta H = KA \qquad \textbf{Equation 2-26}$$

Where ΔH is the enthalpy of transition, K is the calorimetric constant and A is the area under the curve. The calorimetric constant varies from instrument to instrument and can be determined by analyzing a well characterized sample with known ΔH.

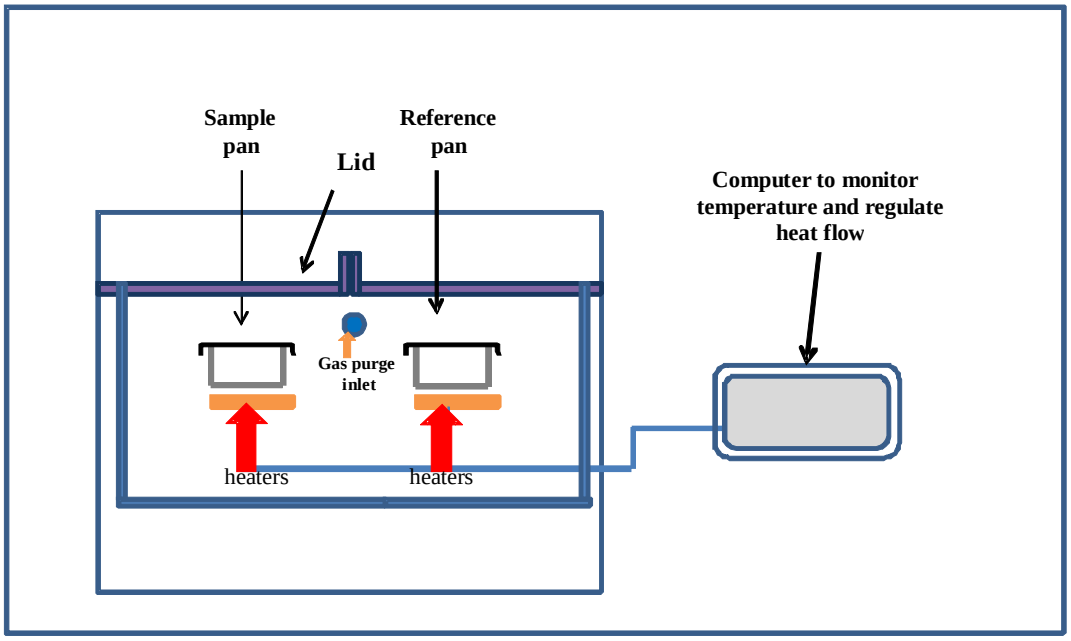

Figure 2-22: Schematic diagram of Differential Scanning Calorimetry instrumentation

DSC is a popular technique for phase diagram studies of samples. The most common theoretical DSC curves are those observed for fusion, crystallization and glass transition temperatures. For instance, at increased temperature, amorphous semicrystalline solid molecules will become less viscous and have enough freedom of motion to rearrange the molecular structure spontaneously into crystalline form. The value of crystallisation temperature, T_c, indicates this as an exothermic process. Conversely, as the temperature increases to melting temperature, T_m, the sample will have enough energy to melt, indicated as an endothermic curve. Similarly, glass transition temperature, T_g, will be reached as the temperature of an amorphous solid increases. On the DSC curve, T_g appears as a step in the baseline of the recorded DSC signal.

2.9. References

1. Yu, L.; Reutzel-Edens, S. M.; Mitchell, C. A., Crystallization and Polymorphism of Conformationally Flexible Molecules: Problems, Patterns, and Strategies. *Org. Process Res. Dev.* **2000,** 4, 396-402.

2. Docherty, R.; Clydesdale, G.; Roberts, K. J.; Bennema, P., Application of Bravais-Friedel-Donnay-Harker, attachment energy and Ising models to predicting and understanding the morphology of molecular crystals. *J. Phys. D. Appl. Phys.* **1991**, 89-99.

3. Carvalho, P. O.; Cass, Q. B.; Calafatti, S. A.; Contesini, F. J.; Bizaco, R., Review-Alternatives for the separation of drug enantiomers: ibuprofen as a model compound. *Braz. J. Chem.Eng.* **2006,** 23, 291-300.

4. Mullin, J. W., *Crystallization*. Fourth Edition ed.; Butterworth-Heineman: Oxford, 1993; p 610.

5. Davey, R.; Garside, J., *From Molecules to Crystallizers . An Introduction to Crystallization*. Oxford University Press: New York, United States, 2000; p 81.

6. Ristic, R. I.; Finnie, S.; Sheen, D. B.; Sherwood, J. N., Macro- and Micromorphology of Monoclinic Paracetamol Grown from Pure Aqueous Solution. *J. Phys. Chem. B* **2001,** 105, 9057-9066.

7. Boistelle, R.; Astier, J. P., Crystallization mechanisms in solution. *J. Cryst. Growth* **1988,** 90, 14-30.

8. Grimbergen, R. F. P.; Meekes, H.; Bennema, P.; Strom, C. S.; Vogels, L. J. P., On the Prediction of Crystal Morphology. I. The Hartman-Perdok Theory Revisited. *Acta Crystallogr. A* **1998**, 491-500.

9. Gavezzotti, A., Structure and intermolecular potentials in molecular crystals. *Model. Simul. Mater. Sci.* **2002,** 10, R1-R29.

10. Winn, D., Modeling crystal shapes of organic materials grown from solution. *AIChE J.* **2000,** 46, 1348.

11. Hartman, P.; Perdok, W. G., On the relations between structure and morphology of crystals. I. *Acta Crystallogr.* **1955**, 49-52.

12. Boerrigter, S. X. M.; Cuppen, H. M.; Ristic, R. I.; Sherwood, J. N.; Bennema, P.; Meekes, H., Explanation for the Supersaturation-Dependent Morphology of Monoclinic Paracetamol. *Cryst.Growth Des.* **2002,** 2, 357-361.

13. Cuppen, H. M.; Day, G. M.; Verwer, P.; Meekes, H., Sensitivity of Morphology Prediction to the Force Field: Paracetamol as an Example. *Cryst.Growth Des.* **2004,** 4, 1341-1349.

14. Shekunov, B. Y., In Situ Optical Interferometric Studies of the Growth and Dissolution Behavior of Paracetamol (Acetaminophen). 1. Growth Kinetics. *J. Phys. Chem. B* **1997,** 101, 3973-3979.

15. Thompson, C.; Davies, M. C.; Roberts, C. J.; Tendler, S. J. B.; Wilkinson, M. J., The effects of additives on the growth and morphology of paracetamol (acetaminophen) crystals. *Int.J. Pharm.* **2004,** 280, 137-150.

16. Espeau, P.; Céolin, R.; Tamarit, J.-L.; Perrin, M.-A.; Gauchi, J.-P.; Leveiller, F., Polymorphism of paracetamol: Relative stabilities of the monoclinic and orthorhombic phases inferred from topological pressure-temperature and temperature-volume phase diagrams. *J. Pharm.Sci.* **2005,** 94, 524-539.

17. Vasil'chenko, M. A.; Shakhtshneider, T. P.; Naumov, D. Y.; Boldyrev, V. V., Topochemistry of the initial stages of the dissolution of single crystals of acetaminophen. *J.Pharmaceutic.Sci.* **1996,** 85, 929-934.

18. Prasad, K. V. R.; Sheen, D. B.; Sherwood, J. N., Fracture Property Studies of Paracetamol Single Crystals Using Microindentation Techniques. *Pharm. Res.* **2001,** 18, 867-872.

19. Behzadia, H.; Esrafilia, M. D.; Hadipour, N. L., A theoretical study of 17O, 14N and 2H nuclear quadrupole coupling tensors in the real crystalline structure of acetaminophen. *Chem.Phys.* **2007,** 333, 97-104.

20. Naumov, D. Y.; Vasilchenko, M. A.; Howard, J. A. K., The Monoclinic Form of Acetaminophen at 150K. *Acta Crystallogr. C* **1998**, 653-655.

21. Esrafili, M. D.; Behzadi, H.; Hadipour, N. L., Influence of N-H...O and O-H...O hydrogen bonds on the 17O, 15N and 13C chemical shielding tensors in crystalline acetaminophen: A density functional theory study. *Biophys. Chem.* **2007,** 128, 38-45.

22. Saha, A.; Tiwary, A. S.; Mukherjee, A. K., Charge transfer interaction of 4-acetamidophenol (paracetamol) with 2,3-dichloro-1,4-naphthoquinone: A study in aqueous ethanol medium by UV-vis spectroscopic and DFT methods. *Spectrochim. Acta A* **2008,** 71, 835-840.

23. Di Martino, P.; Guyot-Hermann, A. M.; Conflant, P.; Drache, M.; Guyot, J. C., A new pure paracetamol for direct compression: The orthorhombic form. *Int.J. Pharm.* **1996,** 128, 1-8.

24. Al-Zoubi, N.; Koundourellis, J. E.; Malamataris, S., FT-IR and Raman spectroscopic methods for identification and quantitation of orthorhombic and monoclinic paracetamol in powder mixes. *J. Pharm. Biomed.Anal.* **2002**, 459-467.

25. Al-Zoubi, N.; Nikolakakis, I.; Malamataris, S., Crystallization conditions and formation of orthorhombic paracetamol from ethanolic solution. *J. Pharm. Pharmacol.* **2002,** 54, (3), 325-333.

26. Heng, J. Y. Y.; Bismarck, A.; Lee, A. F.; Wilson, K.; Williams, D. R., Anisotropic surface energetics and Wettability of macroscopic form I paracetamol crystals. *Langmuir* **2006,** 22, 2760-2769.

27. Alander, E. M.; Uusi-Penttila, M. S.; Rasmuson, A. C., Agglomeration of Paracetamol during Crystallization in Pure and Mixed Solvents. *Ind. Eng. Chem. Res.* **2004**, 629-637.

28. Nichols, G.; Frampton, C. S., Physicochemical characterization of the orthorhombic polymorph of paracetamol crystallized from solution. *J. Pharm.Sci.* **1998,** 87, 684-693.

29. Oswald, I. D. H.; Allan, D. R.; McGregor, P. A.; Motherwell, W. D. S.; Parsons, S.; Pulham, C. R., The formation of paracetamol (acetaminophen) adducts with hydrogen-bond acceptors. *Acta Crystallogr. B* **2002,** 58, 1057-1066.

30. Sacchetti, M., Thermodynamic analysis of DSC data for acetaminophen polymorphs. *J Therm. Anal. Calorim.* **2001,** 63, 345-350.

31. Qi, S.; Avalle, P.; Saklatvala, R.; Craig, D. Q. M., An investigation into the effects of thermal history on the crystallisation behaviour of amorphous paracetamol. *Eur. J. Pharm. Biopharm.* **2008,** 69, (1), 364-371.

32. Di Martino, P., Molecular mobility of the paracetamol amorphous form. *Chem. Pharmaceut. Bull.* **2000,** 48, (8), 1105-1108.

33. Moynihan, H. A.; O'Hare, I. P., Spectroscopic characterisation of the monoclinic and orthorhombic forms of paracetamol. *Int. J. Pharm.* **2002,** 247, 179-185.

34. Burgina, E. B.; Baltakhinov, V. P.; Boldyreva, E. V.; Shakhtschneider, T. P., IR Spectra of Paracetamol and Phenacetin. 1. Theoretical and Experimental Studies. *J.Struct.Chem+* **2004,** 45, 64-73.

35. Beyer, T.; Price, S. L., The errors in lattice energy minimisation studies: sensitivity to experimental variations in the molecular structure of paracetamol. *CrystEngComm* **2000,** 2, 183-190.

36. Ålander, E. M.; Rasmuson, Å. C., Agglomeration and adhesion free energy of paracetamol crystals in organic solvents. *AIChE J.* **2007**, 2590-2605.

37. Alves, C. N.; Borges, R. S.; DaSilva, A. B. F., Density functional theory study of metabolic derivatives of the oxidation of paracetamol. *Int. J. Quantum Chem.* **2006,** 106, 2617-2623.

38. Yu, L., Amorphous pharmaceutical solids: preparation, characterization and stabilization. *Adv.Drug Deliver. Rev.* **2001**, 27-42.

39. Wen, H.; Morris, K. R.; Park, K., Study on the interactions between polyvinylpyrrolidone (PVP) and acetaminophen crystals: Partial dissolution pattern change. *J. Pharm.Sci.* **2005,** 94, 2166-2174.

40. Terzyk, A. P., Molecular properties and intermolecular forces--factors balancing the effect of carbon surface chemistry in adsorption of organics from dilute aqueous solutions. *J.Colloid Interf. Sci.* **2004,** 275, 9-29.

41. An, G.-W.; Zhang, H.; Cheng, X.-L.; Zhuo, Q.-L.; Lv, Y.-C., Electronic structure and hydrogen bond in the crystal of paracetamol drugs. *Struc.Chem.* **2008,** 19, 613-617.

42. Ilieva, S.; Hadjieva, B.; Galabov, B., Theory Supplemented by Experiment. Electronic Effects on the Rotational Stability of the Amide Group in p-Substituted Acetanilides. *J.Org.Chem.* **2002,** 67, 6210-6215.

43. Wilson, C. C.; Shankland, N.; Florence, A. J.; Frampton, C. S., Single-crystal neutron diffraction of bio-active small molecules. *Physica B* **1997,** 234-236, 84-86.

44. Wilson, C. C., Neutron diffraction of p-hydroxyacetanilide (Paracetamol): libration or disorder of the methyl group at 100 K. *J. Mol. Struct.* **1997,** 405, 207-217.

45. Germaine L Defendi, M., MS, FAAP, Toxicity, Acetaminophen. In *e-Medicine from webMD*, May, 15, 2007. http://emedicine.medscape.com/article/1008683-overview.

46. Jiao, J., Polyoxyethylated nonionic surfactants and their applications in topical ocular drug delivery. *Adv. Drug Deliver. Rev.* **2008**, 1663-1673.

47. Law, S. L.; Kayes, J. B., Adsorption of non-ionic water-soluble cellulose polymers at the solid-water interface and their effect on suspension stability. *Int.J. Pharm.* **1983,** 15, 251-260.

48. Changquan Calvin Sun, Y. H. K., On the identification of slip planes in organic crystals based on attachment energy calculation. *J. Pharm.Sci.* **2008,** 97, 3456-3461.

49. Wells, J. I., *Pharmaceutical preformulation : the physicochemical properties of drug substances*. Ellis Horwood: Chichester, 1988.

50. Feng, Y.; Grant, D. J. W.; Sun, C. C., Influence of crystal structure on the tableting properties of n-alkyl 4-hydroxybenzoate esters (parabens). *J. Pharm.Sci.* **2007,** 96, 3324-3333.

51. Kazarian, S. G.; Martirosyan, G. G., Spectroscopy of polymer/drug formulations processed with supercritical fluids: in situ ATR-IR and Raman study of impregnation of ibuprofen into PVP. *Int.J.Pharm.* **2002,** 232, 81-90.

52. Brostow, W.; Chiu, R.; Kalogeras, I. M.; Vassilikou-Dova, A., Prediction of glass transition temperatures: Binary blends and copolymers. *Mater. Lett.* **2008,** 62, 3152-3155.

53. Marsac, P. J.; Li, T.; Taylor, L. S., Estimation of drug-polymer miscibility and solubility in amorphous solid dispersions using experimentally determined interaction parameters. *Pharm. Res.* **2009,** 26, 139-151.

54. David, J. G.; Adrian, C. W.; Peter, T.; Peter, Y., Solubility parameters as predictors of miscibility in solid dispersions. *J. Pharm.Sci.* **1999,** 88, 1182-1190.

55. Stefanis, E., Prediction of hansen solubility parameters with a new group-contribution method. *Int. J. Thermophys.* **2008,** 29, 568-585.

56. Ghebremeskel, A. N.; Vemavarapu, C.; Lodaya, M., Use of surfactants as plasticizers in preparing solid dispersions of poorly soluble API: Selection of polymer-surfactant combinations using solubility parameters and testing the processability. *Int. J.Pharm.* **2007,** 328, 119-129.

57. Forster, A.; Hempenstall, J.; Tucker, I.; Rades, T., Selection of excipients for melt extrusion with two poorly water-soluble drugs by solubility parameter calculation and thermal analysis. *Int. J. Pharm.* **2001,** 226, 147-161.

58. Hancock, B. C.; York, P.; Rowe, R. C., The use of solubility parameters in pharmaceutical dosage form design. *Int. J.Pharm.* **1997,** 148, 1-21.

59. Adamska, K.; Voelkel, A.; Héberger, K., Selection of solubility parameters for characterization of pharmaceutical excipients. *J. Chromatogr. A* **2007**, 90-97.

60. Mermet, C. R., Significance of partial and total cohesion parameters of pharmaceutical solids determined from dissolution calorimetric measurements. *Pharm. Res.* **1991,** 8, 636.

61. Pospiech, D., Determination of interaction parameters of block copolymers containing aromatic polyesters from solubility parameters obtained from solution viscosities. *Colloid Polym. Sci.* **2002,** 280, 1027.

62. Patel, S.; Lavasanifar, A.; Choi, P., Application of Molecular Dynamics Simulation To Predict the Compatability between Water-Insoluble Drugs and Self-Associating Poly(ethylene oxide)-b-poly(ε-caprolactone) Block Copolymers. *Biomacromolecules* **2008,** 9, 3014-3023.

63. Barra, J.; Lescure, F.; Doelker, E., Influence of Surface Free Energies and Cohesion Parameters on Pharmaceutical Material Interaction Parameters–Theoretical Simulations. *Pharm.Res.* **1996,** 13, 1746-1751.

64. Guo, C.; Liu, H.; Wang, J.; Chen, J., Conformational Structure of Triblock Copolymers by FT-Raman and FTIR Spectroscopy. *J.Colloid Interf.Sci.* **1999**, 368-373.

65. Schmolka, I., Physical Basis for Poloxamer Interactions. *Annal. NY Acad.Sci.* **1994,** 720, 92-97.

66. Brandani, P.; Stroeve, P., Adsorption and Desorption of PEO-PPO-PEO Triblock Copolymers on a Self-Assembled Hydrophobic Surface. *Macromolecules* **2003,** 36, 9492-9501.

67. Giffard, M.; Delfosse, V.; Sciara, G.; Mayer, C.; Cambillau, C.; Hajji, M. E.; Castro, B.; Bonnet, F., Surfactant Poloxamer 188 as a New Crystallizing Agent for Urate Oxidase. *Cryst. Growth Des.* **2009,** 9, 4199-4206.

68. Fusco, S., Perspectives on: PEO-PPO-PEO triblock copolymers and their biomedical applications. *J. Bioact.Compat.Pol.* **2006,** 21, 149-164.

69. Ali, W.; Williams, A. C.; Rawlinson, C. F., Stochiometrically governed molecular interactions in drug: Poloxamer solid dispersions. *Int.J. Pharm.* 391, 162-168.

70. Musoke, M.; Luckham, P. F., Interaction forces between polyethylene oxide-polypropylene oxide ABA copolymers adsorbed to hydrophobic surfaces. *J, Colloid Interf. Sci.* **2004,** 277, 62-70.

71. Cassidy, O. E., Surface modification and electrostatic charge of polystyrene particles. *Int. J. Pharm.* **1999,** 182, 199-211.

72. Ghareeb, M.; Abdulrasool, A.; Hussein, A.; Noordin, M., Kneading Technique for Preparation of Binary Solid Dispersion of Meloxicam with Poloxamer 188. *AAPS PharmSciTech* **2009,** 10, (4), 1206-1215.

73. Lee, B.; Firestone, M. A., Electron Density Mapping of Triblock Copolymers Associated with Model Biomembranes: Insights into Conformational States and Effect on Bilayer Structure. *Biomacromolecules* **2008,** 9, 1541-1550.

74. Nefedov, V. I., *X-ray photoelectron spectroscopy of solid surfaces*. VSP BV: Utrecht, 1988; p vii, 191.

75. Briggs, D., *Surface analysis of polymers by XPS and static SIMS*. Cambridge University Press: Cambridge, 1998.

76. Bagus, P. S.; Illas, F.; Pacchioni, G.; Parmigiani, F., Mechanisms responsible for chemical shifts of core-level binding energies and their relationship to chemical bonding. *J. Electron Spectroc.* **1999**, 215-236.

77. Brisk, M. A.; Baker, A. D., Shake-up satellites in X-ray photoelectron spectroscopy. *J. Electron Spectroc.* **1975,** 7, 197-213.

78. Rouxhet, P. G.; Doren, A.; Dewez, J. L.; Heuschling, O., Chemical composition and physico-chemical properties of polymer surfaces. *Prog.Org.Coat.* **1993,** 22, 327-344.

79. Riga, J.; Pireaux, J.-J.; Verbist, J. J., An ESCA study of the electronic structure of solid benzene. -- Valence levels, core level and shake-up satellites. *Mol. Phys.* **1977,** 34, 131 - 143.

80. Turner, N. H.; Schreifels, J. A., Surface Analysis: X-ray Photoelectron Spectroscopy and Auger Electron Spectroscopy. *Anal. Chem.* **1996,** 68, 309-332.

81. Echenique, P. M., Theory of inelastic lifetimes of low-energy electrons in metals. *Chem. Phys.* **2000,** 251, (1-3), 1-35.

82. Tanuma, S., Calculations of electron inelastic mean free paths for 31 materials. *Surf. Interface Anal.* **1988,** 11, 577-589.

83. Tanuma, S.; Powell, C. J.; Penn, D. R., Calculations of electron inelastic mean free paths. V. Data for 14 organic compounds over the 50–2000 eV range. *Surf. Interface Anal.* **1994,** 21, 165-176.

84. Seah, M. P., Quantitative electron spectroscopy of surfaces: A standard data base for electron inelastic mean free paths in solids. *Surf. Interface Analysis* **1979,** 1, 2-11.

85. Chappell, P. J. C.; Williams, D. R.; George, G. A., XPS analysis of model p-aramid compounds and poly (p-phenylene terephthalamide) fibers. *J.Colloid Interf. Sci.* **1990,** 134, 385-396.

86. Joanna, S. S.; Sven, L. M. S., Quantitative analysis of saccharides by X-ray photoelectron spectroscopy. *Surf. Interface Anal.* **2009,** 41, 453-462.

87. Fultz, B.; Howe, J. M., *Transmission Electron Microscopy and Diffractiometry of Materials*. Springer: Berlin, 2001; p 3.

88. Jenkins, R.; Snyder, R. L., *Introduction to X-ray powder diffractometry*. Wiley: New York ; Chichester, 1996.

89. Accelrys Material Studio Datasheet. Morphology. http://accelrys.com/products/datasheets/morphology.pdf (20 April),

90. Davey, R. J.; Black, S. N.; Logan, D.; Maginn, S. J.; Fairbrother, J. E.; Grant, D. J. W., Structural and kinetic features of crystal growth inhibition: adipic acid growing in the presence of n-alkanoic acids. *Journal of the Chemical Society, Faraday Transactions* **1992,** 88, (23), 3461-3466.

91. Grimbergen, R. F.; Bennema, P.; Meekes, H., On the prediction of crystal morphology. III. Equilibrium and growth behaviour of crystal faces containing multiple connected nets. *Acta Crystallogr. Sect. A: Found.Crystallogr.* **1999**, 84-94.

92. Hartman, P., The Attachment Energy as a Habit Controlling Factor. I--Theoretical Considerations. *J. Cryst. Growth* **1980**, 145.

93. Andrews, D. H., The Collected Works of J. Willard Gibbs. Two volumes. *Journal of Chemical Education* **1929,** 6, (3), 591-null.

3. CHAPTER 3: CRYSTAL CRYSTALLISATION

3.1. Objectives

The objectives of the work described in this chapter were:

i) To differentiate the crystal habits obtained by using three different solvents: acetone, ethanol and methanol.

ii) To obtain high quality single crystals of at least 1 cm diameter by slow cooling crystallisation.

3.2. Crystallisation Techniques

The cooling process affects the growth rate and the size of crystals. Rapid cooling will reduce crystal size due to the incomplete growth of a large number of small crystals[1]. While overly slow cooling may also cause incomplete growth due to the very long time required to complete growth,[2] theoretically, through slow cooling, all solute molecules (unit cells) will become aligned and a regular crystal shape will be obtained. This is illustrated in **Figure 3-1**, where hexagons represent the solute and triangles the impurities. If the hot solution is left to cool slowly, the impurities may settle briefly in the growing crystal lattice, but after a time they will move out and a regular crystal geometry of hexagon shapes will be formed. In rapid cooling, by contrast, the impurities will be trapped in the crystal units and irregular shapes obtained (**Figure 3-2**).

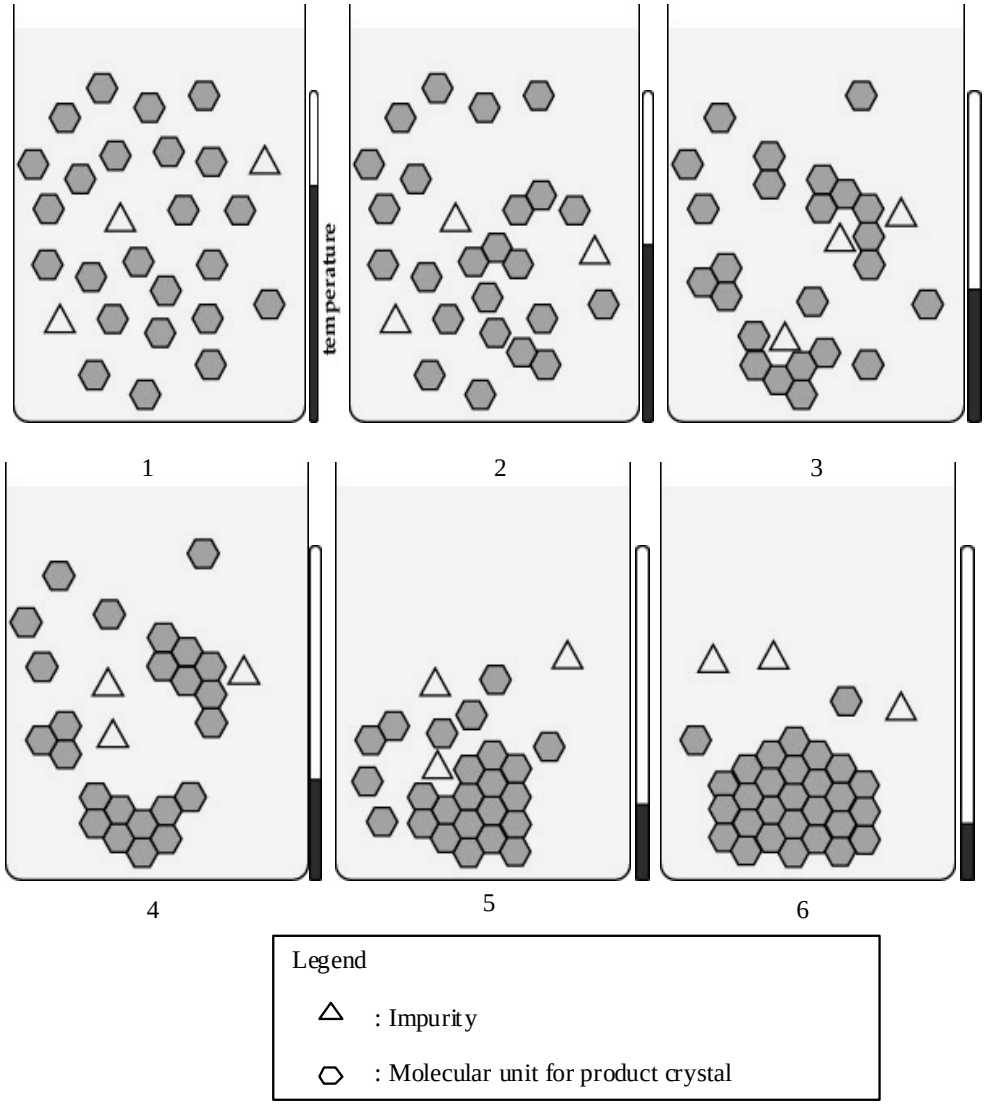

Figure 3-1: Schematic illustration for crystallisation of pure product during slow crystallisation

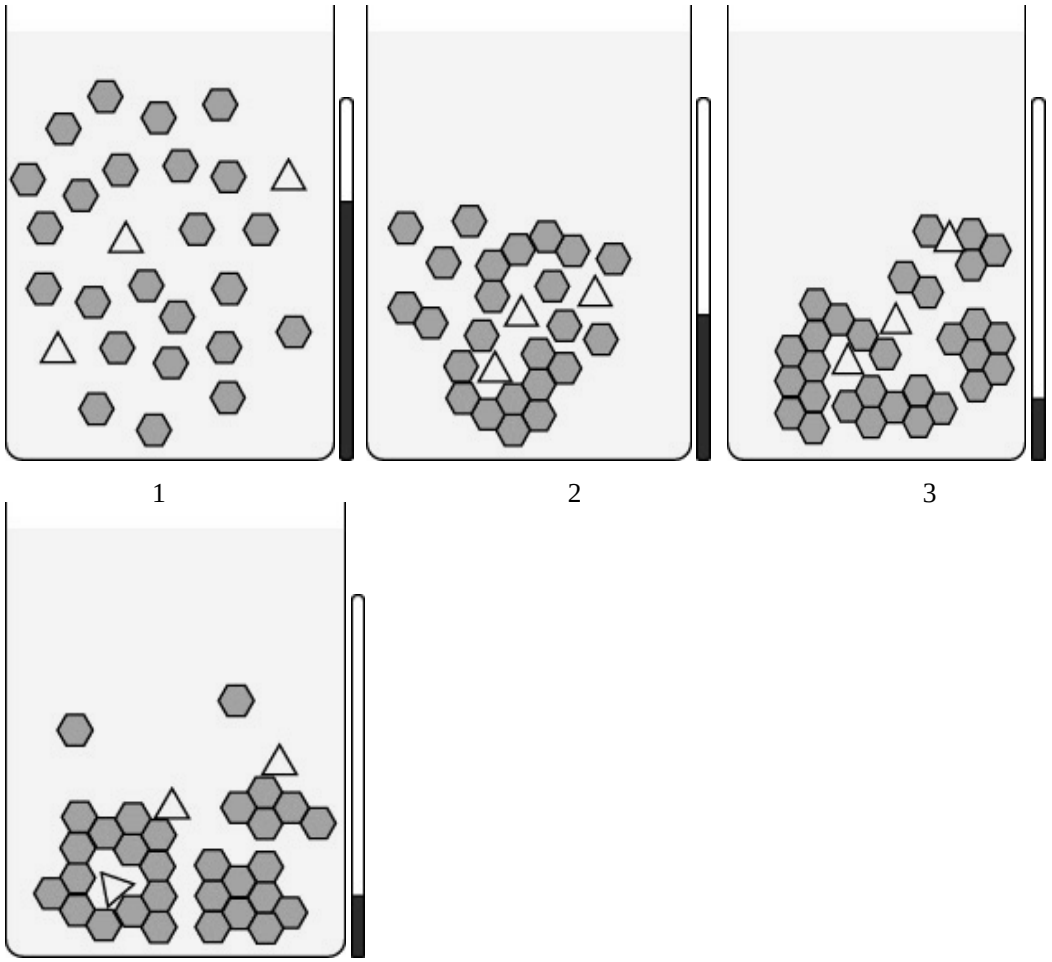

Figure 3-2: Schematic illustration for formation of impure product during fast crystallisation induced by rapid cooling

Slow evaporation, in which the temperature of the solution is increased slowly over time, is among the easiest and best known of the crystallisation techniques. It is very sensitive to the choice of solvent and a major disadvantage is that the crystals tend to adhere to the glass walls, which can make it more difficult to retrieve them without damage[3].

3.2.1. Vapour Diffusion

A method which is suitable for milligram amounts of material is vapour diffusion, shown in **Figure 3-3**. A solution of the substance is prepared using first solvent S1 and placed in test tube T. A second solvent, S2, is placed in a closed beaker, B. S2 is chosen such that when it is mixed with S1 the solute will become less soluble. The test tube containing S1 is then placed in the beaker and the beaker is sealed. The slow diffusion of S2 into test tube T and S1 out of T will cause crystals to form. If S2 is more volatile than S1, the solvent level will increase and prevent microcrystalline crusts from forming on the sides of T[3, 4].

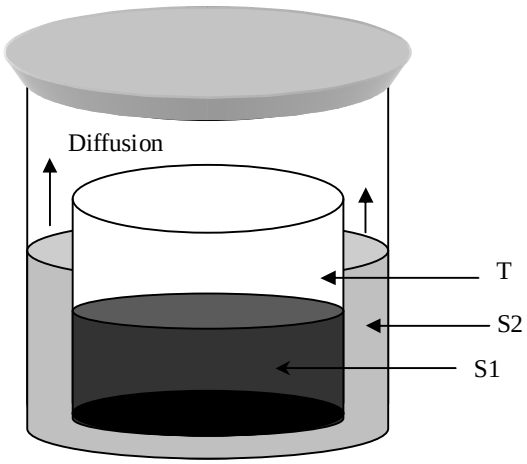

Figure 3-3: Schematic diagram of vapour diffusion crystallisation technique. S1- first solvent, S2- second solvent, T- test tube

A crucial step in the vapour diffusion technique is the selection of the solvents: S2 must have a lower melting point than S1.

3.2.2. Paracetamol Solubility

In the present study, paracetamol (monoclinic, form I) was prepared using several different solvents. An understanding of the crystallisation process is essential to the preparation of single crystals. **Figure 3-4** shows the paracetamol solubility curve for all three solvents, using solubility data from the literature[5].

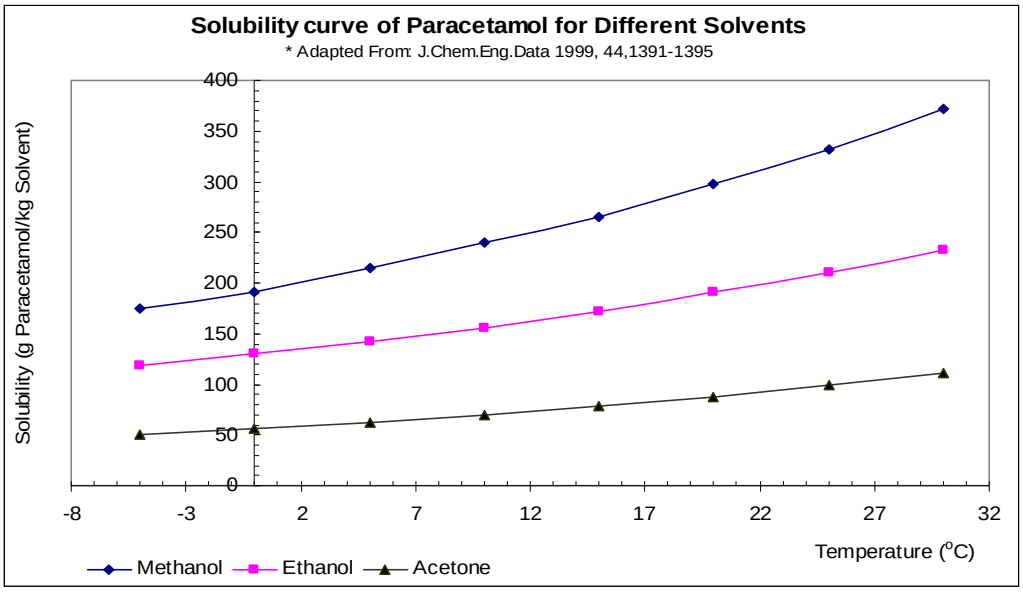

Figure 3-4: Solubility curves of paracetamol in different solvents

These solubility curves were used to prepare single paracetamol crystals with three other solvents: ethanol, methanol and acetone. **Table 3-1** below shows the paracetamol mass of 20 mL solvents calculated from the solubility curves (**Figure 3-4**).

Table 3-1: Mass of paracetamol (PA) for 20 mL solvent calculated from the solubility data.

Temperature (°C)	g PA/ 20 mL MeOH	g PA/ 20 mL EtOH	g PA/ 20 mL Acetone
10	3.79	2.46	1.09
15	4.20	2.70	1.23
20	4.71	3.01	1.38
25	5.25	3.31	1.57
30	5.88	3.67	1.76

3.3. Preparation of Monoclinic Single Paracetamol Crystal by Slow Crystallisation

Prior to preparation of paracetamol single crystal, two types of apparatus cleaning were conducted.

i) First, the container was washed with a 2% solution of ammonium peroxydisulphate (APS) in 99% sulphuric acid. The APS solution was prepared by a lab technician immediately prior to the cleaning process. After this acid wash, the container was thoroughly rinsed with tap water, followed by deionised water. The apparatus was then dried in an oven at 60 °C.

ii) The second method of cleaning was using a high temperature furnace, in which the apparatus was heated to 450 °C for 2 hours to eliminate all organic particles sticking to the apparatus wall. The heating method is normally used for big glass cleaning.

Pure paracetamol single crystals were prepared using three types of solvent: absolute ethanol, acetone and methanol. The acetone and methanol were HPLC grade (99.9% purity). Ethanol (20 ml) in the jacketed vessel was held at a temperature of 20 °C. Paracetamol powder was weighed as calculated on **Table 3-1.** The saturated solution was prepared by dissolving all the powder in ethanol at a temperature of 23 °C. After a clear solution was achieved, its temperature was reduced to 20 °C, producing a supersaturated solution, which was stirred for 24 hours at 20 °C, when it was assumed that the solubility limit of the solution had been achieved. The magnetic stirrer was then removed from the vessel and the bath temperature decreased by 0.10 °C per day to 19.80 °C, when a single crystal seed was placed in the solution. The seed was prepared by evaporating the saturated solution in a small crystallisation disk for 1 day. The circulating bath (Thermo Scientific NESLAB Digital Plus RTE 7, refrigerated bath chiller circulator) was then programmed to reduce the temperature by 0.50 °C per day until last temperature was 16.3^{o}C. The crystallisation was terminated approximation for 7 days. Care was taken that the crystallisation setup should not be affected by any vibration, stirring or disturbance until a sufficient size of single crystal was obtained. The crystal was then removed from the vessel by means of a Büchner filter.

3.4. Preparation of a Single Orthorhombic Paracetamol Crystal

Form II (orthorhombic) paracetamol is very sensitive to the presence of any contamination during the crystallisation process. Any impurities or debris present in the

crystallisation vessel will lead to recrystallisation to form I. Therefore, all the glassware was cleaned in APS prior to the experiment.

12.50 g of pure paracetamol was dissolved at 40 °C in 500 ml of deionised water in a conical flask. The solution was then heated to boiling point and kept boiling for 15 minutes to ensure that all the powder had fully dissolved, before being filtered and transferred to a jacketed vessel where it was kept at 40 °C for 24 hours. Next, the solution was cooled at a rate of 3 °C per day until it reached the appropriate saturation temperature of 4 °C[6, 7], when the seed was introduced into the vessel. This had been prepared by melting form I paracetamol powder at 175 °C. The crystallisation process took 15 days.

3.5. Sample Preparation and Characterisation

The single crystals prepared as above were ground prior to characterisation by ATR-IR and XRD analysis. An amount sufficient for the analysis, approximately 1-2 mg, was ground in a mortar until a homogenous powder was formed. The ground crystal analysed by XRD and ATR-IR were labelled as AceGround (single crystal grown in acetone), EtGround (ground single crystal grown in ethanol), MeGround (ground single crystal grown in methanol). For single crystal XRD analysis, a single seed crystal of less than 0.25 mm was selected for the unit cell and indexes. No further treatment was done. Single crystal X-ray diffraction data were collected at 100 K with an Oxford Diffraction X-Calibur 2 diffractometer utilising Mo K_α radiation ($\lambda = 0.71073$ Å) and an Oxford Cryosystems cryostream Controller 700. Data were recorded with the X-ray source operating at 50 kV and 40 mA. Data reduction, cell refinement, and multi-scan absorption corrections were carried out using the program Crysalis RED (Oxford Diffraction Ltd., version 1.171.32.24, 2008). The X-ray powder diffraction patterns were collected using a Rigaku Miniflex instrument utilising Cu K_α radiation (1.5406 Å), operating over 5-40^o 2θ at 1.5^o min^{-1} with a 0.03^o step, 30 kV voltage, and 15 mA current. Typically 5 mg of sample was placed on a sample attachment and smoothed to achieve a level surface.

ATR-IR spectra were obtained with a ThermoNicolet Avatar 360 ESP FT-IR spectrometer with a Specac Golden Gate ATR attachment. A background spectrum was taken before each session of characterisation. Spectra were recorded over the range 4000-400 cm^{-1}. Spectra were analysed using Nicolet OMNIC E.S.P.5.1 software.

3.6. Results and Discussion

3.6.1. Paracetamol crystal

Many authors report the preparation of single paracetamol crystals by the solvent evaporation technique[7, 8] with a seed. However, the technique chosen for use in this study was slow cooling with a seed as a precursor because of the good outcomes in terms of the single crystals produced (**Figure 3-5a**). The slow cooling crystallisation would produce larger crystals and good temperature control led to the production of clear single crystals. Crystal growth is very sensitive to temperature, environment, the cleanliness of the container and vibration. Therefore, a programmed circulating bath was used in the crystallisation process. The solubility curve shows that at 20 °C a saturated solution of paracetamol becomes supersaturated; therefore the ideal temperature to introduce the seed was considered to be 19.80 °C. Two different types of crystallisation solution are compared in **Figure 3-5**. The photographs were captured to differentiate the arrangement of crystal in solution. **Figure 3-5 (a)** formed a single crystal at the bottom of jacketed vessel at the end of crystallisation period. However, **Figure 3-5 (b)** resulted no single crystal formed at the end of crystallisation period (attempt had been made until 2 months, the single crystal was not appeared at the end of the period).

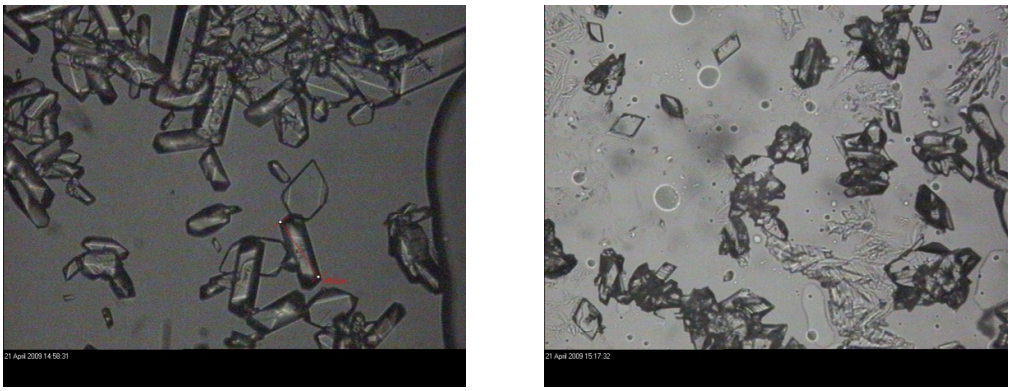

(a) (b)

Figure 3-5: Comparison of two crystallisation solutions. (a) Solution which crystallised to single crystals (b) Non-crystallised solution which would not formed single crystal.

.

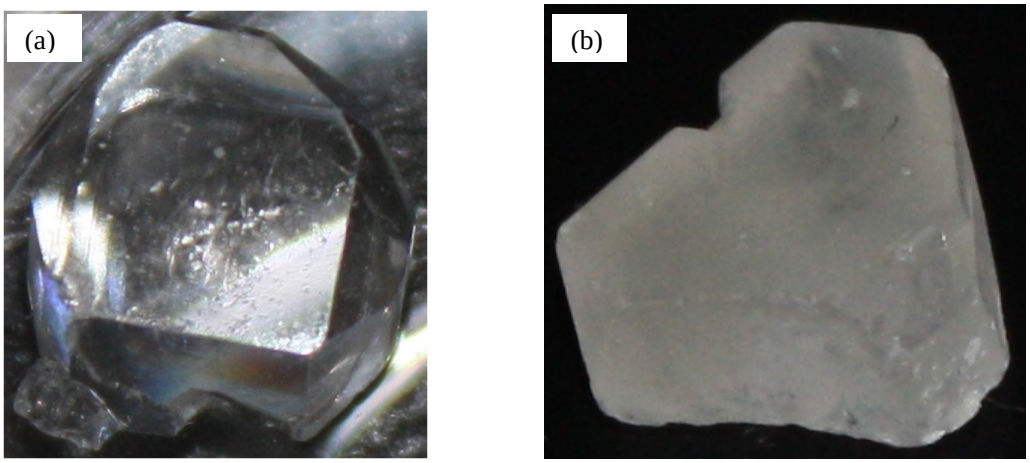

Figure 3-6: Paracetamol single crystal (a) From acetone solution where the crystallisation apparatus was washed with APS (b) Ethanol single crystal where the apparatus was cleaned with detergent and water.

All the apparatus for the crystallisation experiment must also be very clean and the solvent used must be absolute or HPLC grade. **Figure 3-6** shows images of two single crystals produced in apparatus (a) cleaned in APS and (b) cleaned with detergent then rinsed with deionised water. The figures show that the clarity of single crystal prepared was affected by the cleanliness of the crystallisation containers.

3.6.2. X-ray Diffraction

The single crystals of polymorph form I and form II diffraction patterns prepared were ground and analysed with powder XRD. **Figure 3-7** compares XRD patterns of the two forms according to the Crystal Database Structure (CDS) data, while **Figure 3-8** compares experimental spectra for the two forms obtained from the prepared crystals. The results show that the main difference between forms I and II is visible at 2θ values of 25.32° and 25.62°, for CDS data and experimental data respectively. The XRD diffraction patterns thus indicate that the paracetamol prepared was of polymorph forms I and II.

Because the single crystal XRD (SXRD) diffractometer was restricted to characterising the structure of single crystals up to 0.2 mm, only seed crystals were used for the confirmation of form I paracetamol. **Figure 3-9** depicts the SXRD analysis at different face orientations, showing measurements of the cell angles: α was at 90°, β at 97.75° and γ at 90°, while the a axis was 7.14 Å, b was 9.34 Å and c was at 11.69 Å. It was confirmed that the crystal was monoclinic with a cell volume of 772 $Å^3$. These

results are in agreement with values given in the literature of α = 90°, β = 97.82° and γ = 90°; length a = 7.09 Å, b = 9.23 Å and c = 11.62 Å. The reference CDS crystal cell volume was 753.94 $Å^3$ and the dominant facets were at (0-1-1), (10-1) and (1-1-1).

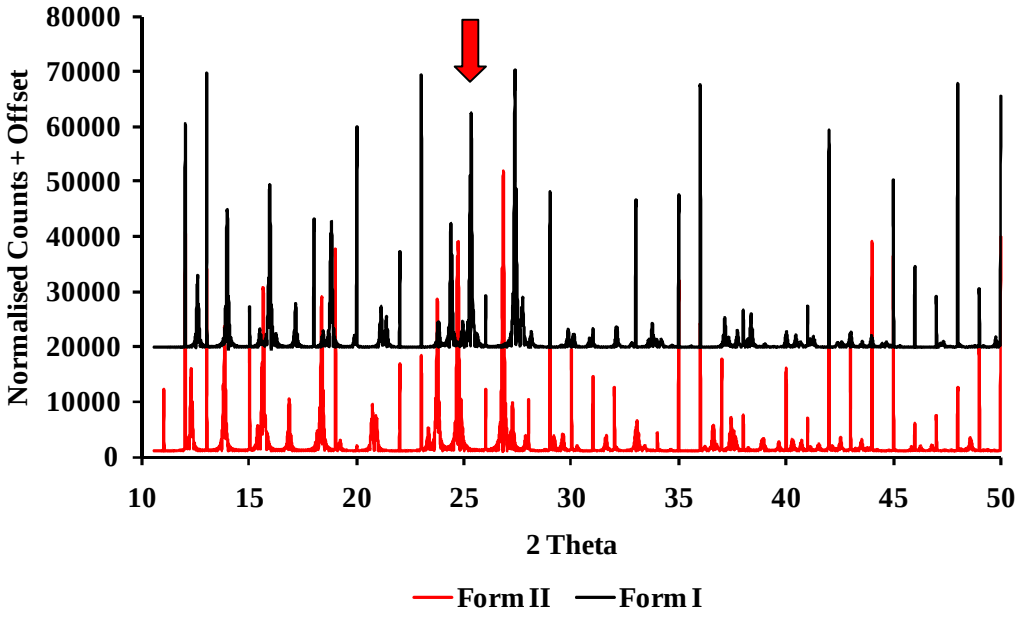

Figure 3-7: XRD paracetamol diffraction patterns for form I and form II from the CDS database.

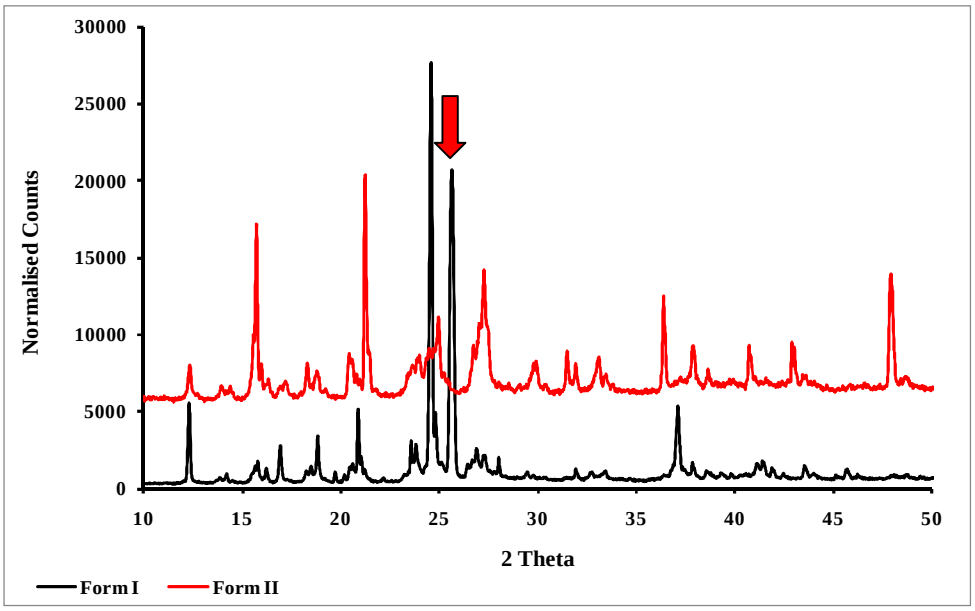

Figure 3-8: PXRD Paracetamol diffraction patterns for form I and form II from the prepared crystals

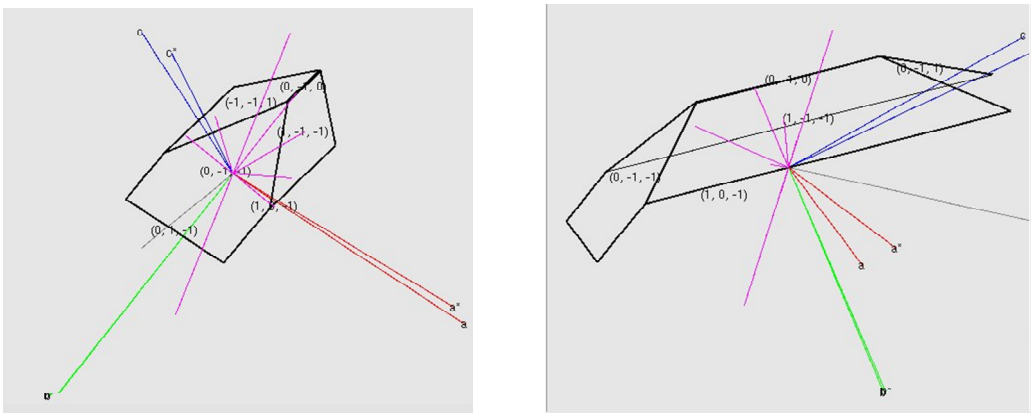

Figure 3-9: Single crystal- XRD (SXRD) facet analysis of paracetamol at two different orientations

3.6.3. Attenuated Total Reflection -IR

ATR-IR was utilised to test whether the prepared crystal had similar functional groups to those of powdered paracetamol. **Figure 3-10** shows the spectra of powdered paracetamol and of ground paracetamol obtained from acetone crystal, ethanol crystal and methanol crystal.

Table 3-2: Wave numbers of paracetamol (powder and ground crystal) functional groups

Functional group	Powder	AceGround	EtGround	MeGround
N-H (cm^{-1})	3312.93	3316.19	3318.58	3318.06
C-OH (cm^{-1})	3162.64	3162.44	3166.76	3158.51
N-C=O (cm^{-1})	1645.85	1649.96	1650.09	1649.84
C=C (cm^{-1})	1560.78	1562.88	1561.70	1562.07

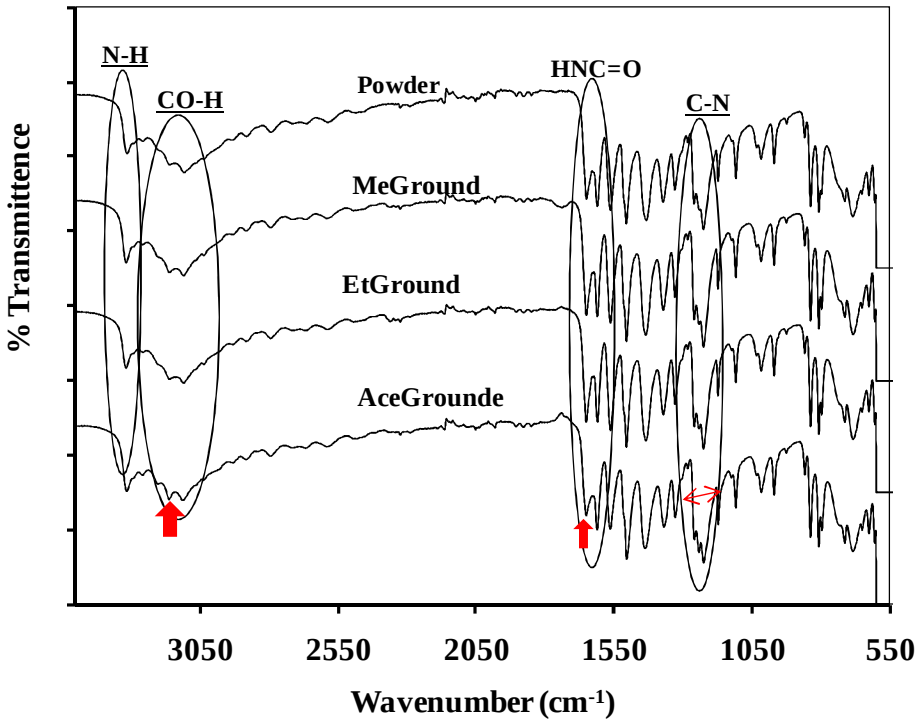

Figure 3-10: ATR-IR spectra of all the ground crystals and powder. AceGround-Single Crystal grown in acetone, MeSingle- Single Crystal grown in Methanol, EtSingle-single Crystal grown in Ethanol

The sharp absorption (**Table 3-2**) at the higher wavenumbers of 3312 cm^{-1} and 3162 cm^{-1} in all the spectra was due to the N-H amide group and the C-OH stretching group. The N-H and C-OH peaks of ground paracetamol crystals were more intense than those of the powdered form. The high intensity of the ground crystal C-OH peak is an indication of free hydroxyl groups in the molecules, while the broadness of the powdered paracetamol C-OH peak is characteristic of hydrogen bonds of paracetamol molecules. The high intensity of the asymmetric N-C=O peaks at 1650 and 1610 cm^{-1}, especially in EtGround and MeGround, reveals the interaction of paracetamol N-C=O and solvent molecules. The reduced intensity of the C=O peak of the ground acetone crystal was most probably caused by the C=O acetone dipole moment with the paracetamol solute. The prominent peaks at 1560 and 1510 cm^{-1} are characteristic of the aromatic C-C stretching bands of paracetamol. The C-N stretching band was detected at 1220 cm^{-1} and the methyl (CH_3) group of paracetamol was characterised by a vibration at 1432 cm^{-1}.

3.6.4. Paracetamol vapour pressure

XPS cannot be applied when the vapour pressure of a sample is high enough to cause significant sublimation under ultra-high vacuum conditions. The vapour pressure of paracetamol Form I increases from 2.2×10^{-5} Pa at a temperature of 40 °C to 0.0671 Pa at 74 °C, with an enthalpy of sublimation of 238.85 kJ/mol[9]. Form II was reported as thermodynamically unstable[10, 11]. XPS experiment on Form II were attempted but was failed due to the high vapour pressure of the solid and sublimation during analysis.

3.6.5. Paracetamol crystallisation with acetone, ethanol and methanol

The crystal habit results from the relative growth rates of parent molecule surfaces in different directions. Therefore, preferential growth inhibition of different crystal faces changes the shape of the crystal. The interaction between crystal surfaces and the solvent or impurities will result in variations of crystal habit[12]. Paracetamol crystals were prepared in three ways, using acetone, methanol and ethanol as solvents respectively. In each case, many attempts at crystallisation were made and similar habits were observed for all types of solvent used. Two habits were observed: pinacoidal and prismatic. The results (illustrated in **Figure 3-11**), indicate that the choice of solvents in the present work did not influence the paracetamol crystal habit.

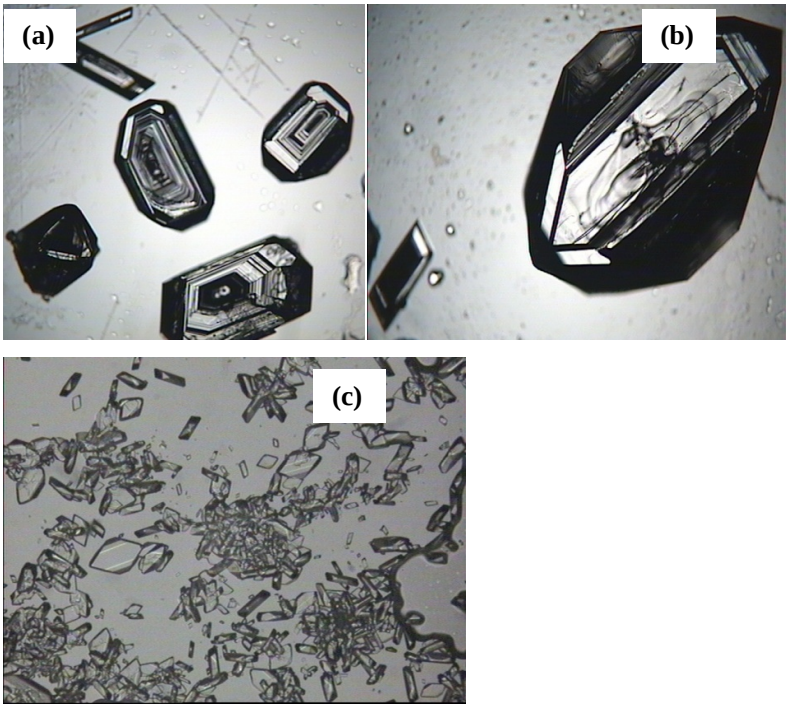

Figure 3-11: Crystal habit for crystals growth in three different solvents. (a) Crystal growth in acetone, (b) crystal growth in ethanol, (c) crystal growth in methanol

The selection of seed was very important for the final habit of the paracetamol single crystal. When a needle-shaped seed was chosen instead of a prismatic one, the resultant single crystal would have a pinacoidal habit, as shown in **Figure 3-11. Figure 3-12** shows an EtSingle sample with a diameter of 1.5 cm (a) and 1.0 cm (b).

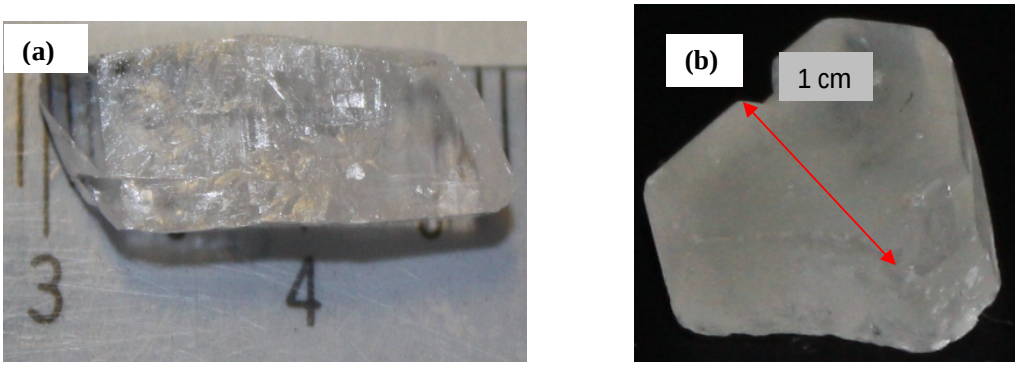

Figure 3-12: EtSingle. (a) Single crystal from needle seed (b) single crystal from prismatic seed

3.7. Conclusions

Paracetamol single crystals were successfully grown by slow crystallisation from acetone, ethanol and methanol solutions, using seed crystals and the slow evaporation technique. Paracetamol form II was prepared and characterised by PXRD analysis, as indicated by agreement of the diffraction pattern with CDS reference data. The monoclinic (form I) single crystal was characterised by single crystal PXRD, confirming that it had the same structural parameters as previously reported for its crystal structure. ATR-IR results support the PXRD findings, with very similar spectra for powdered paracetamol and ground crystals grown from acetone, ethanol and methanol solutions. The ATR-IR results revealed a broadened C-OH peak in powdered paracetamol, which is an indication of hydrogen bonds. The choice of solvent did not influence the paracetamol crystal habit.

3.8. References

1. Mullin, J. W., *Crystallization*. Fourth Edition ed.; Butterworth-Heineman: Oxford, 1993; p 610.

2. Nikolakakis, I.; Kachrimanis, K.; Malamataris, S., Relations between crystallisation conditions and micromeritic properties of ibuprofen. *Int. J. Pharm.* **2000,** 201, 79-88.

3. Getting Crystals Your Crystallographer Will Treasure. http://www2.chemistry.msu.edu/facilities/crystallography/xtalgrow.pdf

4. Heng, J. Y. Y.; Bismarck, A.; Williams, D. R., Anisotropic surface chemistry of crystalline pharmaceutical solids. *AAPS PharmSciTech* **2006,** 7, 84.

5. Granberg, R. A.; Rasmuson, A. C., Solubility of Paracetamol in Pure Solvents. *J. Chem. Eng. Data* **1999,** 44, (6), 1391-1395.

6. Mikhailenko, M. A., Growth of large single crystals of the orthorhombic paracetamol. *J. Cryst. Growth* **2004,** 265, 616-618.

7. Heng, J. Y. Y.; Williams, D. R., Wettability of paracetamol polymorphic forms I and II. *Langmuir* **2006,** 22, 6905-6909.

8. Heng, J. Y. Y.; Bismarck, A.; Lee, A. F.; Wilson, K.; Williams, D. R., Anisotropic surface energetics and Wettability of macroscopic form I paracetamol crystals. *Langmuir* **2006,** 22, 2760-2769.

9. D. Williams , D. W., R. Storey , P. Basford Vapour Pressure Determination of Pharmaceutical Powders. In *7th International Conference/Workshop on Pharmacy and Applied Physical Chemistry, University of Innbruck, Austraia, 2004*

10. Wang, S.-L.; Lin, S.-Y.; Wei, Y.-S., Transformation of Metastable Forms of Acetaminophen Studied by Thermal Fourier Transform Infrared (FT-IR) Microspectroscopy. *Chem. Pharmaceut. Bull.* **2002,** 50, 153-156.

11. Sacchetti, M., Thermodynamic analysis of DSC data for acetaminophen polymorphs. *J Therm. Anal. Calorim.* **2001,** 63, 345-350.

12. C.Stoica; Verwer, P.; H.Meekes; Van-Hoof, P. J. C. M.; Kasperson, F. M.; E.Vlieg, Understanding the effect of Solvent on the Crystal Habit. *Cryst. Growth Des.* **2004,** 4, 765-768.

CHAPTER 4: POLOXAMER CHARACTERISATION

4.1. Objectives

The objectives of the works described in this chapter were:

i) To analyse surface degradation of three different composition of Poloxamers using X-ray Photoelectron Spectroscopy (XPS)

ii) To differentiate the surface composition of three different Poloxamers composition using XPS.

4.2. Introduction

Effective tableting or compaction of pure drugs or active pharmaceutical ingredients may require the inclusion of excipients in the formulations. An excipient is an inactive ingredient that often helps to bind a dose of API. Other excipients may improve bioavailability, release or stability of a drug. Excipients in drug formulations are normally inert materials. However, polymer excipients can initiate, propagate or participate in chemical or physical interactions with the drugs. In the case of chemical interaction this may lead to the degradation of the API and so reduce the amount available for therapeutic effect or compromise the safety of the medication, while physical interaction may affect the rate of dissolution, uniformity of dose or ease of administration of the drug[1].

Nonionic surfactants with polyoxyalkane chains are often used as excipients even though they are quite sensitive to autoxidation[2]. The autoxidation process leads to the formation of hydroperoxides and free radicals, which are responsible for the degradation and ageing of pharmaceutical formulations. Poly(ethylene oxide)-poly(propylene oxide)-poly(ethylene oxide) triblock copolymers of the ABA type, often denoted PEO-PPO-PEO or $(EO)_a(PO)_b(EO)_a$ and commercially known as Poloxamers, Pluronics or Synpronics, are nonionic macromolecular surface active agents[3] with *a* and *b* are Poloxamers repetition units.

Poloxamers differ from classic many other surfactants through their molar mass, which ranges from 1000 to 15,000, whereas other commonly used surfactants often have lower molar masses. The chemical structure of poloxamers consists of two different blocks of ethylene oxide (EO) and propylene oxide (PO) (**Figure 4-1**).

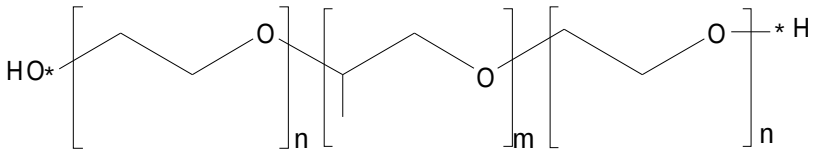

Figure 4-1: Chemical structure of poloxamers (m and n are the Poloxamers repetition unit)

The two outer blocks are the same size, synthesised from ethylene oxide, monomer and constitute the hydrophilic components of the molecule, while the inner block is constructed from propylene oxide, and represents the hydrophobic moiety[4]. The sizes of the blocks are varied to provide the molecule with a range of surface activity.

Poly(oxyethylene), EO, is very sensitive to photoxidation, as it can absorb radiation with wavelengths below 300 nm. Its degradation can be initiated particularly by chromophoric impurities which absorb UV light and produce radicals[5]. The presence of oxygen in the polyethylene oxide, EO, facilitates autoxidation of EO. The EO chain undergoes oxidation more rapidly than poly(oxypropylene), PO. EO degradation starts with the formation of radicals by hydrogen abstraction on the polymeric backbone,[5] then the reaction of these free radicals with oxygen produces peroxy radicals or hydroperoxides at the α-carbon atoms of ethylene chains [2, 5]. EO chains degrade to low molecular weight products [2]. It has been shown[2, 5] that the main mainly C-cleavage of poloxamers takes place. In response to their high sensitivity to autoxidation, poloxamer manufacturers add butylated hydroxytoluene (BHT) as an antioxidant. The BHT concentration in the formulation varies from one poloxamer product to another, so the rate of poloxamer degradation varies as a function of BHT concentration [1].

Poloxamer thermoxidation studies showed that PO blocks were thermally less stable than EO blocks, due to the rapid formation of radicals on the tertiary carbon of PO [2]. The thermoxidation of PO at 125 °C resulted in the formation of acetate, formate and ketone chain ends from the decomposition of hydroperoxides formed on the backbone during oxidation [1]. Other studies using the MALDI-TOF technique have shown that at 155 °C the thermoxidation pathways of PO were at the secondary alkoxy radical [2, 6]. An NMR study at 150 °C showed that the oxidation of EO blocks produced formate end groups through intramolecular decomposition and esterification of hydroxyl chain ends,

while the PO tertiary alkoxy radical was predominant at the beginning of the polymer breakdown [7]. The chain breaking stages of thermoxidation were β-scission and cage reactions [8]. The thermoxidation product was confirmed as acetaldehyde, which was oxidised to acetic acid. The acetic acid then esterified 1,2-propanediol, 2 formate into 1,2-propanediol, 1-acetate, 2 formate. PO exposed to radiolysis revealed the formation of CO and OH groups on the polymer chains [1, 9]. It has been shown that the radiolysis of ethylene-propylene copolymers caused the rupture of C-C bonds and the formation of primary radicals [10].

To date, no XPS study of poloxamer degradation has been carried out. Also, the NIST binding energy data applies only to poly(ethylene oxide) and poly(propylene glycol) as separate species, so no data on the pure copolymer has been recorded in the XPS database. Before analysing paracetamol/poloxamer formulations an XPS study of poloxamers and their degradation was undertaken.

4.3. Experimental

Poloxamer samples Poloxamer188 (P188), Poloxamer338 (P338) and Poloxamer407 (P407) were obtained from two main sources. Aged samples (analysis after 24 months storage in the laboratory) were obtained from Sanofi and their properties were not found due to the lost of MSDS. These samples had been stored in transparent glass containers. The other set of samples were freshly obtained from BASF and stored in opaque plastic containers in a dark place, thus having no exposure to light. Samples analysed were:

i) Three aged samples, P188, P338 and P407 aged after 24 months stored. No notes had been found stated the manufacturing date of the sample. 24 months was duration of the sample delivered from the manufacturer.

ii) Three fresh samples, P188, P338 and P407 freshly from supplier and stored as advised by MSDS sheet. No data of manufacturing date was found.

As mentioned above, poloxamers degrade in air; therefore, in the manufacturing process an antioxidant, BHT, had been added. The concentration of BHT in each of the fresh poloxamer samples was as presented in **Table 4-1** according to the MSDS from BASF.

Table 4-1: Butylated hydroxytoluene content in poloxamers 188, 338 and 407

Poloxamers	BHT (ppm)
P188	100
P338	100
P407	82.4

The samples were used as provided by the supplier. During the XPS mounting, samples were spread on double-sided tape and care was taken to ensure that poloxamer particles covered the tape entirely. Exposure of the samples to the laboratory ambient conditions before analysis was minimised to within approximately 10 minutes. The chemical structures and formulas of all the poloxamers used are illustrated in **Figure 4-2**. P188 and P338 had the same percentage of EO block (80%) but different molecular weights (MW) of PO block.

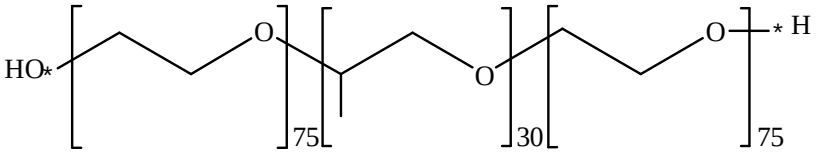

Poloxamer 188

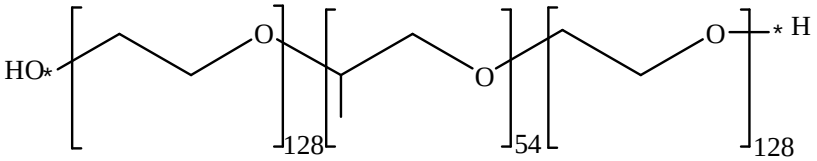

Poloxamer 338

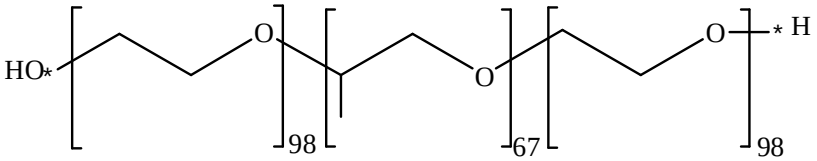

Poloxamer 407

Figure 4-2: Chemical structure of the poloxamers used in this study.

From **Figure 4-2**, the ratio of EO to PO block of P188 and P338 is approximately similar; 5.00 and 4.74 respectively while P407 has lowest value of 2.93. The ratio indicated that P407 had the highest PO segment to EO, while P338 had the lowest PO content relative to EO.

4.4. Results and Discussion

4.4.1. ATR-IR

The initial interest of the Poloxamers degradation analysis was IR comparison of fresh and aged P188 (≥ 3 years after manufacturing). The existence of a C=O peak at 1738.03 cm^{-1} from aged P188 indicated that degradation had taken place. P188 chemical structure reveals no C=O bond, as shown in **Figure 4-3**.

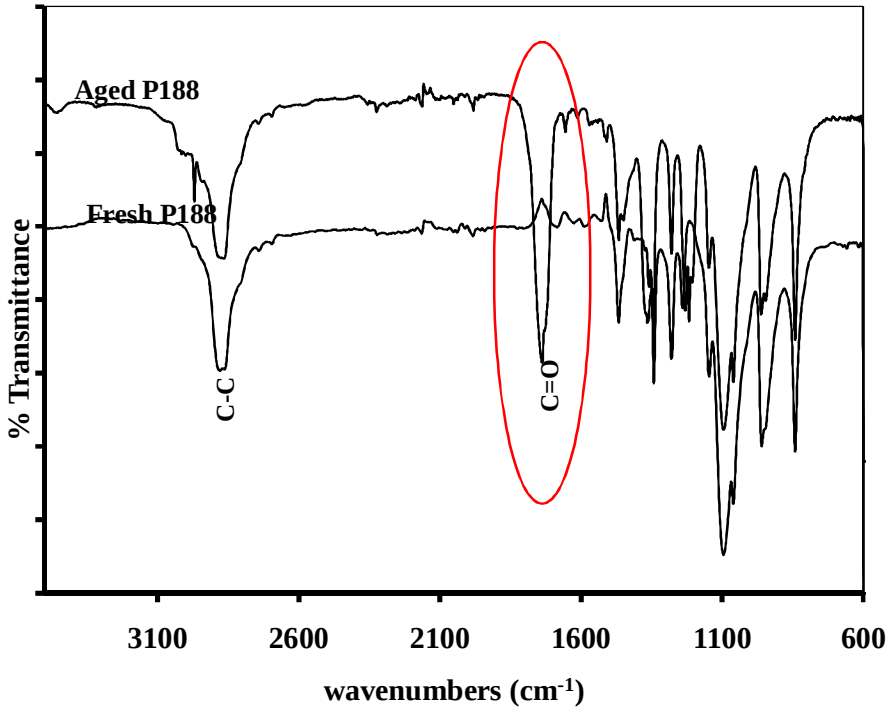

Figure 4-3: Comparison spectra of aged and fresh P188. Red circle reveals the C=O peak from aged P188.

4.4.2. Survey Spectra

Survey XPS spectra of all poloxamers are shown in **Figure 4-4**, illustrating the C 1s and O 1s photoelectron lines. Analysis of the emission intensities in the survey (**Table 4-2**) revealed that the C 1s intensities were higher than expected from the poloxamer stoichiometry, while O 1s concentrations were lower than expected. The existence of a

C=O peak in the analysis of C 1s high resolution data **(see section 4.4.4**) indicated that the deviations in carbon and oxygen content in the survey spectra stemmed from the formation of oxidised degradation products.

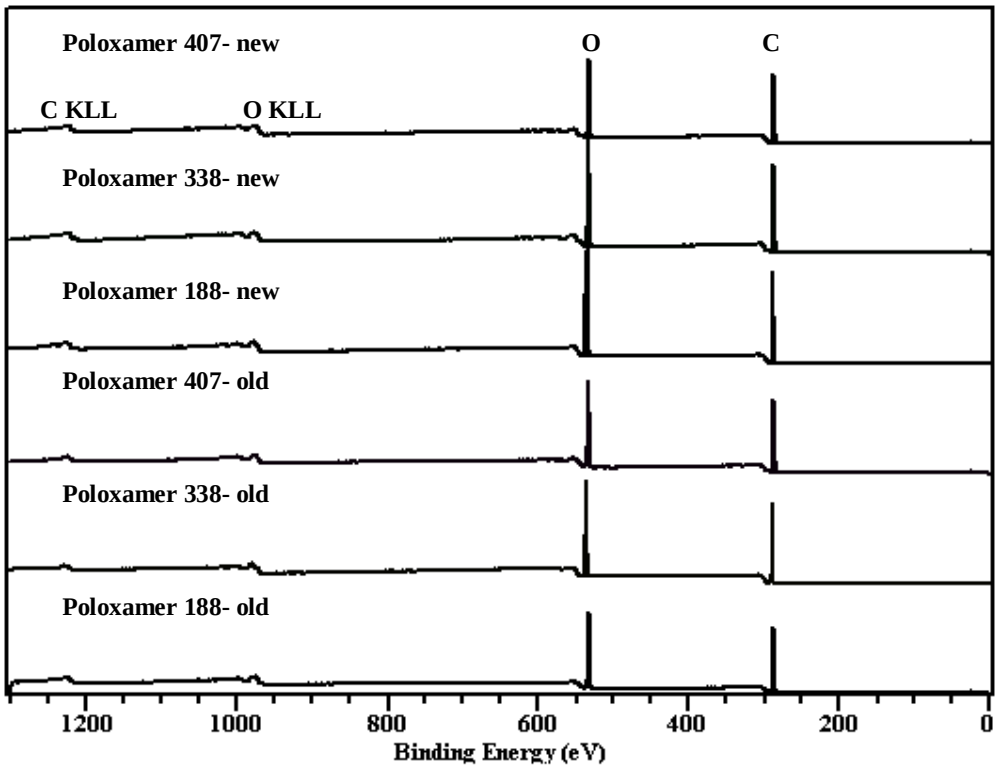

Figure 4-4: Survey spectra of analysed Poloxamers

In line with this, after the carbonyl percentage from high resolution analysis had been subtracted from the carbon and added to the oxygen composition in the survey spectra, the carbon and oxygen composition data were much more in line with the expected stoichiometry (**Table 4-2**). Significantly, removal of the C=O contribution allows distinguishing between the stoichiometries of P188, P338 and P407, especially for the fresh poloxamers.

Table 4-2: Stoichiometrically expected and experimental elemental composition of P188, P338 and P407 including removal of C=O contamination specified in the C 1s high resolution data

Types & age of Poloxamers	C(%)	O(%)	C(%) Removing C=O	O% Removing C=O
$P188_{calculated}$	68.4	31.6	-	-
$P188aged_{exp}$	71.7	28.3	68.4	31.6
$P188fresh_{exp}$	71.6	28.4	69.5	30.5
$P338_{calculated}$	68.5	31.5	-	-
$P338aged_{exp}$	72.3	27.9	70.3	29.7
$P338fresh_{exp}$	72.1	27.9	69.7	30.3
$P407_{calculated}$	69.3	30.7	-	-
$P407aged_{exp}$	73.0	27.0	69.9	30.1
$P407fresh_{exp}$	73.2	26.8	71.9	28.1

4.4.3. High Resolution C 1s and O 1s analysis without C=O

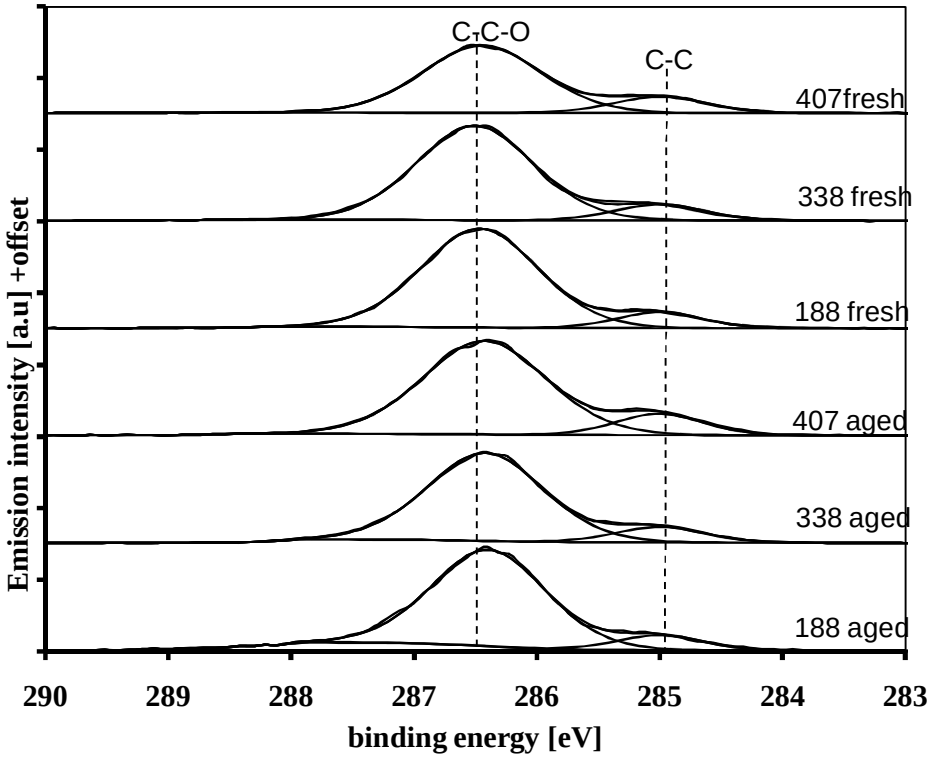

Figure 4-5: C1s spectra of Poloxamers fitting without fixing C=O groups.

In the C 1s spectra (**Figure 4-5**), C-C-O units were found between 286.4 and 286.6 eV, while C-C contributions were found between 285 and 285.2 eV. The results (**Table 4-3**) were in agreement with the presence of EO segments; the C-C-O E_B was at 286.4 eV, and the PO contribution was clearly visible through emission from a C-C environment.

Table 4-3: Calculated, experimental, binding energy and FWHM data for C-C-O and C-C environments fitted without C=O for all aged and fresh poloxamers

Types of Poloxamers	Atomic Concentration	Atomic Concentration		Binding Energy [eV]			
	$[C\text{-}C]_{cal}$%	$[C\text{-}C]_{exp}$ %		C-C		FWHM	
		Aged	Fresh	Aged	Fresh	Aged	Fresh
Poloxamer188	14.3	10.1	10.3	285.0	285.0	0.8	0.8
Poloxamer338	14.8	12.1	11.4	285.0	285.0	0.8	0.9
Poloxamer407	20.3	13.8	16.1	285.0	285.0	0.8	0.9
	$[C\text{-}C\text{-}O]_{cal.}$ %	$[C\text{-}C\text{-}O]_{exp}$ %		C-C-O [eV]		FWHM	
		Aged	Fresh	Aged	Fresh	Aged	Fresh
Poloxamer188	85.7	89.9	89.7	286.4	286.5	1.1	1.1
Poloxamer338	85.2	87.9	88.6	286.4	286.5	1.1	1.1
Poloxamer407	79.7	86.2	83.9	286.4	286.5	1.2	1.1

Table 4-3 shows the concentration of all the C 1s poloxamers in comparison with the expected concentrations, indicating that all the aged poloxamers (P188, P338 and P407) had enhanced concentrations of C-C-O, while the C-C concentration were too low. It has been stated that exposure of chain termination leads to the formation of more C-C-O chains at the surface. Previous reports suggest that the aged poloxamer samples were prone to coupling termination of radicals, rather than disproportionation termination [5, 11].

A similar phenomenon was detected in the fresh poloxamer C-C and C-C-O chains. This result, in agreement with a previous study [5, 7, 12-15] shows that there was chain scission of the C-C chain and formation of the alkoxy radical from natural degradation, allowing the fixing of the oxygen to another polymeric chain after the abstraction of hydrogen for the radical reaction and further oxidation, yielding aldehyde or ketone, or ester end group compounds. The bond dissociation energies associated with these bonds (C-C-O and C-C) are approximately at 360 kJ/mol and 347 kJ/mol respectively [1]. It is indicated dissociation of C-C-O bond needs higher energy than C-C which reveals to

bond breaking the C-C-O is harder than C-C. Concurrent with results, C-C-O was high concentration on the surface distinguish with C-C. No significance difference reveals on the binding energy of all the samples.

The greatest difference between expected results and experimental data **(Table 4-3**) for C-C and C-C-O environments was found in both aged and fresh samples of P407, while the smallest differences were found in aged and fresh P338. This can be explained by the higher PO molecular weight of P407, influencing the rate of degradation. At low temperature, the PO block would degrade faster than the EO block,[1, 16] because of the greater radical formation at tertiary carbon as opposed to secondary carbon. On top, P407 (**Table 4-3**) showed the greatest difference between calculated and experimental results, due to its lower BHT content (see **Table 4-1**). These results were in agreement with a previous study which found that poloxamers with lower BHT content degraded faster [1].

4.4.4. High resolution C 1s and O 1s analysis with C=O fitted

The analysis reported in this section will be divided into three sub-sections. First, comparison between fresh and aged Poloxamers based mainly on C 1s data will be carried out. Then the relationship between C=O (C 1s) related to O-H (O 1s) binding energy and composition concentration will be analysed, distinguishing between aged and fresh Poloxamers through O 1s data. Finally, a possible degradation mechanism compatible with the obtained data will be suggested.

Table 4-4: Binding energy (eV) and atomic concentration percent of the poloxamers for the C 1s peak components with C=O fitted

C environment	$P188_{aged}$	$P188_{fresh}$	$P338_{aged}$	$P338_{fresh}$	$P407_{aged}$	$P407_{fresh}$
$C\text{-}C\text{-}O_{expected}$	(286.1-286.8) eV Mean: 286.4 eV					
$C\text{-}C\text{-}O_{exp.}$ [eV]	286.4	286.5	286.4	286.5	286.5	286.5
[C-C-O]%	86.6	85.6	82.5	84.5	79.3	80.0
$C\text{-}C_{expected}$	(285.0-285.2) eV Mean: 285.1 eV					
$C\text{-}C_{exp.}$[eV]	285.0	285.1	285.1	285.1	285.1	285.1
[C-C]%	9.1	12.2	13.8	13.3	17.4	18.4
$C{=}O_{expected}$	(286.9- 291.7) eV Mean: 289.3 eV					
$C{=}O_{exp}$[eV]	288.1	287.8	287.8	287.8	287.8	287.9
[C=O]%	4.3	2.2	3.7	2.2	3.3	1.6

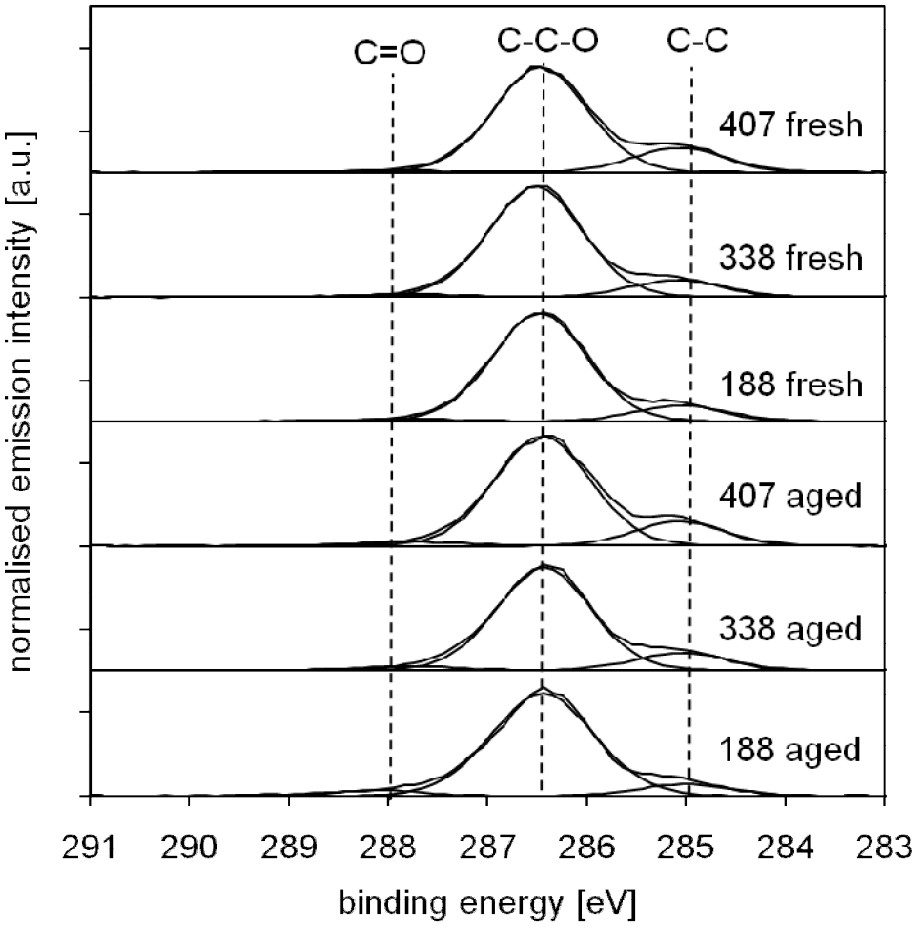

Figure 4-6: Poloxamers C 1s spectra representing XPS fitting with C=O group

Table 4-4 gives the C1s binding energy data for all poloxamers detected by XPS, analysed by CasaXPS with C=O fitting, while **Figure 4-6 and 4-7** (C=O peaks) represent the C=O peak. The data reveal that all C-C-O and C-C E_B values were similar and in the range expected and reported in the literature. The C 1s emission from all poloxamers indicated the existence of C=O species (**Table 4-4**) at a binding energy ranging from 287.8 eV to 288.1 eV. The binding energy of 287.5 to 287.9 eV (**Table 4-4**) is related to the carbon environment of several compounds such as formaldehyde, acetaldehyde, formate or alcohol ketone polymer. The peaks support the effect of formaldehyde or acetaldehyde or ketone on the degradation of poloxamers. However, other analysis is needed to certain weather aldehyde or ketone was detected due to the weakness of XPS in detected hydrogen atomic concentration.

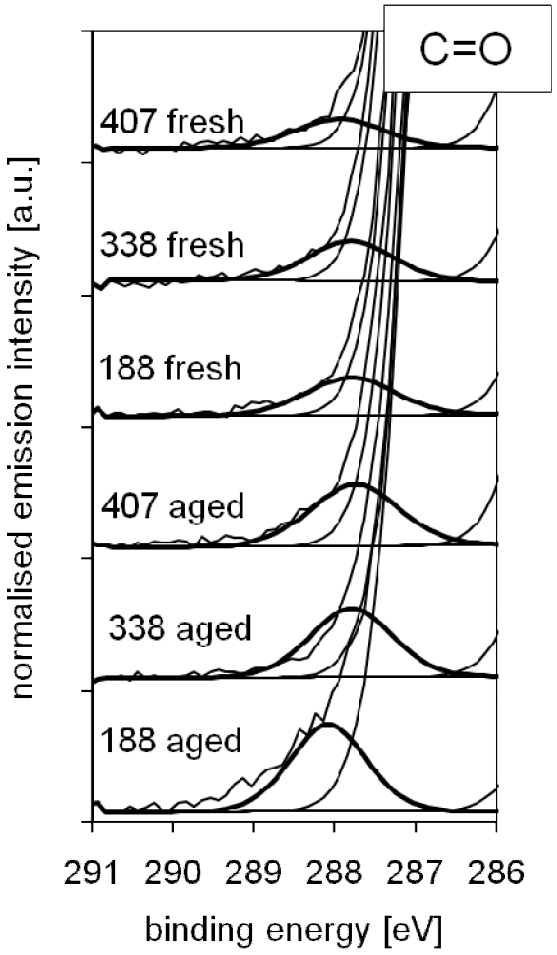

Figure 4-7: C=O emission intensity peak from high resolution C1s Poloxamers

The aged P338 and P407 samples, with C=O E_B values at 287.8 eV (**Table 4-4**), had pronounced formaldehyde, acetaldehyde, hemiacetal or ketone peaks. In some studies, acid formation has been found on the degradation of EO or PO blocks [1, 13, 17]. The absence of a C-OOH peak above 288.5 eV [18] indicates that no carboxylic group of formic acid was detected on the surface of any poloxamer samples.

Analysis of the aged samples of P188 showed a chemical shift of C=O towards a higher binding energy of 288.1 eV compared to fresh P188 at 287.8 eV. The difference (0.3 eV) was significant. The 288 eV peak also appeared clearly in previous PO block analysis [12, 13] (the analysis was only on Poly (propyleneoxide, PPO) but to date, no explanation of the peak has been reported. The O-H peak in the O 1s environment was detected at 534 eV (**Table 4-5**). The high O-H (water) concentration of O 1s (**Table 4-5**) of aged P188 distinguishes it from other poloxamers and may cause the existing

formaldehyde to react with water molecules to form a new chain of poly(oxymethylene) glycol (**Figure 4-8**), for which a peak was detected at 288.1 eV of aged P188.

However, C=O (C1s, **Table 4-4**) concentration of fresh P188 was not reveals significance different with fresh P338, while O-H concentration (O1s, **Table 4-5**) of P188 reveals the lowest value among all the fresh poloxamers. The highest O-H concentration of fresh Poloxamers was P407 and P338. Both P407 and P338 have high PO percent. The explanation is that the PO (particularly on fresh P407) block was actively degraded at the initial stage, then after some time the EO (referred to aged P188) block was more actively degraded, with the absorption of moisture from the environment [1].

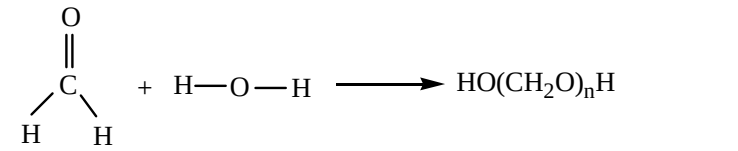

Figure 4-8: Chemical reaction of formaldehyde and water to produce poly (oxymethylene) glycol

Table 4-5: Binding energy (eV) and atomic concentration (%) for the O 1s peak components of the poloxamers

O environment	**P188$_{aged}$**	**P188$_{fresh}$**	**P338$_{aged}$**	**P338$_{fresh}$**	**P407$_{aged}$**	**P407$_{fresh}$**
C-C-O$_{expected}$	(532.5-532.8) eV					
C-C-O$_{exp}$	532.7	532.6	532.7	532.8	532.8	532.7
[C-C-O]	88.5	96.3	93.1	94.8	90.4	95.3
O-H$_{expected}$	(533-535) eV					
O-H$_{exp}$	534.3	534.7	534.2	534.3	534.2	534.2
[O-H]	7.6	1.2	3.2	2.7	6.0	2.7
C=O$_{expected}$	(532.3-532.4) eV					
C=O$_{exp.}$[eV]	532.4	532.1	532.4	532.4	532.4	532.3
[C=O]	4.0	2.5	3.7	2.5	3.6	2.0

Table 4-5 presents the data of O 1s fitting with the O-H peak. The asymmetrical tailing in the O 1s spectra (**Figure 4.9**) of all samples at both ends of the spectra needs fitting to support the existence of C=O and a suggested O-H peak. Peaks of both C=O

and O-H were detected, at 532.1 to 532.4 eV and at 534.1 to 534.7 eV. The ether O peak of the poloxamers was defined between 532.4 and 532.8 eV. Among aged samples, the O-H concentration was highest for P188 and lowest for P338. The difference in PO block concentration between aged P188 and aged P338 had an effect on the O-H concentration. Interestingly, aged P407 was found to have a higher concentration of O-H than aged P338. The most probable explanation for the high O-H concentration in high MW poloxamers (P407) is the active neutralisation of the PO hydroperoxide charged at tertiary carbon by a proton-forming tert-alcohol [12].

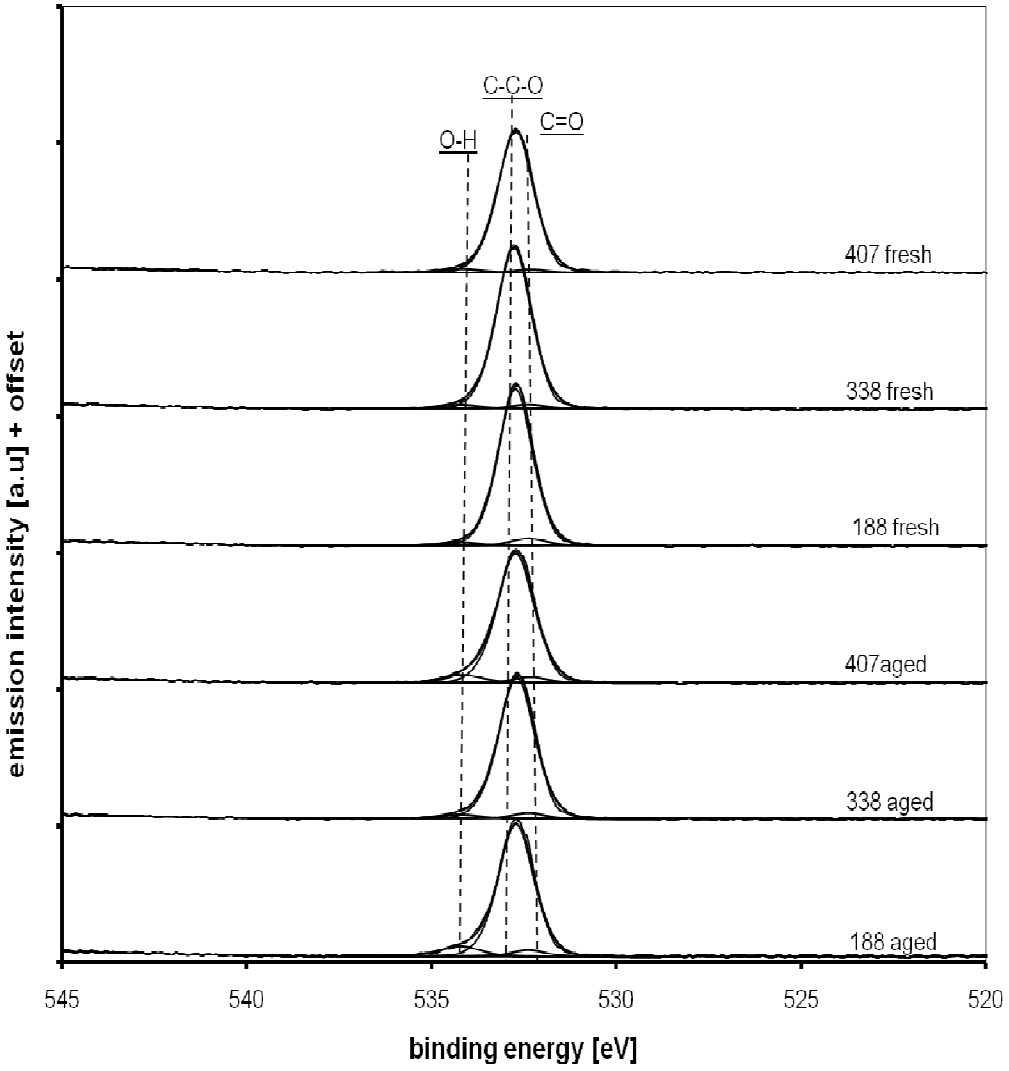

Figure 4-9: O1s spectra for all analysed Poloxamers

It is evident that radical formation over a period of two years had degraded P188, P338 and P407 by autoxidation or photoxidation to produce such impurities as esters,

aldehydes, ketones and water[17, 19]. As indicated above, the formation of poloxamer radicals may have been initiated by the presence of oxygen, heat, pressure or a catalyst that had been used during a previous experiment. The abstraction of hydrogen from EO or PO blocks produces hydroperoxide. As suggested previously,[1,5,14,16] tertiary hydroperoxide is prone to be formed on the PO block, while secondary hydroperoxide would form on the EO block. Decomposition of the hydroperoxides produces alkoxy and hydroxyl radicals, formed on both EO and PO blocks. With time, alkoxy radicals lead to the formation of more hydroperoxide from both blocks. The formation of C=O (**Table 4-4**) at 287.5 eV to 288.1 eV results from the breaking of peroxy chains. These chains can be cleaved through β-scission in several ways to produce aldehyde, ketone and alkoxy radicals. It is evidence that the O 1s spectra of all aged poloxamers had been shifted to a higher binding energy. C-O-C and O-H peaks were higher in aged than fresh samples. Spectrum tailing indicated the O-H environment. **Figure 4-10 and 4-11** show the mechanisms of radical formation and chain scission for EO and PO blocks proposed by several studies [1,5,7,14,16,17].

A: **General Poloxamer chemical formula**

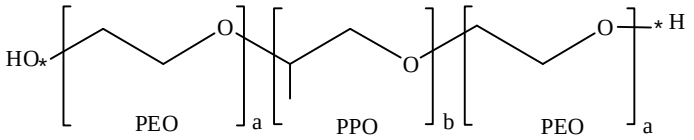

B: **EO radical degradation mechanism**

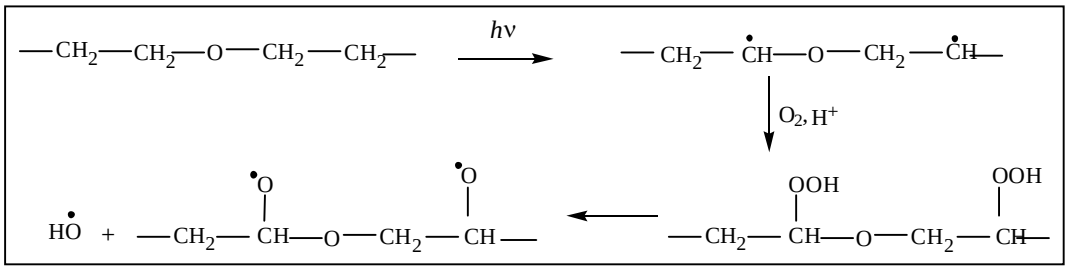

C: **PO radical degradation mechanism**

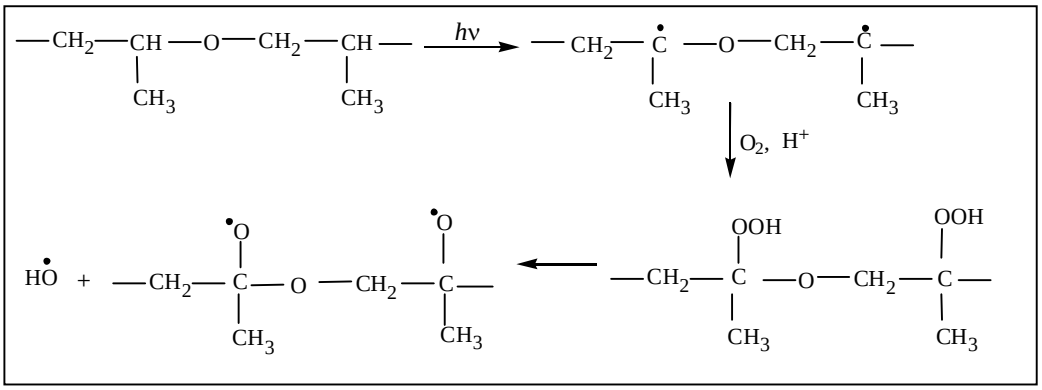

Figure 4-10: Polyoxyethylene (EO) and Polyoxypropylene (PO) block degradation mechanism

4.5. Conclusions

The XP spectra of aged and fresh poloxamers of three different types have been investigated. The stoichiometry of each type of poloxamer could be determined from a combination of survey and high resolution analysis. During ageing, oxidative degradation leads to the formation of carbonyl functional groups and absorption of moisture from the environment leads to the formation of water on the polymer surface. The concentration of C=O and water content was related with the Poloxamers EO and PO percent. It is also evident that the BHT concentration influences the rate of Poloxamers degradation.

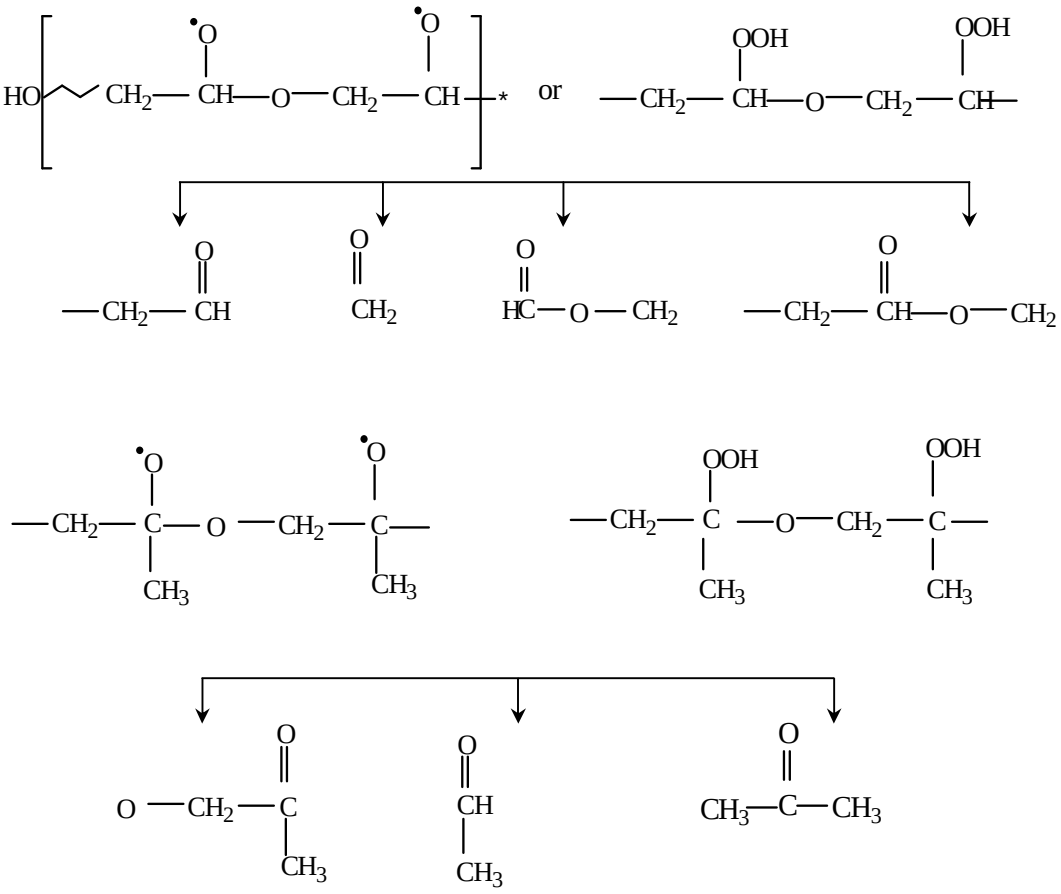

Figure 4-11: Scissions of Polyoxyethylene (EO) and Polyoxypropylene (PO) block radicals

4.6. References

1. Erlandsson, B., Stability-indicating changes in poloxamers: the degradation of ethylene oxide-propylene oxide block copolymers at 25 and 40 °C. *Polymer degradation and stability* **2002,** 78, (3), 571.

2. Gallet, G.; Carroccio, S.; Rizzarelli, P.; Karlsson, S., Thermal degradation of poly(ethylene oxide-propylene oxide-ethylene oxide) triblock copolymer: comparative study by SEC/NMR, SEC/MALDI-TOF-MS and SPME/GC-MS. *Polymer* **2002,** 43, (4), 1081-1094.

3. Alexandridis, P.; Alan Hatton, T., Poly(ethylene oxide)---poly(propylene oxide)---poly(ethylene oxide) block copolymer surfactants in aqueous solutions and at interfaces: thermodynamics, structure, dynamics, and modeling. *Colloids and Surfaces A: Physicochemical and Engineering Aspects* **1995,** 96, (1-2), 1-46.

4. Dong, J.; Chowdhry, B. Z.; Leharne, S. A., The relationship between the surface activity of poly(ethylene oxide)-poly(propylene oxide)-poly(ethylene oxide) triblock copolymers and molecular composition. *Colloids and Surfaces A: Physicochemical and Engineering Aspects* **2006,** 277, (1-3), 249-254.

5. Morlat, S.; Gardette, J.-L., Phototransformation of water-soluble polymers. I: photo- and thermooxidation of poly(ethylene oxide) in solid state. *Polymer* **2001,** 42, (14), 6071-6079.

6. Barton, Z., Mass spectral characterization of the thermal degradation of poly (propylene oxide) by electrospray and matrix-assisted laser desorption ionization. *Polymer* **1995,** 36, (26), 4927.

7. Yang, L.; Heatley, F.; Blease, T. G.; Thompson, R. I. G., A study of the mechanism of the oxidative thermal degradation of poly(ethylene oxide) and poly(propylene oxide) using 1H- and 13C-NMR. *European Polymer Journal* **1996,** 32, (5), 535-547.

8. Posada, F.; Malfreyt, P.; Gardette, J. L., Hydrogen abstraction from poly(propylene) and poly(propylene oxide) by hydroxyl radicals: a computational quantum semi-empirical study. *Computational and Theoretical Polymer Science* **2001,** 11, (2), 95-104.

9. G. P. Roberts, M. B. M. D., Radiation chemistry of poly(propylene oxide). *Journal of Polymer Science Part A-2: Polymer Physics* **1971,** 9, (10), 1729-1745.

10. Kabamba, M. S., Mechanisms of chain scission and the role of oxidation products in the oxidative radiolysis of ethylenepropylene copolymer. *Journal of radioanalytical and nuclear chemistry* **1988,** 126, (3), 211.

11. Fessenden, R. J.; Fessenden, J. S.; Logue, M. W., *Organic chemistry*. Brooks/Cole Publishing Co.: Pacific Grove, CA, 1998.

12. Massey, S.; Roy, D.; Adnot, A., Study of natural ageing of polypropylene by X-ray photoelectron spectroscopy. *Nuclear Instruments and Methods in Physics Research Section B: Beam Interactions with Materials and Atoms* **2003,** 208, 236-241.

13. Rjeb, A.; Letarte, S.; Tajounte, L.; El Idrissi, M. C.; Adnot, A.; Roy, D.; Claire, Y.; Kaloustian, J., Polypropylene natural aging studied by X-ray photoelectron spectroscopy. *Journal of Electron Spectroscopy and Related Phenomena* **2000,** 107, (3), 221-230.

14. Griffiths, P. J. F., The autoxidation of poly(propylene oxide)s. *European polymer journal* **1993,** 29, (2-3), 437-442.

15. de Sainte Claire, P., Degradation of PEO in the Solid State: A Theoretical Kinetic Model. *Macromolecules* **2009,** 42, (10), 3469-3482.

16. Gallet, G., Thermal oxidation of poly (ethylene oxide-propylene oxide-ethylene oxide) triblock copolymer: focus on low molecular weight degradation products. *Polymer degradation and stability* **2002,** 77, (1), 55.

17. Hassouna, F.; Morlat-Thérias, S.; Mailhot, G.; Gardette, J. L., Influence of water on the photodegradation of poly(ethylene oxide). *Polymer Degradation and Stability* **2007,** 92, (11), 2042-2050.

18. Briggs, G. B. a. D., *The XPS of Polymers Database*. Surface Spectra Ltd.: Manchester, 2000.

19. Forshed, J.; Erlandsson, B.; Jacobsson, S. P., Quantification of aldehyde impurities in poloxamer by 1H NMR spectrometry. *Analytica Chimica Acta* **2005,** 552, (1-2), 160-165.

CHAPTER 5: POLYCRYSTALLINE PARACETAMOL CHARACTERISATION

5.1. Objectives

The objective of this chapter is to examine the possibility to detect differences in local interactions within different forms of paracetamol by core level spectroscopy.

5.2. Introduction

X-ray photoelectron spectroscopy (XPS) is a well-established technique for elemental analysis at surface and for the determination of the chemical state of atoms at surfaces. The technique has been used extensively for surface science studies of single crystal surfaces, adsorbed molecules and thin films, including studies of their growth and of surface reactions.[1] Over the last decade or so the technique has also been established in studies of biomaterials,[2-5] where it has proved useful especially for the determination of thin films and overlayers of functionalised organic moieties anchored at surfaces.

In the context of pharmaceutical research XPS has mostly been used in studies of controlled release drug delivery systems, especially in the context of active pharmaceutical ingredient (API) absorption and adsorption on drug delivery carrier materials, including particulates[6-17] and films[18-22]. Already in 1991 Buckton introduced the idea to correlate XPS–determined surface chemical compositions with the wettability of API surfaces ,[23] but this experimental approach was subsequently taken up only 15 years later, in studies addressing the crystal facet anisotropy of wetting behavior [24-26] and the wetting of polycrystalline powder samples [27-29]. Very recently, the technique has also been applied to detect free base segregation at the surfaces of an API salt powder[30] because the free base layer impacted on the flowability of the milled drug. The ability of XPS to sensitively probe inter- and intramolecular proton transfer in organic solids can be applied to distinguish between salts and co-crystals of APIs with a nitrogen proton-acceptor group [31-33], establishing the technique as complementary to X-ray diffraction and solid state NMR characterization of proton transfer.

While proton transfer leads to sizable chemical shifts in high resolution XP spectra, it is currently not clear whether XPS is also sensitive to more subtle variations in local structure in molecular organic solids, for example due to polymorphism, disorder or crystal facet specific termination effects. In the absence of strong electronic interactions

due to, e.g., inter- or intramolecular π-π interactions or electron transfer, the expected effects on the core level binding energies probed by XPS should be small, because the cohesive energy of molecular crystals derives typically from relatively weak dipole, van der Waals and London interactions. However, no systematic studies of their effects have been performed. In the following the issue is directly addressed through a study of a number of polycrystalline paracetamol samples that were obtained by different preparations routes. They include commercial Form I paracetamol powder, a different polymorphic form (Form III) of paracetamol, and various quench-cooled melts and ball-milled paracetamol samples with varying degrees of disorder. Paracetamol was chosen because it represents one of the few compounds for which literature data already exist.[26]

5.3. Experimental Section

5.3.1. Materials

Seven paracetamol powder and blends were prepared for the comparative analysis.

i) Untreated paracetamol powder (Form I), as received from Sigma Aldrich, UK.

ii) Ground paracetamol obtained by grinding material i) using a mortar and pestle.

iii) Milled paracetamol, obtained by milling i) in a Retsch MM200 mixer mill at a rate of 30 Hz, using 5 mL stainless steel jars, each containing one 7 mm diameter stainless steel ball mill. The milling time was 5 min.

iv) A liquid nitrogen (LN2) quench-cooled melt of paracetamol [34-36]. Powdered paracetamol i) was melted in an aluminium foil envelope and immediately immersed in liquid nitrogen (LN2).

v) 5 min milled LN2-quench-cooled paracetamol, obtained by milling an aliquot of sample iv) in a Retsch MM200 mixer mill at a rate of 30 Hz, using 5 mL stainless steel jars, each containing one 7 mm diameter stainless steel ball mill.

vi) 15 min milled LN2-quench-cooled paracetamol, obtained by milling an aliquot of sample iv) in the same way as v).

vii) Glassy paracetamol obtained through a DSC heat-cool cycles (see section on DSC results below) performed under a flow of N_2 gas.

Besides XPS characterization all the above samples were investigated by PXRD and DSC. Due to the difficulties of obtaining sufficient sample from the small pans used in DSC, no characterisation of the DSC-derived sample vii) by ATR-IR could be performed.

5.3.2. X-ray Powder Diffraction (PXRD)

PXRD reference patterns of untreated paracteamol and aged samples were collected on a PANalytical X'Pert Pro Multipurpose Diffractometer (MPD) in transmission Bragg-Brentano geometry with a Cu anode operating at a power of 1.6 kW (40 kV, 40 mA). Polycrystalline samples were mounted as received on XRF grade Mylar film and rotated at 0.5 Hz. The incident beam was conditioned with a focusing mirror, 0.04 rad Soller slits and a 0.5° antiscatter slit. The diffracted beam passed through 0.04 rad Soller slits and 0.5° antiscatter slit before entering the PIXcel detector operating in scanning mode with an effective step size of 0.013° between data points and a dwell time of 18.69 s per data point.

PXRD patterns of solidified melts and milled samples were recorded immediately after preparation using a Rigaku Miniflex Instrument utilizing CuK_α radiation (1.5406 Å), operating over 5-40° at 1.5° min^{-1} with a potential of 30 kV and current of 15 mA in steps of 0.03°. Typically 1 to 2 mg of sample was placed on the top holder and smoothed to achieve a level surface.

5.3.3. Differential Scanning Calorimetry (DSC)

Thermal analysis was conducted using a TA Instruments DSC Q100 with a low temperature attachment (Refrigerated Cooling System, TA Instruments) for subambient operation. The instrument was calibrated with high purity indium (ΔH_{fusion} = 28.57 J g^{-1} and T_m = 156.36 ℃). The specific software of TA Universal Analysis 2000 was used for heat capacity calculations in the study. All scans were conducted at 10°C/min with nitrogen purge to minimise oxidative decomposition. A sample (5-12 mg) was weighed and crimped in the DSC pan, which was weighed again to ensure that the sample had not spilled out during the crimping process. Each of the samples was programmed to the methods needed. Most of the samples were analysed more than twice. A few samples were run more than once, as good thermograms were obtained.

5.3.4. X-ray Photoelectron Spectroscopy (XPS)

XPS spectra were recorded with a Kratos Axis Ultra instrument employing a monochromatic Al K_α source (1486.69 eV), a hemispherical analyser with a hybrid (electrostatic and magnetic) lens system, charge neutralization by filament-generated,

magnetically channeled low-energy electrons[37], and a delay line detector (DLD). The powder samples were spread over double-sided tape for the XPS analysis, and care was taken to ensure that the sample particles completely covered the tape. However, throughout the study, measurement and analysis was not ruled out for the tape contribution affected the samples composition or element (C, O and N). Experiments were performed while operating the X-ray source with a power of 180 W (15 kV and 12 mA), with the pressure below 10^{-8} mbar during analysis.

The instrument was operated in CAE (constant analysis energy) mode, with a pass energy of 80 eV for survey scans, and 20 eV for high resolution scans of the photoemission from individual core levels, with a calibrated intensity/energy response and transmission function[38]. Surveys were measured in steps of 0.5 eV, with 300 ms dwell time per data point. High resolution spectra were measured within the spectral range of interest (± 20 eV around the core level emission peaks of interest), with 0.1 eV steps and 300 ms dwell time per data point for C 1s, 400 ms for O 1s, and 500 ms for N 1s spectra. Repeats were carried out to check for radiation damage.

Analysis of the data was carried out with Casa XPS software[39]. A Linear background was used in all curve-fitting along with a GL(30) lineshape (70% Gaussian, 30% Lorentzian using the Gaussian/Lorentzian product form[39]) and samples were referenced to adventitious hydrocarbon contamination at 285 eV. Positions of photoemission peaks assigned to chemical environments are in agreement with the ranges commonly reported for similar chemical environments[1,40]. Individual chemical environments/functional groups often exhibit similar ranges of binding energy values where the bonding or electronegativity is similar, thus where peaks arising from photoemission from different chemical environments occurred at the same position or within ±0.1 eV, a single peak was used to represent both environments for clarity and ease of discussion. The elemental compositions were calculated using an O 1s relative sensitivity factor (RSF) of 2.52 relative to C 1s, using the Scofield values corrected for angular anisotropy of 60°, and an inelastic mean free path energy dependency of –0.66. Repeatability of the binding energy measurements was ±0.1 eV, while repeatability for the elemental composition values was within ±1.0%.

5.4. Results and Discussion

5.4.1. DSC of Untreated Form I Powder

To establish that the supplied paracetamol Form I powder followed the established phase behavior[36,41-44] it was analysed by DSC (**Figure 5-1**). The first cycle of the thermogram indicates that melting of the Form I powder commences at about 169.4°C, and that the phase transition rate goes through the maximum at 171.7°C. After cooling this melt to 10°C, the second thermogram follows closely the previously reported progression of phase transitions, including (i) crystallization of the glassy state of the solidified melt to paracetamol Form III (onset at 76.0°C, maximum at 82.3°C), (ii) recrystallisation of Form III to Form II (onset at 124.2°C, maximum at 128.5°C), and (iii) melting of Form II (onset at 157.0°C, maximum at 159.8°C). [41] The T_g of the solidified paracetamol melt was at 24.6°C, which is also in agreement with previous observed values.[41]

We also investigated the milled sample iii) by DSC. It exhibited a weak and broad glass transition at a slightly higher T_g value of 42.9°C, indicating that the amorphous component introduced by milling was non-uniform and not as strongly disordered as the solidified melt. Evidence for Forms III and II was not observed; only melting at the temperature characteristic for form Form I was observed. Subsequent cooling and re-heating resulted in the same behavior as for the unmilled sample.

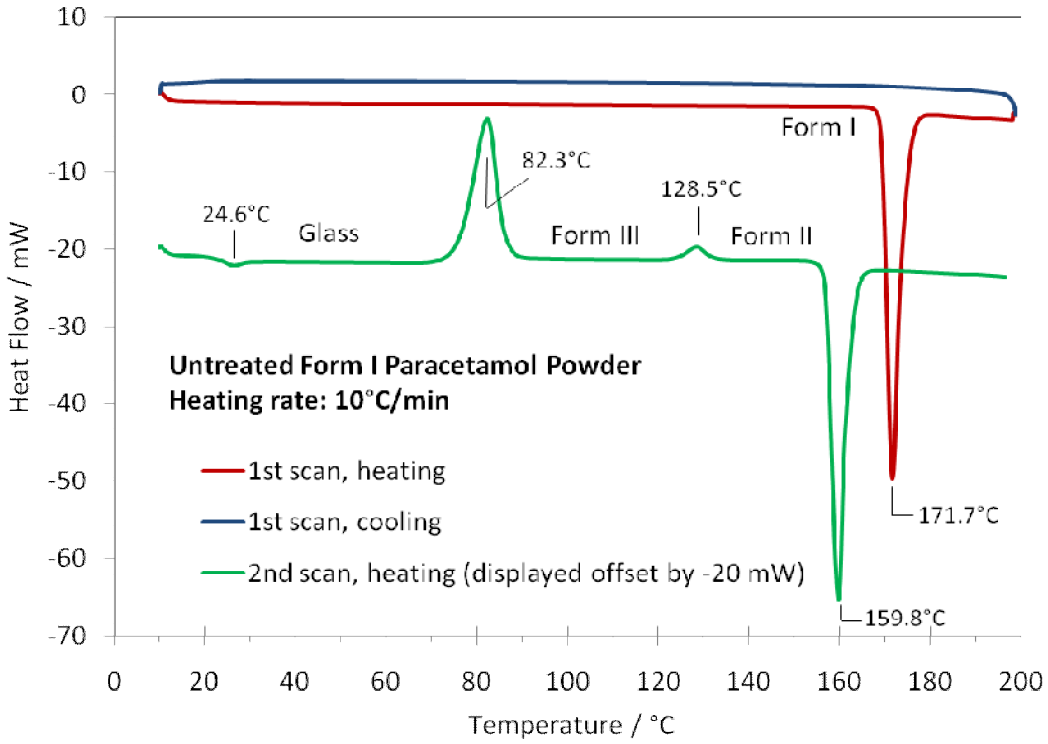

Figure 5-1:. DSC curve of the untreated commercial Form I paracetamol powder, indicating how the glassy paracetamol as well as Forms II and II are obtained by heating a melt of Form I

5.4.2. PXRD

Powder diffraction patterns were generated from the DSC-melted sample as well as from the samples obtained by milling directly after preparation. The patterns are displayed in **Figure 5-2**. All patterns exhibit strongly broadened lines, indicating the presence of significant disorder. Comparison with calculated reference diffraction patterns of Form I[45], Form II[46] and Form III[47] (**Figure 5-2**) reveals that the composition of the solidified melt obtained from the DSC experiment is dominated by a disordered Form III component, but some disordered Form I component is present as well. Disordered Form I dominates the composition of the milled samples. Unfortunately the pattern of the LN2-quenched sample could not be reliably acquired due to instrument failure.

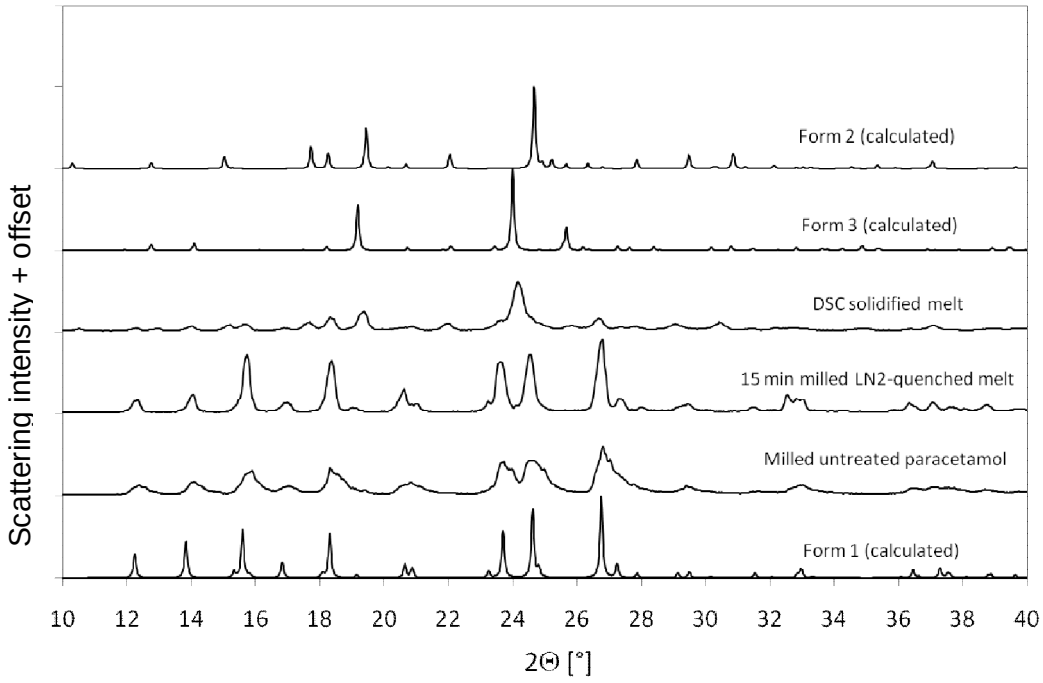

Figure 5-2: X-ray powder diffraction patterns for the non-crystalline samples compared to calculated patterns for Form 1, Form 2 and Form 3 of paracetamol. Data acquired with a Rigaku benchtop XRD system.

Untreated paracetamol exhibited the expected diffraction pattern of Form I with a high degree of crystallinity and phase purity (**Figure 5-3**). **Figure 5-3** also displays the diffraction patterns of the LN2-quenched sample alongside two milled samples after storage for 8 months. It can be seen that the broadening of the diffraction lines observed directly after preparation (**Figure 5-2**) has given way to sharp diffraction lines characteristic for Form I of paracetamol. Clearly re-crystallisation of the disordered phases to Form I take place at a significant rate. These data were acquired with a rotating capillary powder sample holder, allowing identification of preferred orientation effects through the intensity distribution of the diffraction peaks. It can be seen that the LN2-quenched sample exhibits a strong reflection at $2\theta = 36°$ (CDS: plane of (132)), indicating that it has recrystallised to crystallites with strongly preferred orientation of the crystal planes. No such strong preferred orientation effects were observed for the milled samples.

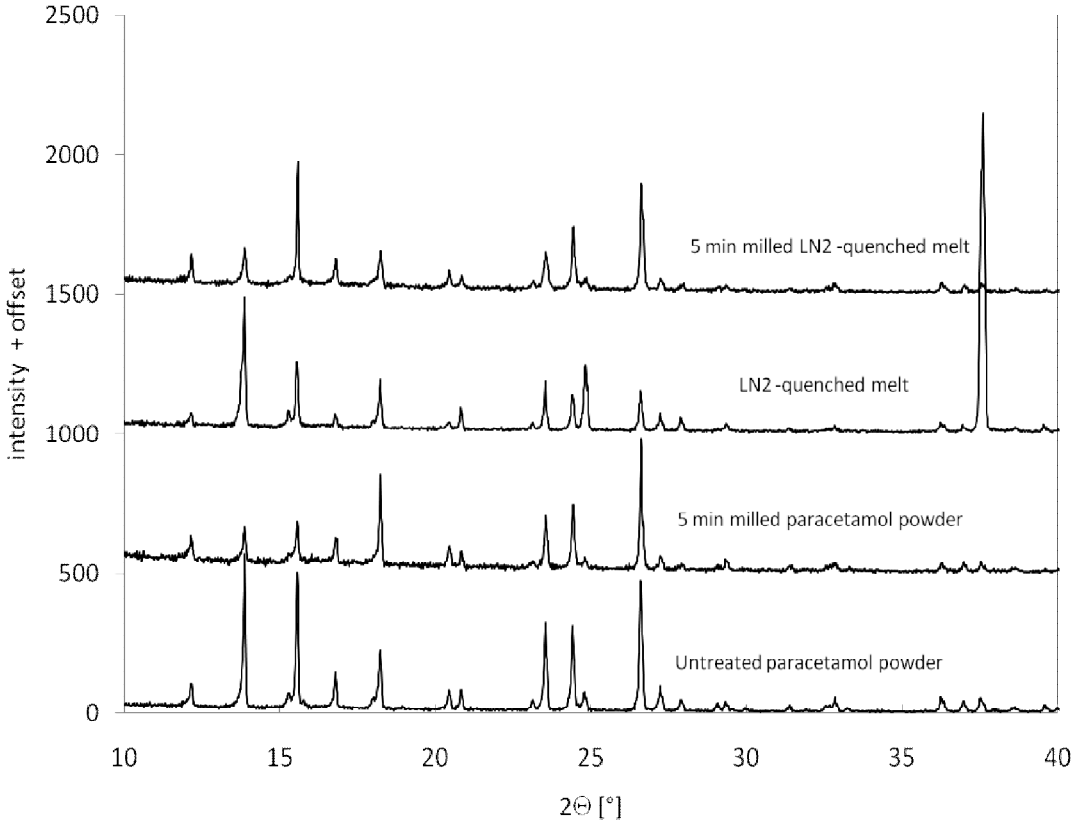

Figure 5-3: X-ray powder diffraction patterns of untreated paracetamol (Form I) compared to for milled samples compared to the pattern of untreated paracetamol. Data acquired with a rotatingcapillary in the Philips Panalytical XRD system approximately 8 months after measuring the data displayed in Figure 5-2.

5.4.3. XPS Survey Data

Survey spectra (**Figure 5-4**) show the 1s photoemission from C, O, and N for all samples and their KLL Auger peaks. The elemental composition of the sample region probed by XPS can be determined from the survey spectra (**Table 5-1**). It can be seen that the C, O, and N percentages are close to those expected from the stoichiometry of a pure paracetamol sample, but an excess of C intensity at the expense of O and particularly N intensity suggest the presence of significant contributions from adventitious hydrocarbon contamination on all samples. An excess of C is also borne out by the higher than expected C:O and C:N intensity ratios (**Table 5-1**). The observed level of contamination indicated by these data is similar to that commonly observed in studies of inorganic materials handled in a laboratory environment[1]. In recent studies of other molecular materials with the same XPS instrument [31,32,38] similar levels were also observed.

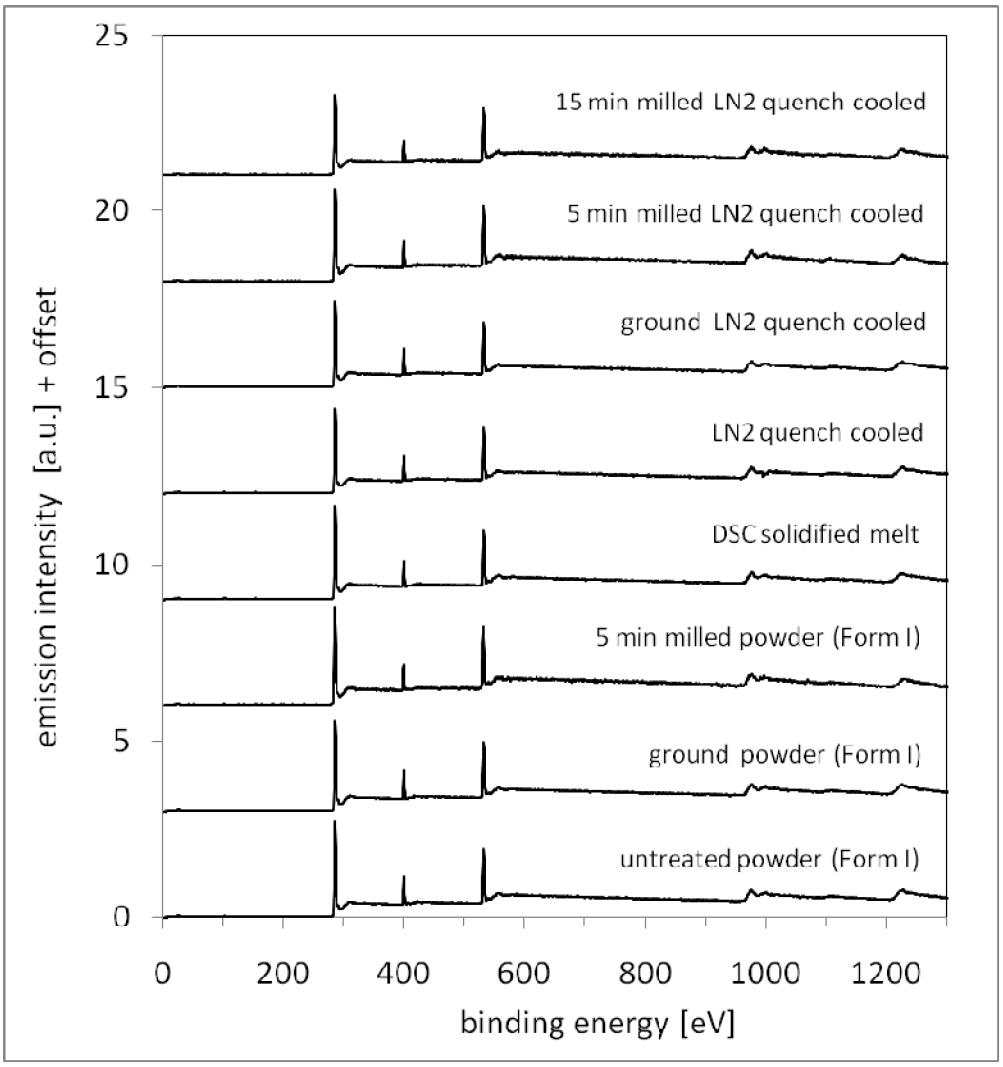

Figure 5-4: XPS survey spectra of all paracetamol powder samples.

Table 5-1: Comparison of expected elemental composition of pure paracetamol with the composition actually determined from the XPS survey data.

	C	O	N	C:O	C:N	O:N
Paracetamol, expected (atom%)	72.7	18.2	9.1	4.00	8.00	2.00
Untreated powder (%) E_B (eV)	76.55± 0.64 284.7	15.69 ± 0.58 532.2	7.76± 0.06 400.0	4.88	9.86	2.02
Milled powder (%) E_B (eV))	73.91 284.7	18.53 531.7	7.56 399.7	3.99	9.77	2.45
Ground Powder (%) E_B (eV)	76.65 284.7	15.52 532.7	8.13 400.2	4.94	9.43	1.91
DSC (%) E_B (eV)	75.09 284.7	17.07 532.7	7.84 400.2	4.40	9.58	2.18
LN_2 quenched E_B (eV)	76.65 284.7	15.74 532.7	7.67 400.2	4.87	9.99	2.05
Ground LN_2 quenched E_B (eV)	76.58 284.7	15.55 532.7	7.88 400.2	4.92	9.72	1.97
5 min milled LN_2 quench E_B (eV)	74.04 284.7	17.60 532.2	8.36 400.2	4.21	8.86	2.11
15 min milled LN_2 quench E_B (eV)	74.84 284.7	17.28 532.2	7.88 400.2	4.33	9.50	2.19

5.4.4. XPS High Resolution Data

For the discussion of the chemical shifts in the high resolution data we recall the numbering of the various atom species in paracetamol in **Figure 5-5.**

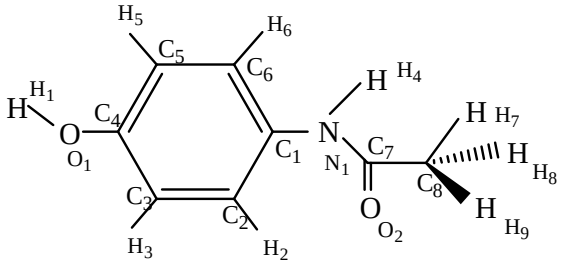

Figure 5-5: Numbering of atoms in paracetamol, $C_8H_9NO_2$

C1s

The photoemission from the C 1s core level of paracetamol reveals three clear peaks. Peaks of increasing E_B are assigned to the carbon environments with increasing

electronegative neighbours (decreasing electron density on carbon), with the lowest E_B peak at 284.7 to 285.4 eV; two deconvoluted C environments were fitted: C=C (C2, C3, C5, C6) and C-C (C8). The shoulder peaks ranging from 285.76 to 286 eV arise from C-OH (C4) and C-N (C1). The well resolved peak at 287.92 to 288.02 eV arises from carbon in the amide group, N-C=O. The aromatic structure of paracetamol results in a broad π-π^* shake-up satellite at high E_B values around 291 eV.

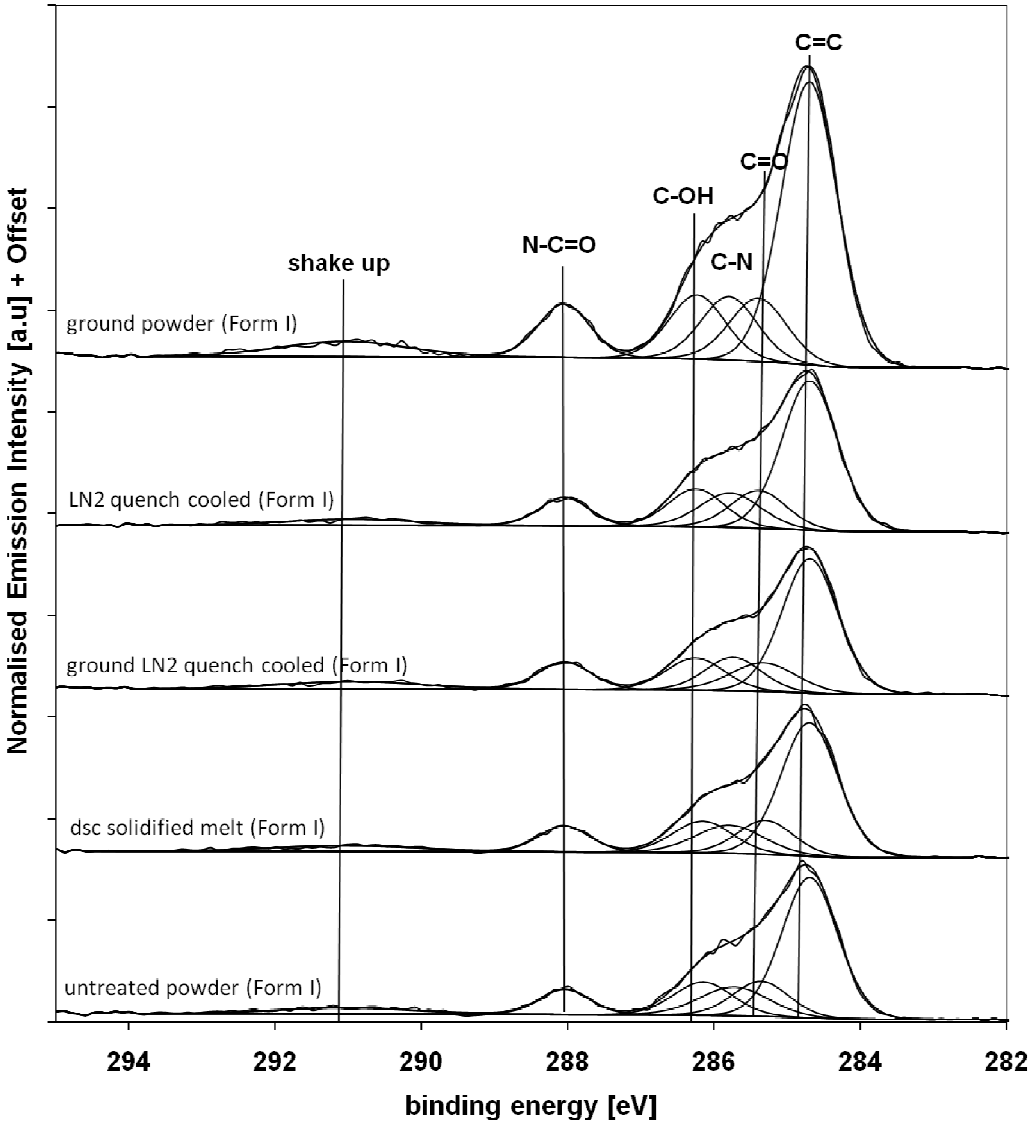

Figure 5-6: C1s photoemission spectra of some paracetamol powdered samples.

Visual inspection of the C 1s data displayed in **Figure 5-6** already indicates that variations between the samples are only minor. The vertical lines drawn through the spectra show that the chemical shifts in the binding energies of the various carbon moieties are negligible. The relative intensities of the three fitted curves under each

spectrum are comparable as well. The numerical results of the curve fitting analysis (curves displayed in **Figure 5-6**) underline these observations (**Table 5-2, and Figure 5-7**). Most interestingly, the intensity of the N-C=O (amide) group of paracetamol does not vary very much across the various preparations (**Table 5-2, Figure 5-7**). This is interesting, because the strongly chemically shifted C1s emission from the amidic carbon atom is specific for emission from paracetamol because adventitious carbon contamination does not contain amide species. The reduction of the amide emission is for all samples approximately 30-40%, which is too large to be compatible with a reduction due to crystal facet orientation effects, because the C1s signal escapes from a depth of a few nm,[48] i.e., from a region in the crystal that is significantly larger than the thickness of a single molecular layer. Moreover, the amide emission is unaffected by either crystal structure, crystallinity or preferred orientation of the crystallites in the powder samples. This suggests that the observed variations relate predominantly to the presence of adventitious carbon contamination species at the surface, a conclusion that is also in line with the elemental analysis data derived from the survey spectra (see **Figure 5-4**). Finally, the C1s emission contributions from the C=C/C-C=O and C-N/C-OH groups support this conclusion as well, because a lower than expected intensity value for C=C/C-C=O groups was associated with an increased concentration of C-N/C-OH (**Table 5-2**). This trend was observed for all the samples. A quantitative interpretation of the C-N/C-OH enhancement is not entirely straightforward because the intensities of all peaks in the C 1s data are affected by the presence of the shake-up peak at higher binding energy. It is not clear how its intensity is related to the intensities of the three main peaks in the spectra. However, in a first approximation, the magnitude of the enhancement in the C-N/C-OH component of the C1s emission is around 10% (**Table 5-2**), indicating that the adventitious carbon contamination contains significant concentrations of functional groups with C-O bonds.

Table 5-2: Results of quantification of the C1s emission by curve fitting analysis. The emission intensities [%] do not add up to 100% because of the presence of the shake-up peak in the spectra.

Samples	**C=C**	**C-C=O**	**C-N**	**C-OH**	**N-C=O**
Expected (%)	50.0	12.5	12.5	12.5	12.5
Untreated powder	49.3	12.3	12.3	12.3	8.0
E_B (eV)	284.7	285.4	285.7	286.2	288.1
5 min milled powder	48.1	12.1	12.0	12.0	12.0
E_B (eV)	284.7	285.2	285.7	286.3	288.0
Ground powder	50.9	11.4	12.4	12.4	8.7
E_B (eV)	284.7	285.4	285.8	286.2	288.1
DSC	49.1	12.3	12.3	12.3	8.5
E_B (eV)	284.7	285.0	286.0	286.0	288.0
Untreated LN_2	49.1	12.4	12.4	12.4	8.3
E_B (eV)	284.7	285.4	285.8	286.3	288.1
Ground LN_2	48.1	12.0	12.0	12.0	9.3
E_B (eV)	284.7	285.3	285.8	286.3	288.1
5 min milled LN_2	47.4	11.9	11.9	11.8	11.8
E_B (eV)	284.7	285.1	285.8	286.2	288.0
15 min milled LN_2	48.4	12.1	12.1	12.1	12.1
E_B (eV)	284.7	285.1	285.8	286.2	287.9

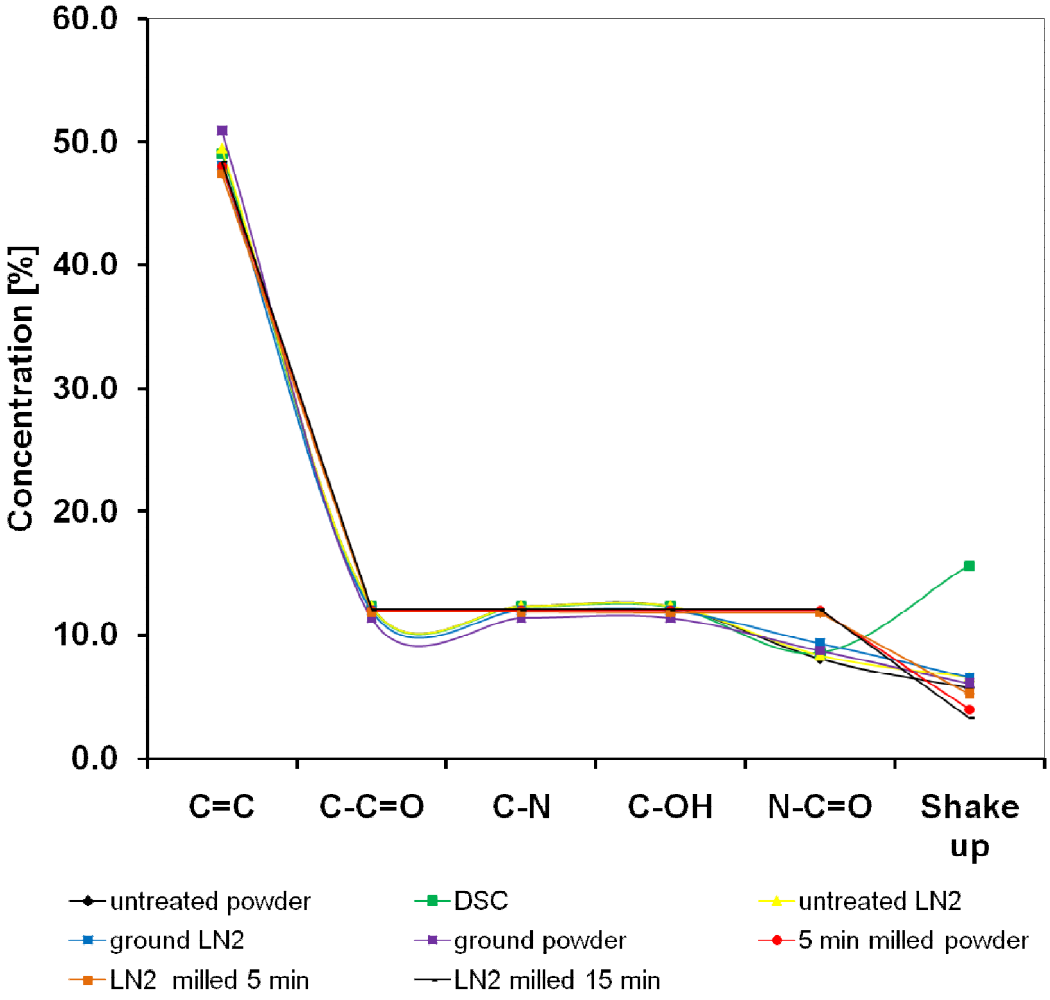

Figure 5-7: Plot of the intensities of the C 1s emission components for all samples. The concentrations [%} do not add up to 100% because of the presence of the shake-up peak in the spectra.

O1s

Paracetamol is characterized by two O 1s emission peaks, a carbonyl oxygen component at 531.3 eV and a hydroxyl emission at 532.76 eV (**Figure 5-8, Table 5-3**). The results of the curve fitting analysis of the O 1s data of all samples are summarized in **Table 5-3**. The binding energies are compatible with previously observed values for these functional groups,[40] and there is little variation between the samples. From the stoichiometry of paracetamol one would expect intensities of the two peak components to be in a ratio of 1:1. In contrast to this expectation the data in **Figure 5-8** are characterized by generally stronger emission from the OH than the carbonyl component. This is clearly

borne out by the results of the quantitative curve fitting analysis (**Table 5-3**), which indicates that on average 59% of the O 1s emission stems from the OH region of the spectrum. A very similar enhancement of the OH concentration has previously been reported for individual facet surfaces of paracetamol.[26] The inelastic mean free path of the O1s electrons is on the order of 2.9 nm,[48] indicating that the surface region probed by the O 1s signal is several nm. This length is too large to be compatible with an enhanced OH concentration due to crystal facet termination effects, which would be restricted to a surface region with a thickness similar to a C-OH bond (~0.3 nm). It is more plausible to assume that OH groups from the adventitious carbon contamination cause the observed enhancement of the OH signal. The observed enhancement of the O 1s signal is on the order of 10% of the signal expected for the two oxygen atoms in paracetamol. We noted above that the observed attenuation of the C1s signal from the paracetamol amide group was about 30-40%, indicating that the adventitious carbon contaminations contains approximately one oxygen atom for every four carbons atoms.

Table 5-3: O 1s high resolution binding energy analysis of all the samples

Samples	**OH (eV)**	**C=O (eV)**
Expected (%)	50 %	50 %
Untreated powder	57.36%	42.64%
E_B (eV)	532.8	531.3
Milled powder	55.06%	44.94%
E_B (eV)	532.8	531.3
Ground powder	57.72%	42.28%
E_B (eV)	532.8	531.3
DSC	57.06%	42.94%
E_B (eV)	532.7	531.3
Untreated LN_2	58.27%	41.73%
E_B (eV)	532.8	531.3
Ground LN_2	56.10%	43.90%
E_B (eV)	532.8	531.3
5 min milled LN_2	59.61%	40.39%
E_B (eV)	532.8	531.3
15 min milled LN_2	63.73%	36.27%
E_B (eV)	532.8	531.3

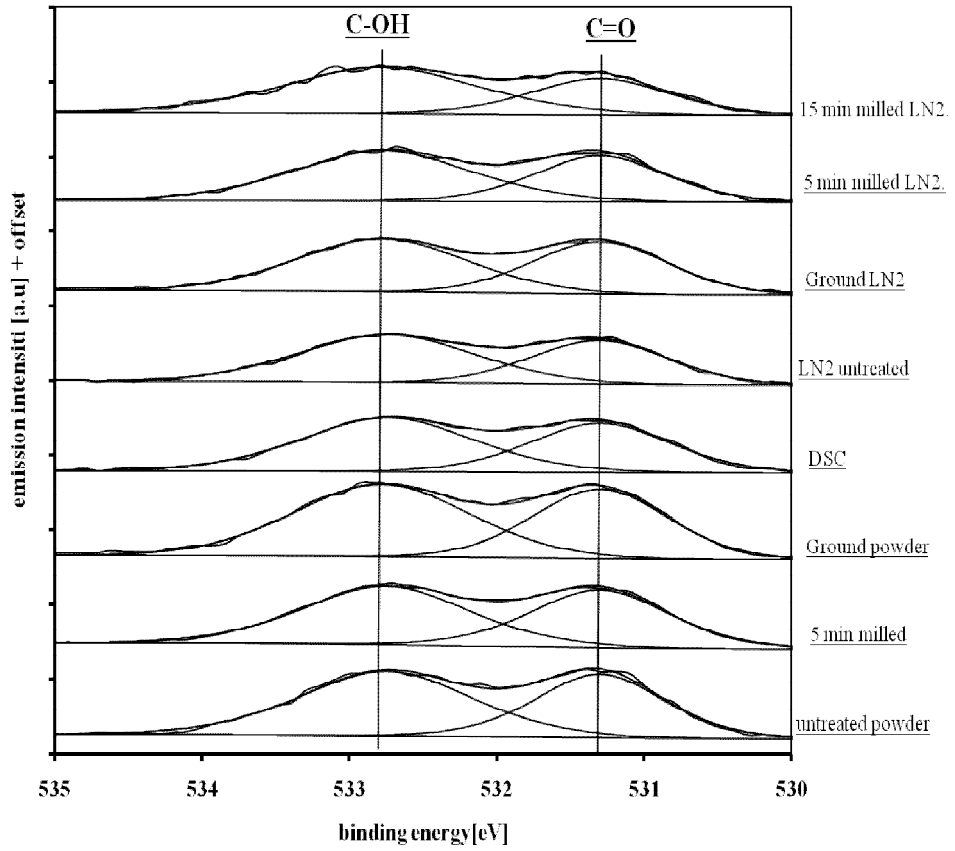

Figure 5-8: **O1s photoemission spectra of all paracetamol samples.**

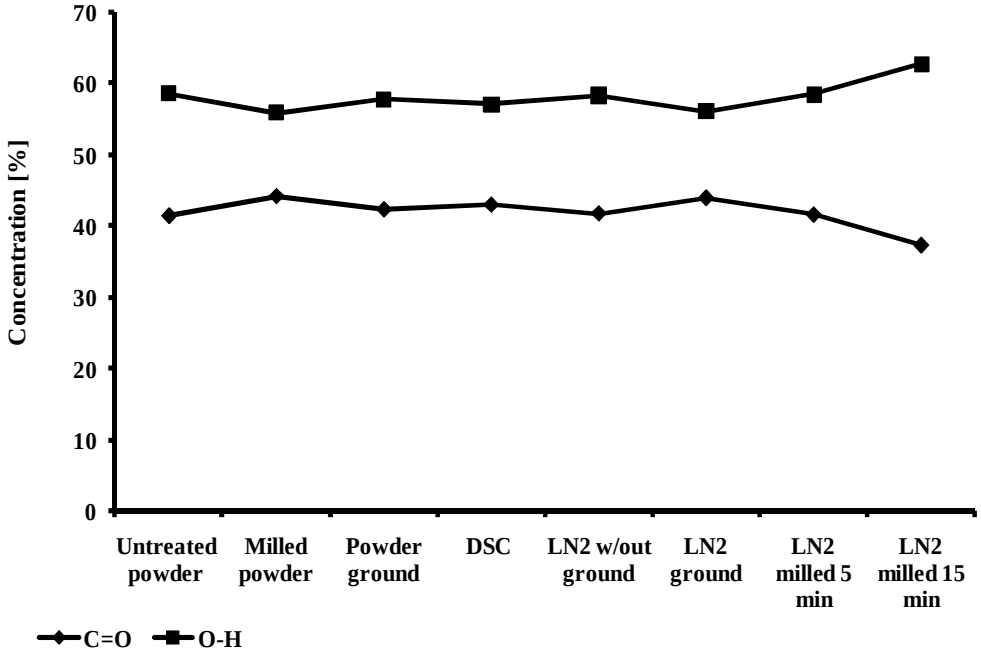

Figure 5-9: O 1s analysis of tested samples

N1s

For all samples only one peak of N was observed in the N 1s emission, with a binding energy of approximately 400 eV, which is compatible with the N-C=O amide species. **Table 5-4** summarises the N 1s (bottom) high resolution binding energy analysis of all the samples. No additional quantitative information can be derived from the high resolution N1s data, which are therefore not displayed here.

Table 5-4: Results of N 1s high resolution binding energy analysis of all the samples

Samples	**N-C=O (eV)**
Untreated powder	400.2
Milled powder	400.0
Ground powder	400.2
DSC	400.2
LN_2 without ground	400.2
LN_2 ground	400.2
LN_2 milled 5 minutes	400.1
LN_2 milled 15 min	400.0

5.5. Discussion

The first high resolution XPS data of paracetamol reveal that the C 1s and O 1s photoemission spectra contain a number of emission features that have previously not been observed in XPS data obtained with a non-monochromatised X-ray source.[26] Especially the well resolved C 1s and O 1s emission features from the amide group of paracetamol can be used to characterize surface cleanliness, phase purity and local structure. However, the XPS examination of a number of paracetamol powder samples with different degrees of crystallinity, crystal structure or preferred orientation of the crystallites produced very similar results for all samples. Most notable is a significant attenuation of the signal from the paracetamol amide group, which is evident from the elemental analysis, from the analysis of the high resolution C 1s emission data and from the hydroxyl/carbonyl intensity ratio of the O 1s emission. The surface sensitivity of XPS is not sufficient[48] to explain this attenuation through structural variations in the top layers due to facet specific crystal surface terminations or reconstructions. It is more likely that the observed amide attenuation and the associated variations of the sample composition

within the near-surface region probed by XPS are due to contamination acquired by the samples during preparation and handling in the laboratory environment. This so-called adventitious carbon and oxygen contamination is a well known phenomenon in surface analysis[1] and very difficult to avoid unless samples are prepared under conditions of cleanliness that cannot be achieved without very considerable effort (for example evaporation and sublimation under ultra-high vacuum conditions). However, no measurement on the effect of tape was done due to the constaint of instrument availability and analysis cost. This explanation of the observed variations is given particular credibility by the fact that amides are not a common component in adventitious surface contamination layers. The well resolved features of the amide group in the C 1s, N 1s and O 1s emission from paracetamol thereby provide a reliable means for determining the amount of contamination on the surface. The quantitative analysis of the data suggests that the adventitious contamination layer constitutes about 30-40% of the carbon content within the near-surface layer probed by XPS, and that it contains carbon and oxygen approximately in a ratio of 4:1. These substantial amounts of surface contamination are likely to have a pronounced effect on commonly used macroscopically observable surface parameters such as contact angles.

5.6. Conclusions

The reported study of polycrystalline paracetamol samples underlines the fact that extreme care must be taken when surface properties are determined by surface sensitive techniques that do not permit insight into the chemical composition of the top molecular layers.

5.7. References

1. *Practical Surface Analysis. Vol.1 - Auger and X-ray Photoelectron Spectroscopy;* 2 ed.; John Wiley & Sons: Chichester, New York, Brisbane, Toronto, Singapore, 1990.

2. Castner, D. G.; Ratner, B. D. Biomedical Surface Science: Foundation to Frontiers. *Surf. Sci.* **2002,** 28-60.

3. Banerjee, R.; Katsenovich, Y.; Lagos, L.; McIintosh, M.; Zhang, X.; Li, C. Z. Nanomedicine: Magnetic Nanoparticles and their Biomedical Applications. *Curr. Med. Chem.* **2010,** 3120-3141.

4. McArthur, S. L. Applications of XPS in bioengineering. *Surf. Interface Anal.* **2006,** 1380-1385.

5. Ma, Z. W.; Mao, Z. W.; Gao, C. Y. Surface modification and property analysis of biomedical polymers used for tissue engineering. *Colloids Surf. , B* **2007,** 137-157.

6. Carli, F.; Garbassi, F. Characterization of Drug Loading in Crospovidone by X-ray Photoelectron-Spectroscopy. *J. Pharm. Sci*. **1985,** 963-967.

7. Morales, M. E.; Ruiz, M. A.; Oliva, I.; Oliva, M.; Gallardo, V. Chemical characterization with XPS of the surface of polymer microparticles loaded with morphine. *Int. J. Pharm.* **2007,** 162-166.

8. Mu, L.; Teo, M. M.; Ning, H. Z.; Tan, C. S.; Feng, S. S. Novel powder formulations for controlled delivery of poorly soluble anticancer drug: Application and investigation of TPGS and PEG in spray-dried particulate system. *J. Control Release* **2005,** 565-575.

9. Bosquillon, C.; Rouxhet, P. G.; Ahimou, F.; Simon, D.; Culot, C.; Preat, V.; Vanbever, R. Aerosolization properties, surface composition and physical state of spray-dried protein powders. *J. Control Release* **2004,** 357-367.

10. Scholes, P. D.; Coombes, A. G. A.; Illum, L.; Davis, S. S.; Watts, J. F.; Ustariz, C.; Vert, M.; Davies, M. C. Detection and determination of surface levels of poloxamer and PVA surfactant on biodegradable nanospheres using SSIMS and XPS. *J. Control Release* **1999,** 261-278.

11. Bouillot, P.; Babak, V.; Dellacherie, E. Novel bioresorbable and bioeliminable surfactants for microsphere preparation. *Pharmaceut. Res.* **1999,** 148-154.

12. Lacasse, F. X.; Hildgen, P.; McMullen, J. N. Surface and morphology of spray-dried pegylated PLA microspheres. *Int. J. Pharm.* **1998,** 101-109.

13. Binns, J. S.; Davis, S. S.; Melia, C. D.; Watts, J. F.; Davies, M. C. The Application of Xps to the Surface Characterization of Polymeric Drug Delivery Systems. *J. Pharm. Pharmacol.* **1989,** *41*.

14. Evora, C.; Soriano, I.; Rogers, R. A.; Shakesheff, K. M.; Hanes, J.; Langer, R. Relating the phagocytosis of microparticles by alveolar macrophages to surface

chemistry: the effect of 1,2-dipalmitoylphosphatidylcholine. *J. Control Release* **1998,** 143-152.

15. Mellaerts, R.; Houthoofd, K.; Elen, K.; Chen, H.; Van Speybroeck, M.; Van Humbeeck, J.; Augustijns, P.; Mullens, J.; Van den Mooter, G.; Martens, J. A. Aging behavior of pharmaceutical formulations of itraconazole on SBA-15 ordered mesoporous silica carrier material. *Micropor. Mesopor. Mat.* **2010,** 154-161.

16. Zimmermann, A.; Millqvist-Fureby, A.; Elema, M. R.; Hansen, T.; Mullertz, A.; Hovgaard, L. Adsorption of pharmaceutical excipients onto microcrystals of siramesine hydrochloride: Effects on physicochemical properties. *Eur. J. Pharm. Biopharm.* **2009,** 109-116.

17. Janssens, S.; Roberts, C.; Smith, E. F.; Van den Mooter, G. Physical stability of ternary solid dispersions of itraconazole in polyethyleneglycol 6000/hydroxypropylmethylcellulose 2910 E5 blends. *Int. J. Pharm.* **2008,** 100-107.

18. Rafati, A.; Davies, M. C.; Shard, A. G.; Hutton, S.; Mishra, G.; Alexander, M. R. Quantitative XPS depth profiling of codeine loaded poly(L-lactic acid) films using a coronene ion sputter source. *J. Control Release* **2009,** , 40-44.

19. Sumi, V. S.; Kala, R.; Praveen, R. S.; Rao, T. P. Imprinted polymers as drug delivery vehicles for metal-based anti-inflammatory drug. *Int. J. Pharm.* **2008,** 30-37.

20. Watts, P. J.; Lynn, R. A. P.; Watts, J. F.; Melia, C. D.; Davies, M. C. Surface Characterization of Eudragit Rs-Sulphasalazine Microspheres Using X-ray Photoelectron Spectroscopy Xps. *J. Pharm. Pharmacol.* **1991,** ABSTRACT.

21. Davies, M. C.; Wilding, I. R.; Short, R. D.; Khan, M. A.; Watts, J. F.; Melia, C. D. An Analysis of the Surface Chemical-Structure of Polymethacrylate (Eudragit) Film Coating Polymers by Xps. *Int. J. Pharm.* **1989,** 183-187.

22. Bridgett, M.; Davies, M.; Denyer, S. An XPS analysis of pluronic surfactants adsorbed to poly(styrene) surfaces. *J. Pharm. Pharmacol.* **1992,** *44*.

23. Buckton, G.; Bulpett, R.; Verma, N. Surface-Analysis of Pharmaceutical Powders - X-ray Photoelectron-Spectroscopy (Xps) Related to Powder Wettability. *Int. J. Pharm.* **1991,** 157-162.

24. Heng, J. Y. Y.; Bismarck, A.; Lee, A. F.; Wilson, K.; Williams, D. R. Anisotropic surface chemistry of aspirin crystals. *J. Pharm. Sci.* **2007,** 2134-2144.

25. Heng, J. Y. Y.; Bismarck, A.; Williams, D. R. Anisotropic surface chemistry of crystalline pharmaceutical solids. *AAPS PharmSciTech* **2006,** *7*.

26. Heng, J. Y. Y.; Bismarck, A.; Lee, A. F.; Wilson, K.; Williams, D. R. Anisotropic surface energetics and Wettability of macroscopic form I paracetamol crystals. *Langmuir* **2006,** 2760-2769.

27. Puri, V.; Dantuluri, A. K.; Kumar, M.; Karar, N.; Bansal, A. K. Wettability and surface chemistry of crystalline and amorphous forms of a poorly water soluble drug. *European Journal of Pharmaceutical Sciences* **2010,** 84-93.

28. Dahlberg, C.; Millqvist-Fureby, A.; Schuleit, M. Surface composition and contact angle relationships for differently prepared solid dispersions. *Eur. J. Pharm. Biopharm.* **2008,** 478-485.

29. Heng, J. Y. Y.; Thielmann, F.; Williams, D. R. The effects of milling on the surface properties of form i paracetamol crystals. *Pharmaceut. Res.* **2006,** 1918-1927.

30. Stevens, J. S.; Byard, S. J.; Zlotnikov, E.; Schroeder, S. L. M. Detection of Free Base Surface Enrichment of a Pharmaceutical Salt by X-ray Photoelectron Spectroscopy (XPS). *J. Pharm. Sci.* **2011,** *12*, in press.

31. Stevens, J. S.; Byard, S. J.; Schroeder, S. L. M. Characterization of Proton Transfer in Co-Crystals by X-ray photoelectron spectroscopy (XPS). *Cryst. Growth Des.* **2010,** 1435-1442.

32. Stevens, J. S.; Byard, S. J.; Schroeder, S. L. M. Salt or Co-Crystal? Determination of Protonation State by X-ray Photoelectron Spectroscopy (XPS). *J. Pharm. Sci.* **2010,** 4453-4457.

33. Stevens, J. S.; Byard, S. J.; Muryn, C. A.; Schroeder, S. L. M. Identification of Protonation State by XPS, Solid-state NMR, and DFT: Characterization of the Nature of a New Theophylline Complex by Experimental and Computational Methods. *J. Phys. Chem. B* **2010,** *submitted*.

34. Feng, T.; Pinal, R.; Carvajal, M. T. Process induced disorder in crystalline materials: Differentiating defective crystals from the amorphous form of griseofulvin. *J. Pharm. Sci.* **2008,** 3207-3221.

35. Miyazaki, T.; Yoshioka, S.; Aso, Y. Physical stability of amorphous acetanilide derivatives improved by polymer excipients. *Chem. Pharm. Bull.* **2006,** 1207-1210.

36. Qi, S.; Avalle, P.; Saklatvala, R.; Craig, D. Q. M. An investigation into the effects of thermal history on the crystallisation behaviour of amorphous paracetamol. *Eur. J. Pharm. Biopharm.* **2008,** 364-371.

37. *AXIS Charge Balance System*; Kratos Analytical: Manchester, 10.

38. Stevens, J. S.; Schroeder, S. L. M. XPS Analysis of Saccharides and Their X-ray Induced Degradation. *Surf. Interface Anal.* **2009,** 453-462.

39. Fairley, N.; Carrick, A. *The CASA Cookbook: Recipes for XPS Data Processing, pt. 1;* Acolyte Science: Knutsford, Cheshire, 2005.

40. *The XPS of Polymers Database;* 1 ed.; Surface Spectra Ltd: Manchester, UK, 2000.

41. Burley, J. C.; Duer, M. J.; Stein, R. S.; Vrcelj, R. M. Enforcing ostwald's rule of stages: Isolation of paracetamol forms III and II. *European Journal of Pharmaceutical Sciences* **2007,** 271-276.

42. Giordano, F.; Rossi, A.; Bettini, R.; Savioli, A.; Gazzaniga, A.; Novak, C. Thermal behavior of paracetamol-polymeric excipients mixtures. *J. Therm. Anal. Calorim.* **2002,** 575-590.

43. DiMartino, P.; Conflant, P.; Drache, M.; Huvenne, J. P.; GuyotHermann, A. M. Preparation and physical characterization of forms II and III of paracetamol. *J. Thermal Anal.* **1997,** 447-458.

44. Di Martino, P.; Beccerica, M.; Joiris, E.; Palmieri, G. F.; Gayot, A.; Martelli, S. Influence of crystal habit on the compression and densification mechanism of ibuprofen. *J. Cryst. Growth* **2002,** 345-355.

45. Naumov, D. Y.; Vasilchenko, M. A.; Howard, J. A. K. The monoclinic form of acetaminophen at 150K. *Acta Crystallogr. , Sect. C: Cryst. Struct. Commun*. **1998,** 653-655.

46. Nichols, G.; Frampton, C. S. Physicochemical characterization of the orthorhombic polymorph of paracetamol crystallized from solution. *J. Pharm. Sci.* **1998,** 684-693.

47. Perrin, M. A.; Neumann, M. A.; Elmaleh, H.; Zaske, L. Crystal structure determination of the elusive paracetamol Form III. *J. Chem. Soc. Chem. Comm.* **2009,** 3181-3183.

48. Tanuma, S.; Powell, C. J.; Penn, D. R. Calculations of Electron Inelastic Mean Free Paths .5. Data for 14 Organic-Compounds Over the 50-2000 Ev Range. *Surf. Interface Anal.* **1994,** 165-176.

49. Heng, J. Y. Y.; Williams, D. R. Wettability of paracetamol polymorphic forms I and II. *Langmuir* **2006,** 6905-6909.

CHAPTER 6: SINGLE CRYSTAL PARACETAMOL

6.1. Objectives

The objectives of the studies reported in this chapter were twofold:

i) To examine the possibility that XPS can establish the chemical composition of paracetamol facets by determining the elemental composition and the chemical state of the elements at selected crystal facets
ii) To examine the surface chemical composition as a function of solvent used during crystal growth.

6.2. Introduction

The affinities of a crystal depend on the presentation of its facets, and the surface properties of a particular crystal facet will be governed by the molecular functionalities at the surface. The dominant facets of a crystal will influence its physical and chemical interfacial properties, including the wettability, surface energy and chemical composition[1]. The crystal structure determines the macroscopic crystal shape. Therefore the knowledge of crystal structure at a molecular level is a prerequisite to the understanding and potential control of pharmaceutically important bulk properties of crystalline pharmaceutical solids.

The most prominent characteristic features of an individual crystal are its facets and the angles between them[2]. The Miller indices of the crystal facets are associated with surface coverage by characteristic functional groups, which depend on conformation of molecules in the crystal structure and the chemical composition determined by the crystal termination. The crystal system, structure and Miller indices of the prominent facets can often be determined by powder XRD, and always by single crystal XRD techniques. Scanning electron microscopy (SEM) has been used as well, especially in early work in conjunction with computer programs based on geometric considerations[3]. The Cambridge Structural Database acts as a repository of small molecule crystal structures, so data needed for crystal structure visualization, analysis and structural knowledge can be obtained without experiments[4]. There have been numerous studies of paracetamol, whose crystal structure was first studied by Haisa[5], followed by studies of electron density[6], the

interaction of paracetamol solute with crystallization solvents and density functional theory (DFT), including electronic distribution [7].

Paracetamol was chosen for the X-ray Photoelectron Spectroscopy study in this thesis for three main reasons. Firstly, there have to date been no detailed studies of single paracetamol crystals using high resolution XPS analysis. Secondly, paracetamol crystals are sufficiently stable under UHV conditions compared to other available API such as ibuprofen and aspirin. Thirdly, only one study has previously addressed the composition of single crystal facets, but without reference to the solvents used for crystallisation. XPS analysis will also provide an opportunity to gain information on the influence of contaminants in the crystallization process and of the solvents used during crystallization.

BFDH (Bravais-Friedel-Donnay-Harker) theory was applied to identify the orientation of paracetamol crystal facets. BFDH theory was developed in the first half of the 20th century as a tool for the prediction of crystal morphology. The basis of BFDH predictions is the assumption that the morphological importance, which encompasses both facet size and the statistical frequency of facet occurrence, of an (hkl) facet increases with the interplanar distance d_{hkl} between the (hkl) lattice planes[8, 9]. The d_{hkl} values must also be corrected for the selection rules for each of the 230 space groups, which can be found in the International Tables for X-ray Crystallography [10]. A high frequency of facet occurrence and/or facets with large surface areas are typically associated with slowly growing facets, which leads to the application of BFDH theory in crystal morphology prediction by associating higher growth rates of an (hkl) face with lower d_{hkl} values, and *vice versa*. In the 1950s, Hartman and Perdok developed theoretical methods for the prediction of crystal growth and morphology that put BFDH theory on a sounder physical foundation by calculating relative facet stability based on a consideration of nearest neighbour bonds in the crystal[2].

6.3. Experimental

6.3.1. Preparation of Single Crystal and Ground Crystal Paracetamol

i) **AceSingle1 (single crystal grown in acetone #1)**. HPLC grade acetone was used in the crystallisation experiment. The apparatus was cleaned and dried at 400°C for 2 hours in the oven before use. A single acetone crystal was prepared by the slow cooling crystallisation technique. A saturated acetone-paracetamol solution was prepared by dissolving paracetamol in 20 mL acetone at 20°C. The experiment was

performed in a 50 mL jacketed vessel connected to a programmable circulating water bath, model RTE 740 (Thermo Neslab Digital Plus). The temperature was raised to 23°C in order to form a supersaturated solution for 1 hour, after which the temperature was reduced gradually over 1 hour to 20 °C. During this process the solution was stirred constantly using a magnetic stirrer at scale 4. The solution was kept at 20°C with stirring for 2 hours. Some of the solution was then taken for seed preparation, stirring ceased and the temperature was reduced by 0.1°C per day until it reached 19.8°C, when single crystal nucleation was induced by the addition of seeds. After the initiation of seeding, the bath temperature was reduced by 0.2 °C per day until it reached 16°C. The crystal was dried under ambient conditions before further analysis. The paracetamol weight used in the saturated solution was based on reading the reference solubility curve [10] at a temperature of 20°C. The paracetamol molar concentration was calculated at 0.01 mol in 20 mL of acetone (0.45M).

ii) **AceSingle2 (single crystal grown in acetone #2)**: A single acetone crystal was prepared by the slow cooling technique described above, the only difference being in the cleaning of all the apparatus in detergent, after which it was thoroughly rinsed in deionised water. No further cleaning was done.

iii) **EtSingle (single crystal grown in ethanol)**: A single ethanol crystal was prepared by slow cooling crystallisation. All of the apparatus was first cleaned in detergent and rinsed with deionised water. No further cleaning was done. The only ethanol solvent used was absolute ethanol. A saturated ethanol-paracetamol solution was prepared by dissolving paracetamol in 20 mL ethanol at 20°C. The following steps as stated in AceSingle (**in section i**). 0.019 moles were added to 20 mL of ethanol giving 0.98M of paracetamol solution.

iv) **MeSingle1 (single crystal grown in methanol #1)**: All the apparatus used was washed in APS two days before use, then dried in an oven at 60°C and covered with Parafilm until the crystallisation experiment. The methanol solvent used was HPLC grade. The crystallisation procedure was similar to that described for acetone crystal preparation. 0.03 moles were added to 20 mL of methanol giving 1.55M of paracetamol solution.

v) **MeSingle2 (single crystal grown in methanol #2)**: Before the experiment all the apparatus was prepared as for the acetone crystal experiment. The crystallisation technique was similar to that used in the acetone experiment.

vi) **Powder:** Powdered paracetamol was used without any treatment or modification for XPS analysis.

6.3.2. XPS Analysis

Facets of these crystals were analysed by XPS to examine the near-surface stoichiometry. The single crystals were analysed as a function of facet orientation and indexed with Materials Studio using BFDH calculations [11] **(**see **also Introduction and Chapter 2).** XPS was carried out as described in **Chapter 2**. As given in the table in the previous section, three groups of paracetamol single crystals were analysed: prepared from saturated solutions of paracetamol in acetone, ethanol and methanol respectively. For each single crystal a different number of facets, and in some cases various spots on a facet, were chosen for analysis, depending on facet size, ability to neutralise built-up charges, and the accessibility of under the geometric constraints of the XPS apparatus. The XPS analysis was in two mode; 4 peaks of fitting and 6 peaks of fitting for C1s and O 1s data.

Some of the crystal facets underwent visible beam damage during the XPS investigations, while others were not affected. These observations were as follows:

i) AceSingle1 and AceSingle2: No colour change on the sample surface. The crystals were observed to be unchanged during the XPS analysis.

ii) EtSingle: The sample surface became yellowish after the XPS experiment.

iii) MeSingle1 and MeSingle2: Sample surfaces were observed to be unchanged after the XPS analysis. No colour change was observed.

iv) Ground crystals: All the ground crystals kept their original colour. No colour change to the powder surface was observed.

6.3.3. BFDH Assignment of Crystal Facet Orientation

The AceSingle **(Figure 6-1**) crystal was analysed at four spots, but only two could be used due to excessive charging during the measurements at the other spots.

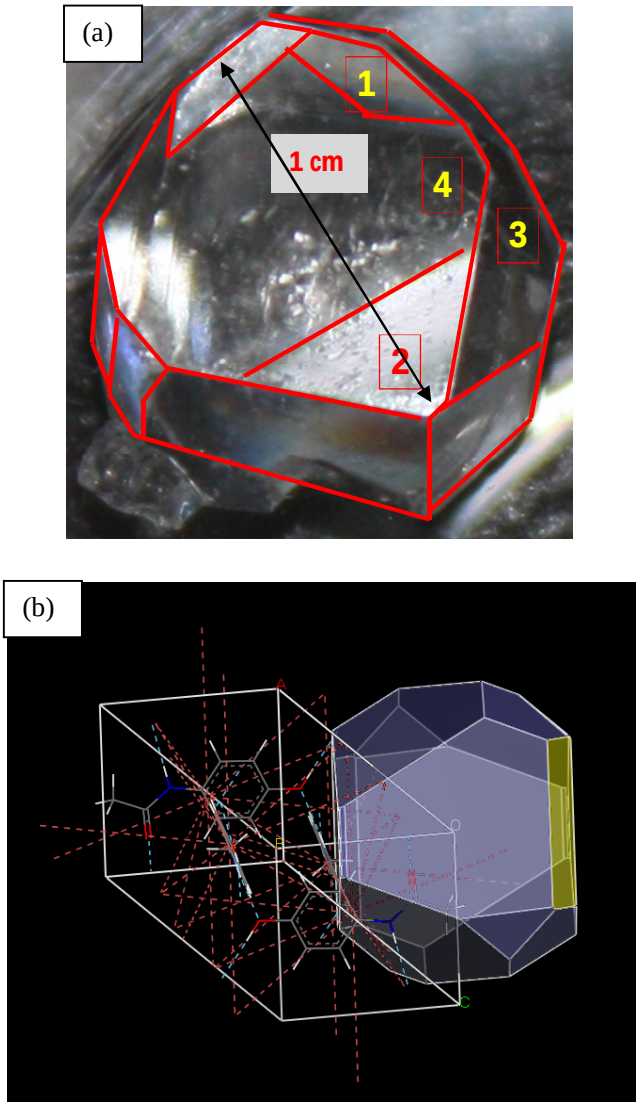

Figure 6-1: (a) Photograph of AceSingle crystal with areas of XPS small spot analysis indicated by numbers; spot 1: (0-20)-facet; spot 2: (0-1-1)-facet; spot 3: (-1-10)-facet, spot 4: (1-10)-facet; (b) BFDH construction that formed the basis for facet orientation assignment.

The EtSingle sample was analysed at 23 spots on a large single facet. The crystal image and schematic BFDH diagram are illustrated in **Figure 6-2.**

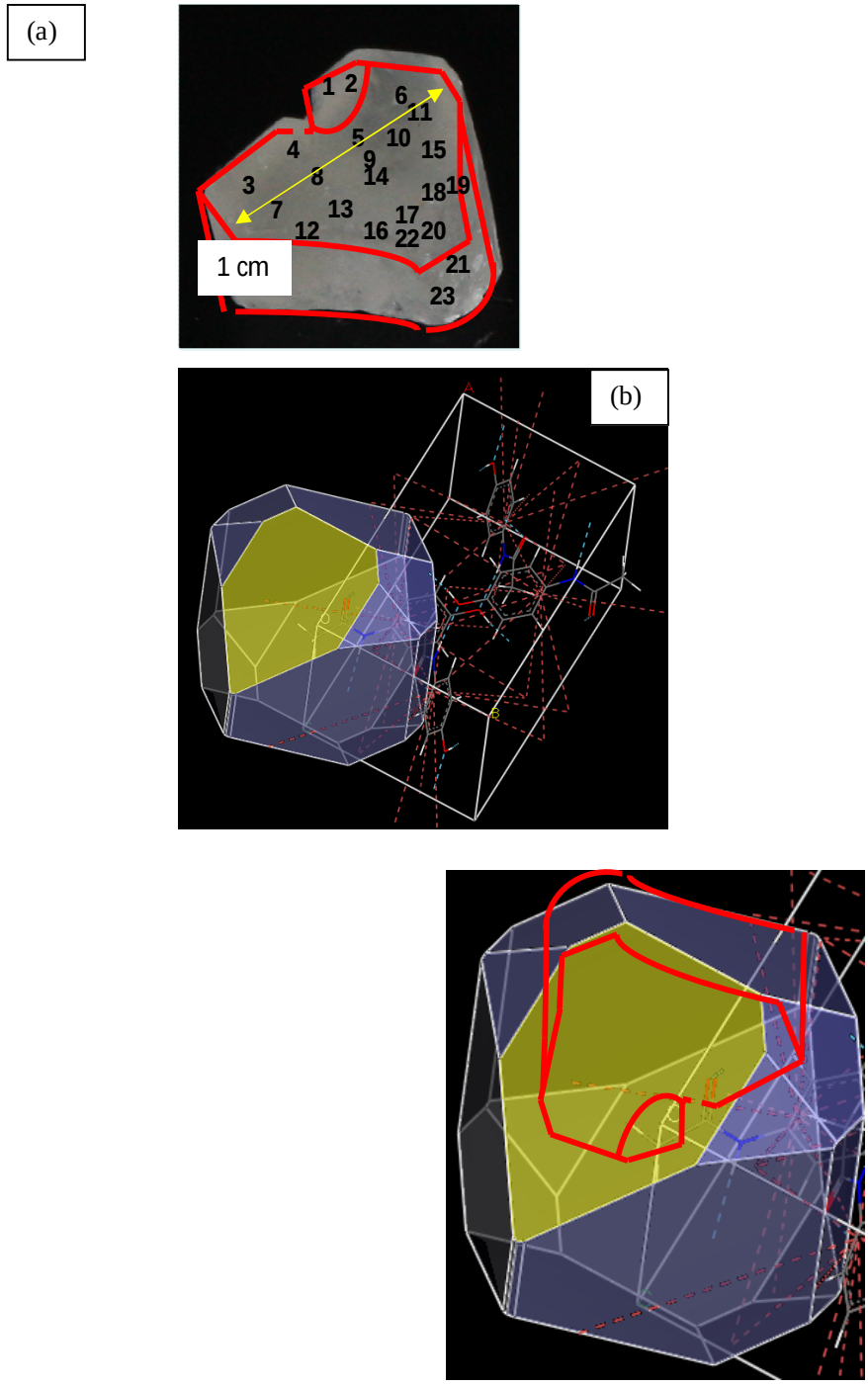

Figure 6-2 (a) Photograph of EtSingle crystal with areas of XPS small spot analysis indicated by numbers; spot 1: (0-1-1)-facet; spot 2: (-1-1-1)-facet; spots 3-20 & 22: (00-1)-facet, spot 21: (01-1)-facet; (b) BFDH construction that formed the basis for facet orientation assignment; bottom: sketch of single crystal superimposed over BFDH construction.

Paracetamol crystallisation from methanol (MeSingle1) generated the highest quality crystals with clear facets (**Figure 6-3**). The BFDH-derived orientations of the

facets were for this crystal independently confirmed through a Laue single crystal orientation (see next section below for details).

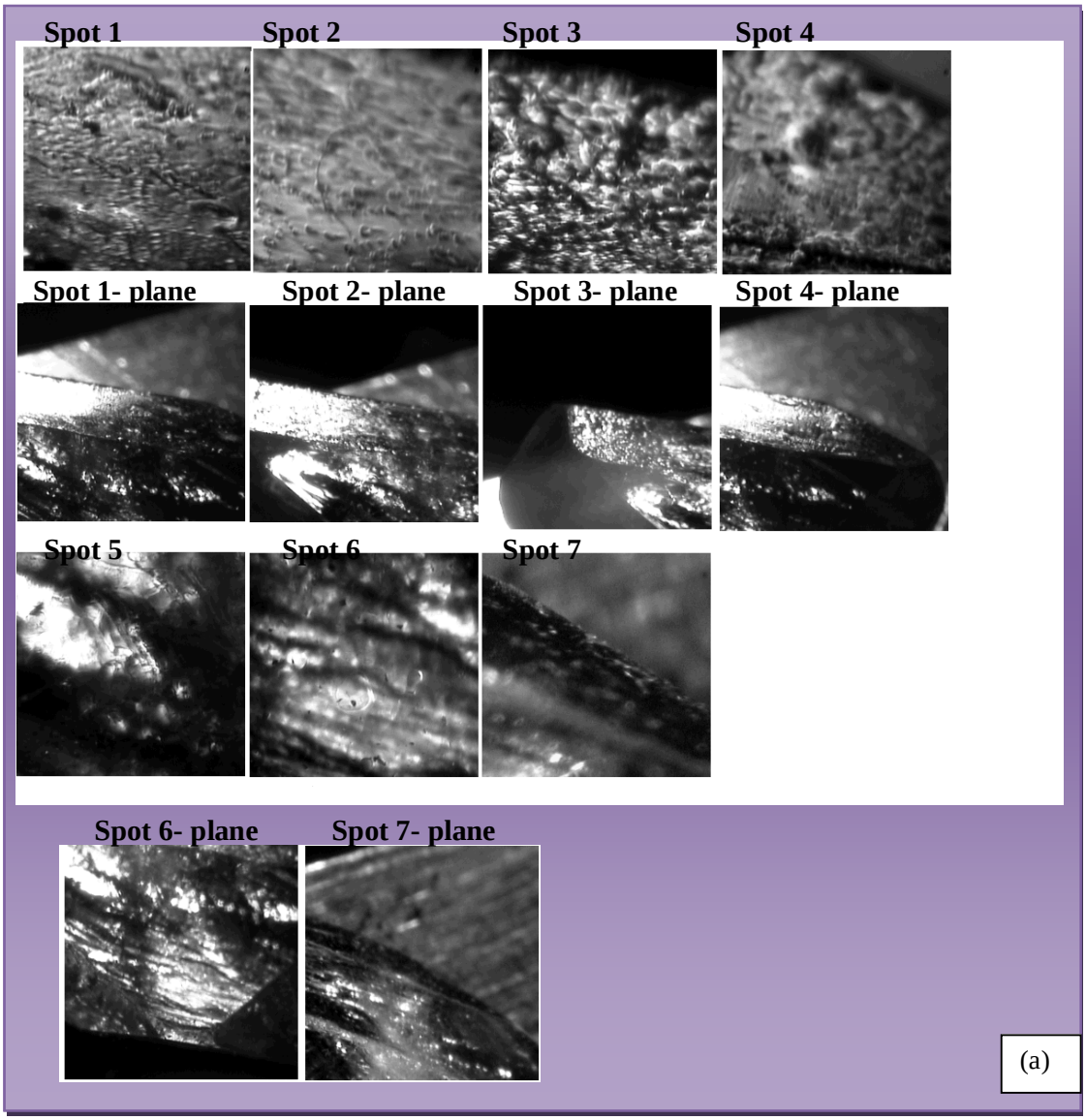

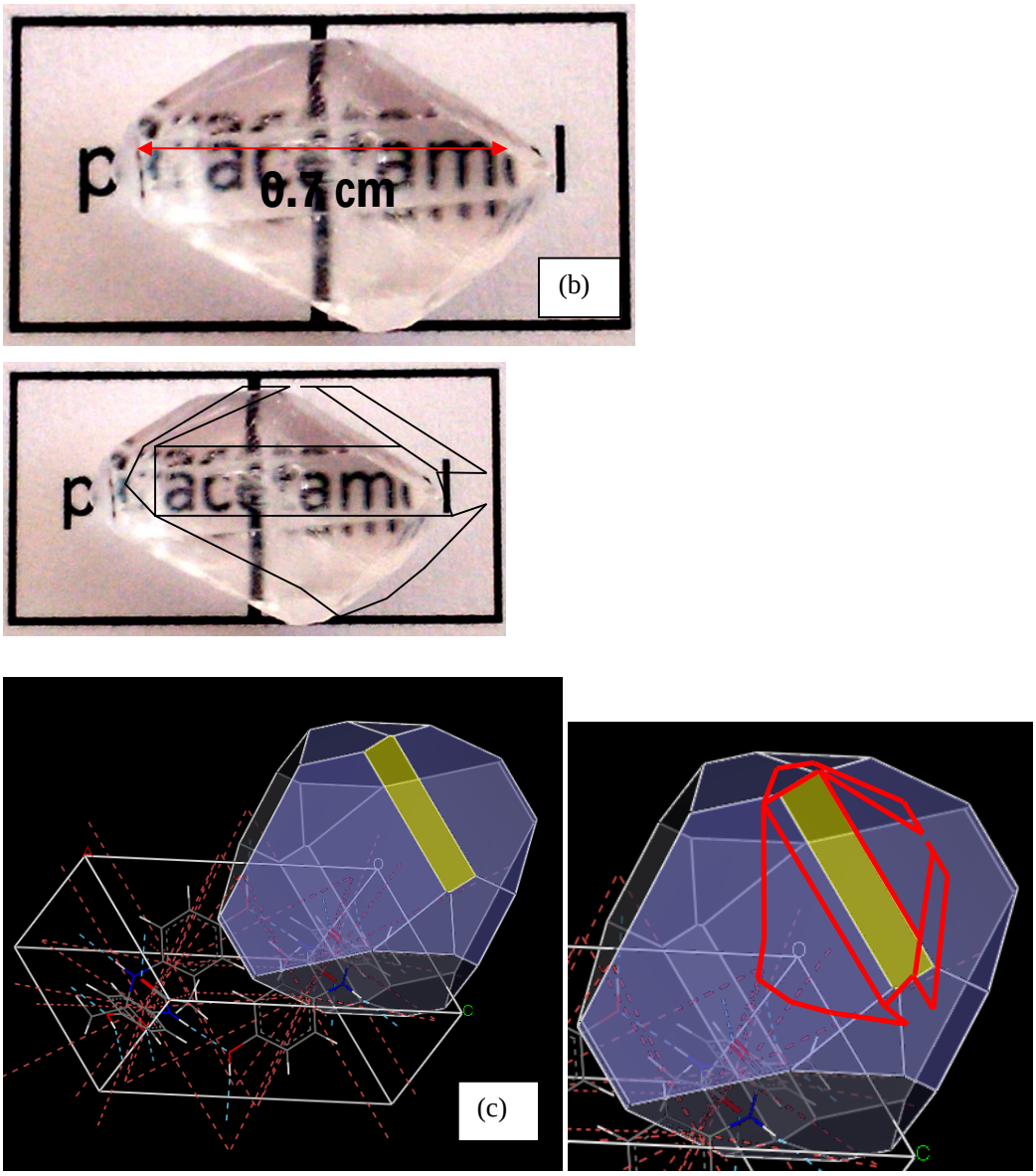

Figure 6-3: (a) Photographs covering 0.8 cm^2 around the XPS analysis spots on the MeSingle1 crystal; images were acquired *in situ* in the XPS analysis chamber; the XPS small spot analysis was taken in the central area of each photograph; Four spots, labeled 1 to 4, were chosen on the main (-101) facet, two spots, labeled 5 and 6, on the (011) facet and one spot (7) on the (11-1) facet. Spots 1 and 2 were in the middle of the (-101) facet, while spots 3 and 4 were at its edge. Tilting the holder at approximately 45° exposed facet (011) of the crystal. Only one spot (7) was analysed on facet (11-1) because of the geometric constraints on the detection of photoelectrons in that position. (b) photographs of the MeSingle1 crystal; (c) BFDH construction that formed the basis for facet orientation assignment, with sketch of single crystal superimposed over the BFDH construction.

Similarly, from the methanol-derived MeSingle2 crystal a total of 8 spots on 3 main facets were analysed, as shown in **Figure 6-4**.

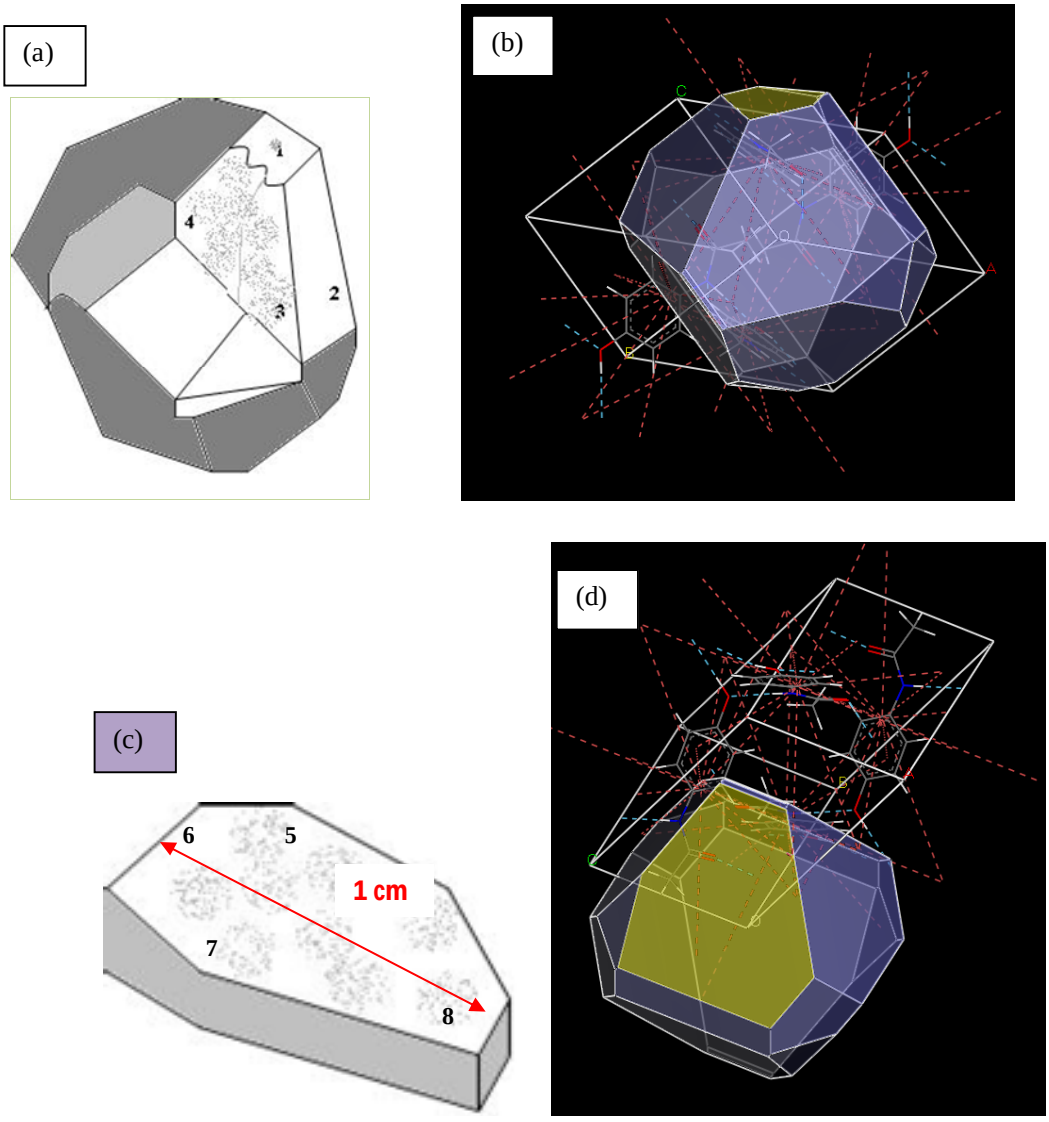

Figure 6-4: (a) Sketch of MeSingle2 crystal with areas of XPS small spot analysis indicated by numbers; spots 1: (1-11)-facet; spot 2: (20-1)-facet; spots 3,4: (00-1)-facet; spot 21: (01-1)-facet; (b) BFDH construction that formed the basis for facet orientation assignment; (c) sketch of MeSingle2 (1-10)-facet with areas of XPS small spot analysis indicated by numbers 5-8; (d) BFDH construction that formed the basis for facet orientation assignment.)

All orientations of investigated facets are summarised in **Table 6-1.** The scheme in **Figure 6-5** summarises which facets were examined by XPS.

Table 6-1: Orientation of all analysed facets of paracetamol single crystals as determined by BDFH analysis

Type of Single Crystal	Spots	Facets orientation
AceSingle	1	(0-20)
	2	(0-1-1)
	3	(-1-10)
	4	(1-10)
EtSingle	1	(0-1-1)
	2	(-1-1-1)
	3-20 &22	(00-1)
	21	(01-1)
MeSingle1	1-4	(-101)
	5 &6	(011)
	7	(11-1)
MeSingle2	1	(1-11)
	2	(20-1)
	3-4	(00-1)
	5-8	(1-10)

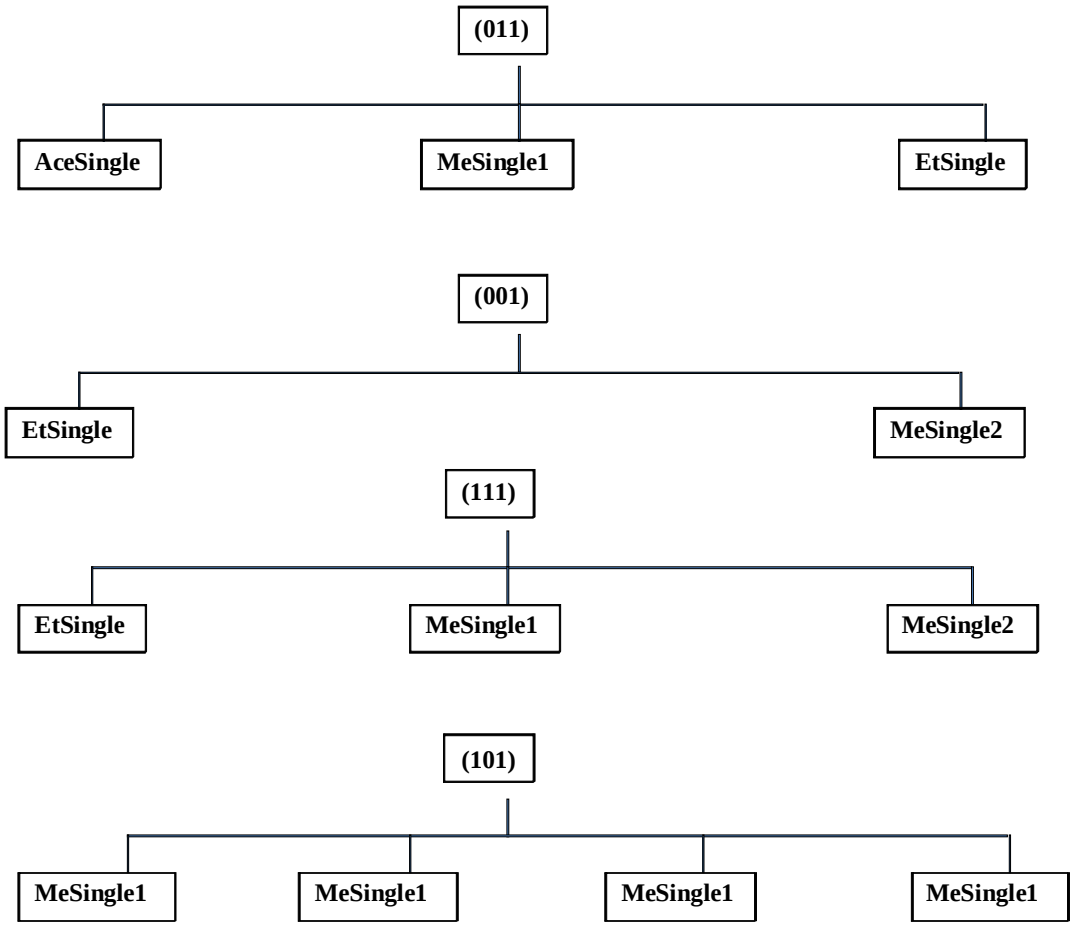

Figure 6-5: Summary of the facets of the single crystals prepared which were analysed

6.3.4. Laue Orientation of MeSingle1 Crystal Facet Orientations

The single crystals were generally too large for orientation in the X-ray goniometer available to the local analytical SXRD service. However, for the methanol-derived crystal, MeSingle1, the structure and the Miller indices of the crystal facets could be checked by single crystal Laue XRD (SXRD). Single crystal X-ray diffraction data were collected at 100 K with an Oxford Diffraction X-Calibur 2 diffractometer utilising Mo K_α radiation (λ = 0.71073 Å) and an Oxford Cryosystems Cryostream Controller 700. Data were recorded with the X-ray source operating at 50 kV and 40 mA. Data reduction, cell refinement, and multi-scan absorption corrections were carried out using the program CrysAlis RED (Oxford Diffraction Ltd., version 1.171.32.24, 2008). The structure was solved with SHELXS-97 and refined on F2 against all reflections with SHELXL-97. All non-hydrogen atoms were refined by direct methods anisotropically; all hydrogen atoms

were located in different Fourier maps and refined isotropically. The CIF file containing full crystallographic details has been deposited with the Cambridge Crystallographic Data Centre (CCDC) as HXACAN01.

The facets of the methanol-derived crystal were ascertained as (-101), (011) and (11-1), in line with the BFDH predictions (see above).

6.3.5. Attenuated Total Reflection IR

Bulk analysis of crystal purity was performed by grinding the single crystals to powders, which were analysed alongside as received powdered paracetamol by ATR-IR spectroscopy, using a Thermo-Nicolet Avatar Model 360 IR. A Golden Gate ATR sampling accessory was employed for the ATR-IR experiments. 1-2 mg of each sample was placed on the ATR sampling device (Ge crystal) and a torque of 20 cNm was applied. The IR spectrum was processed using the OMNIC ESP 5.1 software package. Ground crystal samples were used directly after preparation; no further treatment was needed before ATR analysis. For each experiment, the background was acquired before analysis of the sample. Each spectrum was measured twice for the purpose of monitoring reproducibility.

6.4. Results

Only monoclinic paracetamol single crystals could be analysed by XPS. As mentioned earlier, form II single crystals could not be analysed because their vapour pressure was too high, so that significant sublimation took place in the XPS analysis chamber.

6.4.1. ATR-IR Analysis

Figure 6-6 shows the ATR-IR spectra of ground crystals and powder paracetamol. The spectra of EtGround, MeGround and paracetamol powder were very similar, while AceGround was characterised by some significant differences in the spectrum, mainly at the C-OH peak of 3163 cm^{-1}, indicating that significant amounts of an OH-bearing contaminant were presented in the sample. This peak was much weaker in the spectra of EtGround, MeGround and powder. The C-N peak at 1223 cm^{-1} wavenumber was broader than those of other samples. The C=O characteristic peak was observed at 1651 cm^{-1}. Lower C=O indicates the amide group with lowest intensity on AceGround. No wavenumber shift was observed for any of the samples.

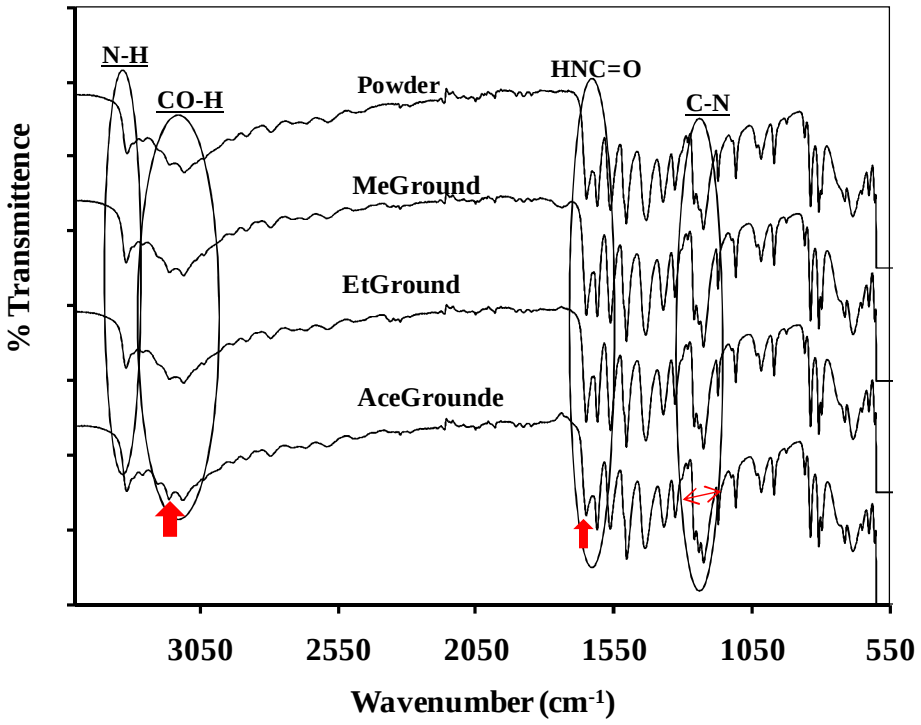

Figure 6-6: ATR-IR spectra of all the tested ground crystal samples compared with powdered paracetamol

6.4.2. PXRD Ground Crystals

PXRD characterisation was used to further examine whether there were any differences between the samples. A comparison by reference to the commercial powder is shown in **Figure 6-7**. Again, the acetone-derived crystal stands out by exhibiting significant evidence for lower crystallinity (less pronounced diffraction reflexes at higher 2θ values), while the ethanol derived sample exhibits evidence for preferred orientation or texturisation particularly through the high intensity peaks at about 40.5° and around 48°.

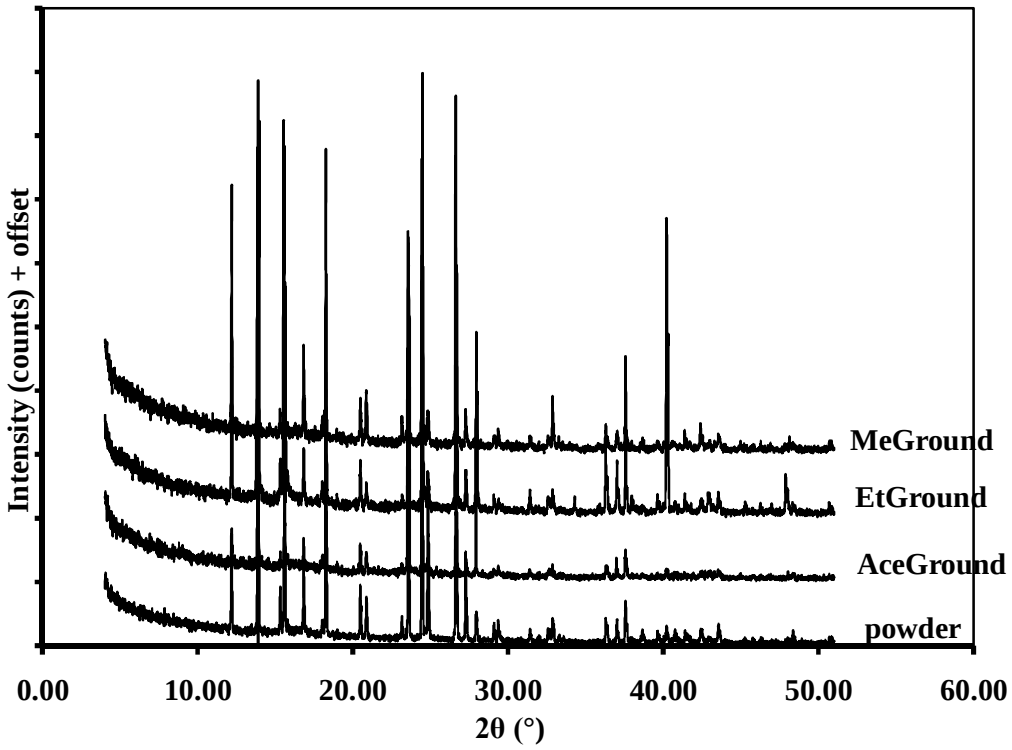

Figure 6-7: PXRD patterns of paracetamol powder and all the ground types of paracetamol crystal

6.4.3. XPS Survey Analysis

Figures 6-8 to 6-11 show the variations of atomic concentration to the selected facets as determined from the intensity of the C1s, N1s and O1s emission lines in XPS survey scans. The bar charts indicate that there were no major differences between single crystal types (AceSingle, MeSingle1, MeSingle2 and EtSingle) for either the (011), (001), (111) and (101) facets. For all samples, the C concentration was significantly higher than expected from the paracetamol stoichiometry (72.7%) while the concentrations of O and N were lower. This observation was broadly in line with previously reported results by Heng *et al.* who also reported higher than expected C 1s signals and lowered N 1s intensities; their results for O 1s emission intensities indicated near-stoichiometry for the (201), (001) and (011) facets, and reduced intensities for the (110) and particularly the (010) facets.

The magnitude the enhancements in C 1s intensities was in line with a number of previous studies of organic substances with our instrument (including the powder data reported in **chapter 5**), which have consistently indicated the presence of excess C on

crystalline organic substances[12-16]. Since it was well known that surfaces exposed to ambient atmosphere exhibit adventitious C contamination[17]; we have previously attributed these slight enhancements to the presence of such contamination. We will discuss below to what extent crystal facet-specific variations in the surface stoichiometry or matrix effects affecting the electron emission process may contribute to these variations.

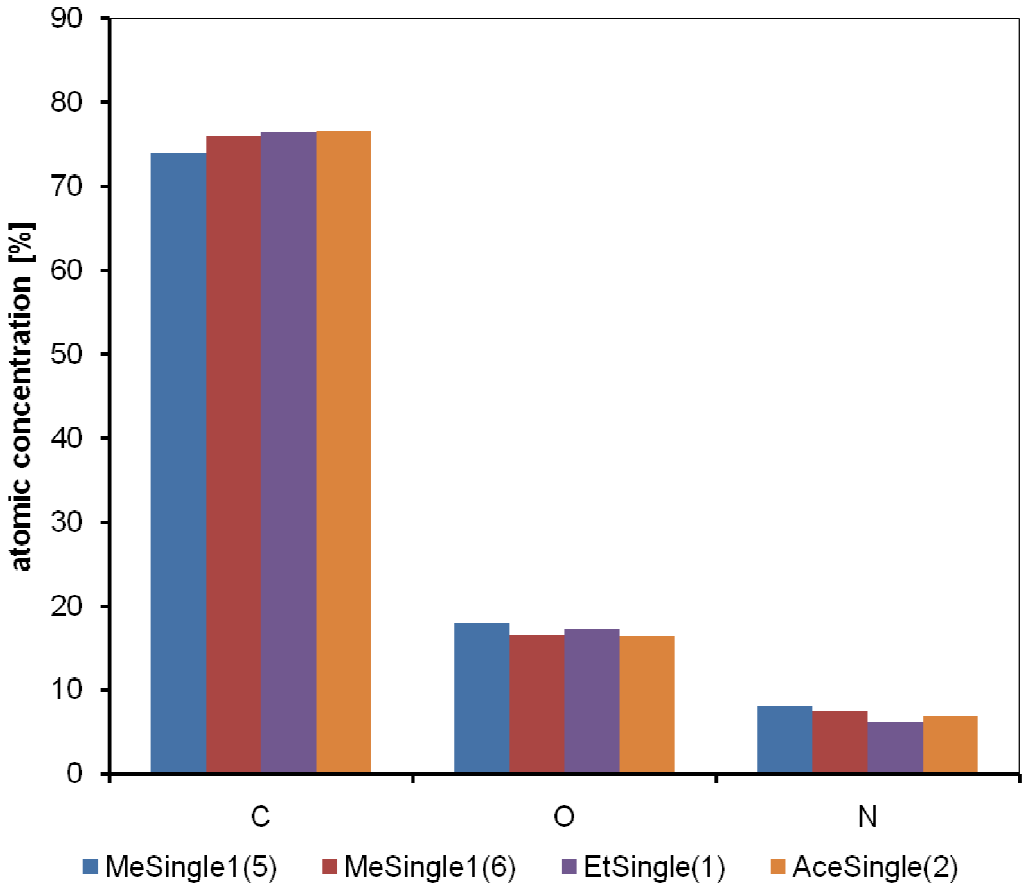

Figure 6-8: Survey elemental analysis of C, O and N elements on (011) facet

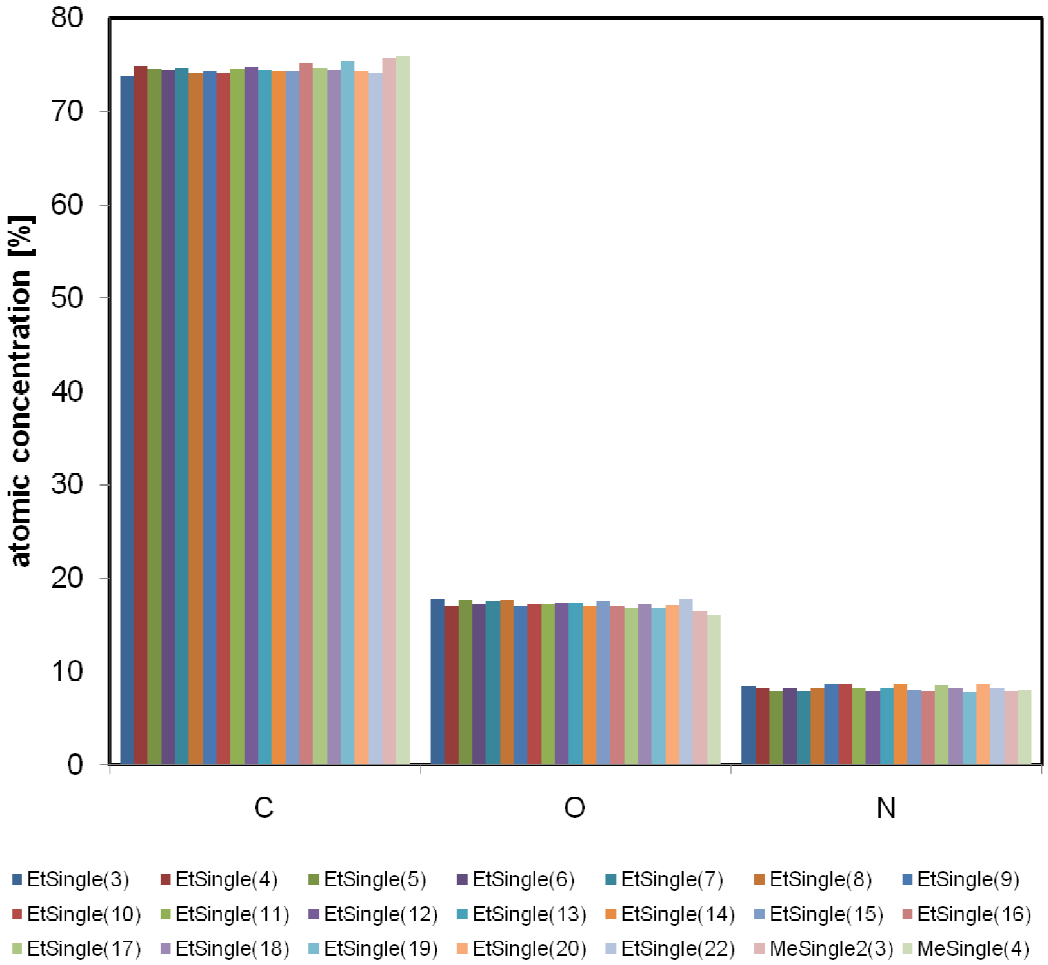

Figure 6-9: Survey elemental analysis of C, O and N elements on (001) facets

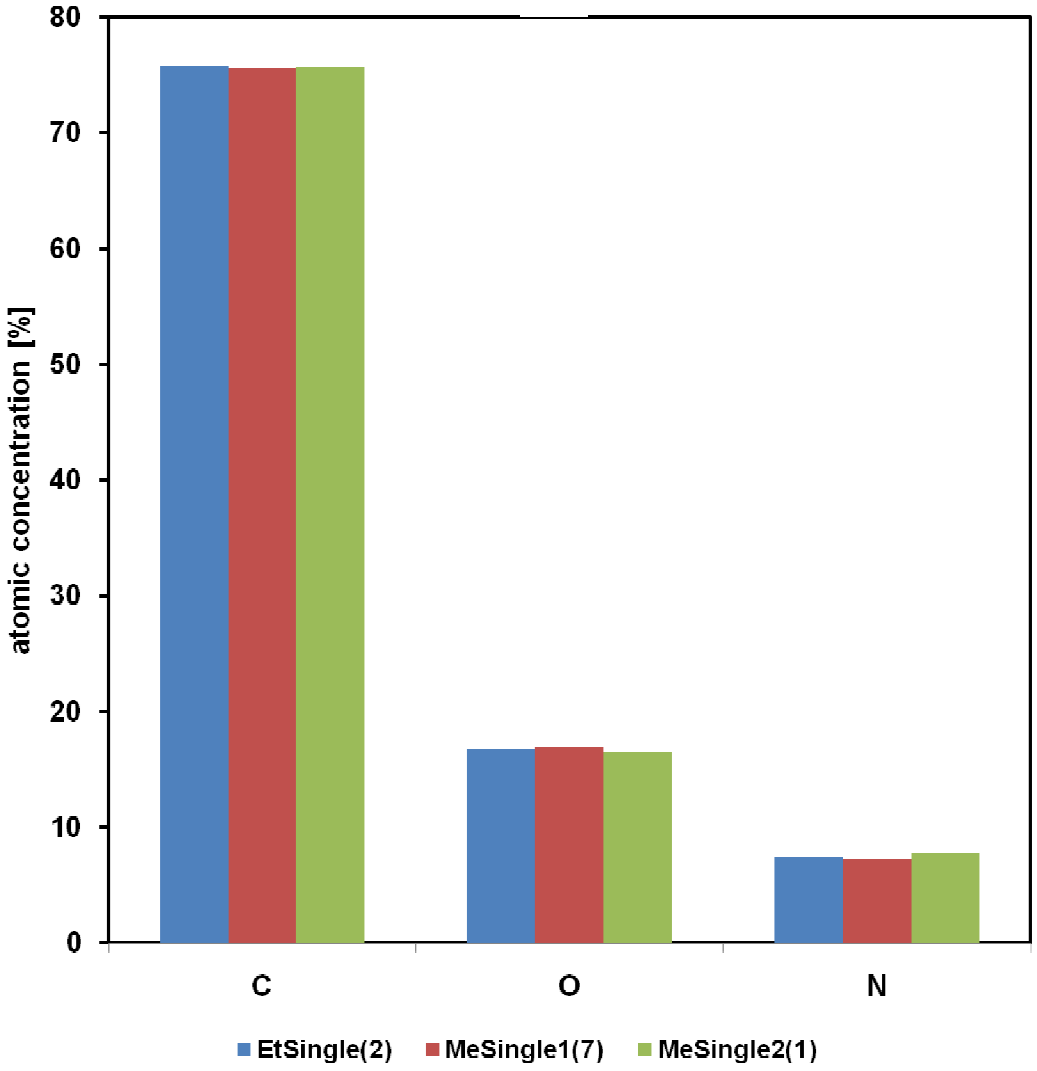

Figure 6-10: Survey elemental analysis of C, O and N elements on (111) facets

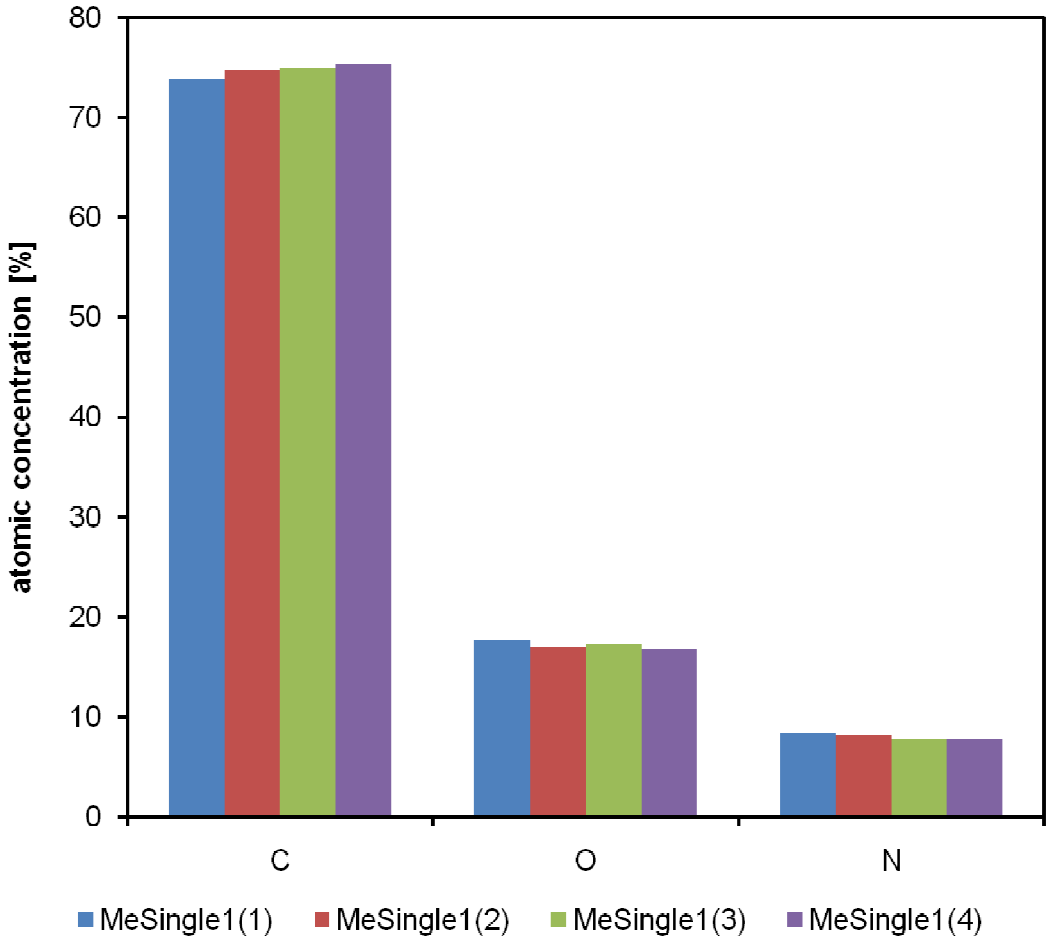

Figure 6-11: Survey elemental analysis of paracetamol crystal (101) facets

The paracetamol molecule is composed of carbon, hydrogen, oxygen and nitrogen atoms. Hydrogen cannot be detected by XPS because of its low photoelectron cross section. Typical survey spectra are shown in the **Appendix 1 and Appendix 5** illustrating the C, O and N 1s photoelectron lines and their KLL Auger peaks of three different single crystal differentiated by solvents used during crystallisation. **Figure 6-5** shows the chart of paracetamol facets analysed at various crystallisation solvents such as acetone (AceSingle), ethanol (EtSingle) and methanol (MeSingle). The stoichiometric ratio for C, O and N expected from the elemental composition of the molecule is 8:2:1. **Table 6-2** summarises the results for the average concentration of spots analysed; the standard deviation was found to be 0.2 to 0.8.

It can be seen (**Table 6-2; column 2**) that the C concentration was a little higher than the expected value for all crystal types. It is likely that the excess C concentration,

which reduced the corresponding O and N percentages **(Table 6-2; column 3 and 4)**, represents hydrocarbon contaminants on the crystal surface[12]. The enhanced C to O ratio is therefore likely also due to contamination with adventitious carbon (hydrocarbon) contamination. **Table 6-2; column 5**, shows that for all samples the results were not significantly different.

Examining the O/N concentration ratio revealed a trend. Because most solvents and common contaminants dissolved in solvents tend to contain a significant amount of oxygen-bearing functional group the O/N ratio was particular instrumental for identifying whether crystallisation solvents generated clean paracetamol surfaces. Both acetone-derived crystals (AceSingle1 and AceSingle2) were characterised by the highest value of the O/N ratio, suggesting that deposition of contaminants from acetone solutions was particularly strong. The lowest O/N ratio was obtained for untreated powder paracetamol, indicating that the supplied material had overall higher surface cleanliness than the single crystals. Methanol- and ethanol-derived crystals had intermediate O/N ratios.

Table 6-2: Elemental analysis of single crystals and powder crystals of paracetamol.

	%C	%O	%N	C:O	C:N	O:N
Stoichiometric composition	72.7	18.2	9.1	4.00	8.00	2.00
AceSingle1	76.14 ± 0.47	17.03 ± 0.20	6.83 ± 0.28	4.47	11.15	2.49
Experim – Stoichiom*	3.44 (+5%)	-1.17 (-6%)	-2.27 (-25%)	0.47	3.15	0.49
AceSingle2	75.03 ± 0.59	17.76 ± 0.16	7.21 ± 0.76	4.22	10.41	2.46
Experim – Stoichiom*	2.33 (+3%)	-0.44 (-2%)	-1.89 (-21%)	0.22	2.41	0.46
EtSingle	74.92 ± 0.57	17.14 ± 0.21	7.92 ± 0.58	4.37	9.46	2.16
Experim – Stoichiom*	2.22 (+3%)	-1.06 (-6%)	-1.18 (-13%)	0.37	1.46	0.16
MeSingle1	74.21 ± 0.58	17.76 ± 0.74	8.03 ± 0.22	4.18	9.24	2.21
Experim – Stoichiom*	1.51 (+2%)	-0.44 (-2%)	-1.07 (-12%)	0.18	1.24	0.21
MeSingle2	75.28 ± 0.74	16.99 ± 0.88	7.73 ± 0.17	4.43	9.74	2.20
Experim – Stoichiom*	2.58 (+4%)	-1.21 (-7%)	-1.37 (-15%)	0.43	1.74	0.20
Powder	75.33 ± 0.54	16.74 ± 0.21	7.93 ± 0.32	4.50	9.50	2.11
Experim – Stoichiom*	2.63 (+4%)	-1.46 (-8%)	-1.17 (-13%)	0.50	1.50	0.11

* Absolute differences between experimental results and expected stoichiometry are reported alongside (in brackets) the relative deviation (in %).

6.4.4. C 1s

High resolution spectra of all the samples are presented in the **Appendix 2, 6.9-11**. All spectra have three peak regions: two low intensity peaks at high binding energies and one main peak at lower binding energy with a complex shoulder.

The C 1s spectra were fitted with six carbon signals to accommodate the six chemical environments in the paracetamol molecules. They first include the aromatic carbon (C=C) between 284.7 eV to 284.8 eV; second, the carbonyl (C–C=O) contributed at 285 4 eV to 285.2 eV; third, the phenolic C (C-OH) at binding energies between 286.0 eV and 286.3 eV; fourth, the C-N emission at higher binding energy between 285.9 eV and 285.7 eV, all in accordance with the increasing electronegativity of the environment around the emitting carbon atom; fifth, the amide N-C=O or C=O group was fitted within 288-288.3 eV[13] **(Table 6-3)**; sixth, the low intensity peak at the high binding energy above 290 eV is a π-π* shake up satellite, which is related to the presence of the aromatic ring[14].

Table 6-3: C 1s values of binding energy (E_B) and expected atomic concentration %

C 1s	No	%	Range (eV)
C=C (Aromatic)	4	50	284.7 to 284.8
C-C=O	1	12.50	285.2 to 285.40
C-N (Aromatic)	1	12.50	285.9 to 286.7
C-OH (Aromatic)	1	12.50	286.0 to 286.3
N-C=O	1	12.50	288.0 to 288.3
Shake-up	2		289 and above

During fitting the binding energy was constrained to within ±0.2 eV of E_B values previously reported for C 1s and O 1s [15]. Relative intensities and peak positions were allowed to vary with a permitted residual standard deviation (RSD) from the ideal paracetamol stoichiometry of 0.9 to 1.3. For instance, from stoichiometry calculations the expected N-C=O concentration was 12.5%, but for an RSD below 1.3 the best fitted N-C=O percentage was only 10.5%. The C=C binding energy was fixed at 284.7 eV and the overlapping peaks in its shoulder fitted applying the above constraints. The peak of N-C=O at 288 eV was separated enough in E_B to not suffer from interference of other peaks during fitting and needed no restraints or constraints. The shake-up peak intensity was

about 5-8% of the whole spectrum and was also fitted without any E_B or fwhm constraints. The overall spectral shapes obtained from all types of single crystal facets and powder paracetamol were much more similar to each other than in the previous study by Heng *et al.*[16] No shake up peaks were apparent in previously reported results (**Figure 6-12**) in contrast to the data for two of the facets reinvestigated here [(011) and (001)]. The reason for the dissimilarities of the results may lie in a different background subtraction method, the use of a non-monochromated MgK_α source, the use of higher detector pass energy of 40 eV or different charge neutraliser settings.

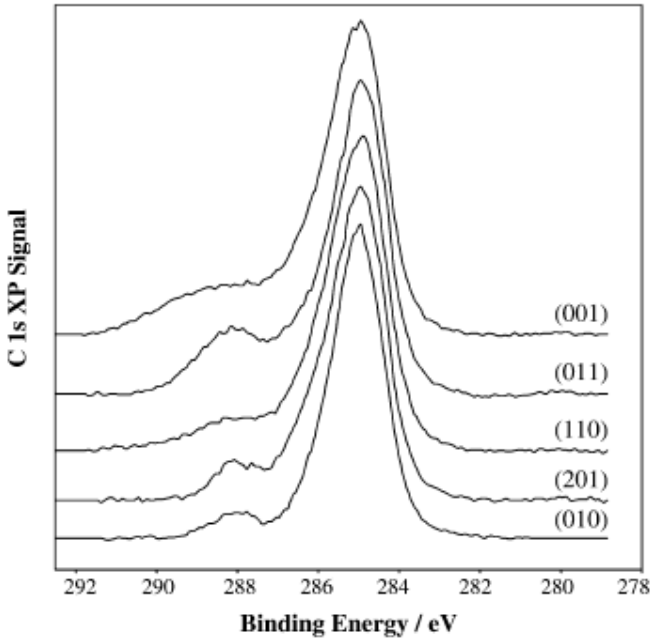

Figure 6-12 : C 1s spectra at 5 facets obtained from previous study by Heng

6.4.5. O1s

The O 1s spectra for all samples revealed similar spectral envelopes. Two peaks were assigned as C-OH and C=O at 531.3 eV and 533 eV, respectively (**Appendix 3, 7, 12-14**).

6.4.6. N 1s

The N 1s spectra **(Appendix 4, 8, 15-17**) exhibit a single peak at 400.1 eV, due to one type of nitrogen environment assigned as amide, N-C=O. The narrow fwhm of 1.2 eV provides strong evidence that for fitting a second peak within the envelope was not necessary.

6.5. Discussion

6.5.1. Probing Depth and Attenuation of C 1s, N 1s, and O 1s Emission Signals

While some aspects of the probing depth of XPS on organic substrates have been touched upon in earlier chapters it still seems worthwhile to delve more into the quantitative aspects of XPS analysis before considering the physical significance of the acquired XPS data. This will facilitate a more meaningful discussion of the data.

Using the TPP-2M formula for the inelastic mean free path (IMFP) of electrons with kinetic energies below 2 keV in organic matter[18], the expected depth attenuation of emission intensities from a semi-infinite sample slab at normal emission can be predicted at least semi-quantitatively. The IMFPs predicted by this method for C 1s, N 1s and O 1s photoelectrons excited by Al K_α are 33.1 Å, 30.6 Å and 27.5 Å, respectively[18]. Facet-specific properties on clean single crystal surfaces are predominantly caused by variations in crystal structure termination in the topmost layer of molecules. We are therefore predominantly interested in this surface region of the crystal, where elastic scattering effects can, in a good first approximation, be neglected because elastic scattering does not influence the depth attenuation of electrons near the surface as strongly as for deeper sub-surface regions of a crystal[19].

Assuming exponential attenuation and the above IMFP values, the resulting depth distribution functions (DDFs) of C 1s, N 1s, and O 1s electrons can be predicted. They are presented in **Figure 6-13**. It can be seen that with the increasing binding energy (i.e., decreasing kinetic energy) of the electrons from C 1s to O 1s the depth attenuation of the signal becomes slightly stronger, but variations between the three signals at no depth exceed differences of more than 10%.

The size of a paracetamol unit cell is, in any direction in the crystal, approximately 10 Å. Assuming a clean stoichiometric single crystal facet of paracetamol, the numbers of atoms of each element probed by an XPS signal from within the 10 Å nearest to this surface must therefore add up to the stoichiometric composition. Consequently, variations of the XP emission intensity from the three elements due to crystal facet-specific molecular orientations principally cannot exceed approximately the fraction of emission intensity coming from the topmost 10 Å of the sample.

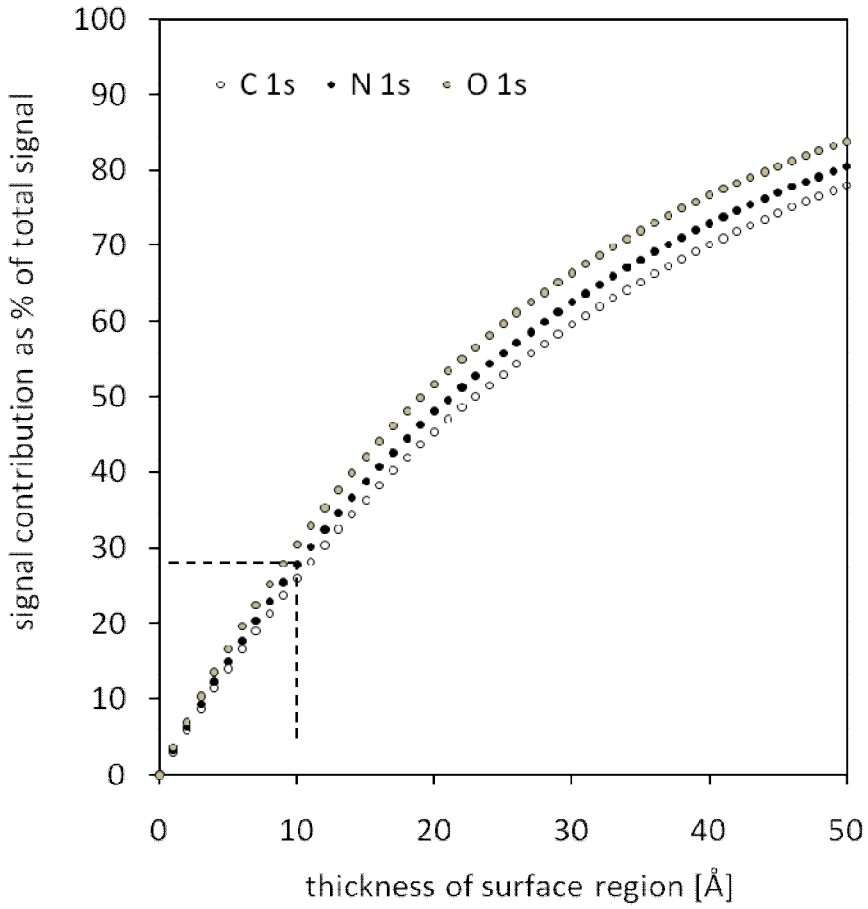

Figure 6-13: Depth distribution functions of the photoemission signals from C 1s, N 1s and O 1s at normal emission, estimated using the TPP-2M formula for the inelastic mean free path of electrons in paracetamol 20. The dashed lines indicate that only about 28% of the signals arise from a depth within about 10 Å near the surface.

Hypothetically contrasting the two most extreme cases, namely all nitrogen moieties exposed right at the surface vs. all nitrogen moieties pointed as far away from the surface as possible into the crystal bulk, the calculated DDFs in **Figure 6-13** indicate that the variation of the N 1s emission could therefore become at most approximately 30%, including an up to 15% *enhancement* of the N 1s emission intensity relative to paracetamol bulk stoichiometry in the case of N moieties exposed at the surface and a corresponding 15% *reduction* in the case of N moieties oriented towards the bulk. In reality of course, the variations in molecular orientation as a function of surface termination are much more subtle (see for example the molecular models for the (010) and (001) surfaces presented by Heng *et al* [21]) and will therefore be much less pronounced. It would seem that a consistent reduction of the N 1s emission by more than

about 10% relative to bulk stoichiometry would therefore almost certainly indicate that the composition of the near-surface region probed by XPS deviates so much from the bulk stoichiometry as to make the surface non-representative of a clean crystal facet. Measurable interfacial properties of such a surface would probably not be representative of a clean equilibrium facet of a paracetamol crystal.

An additional physical factor that may alter depth distribution functions in practice somewhat may be the so-called matrix effect[22], which arises as a result of emission asymmetry caused by direction-dependent variations in crystal composition. Most importantly, the density of crystal lattice planes varies significantly as a function of direction in the crystal. As a result the XPS probing depth at a surface terminating a crystal along a direction with large interplanar lattice spacing will be generally larger than at a surface terminating a direction with low interplanar spacings. Near-the surface, significant additional variations can arise due to reconstruction and lattice relaxation effects. However, the surface tension, and therefore the thermodynamic driving force for the occurrence of surface reconstructions and sub-surface relaxations, of molecular crystal surfaces tends to be much lower than in metallic, covalent and ionic crystals, which are held together by much stronger bonding than the dipole, van-der-Waals, π-π or London forces in molecular crystals. As a result, the mass density of paracetamol is likely to remain reasonably isotropic even in the near-surface and surface region, so relatively weak variations of matrix effects arising from lattice plane variations would be expected. Moreover, because only low-Z atoms are present the differences in inelastic and elastic scattering cross sections as well as forward and backscattering matrices will be similar throughout the crystal structure, with matrix induced differences probably most likely as a result of molecular orientation effects.

That matrix effects are unlikely to have a decisive influence on the C 1s, N 1s and O 1s intensity variations observed is suggested by the quantitative analysis of all XPS survey data, which revealed that deviations from stoichiometric composition do not follow a monotonic trend as a function of photoelectron kinetic energy; consistently, an enhancement of C 1s intensities (highest photoelectron kinetic energy) was observed, while a much stronger decrease of N 1s intensities (somewhat lower kinetic energy) was followed by relatively small deviations (usually a slight enhancement) from bulk stoichiometry for the O 1s emission (lowest kinetic energy). Such strong non-monotonic variations of emission intensities as a function of electron kinetic energy are unlikely due

to matrix effects because both the magnitudes and angle-dependencies of scattering and energy loss cross sections do not exhibit such non-monotonic trends.

Finally, it should be considered that the presence of significant contamination by solvent molecules or other contaminants in the bulk of the crystals may play a role in determining some of the observed variations. FTIR data did indeed indicate that the acetone-derived crystals may perhaps contain some NH or OH-bearing contaminants, which were not detectable for the ethanol- and methanol-derived single crystals. Interestingly, the acetone derived crystals also do exhibit evidence for much stronger N 1s attenuation than the methanol and ethanol-derived crystals, which exhibited N 1s attenuation similar to the pure starting material powder. These results for the alcohol-derived crystals in conjunction with the consistent good quality of the powder diffraction patterns of ground crystals and of the single crystal pattern of the methanol-derived single crystal indicate that strong *bulk* contamination of the crystals is absent.

6.5.2. Attenuation of the N 1s Emission from the Amide Group

The signals associated with the amide group of paracetamol are most diagnostic for the assessment of surface properties because N is an element absent from practically all environmental contaminants commonly found on surfaces handled in a laboratory environment. The N atoms therefore provide us with the most reliable searchlight for examining the effects of surface termination, facet orientation or surface contamination and shall be examined in more depth. The results of the elemental analysis from the survey spectra (**Table 6-2**) indicated that the N 1s emission intensities were *always* reduced, between 12% and 25% relative to bulk stoichiometry, depending on facet orientation and solvent used for the preparation of the crystals. Crystallisation from acetone led to the most pronounced suppression of N 1s intensity. All N 1s intensity results obtained in this study are listed once more in **Table 6-4** below. It can be seen that not a single measurement revealed any *enhancement* of N 1s intensity relative to bulk stoichiometry. If facet–specific molecular orientation effects were the cause of the observed N 1s intensity variations then at least some preparations of facets should exhibit N 1s intensities above or near the stoichiometric value. These results indicate strongly that surface contamination effects have a decisive influence on the measured data, masking any facet-specific molecular orientation effects in the XPS data of the surfaces.

Table 6-4: Experimental XPS-derived N stoichiometries and the relative deviation from paracetamol bulk stoichiometry (9.1%) classified by facet orientation.

(011)		(001)		(111)		(101)	
Experim. [%]	Deviation from Stoich.	Experim. [%]	Deviation from Stoich.	Experim. [%]	Deviation from Stoich.	Experim. [%]	Deviation from Stoich.
8.04	-11.6%	8.44	-7.3%	7.45	-18.1%	8.41	-7.6%
7.46	-18.0%	8.16	-10.3%	7.32	-19.6%	8.2	-9.9%
6.24	-31.4%	7.85	-13.7%	7.79	-14.4%	7.76	-14.7%
6.92	-24.0%	8.31	-8.7%			7.77	-14.6%
		7.89	-13.3%				
		8.22	-9.7%				
		8.62	-5.3%				
		8.68	-4.6%				
		8.21	-9.8%				
		7.87	-13.5%				
		8.22	-9.7%				
		8.63	-5.2%				
		8.09	-11.1%				
		7.86	-13.6%				
		8.55	-6.0%				
		8.3	-8.8%				
		7.81	-14.2%				
		8.65	-4.9%				
		8.19	-10.0%				
		7.85	-13.7%				
		7.99	-12.2%				

As can be seen by consultation of the signal depth distribution functions in **Figure 6-13**, the presence of the commonly observed thin surface contamination layer of adventitious carbon equivalent to a thickness of a few Å would be sufficient to explain the observed reductions in N 1s intensity by typically up to 15%. As argued above, facets exhibiting even higher levels of N 1s emission intensity reductions are almost certain to be highly non-stoichiometric within the depth probed by XPS. That the observed N 1s deviations are for many preparations, especially the methanol and ethanol-derived crystals, weaker than or about the same as the value of –13% observed for the untreated powder (**Table 6-2**) suggests that the cleanliness of the starting materials, the preparation vessels and the media was good. Because of the much lower surface area of the macroscopic crystals one would otherwise expect higher surface concentrations of surface-active contaminants.

6.5.3. Intensity of the C 1s and O 1s Components from the Amide Group

The amide component in the C 1s emission spectra was well resolved and its intensity could thereby be quantitatively analysed relative to the total intensity of the C 1s emission, and the stoichiometry of the surface region probed by the C 1s emission thereby independently double-checked. There is an additional systematic uncertainty in the *relative* error of about ±5% in these data because of the presence of the shake-up losses in the C 1s spectra, for which it is not entirely clear how they will affect the intensities of the various emission components. Moreover, the C 1s emission is slightly less surface-sensitive than the N 1s emission (the signal depth distribution functions in **Figure 6-12** suggest an about 5% *absolute* enhancement of C 1s intensity), so the amide component should be slightly less sensitive to surface contamination than the N 1s emission.

The expected bulk-stoichiometric C 1s contribution from the amide group is 12.5% (one C in eight). The results of the quantitative analysis of the C 1s spectra are documented in **Figures 6-14** to **6-22** below. They show that the N-C=O (amide) intensities were very similar for all facets, around 9 ± 0.5%, equivalent to a reduction of amide concentration by about 28% ± 4%. This reduction is much stronger than that observed in the N 1s analysis, and certainly much stronger than those that facet-specific variations of crystal surface terminations could cause. The E_B of the N-C=O emission was consistently at about 288 eV to 288.1 eV, indicating that no significant variation of the structural environment around the amide group takes place between the samples. The

most plausible explanation for the very strong attenuation of the amide stoichiometry is again the suggested presence of a significant adventitious carbon contamination layer, which would enhance especially in the C=C regions of the C 1s spectra, which is exactly the observation borne out by the C=C intensity values reported in **Figures 6-14 to 6-22** below. The C=C intensity should be significantly reduced from its stoichiometric value of 50% (four out of eight C atoms) due to the shake-up losses in the aromatic system, but the data indicate for most samples intensities of more than 45%. The remaining C 1s contributions from the other functional groups (expected value: 12.5%, one out of 8 C atoms), while spectroscopically not as well resolved from each other as the amide contribution, are also close to expected bulk stoichiometry, supporting the view that adventitious carbon contamination accounts for most of the observed weakening of the emission from the amide group.

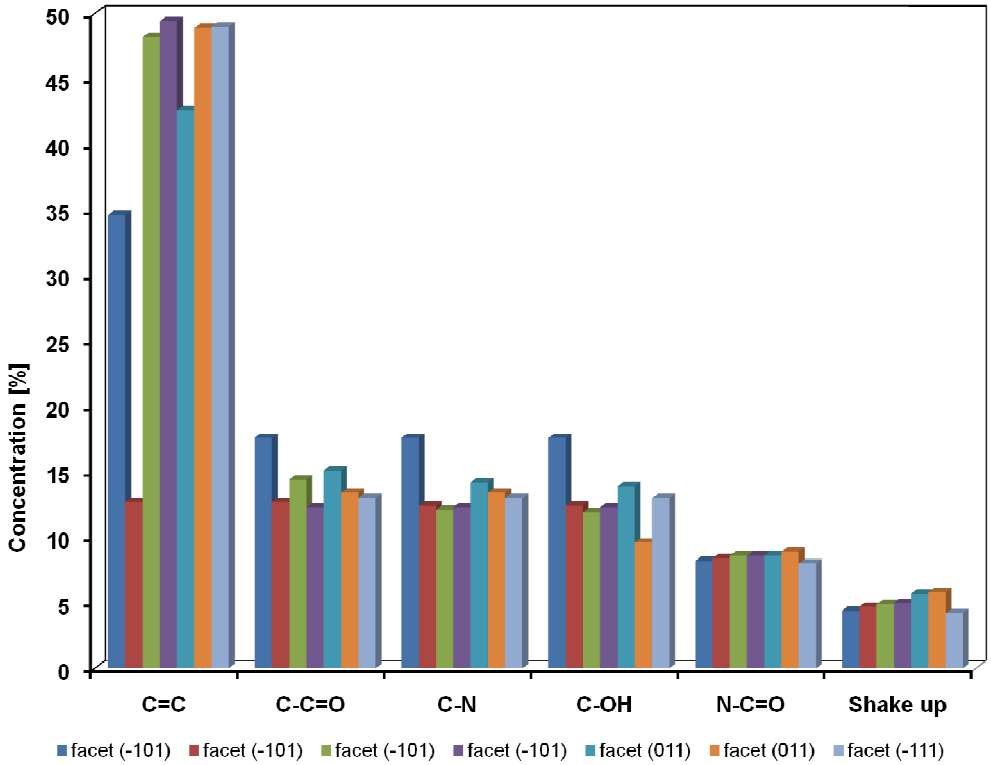

Figure 6-14: Methanol Single Crystal (MeSingle1) analyses for C 1s at all analysed facets

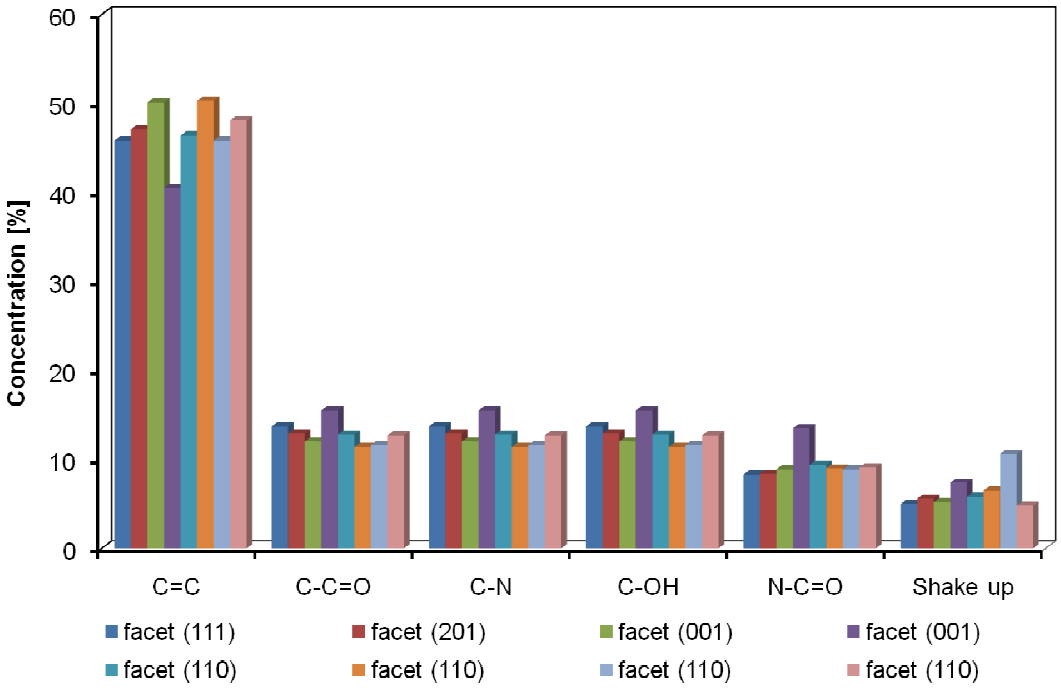

Figure 6-15: Methanol Single Crystal (MeSingle2) analyses for C 1s at all analysed facets

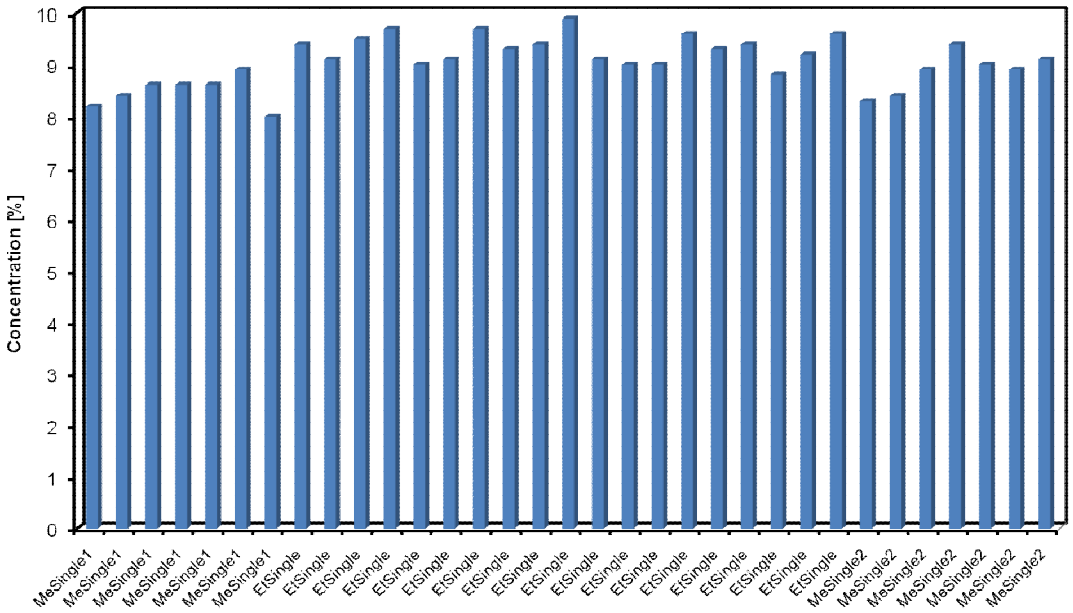

Figure 6-16: N-C=O concentration on MeSingle1, MeSingle2 and EtSingle at all facets analysed

6.5.4. Spatial Variations Across Single Facets

Finally, a few comments shall be made on results examining spatial variations of emission intensities on the crystal facets. For example, spots in the middle and edge of facets were analysed for the purpose of examining the uniformity across a facet. Spot 3 (101), 4 (101) and 6 (011) were at the edge of crystal (**refer to Figure 6-3**), while spot 1 (101), 2 (101) and 5 (011) were on the middle of the MeSingle1 crystal. **Figure 6-14** thus reveals a trend: the C=C concentration was high at the edge of crystal but C-N, C-C=O, C-OH concentrations were smaller in the edge area. Facet (011) shows high concentration of C=C but significantly low concentration of C-N and C-OH relative to (101) facet. However, the O 1s C=O and C-OH (**Figure 6-23**) were not showed a significant different. Reconfirmation of the analysis by MeSingle2 (different crystal) was made. At facet (001) and (110) of spot 3, 6 and 8 **(refer to Figure 6-15)** high concentration of C=C were obtained. Those spots were at the edge of the crystal facet. Consistently, all these data indicate that an enhanced concentration of C=C species is presented at the edges compared to the middle of the facets.

Further analysis focused on the (011) facet, as presented in **Figure 6-17** (this analysis was based on the fitting *without* FWHM and E_B constraints for all C 1s components) and **Figure 6-18** (this analysis was based on the fitting *with* FWHM and E_B constraints of six C 1s components representing all C moieties with different chemical environments). The corresponding O 1s data are presented in **Figures 6-23 and Figures 6-24**. This examination was carried out to reconfirm whether the presence of solvent was influential on the crystal surface. The difference between EtSingle/MeSingle to AceSingle results can be seen on the C=O (**Figure 6-18**), C=O/C=C (**Figure 6-17**), C-OH **(Figure 6-17**) and C-N/C-OH results (**Figure 6-18**). Similarly, **Figure 6-24 and 6-25** reveal no systematic trend of C=O and C-OH between MeSingle1, EtSingle or AceSingle of O 1s analysis. For both types of analysis (FWHM and E_B constrained 6-component *vs* unconstrained 4-component) there were significant differences observed only between spots 5 and 6 of MeSingle1 (**Figure 6-23**), which may well be related to the extreme positioning of spot 6 on the edge of a crystal facet. The trend observed on the facet (111) (**Figure 6-29**) indicates that for EtSingle and MeSingle, the cleanest systems investigated here, C=O and C-OH concentrations do not vary significantly. Unfortunately, due to the constraints in tilting the crystal to certain facets in the XPS analysis chamber, other facets were not investigated in similar detail.

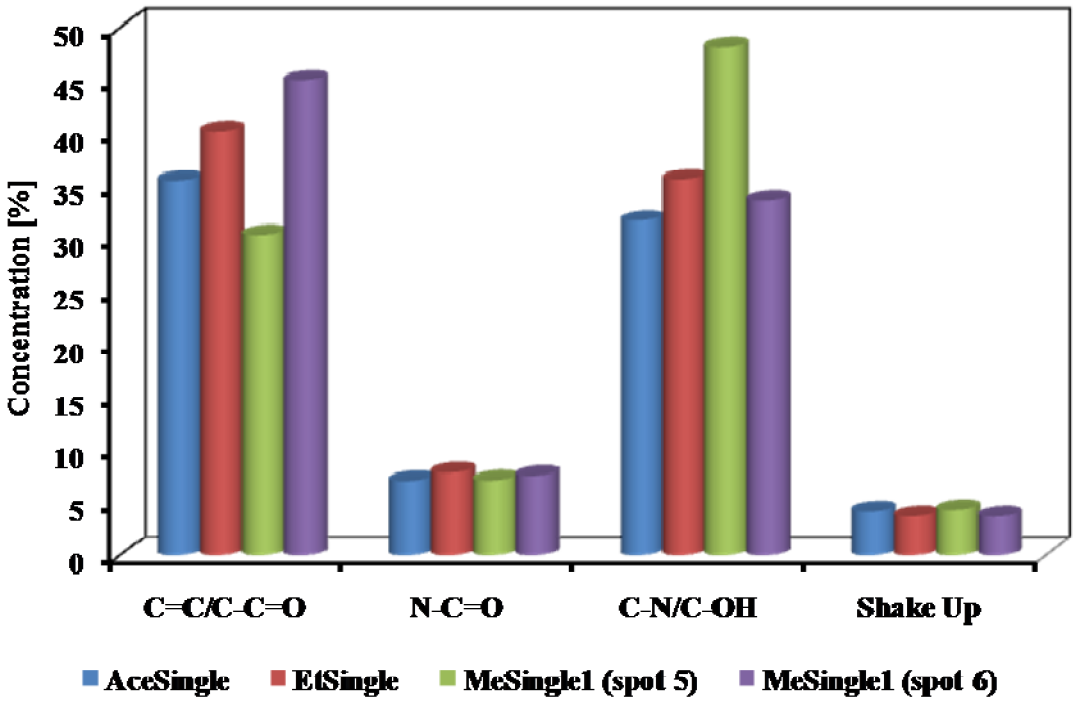

Figure 6-17: (011) facets analysis for three different single crystal at different C environment (4 peaks fitted during CasaXPS fitting)

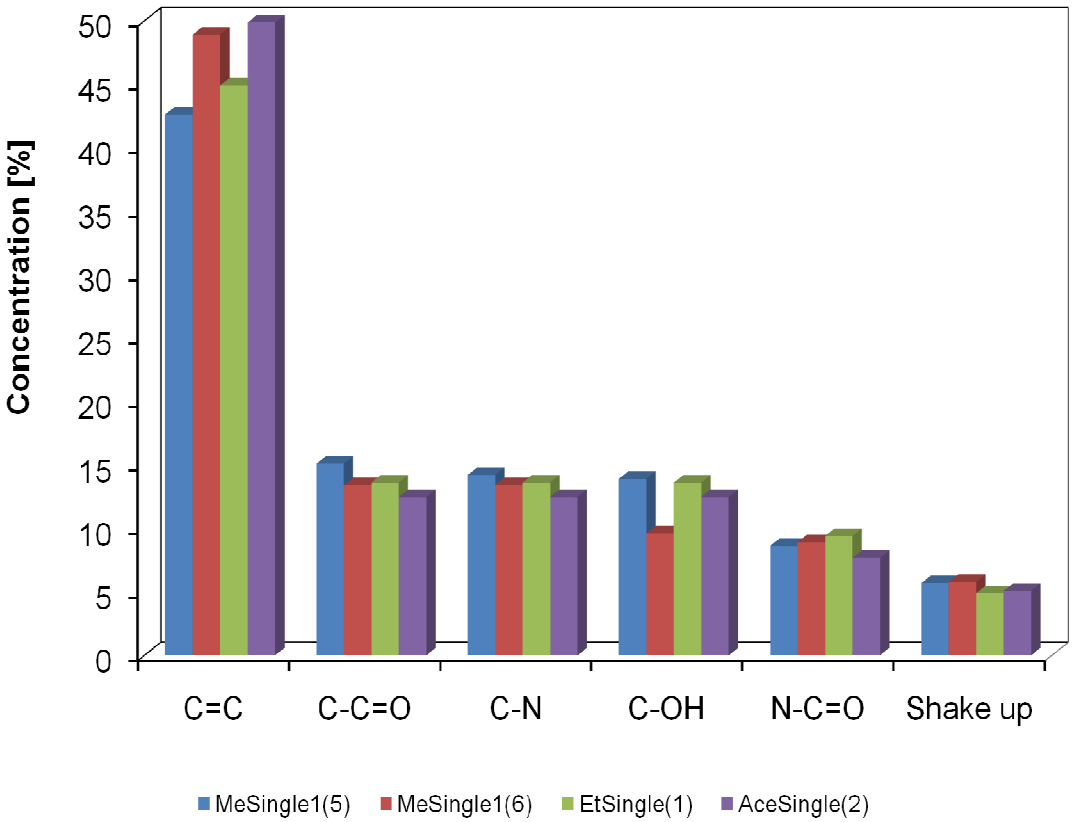

Figure 6-18: (011) facets analysis for three different single crystal at different C environment (6 peaks fitted during CasaXPS fitting)

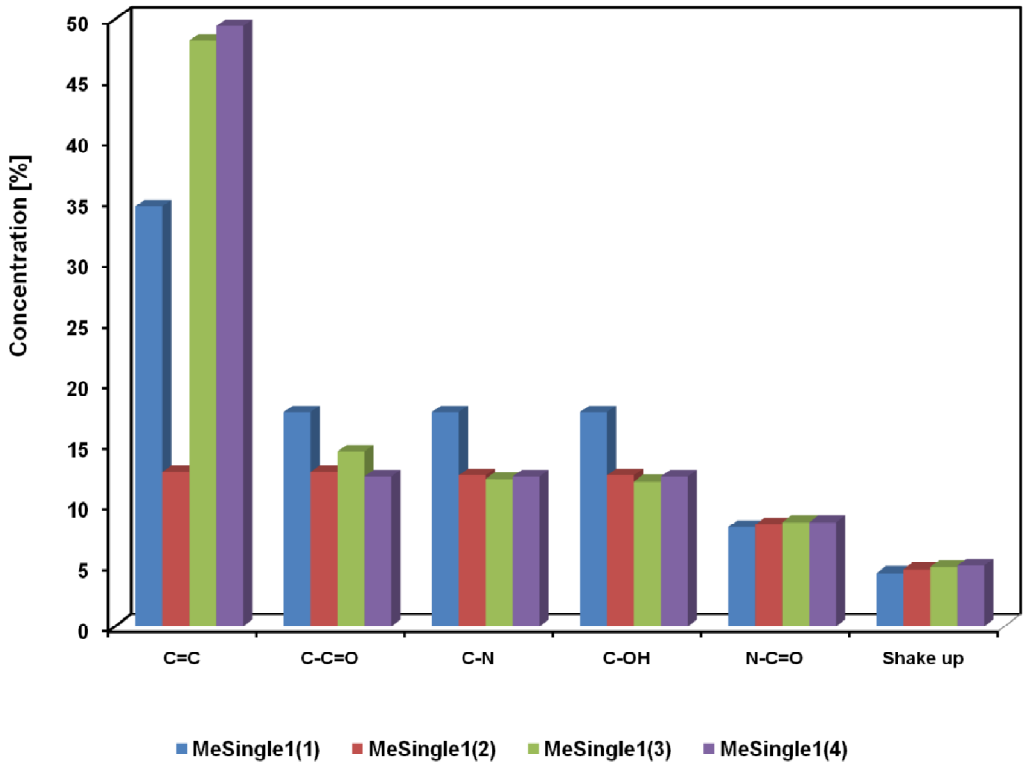

Figure 6-19: (101) facets analysis for three different area of MeSingle1 at different C environment (6 peaks was fitted during CasaXPS fitting)

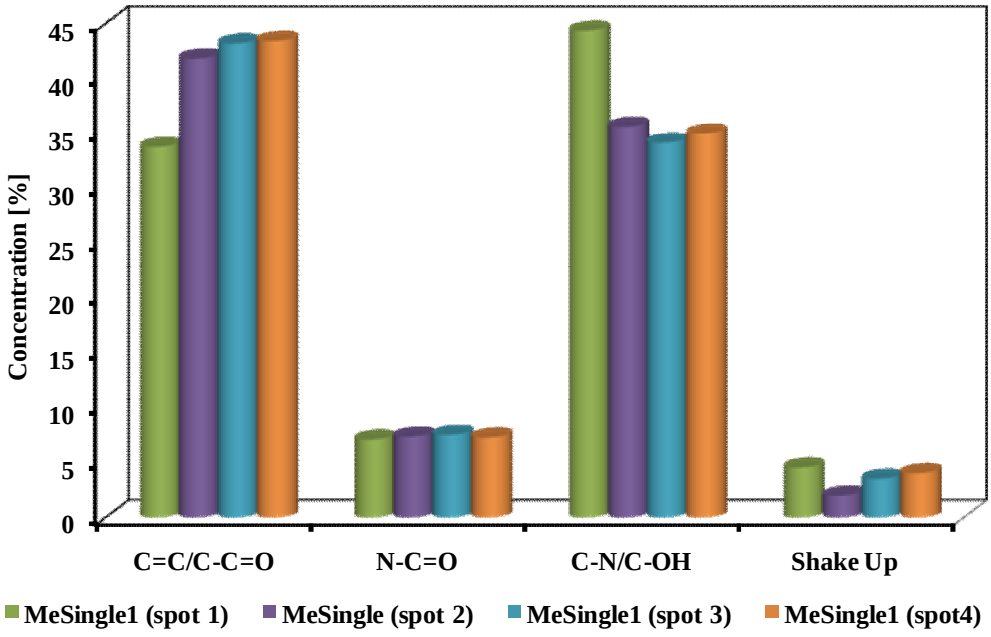

Figure 6-20: (101) facets analysis for three different area of MeSingle1 at different C environment (4 peaks was fitted during CasaXPS fitting)

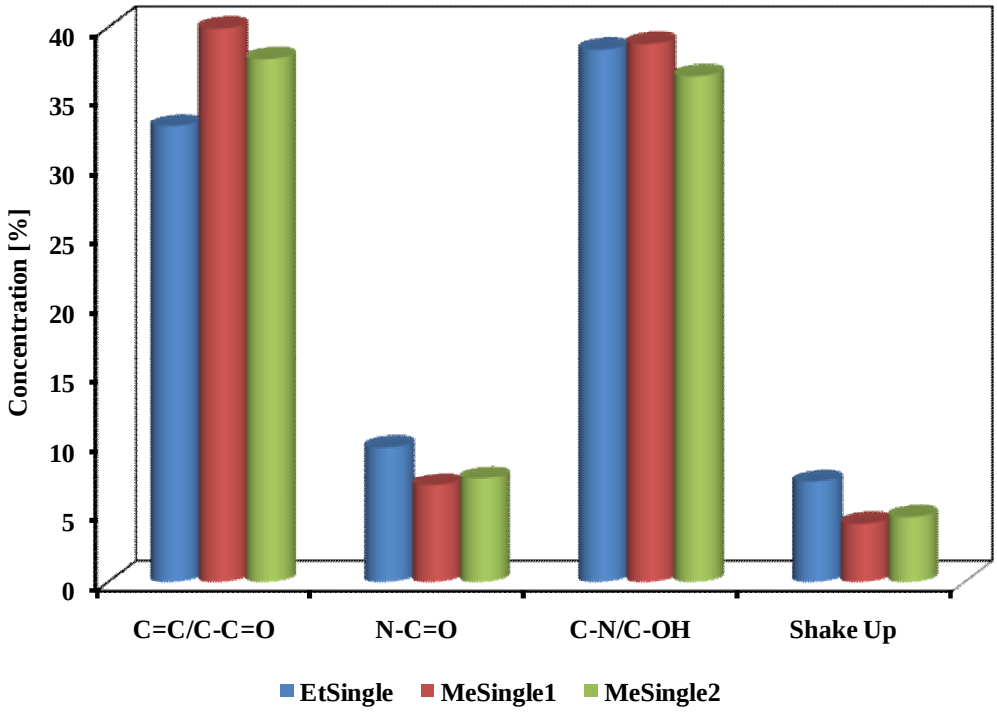

Figure 6-21: (111) facets analysis for three different single crystal at different C environment (4 peaks was fitted during CasaXPS fitting)

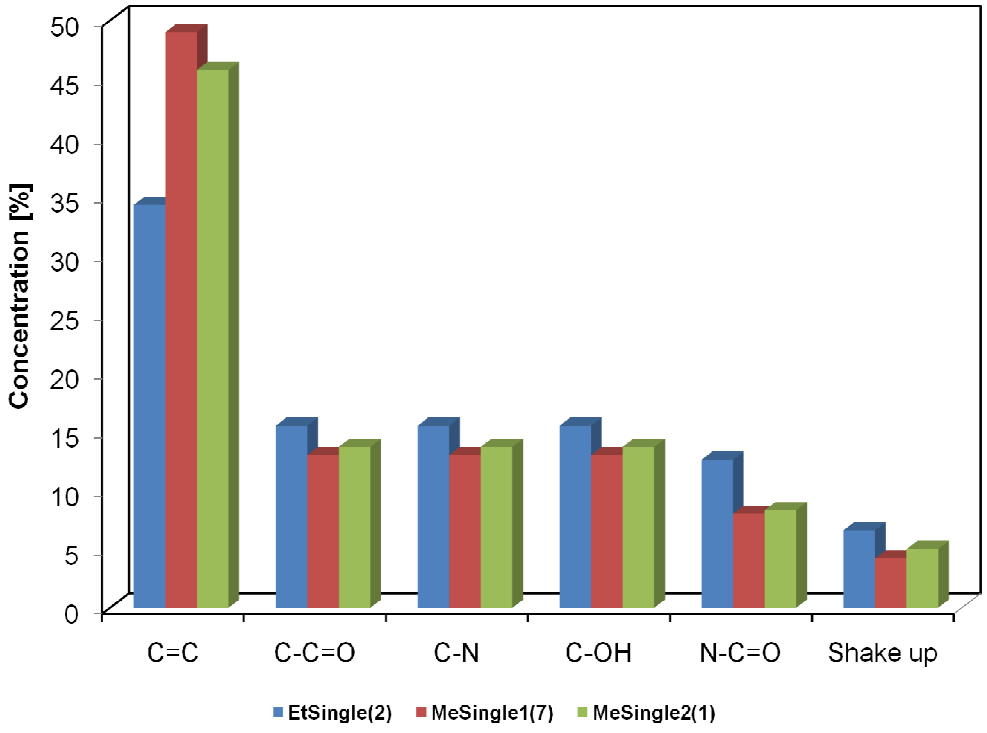

Figure 6-22: (111) facets analysis for three different single crystal at different C environment (6 peaks was fitted during CasaXPS fitting)

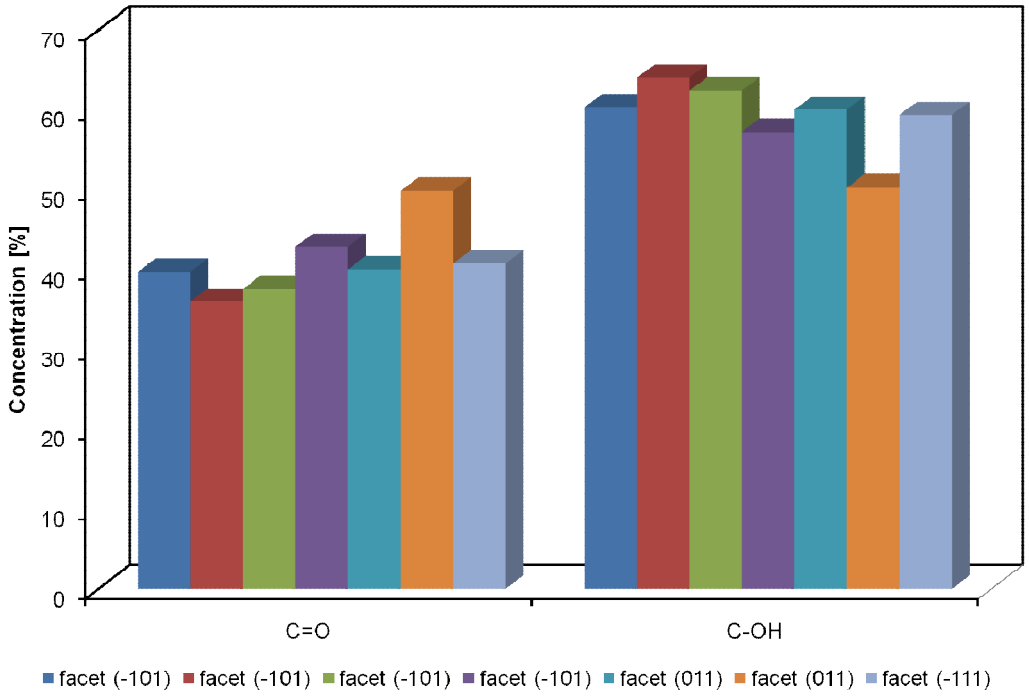

Figure 6-23: Methanol Single Crystal (MeSingle1) analyses for O 1s at all analysed facets

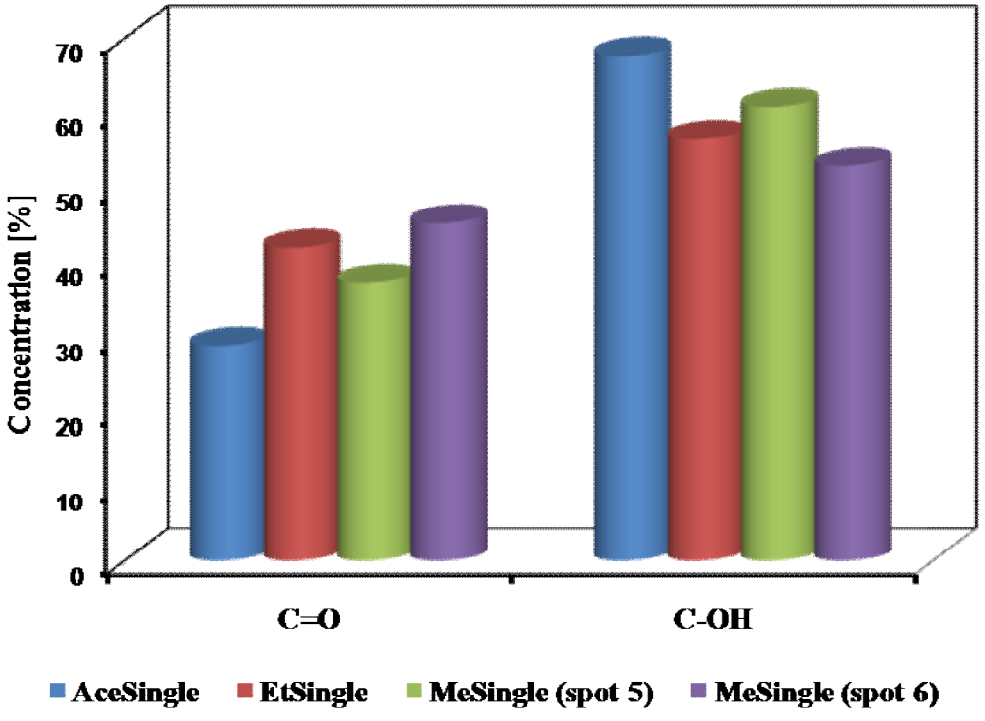

Figure 6-24: (011) facets analysis for three different single crystal at different O environment (4 peaks fitted during CasaXPS fitting)

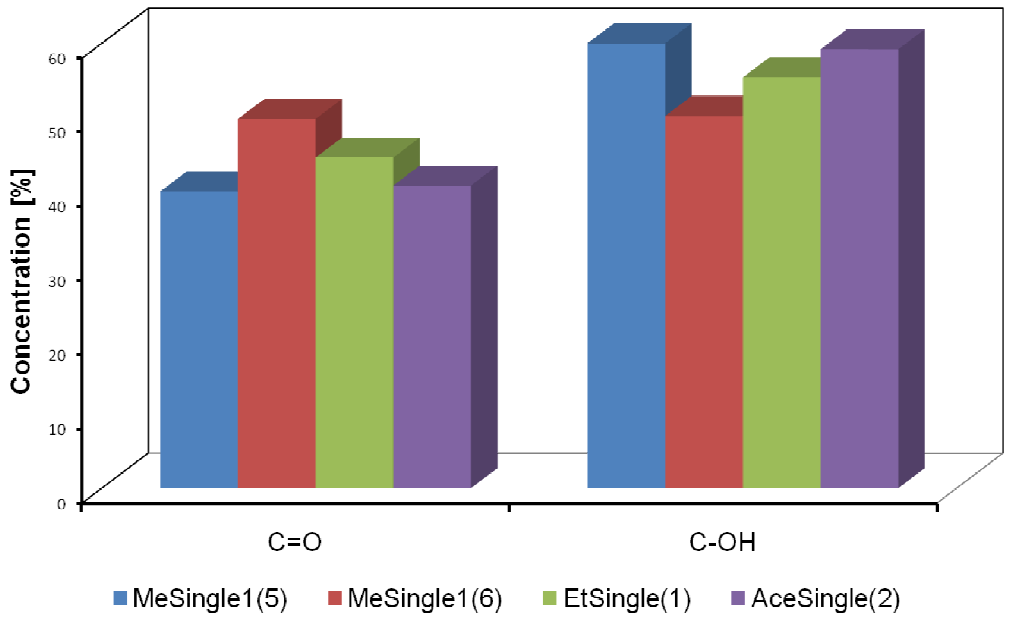

Figure 6-25: (011) facets analysis for three different single crystal at different O environment (6 peaks fitted during CasaXPS fitting)

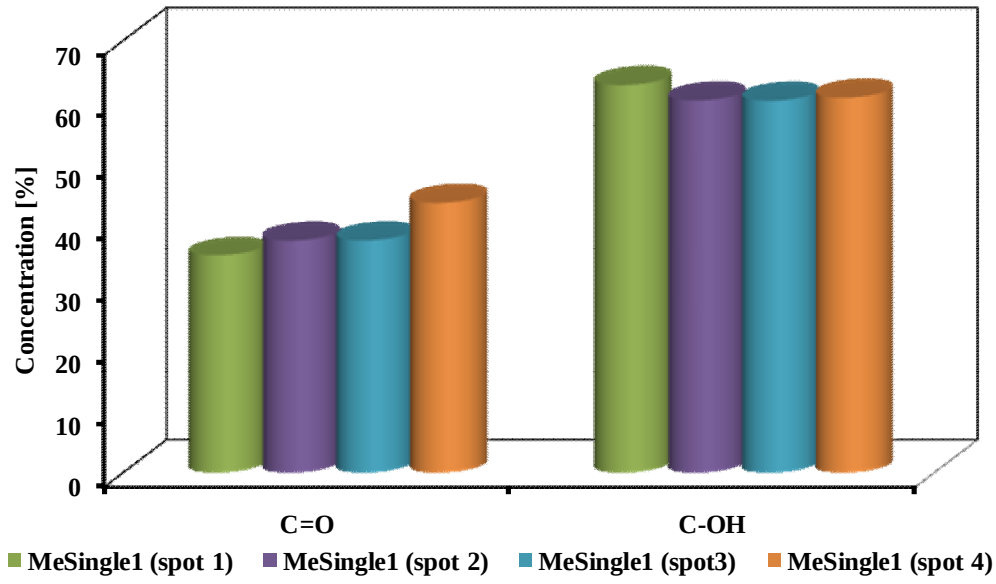

Figure 6-26: (101) facets analysis for three different area of MeSingle1 at different O environment (4 peaks fitted during CasaXPS fitting)

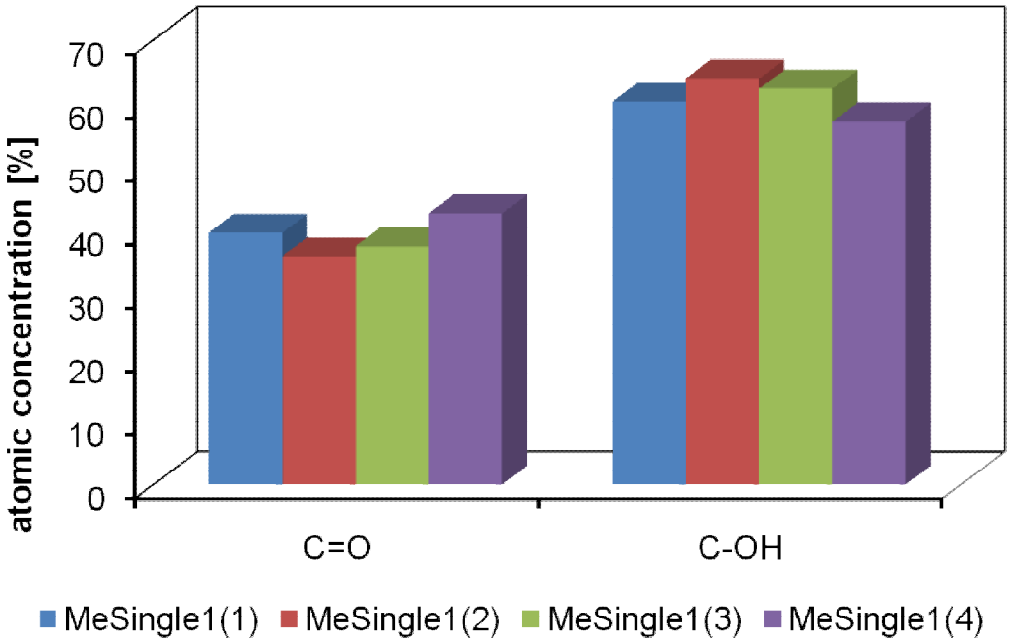

Figure 6-27: (101) facets analysis for three different area of MeSingle1 at different O environment (6 peaks fitted during CasaXPS fitting)

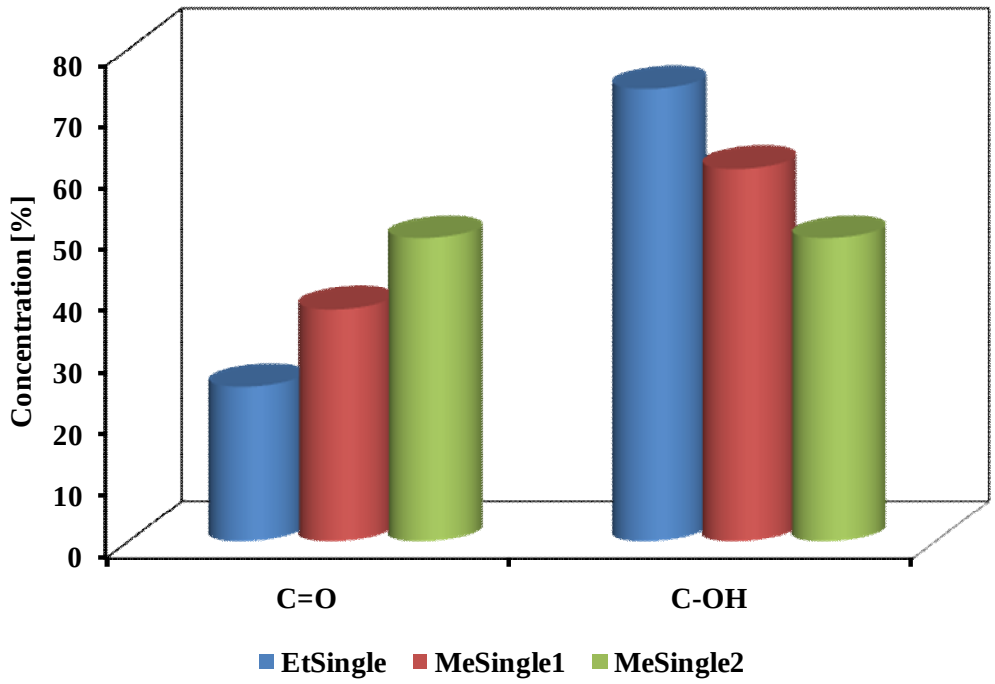

Figure 6-28: (111) facets analysis for three different single crystal at different O environment

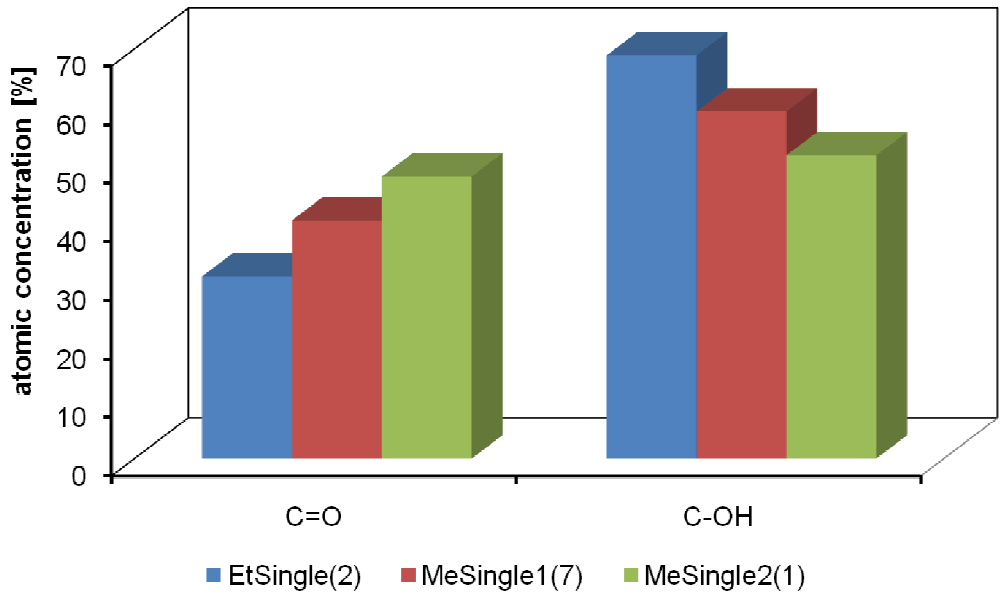

Figure 6-29: (111) facets analysis for three different single crystal at different O environment

6.6. Conclusions

All the results discussed in the previous sections indicate that the prepared single crystal paracetamol specimens at the level of cleanliness one would expect of samples obtained by carefully conducted 'wet chemistry' in the laboratory. Though adventitious carbon contamination levels are clearly evident there was no indication that they were excessive relative to those commonly observed in surface science studies of materials prepared in the laboratory.

The interactions of the solvent and solute (paracetamol) during crystallisation may in principle influence the composition of C 1s or O 1s. Solvent adsorption and that of dissolved solvent contaminants on the crystal surfaces may also affect the concentration of functional groups [23, 24]. The ATR-IR spectra (**Figure 6-5**) include an N-H peak at 3300 cm^{-1}, with the O-H groups visible at 3163 cm^{-1}, but revealed no major differences between functional group signatures for all the single crystals. Only small differences of peak intensity are observable, particularly for the N-C=O vibration at 1650 cm^{-1}, [25] which indicate that the preparations carried out in acetone medium may be more prone to leading to enhanced contamination levels than the preparations in the alcohol media.

The PXRD results **(Figure 6-6)** for AceGround, EtGround and MeGround reveal no shift of diffraction peaks relative to powder paracetamol. This indicates that the solvents used in the crystallisation are not decisively influencing the *bulk* paracetamol composition or local interactions in the crystal structure.

N-related signals (N 1s, amide component of C 1s, C=O component in O 1s) will only source from paracetamol molecules rather than impurities on the surfaces and their analysis leads to the conclusion that the C 1s, O 1s and N 1s XP emission intensity data, and the elemental analyses derived from them, can be interpreted through a model incorporating an adventitious hydrocarbon contamination layer (somewhat oxygenated) on the surface and a stoichiometric composition of the underlying on the crystal surfaces. However, reconfirmation due to the C:H:N elemental analysis was not done throughout this study. Untreated paracetamol powder had one of the lowest ratios of O to N concentrations, suggesting that some solvent may be present at the surfaces of the single crystals. It was observed that both AceSingle1 and AceSingle2 had the highest O/N ratios, followed by MeSingle1 and MeSingle2 and EtSingle. Elemental analysis of some of the crystals should perhaps be carried out to confirm their stoichiometry.

What this study shows is that the use of very pure methanol (HPLC grade) and consistently cleaning the apparatus with APS and drying in the oven at 60°C prior to use allows to preparations of crystal facets with a high degree of cleanliness, though still contaminated by the adventitious carbon contamination layers expected for materials handled in a laboratory environment. The challenge for experimental surface science is now to find additional methodologies for reducing the surface contamination levels further, by reducing contamination levels introduced during crystallisation further and/or handling samples under cleaner (glove box, clean room, special UHV compatible crystallisation chamber) conditions during transfer from solution medium to XPS analysis vacuum.

6.7. References

1. Kiang, Y. H.; Shi, H. G.; Mathre, D. J.; Xu, W.; Zhang, D.; Panmai, S., Crystal structure and surface properties of an investigational drug--A case study. *Int. J.Pharm.* **2004,** 280, 17-26.

2. Vlieg, E., Understanding crystal growth in vacuum and beyond. *Surf.Sci.* **2002,** 500, 458-474.

3. Kiang, Y. H.; Yang, C.-Y.; Staples, R. J.; Jona, J., Crystal structure, crystal morphology, and surface properties of an investigational drug. *Int. J. Pharm.* **2009,** 368, 76-82.

4. Hammond, R. B.; Roberts, K. J.; Docherty, R.; Edmondson, M., Computationally Assisted Structure Determination for Molecular Materials from X-ray Powder Diffraction Data. *J.Phys.Chem.B* **1997**, 6532-6536.

5. Naumov, D. Y.; Vasilchenko, M. A.; Howard, J. A. K., The Monoclinic Form of Acetaminophen at 150K. *Acta Crystallogr. C* **1998**, 653-655.

6. An, G.-W.; Zhang, H.; Cheng, X.-L.; Zhuo, Q.-L.; Lv, Y.-C., Electronic structure and hydrogen bond in the crystal of paracetamol drugs. *Struc.Chem.* **2008,** 19, 613-617.

7. Uusi-Penttilä, M. S.; Rasmuson, Å. C., Experimental Study for Agglomeration Behaviour of Paracetamol in Acetone-Toluene-Water Systems. *Chem. Eng. Res. Des.* **2003,** 81, 489-495.

8. Phillips, F. C., *An introduction to crystallography*. Longmans, Green: 1972.

9. P. Bennema, H. M., W.J.P. van Enckevort, Crystal Growth and Morphology - a multi-faceted approach. In *Growth, dissolution, and pattern formation in geosystems*

Jamtveit, B.; Meakin, P., Eds. Kluwer Academic Publishers: Dordrecht, 1999.

10. International Tables for crystallography. In *International Union of Crystallofraphy*, Hahn, T., Ed. Kluwer Academic Publishers: Dordrecht., 1996.

11. Nichols, G.; Frampton, C. S., Physicochemical characterization of the orthorhombic polymorph of paracetamol crystallized from solution. *J. Pharm.Sci.* **1998,** 87, 684-693.

12. Stevens, J. S.; Schroeder, S. L. M., Quantitative analysis of saccharides by X-ray photoelectron spectroscopy. In John Wiley & Sons, Ltd.: 2009; Vol. 41, pp 453-462.

13. Stevens, J. S.; Byard, S. J.; Schroeder, S. L. M., Characterization of Proton Transfer in Co-Crystals by X-ray Photoelectron Spectroscopy (XPS). *Crystal Growth & Design* 10, (3), 1435-1442.

14. Stevens, J. S.; Byard, S. J.; Schroeder, S. L. M., Salt or co-crystal? determination of protonation state by X-ray photoelectron spectroscopy (XPS). In Wiley Subscription Services, Inc., A Wiley Company: Vol. 99, pp 4453-4457.

15. Stevens, J. S.; Byard, S. J.; Muryn, C. A.; Schroeder, S. L. M., Identification of Protonation State by XPS, Solid-State NMR, and DFT: Characterization of the Nature of a New Theophylline Complex by Experimental and Computational Methods. *The Journal of Physical Chemistry B* 114, (44), 13961-13969.

16. J.S. Stevens, S. J. B., C.S. Seaton, G. Sadiq, R.J. Davey, S.L.M. Schroeder, Crystallography Aided by Atomic Core Level Binding Energies: Proton Transfer vs. Hydrogen Bonding in Organic Crystal Structures. *Angewandte Chemie – International Edition* **2011,** In-press.

17. Briggs, D., *Surface analysis of polymers by XPS and static SIMS*. Cambridge University Press: Cambridge, 1998.

18. Tanuma, S.; Powell, C. J.; Penn, D. R., Calculations of electron inelastic mean free paths. V. Data for 14 organic compounds over the 50–2000 eV range. In John Wiley & Sons Ltd.: 1994; Vol. 21, pp 165-176.

19. Werner, W. S. M., Towards a universal curve for electron attenuation: Elastic scattering data for 45 elements. In John Wiley & Sons Ltd.: 1992; Vol. 18, pp 217-228.

20. Tanuma, S.; Powell, C. J.; Penn, D. R., Calculations of electron inelastic mean free paths. V. Data for 14 organic compounds over the 50–2000 eV range. *Surf. Interface Anal.* **1994,** 21, 165-176.

21. Heng, J. Y. Y.; Bismarck, A.; Lee, A. F.; Wilson, K.; Williams, D. R., Anisotropic surface energetics and Wettability of macroscopic form I paracetamol crystals. *Langmuir* **2006,** 22, 2760-2769.

22. Jablonski, A.; Lesiak, B.; Ebel, H.; Ebel, M. F., Matrix dependence of elastic scattering effects in quantitative AES and XPS. In John Wiley & Sons Ltd.: 1988; Vol. 12, pp 87-92.

23. Li, T.; Wen, H.; Park, K.; Morris, K. R., How Specific Interactions between Acetaminophen and Its Additive 4-Methylacetanilide Affect Growth Morphology: Elucidation Using Etching Patterns. *Cryst.Growth Des.* **2002,** 2, 185-189.

24. Danten, Y.; Tassaing, T.; Besnard, M., Density Functional Theory (DFT) Calculations of the Infrared Absorption Spectra of Acetaminophen Complexes Formed with Ethanol and Acetone Species. *J. Phys. Chem. A* **2006,** 110, 8986-9001.

25. Misra, A. K., Thermoanalytical and microscopic investigation of interaction between paracetamol and fatty acid crystals. *J. Macromol. Sci. A Pure* **2007,** 44, 685-690.

CHAPTER 7: PARACETAMOL AND POLOXAMER MIXTURE

7.1. Objectives

The objectives of the work described in this chapter are:

- To determine the optimum composition of Poloxamer188 required to coat the paracetamol surface by grinding and milling techniques.
- To observe the changing of paracetamol/poloxamer188 surface composition induced by radiation at various mass percentages.

7.2. Introduction

Excipients are used in pharmaceutical formulations to enhance drug properties during processing or in the final product. For example, excipients attached by adsorption on the drug surface may provide many advantages. Recently, the adsorption of crospovidone onto the surface of carbamazepine has been proven to retard the crystallisation of the drug, thus enhancing its release properties[1]. In other work, it has been shown that polymer excipient adsorption can modify the electrostatic surface properties of a drug.[2] The adsorption process can be affected by numerous parameters such as the molecular weight of the adsorbate, the number and position of functional groups, the power of the solvent, the physical and chemical properties of the adsorbent, such as shape, porosity, surface area, polarity and surface energy, including the electrostatic properties of particles.[2]

Adsorption is accomplished by grafting a polyfunctional agent onto the surface, which increases the number of available reactive functional groups per unit surface area. The solid mixture can be categorised by bulk properties such as solubility, compactibility and elasticity, which are primarily dependent on lattice interactions, and surface properties such as interfacial tension, adhesion and cohesion, which are influenced by the surface chemistry and energy[3] of excipients and drugs, through adsorption via electrostatic interactions[4]. The method may be due to the interdiffusion of the components, creating a zone of transition or interphase. It requires mutual solubility and a sufficient molecular solubility[5]. The adsorption of large linear polymer excipients is due to binding of particular sites. However, in practice the individual polymer molecules often adsorb to more than one site and interfere with access to unoccupied adsorption

sites[6]. The adsorption may occur by hydrogen bonding, van der Waals interaction, ion dipole interaction and the hydrophobic effect[6, 7]. The interaction of aniline – a compound similar to paracetamol with a different para-substituent group at the para position – with silicon surfaces is accompanied by the cleavage of either N-H or C-H bonds.[8]

The binding of two molecules by physical interaction or physical forces is the regulating force in all natural and technological phenomena that do not involve chemical reactions and is thus very important in all branches of science and industry.[9] The physical forces acting between molecules are essentially electrostatic or quantum mechanical and make a smaller contribution than gravitational forces due to mass attraction. Electrostatic forces are those between charges and dipoles or induced by dipoles. Quantum mechanical forces are known as dispersion and repulsion forces. In other terms, physical forces between molecules can be categorised as cohesion and adhesion forces. Cohesion describes physical interactions between molecules of the same type, whereas adhesion occurs when molecules of two different types interact. Molecular interaction forces apply at very small separations. Theoretically, they fall off exponentially as the distance between atoms increases.

In the work reported in this chapter, powdered pure paracetamol and several excipients were physically mixed. Powdered materials represent complex systems for fundamental characterisation, being heterogenous in structure, composed of particles of different shapes and sizes with interparticular voids. As a result, powders contain a multitude of interacting surfaces, which leads to wide-ranging physicochemical and mechanical properties.[10] It has been noted that milling, drying and crystallisation may influence the fundamental properties of powdered solids[11]. However, the physical interactions at molecular level are much less well understood[12]. Physical interactions between drugs and excipients are relatively common, because few chemicals are used during the process. Milling or comminution is a common operation employed to reduce particle size. The mechanical stress inherent in the process often produces structural changes in the milled crystalline API. It has been suggested that milling forms a thin amorphous surface layer on particles with disordering of the surface structure rather than the entire bulk [13].

Physically, milling will reduce the particle size of a compound, enhancing the dissolution rate through an increase in the available surface area. However, some reports state that milling is accompanied by a disorder of the crystalline structure, leading to the

formation of amorphous regions, particularly at the surface[14]. These amorphous regions or crystal defects are unstable and can migrate, transform and change in nature[13, 15]. In addition, they will create high energy sites at the surface and thus reduce the activation energy needed for dissolution relative to the more structurally ordered particle surface[13].

Understanding the interactions between polymers and crystal surfaces at the molecular level will make it possible to design polymeric additives to inhibit crystallisation more efficiently[12]. The surface properties of the mixture are determined by the structure and chemical composition of the outermost atomic layer. The effects of an excipient on a drug are linked to the interfacial area of contact between drug and excipient. The amount of excipient will affect the contact between them. Encapsulating a weak acid drug with a polymer excipient will cause polymer-induced degradation[16]. The adsorption of excipients on the layers at the interface was not always homogenous[17].

The adsorption of Poloxamer 188 on the Poly (d,L-lactic-co-glycolic acid), PLGA surface was driven by hydrophobic forces between PO of poloxamer and the adsorbent surface[17]. At the high concentration of Poloxamer and PLGA mixture, the adsorption behaviour of the system suggest a formation of surface Poloxamer aggregates[17].

Polymer adsorption on solid surfaces has been studied using a number of techniques, such as solid state NMR, FTIR, Raman, UV, electron spin resonance (ESR) and photon correlation spectroscopy (PCS), microcalorimetry and surface plasmon resonance (SPR) [12].

7.3. Experimental

7.3.1. Materials

Paracetamol powder and blends were prepared prior to the analysis. Nine paracetamol powder and Poloxamer 188 blends were prepared for the comparative analysis.

i) Untreated paracetamol powder (form I) as received from Sigma Aldrich, UK.

ii) Untreated Poloxamer 188 as received from BASF, UK. No milled Poloxamer 188 was characterized by XPS due to Poloxamer 188 data was only for comparison purposes. No calculation was involved.

iii) Milled paracetamol powder obtained by milling in Retch MM200 mixer mill at a rate of 30 Hz, using 5 mL stainless steel jars, each containing one 7 mm diameter stainless steel ball mill. The milling time was 5 min.

iv) Ground paracetamol and poloxamer 188 at mass percent of poloxamer 188 10 % w/w. Mixtures was ground by using a mortar and pestle.

v) Ground paracetamol and poloxamer 188 at mass percent of poloxamer 188 50 % w/w. Mixtures was ground as (iv).

vi) Ground paracetamol and poloxamer 188 at mass percent of poloxamer 188 90 % w/w. Mixtures was ground as (iv)

vii) Milled paracetamol and poloxamer 188 at mass percent of Poloxamer 188 10 % w/w. Mixture was milled as (iii).

viii) Milled paracetamol and poloxamer 188 at mass percent of Poloxamer 188 50 % w/w. Mixture was milled as (iii).

ix) Milled paracetamol and poloxamer 188 at mass percent of Poloxamer 188 90 % w/w. Mixture was milled as (iii).

7.3.2. Differential Scanning Calorimetry (DSC)

Thermal analysis was performed using a TA Q100 instrument with a low temperature attachment (refrigerated cooling system, TA Instruments) for sub-ambient operation. The specific software used for heat capacity calculations in the study was TA Universal Analysis 2000. All scans were conducted at 10 °C/min with a nitrogen purge to minimise oxidative decomposition. A sample (5-12 mg) was weighed and crimped in the DSC pan, which was re-weighed to ensure that no sample had spilled out during the crimping process. Most of the analyses were repeated once or more; a few samples were analysed only once or twice, when good thermograms were obtained in the initial runs.

The strength of the interaction between drug and excipient was estimated using the Gordon Taylor equation, with the assumption that the mixtures were ideally mixed[18],

$$T_g = \frac{w_1 T_{g1} + K w_2 T_{g2}}{w_1 + K w_2} \text{ ,} \qquad \textbf{Equation 7-1}$$

Where T_{g1} is the glass transition temperature of the drug-polymer blend, w_1, w_2, T_{g1}, T_{g2} are the weight fractions and glass transition temperature of the drug and polymer respectively. The constant, K, is a measurement of the interaction between the components and can be approximated by using equation below.

$$K \approx \frac{\rho_1 T_{g1}}{\rho_2 T_{g2}} \qquad \textbf{Equation 7-2}$$

Where ρ_1 and ρ_2 are the true densities of the paracetamol and excipients respectively[19, 20]. Due to the limitations of the instrument, the true density of paracetamol (1.205 g/cm^3) has been taken from the literature[21], while the poloxamer (0.99 g/cm^3) is the value provided by BASF. If the T_g of a blend was lower than predicted or calculated, the negative deviation from ideal behaviour was obtained. Gordon and Taylor explain such differences by the strength of intermolecular interactions between individual components of the mixture. The polymer will have a strong bond with the drug if the T_g obtained is higher than predicted, because stronger binding will lower the chain mobility. Conversely, if a lower T_g is obtained this indicates that polymer and drug are less strongly bound and prone to self-associate.

7.3.3. Powder X-ray Diffraction (PXRD)

PXRD patterns were recorded on a Rigaku Miniflex Goniometer at 30 kV and 15 mA at steps of 0.01°. About 5 mg of each sample was placed in the top holder and rotated through the range of 5° to 40° at a rate of 3°/minute. The PXRD patterns were converted to the Excel program for further analysis.

7.3.4. Attenuated Total Reflection Infrared (ATR-IR)

ATR-IR experiment was held as stated on **Chapter 6.** The estimation of crystallinity of physical mixtures by ATR-IR spectra was based on the measurement of two selected peaks area; known as intensity of the band and analytical band. Intensity of the band is the spectrum peaks which invariant with the changing of mixture crystallinity. Whilst, analytical band is the spectrum peak which is reduced or increased as the crystallinity of the mixture increased. The peak area percentage is plotted against the mixture compostion [22].

7.3.5. X-ray Photoelectron Spectroscopy (XPS)

Details of the XPS instrument and data acquisition were already are given in **Chapter 2 .**

7.4. Results

7.4.1. Differential Scanning Calorimetry (DSC)

The poloxamer 188 direct heating thermograms revealed two peaks appearing at 56 °C and 390 °C, indicating a melting temperature and a decomposition temperature, respectively. The heating and cooling thermograms showed poloxamer 188 to be a crystalline compound with the detection of melting and crystallisation peaks. The thermograms revealed a broad melting peak at 55.97 ± 0.05 °C (**Table 7-1**), shifting a little from the direct heating peaks. Hence, a broad peak associated with recrystallisation appeared at 32.21 °C and re-melting occurred at 52.99 °C.

Table 7-1: T_m and the enthalpy change, ΔH, for different blends of paracetamol and poloxamer 188

Poloxamer mass (%)	Peak 1/ (°C) ΔH [J/g]
100	55.97 (ΔH – 136.4)
90	53.69 (ΔH – 121.8)
50	52.72 (ΔH – 84.13)
10	51.87 (ΔH – 24.06)
0	171.66 (ΔH – 174.00)

Table 7-2: Correlation between percentage of poloxamer, predicted T_g and experimental T_g

Poloxamer (% w/w)	Predicted T_g (based on Gordon Taylor Equation, °C)	Measured T_g (°C)
100	-	42.59
90	38.53	36.33
50	32.04	52.39
10	26.90	65.35
0	-	24.65

In order to understand the interaction of the paracetamol with poloxamer 188, an attempt was made to correlate the T_g of the mixture with the percentage of poloxamer in the mixture (**Table 7-2**). A positive deviation of the measured from the predicted T_g indicates the region of interaction between the constituents.

7.4.2. Powder X-ray Diffraction (PXRD)

The poloxamer 188 powder X-ray diffraction (PXRD) pattern was compared with that of the pure reference[22] (**Figure 7-1**) for confirmation of compound purity. It was found that the experimental results agreed with the reference, showing 2 main peaks, as expected, at 2θ values of 19° (d spacing: 4.67) and 23° (d spacing: 3.85)[23]

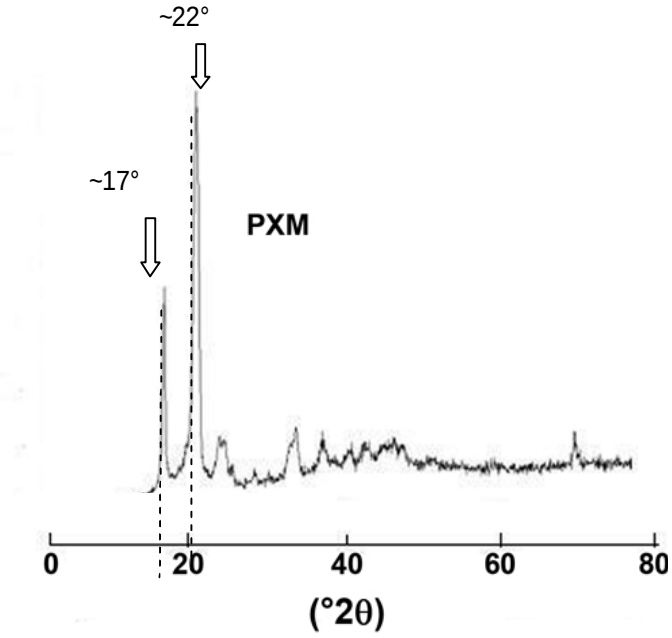

Figure 7-1: PXRD pattern of poloxamer 188 as in the literature[14]

Figure 7-2 shows the PXRD patterns for mixtures of poloxamer 188 and paracetamol. The PXRD pattern of pure poloxamer 188 and paracetamol were compared with the blending peaks (**Figure 7-2**). At higher percentages of poloxamer, (90 % w/w), main peaks at 19° and 23.5° appear that can be assigned to poloxamer 188. It was observed that all the peaks of paracetamol and poloxamer 188 were present in the patterns of all blends. The paracetamol peaks appeared more clearly at lower concentrations of poloxamer 188. For instance, the paracetamol double peaks at 23.57° and 24.14° were obvious and of high intensity only at 10 % w/w of poloxamer 188, while

in other blends these were presented as split peaks. It was observed that an increased proportion of poloxamer 188 would reduce the intensity of the paracetamol peaks.

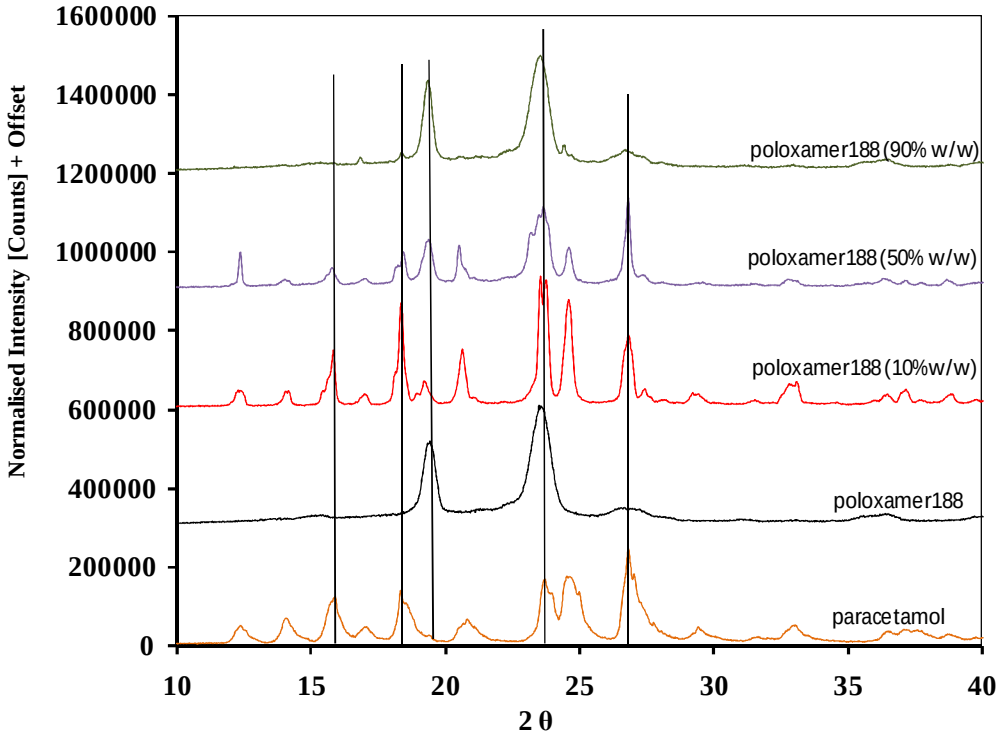

Figure 7-2: PXRD patterns for physical mixtures of paracetamol and poloxamer 188

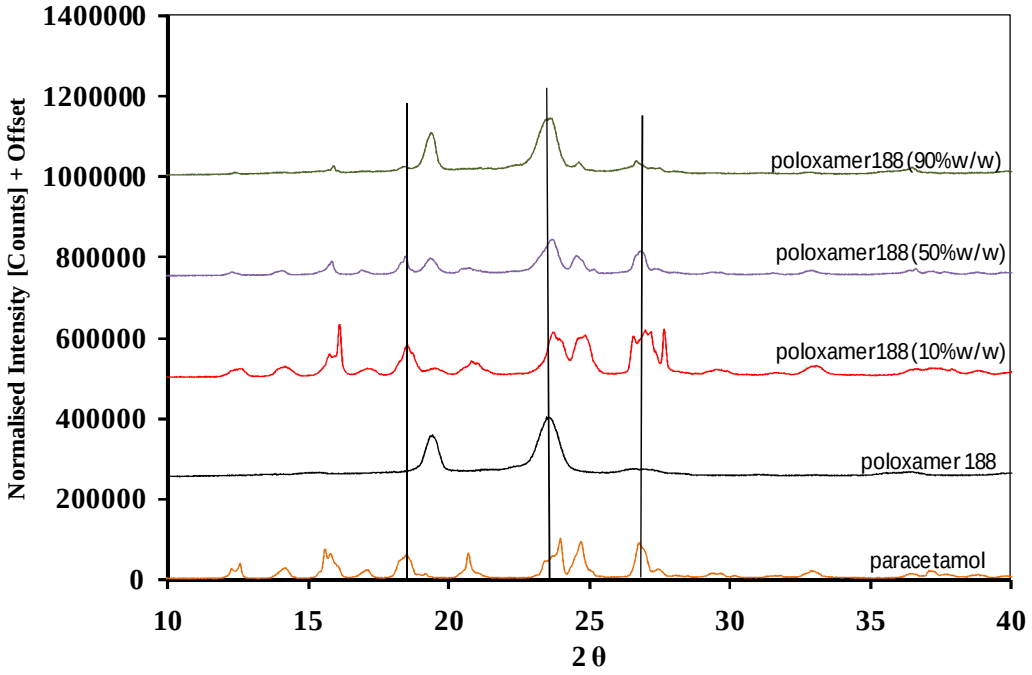

Figure 7-3: PXRD results for milled blends of paracetamol and poloxamer 188

Figure 7-3 shows the PXRD results for milled samples. For all blends, peaks exist indicating paracetamol and poloxamer 188. All the milled samples had similar peaks to those of the parent patterns, indicating that milling does not lead to the formation of new phases. Line broadening indicates reduced crystallinity as the poloxamer 188 concentration is increased.

7.4.3. Attenuated Total Reflection Infra Red (ATR-IR)

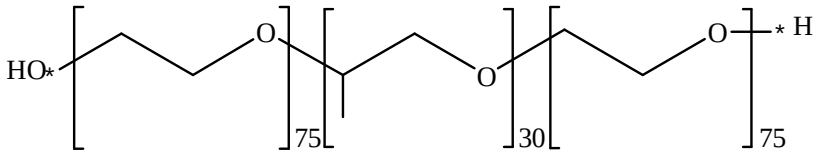

Figure 7-4: Chemical structure of poloxamer 188 with a=70, b=30

The ATR-IR spectrum (**Figure 7-5**) of the poloxamer 188 was found to have a strong C-C-O peak at 1039 cm^{-1} and one of medium intensity at 2890 cm^{-1}, due to C-H aliphatic groups. The peaks at 841 and 949 cm^{-1} were characteristic of the PEO chain of poloxamer [24]. The intense peak at 1100 cm^{-1} is the characteristic band of C-C-O and C-C stretching region[24], while the band at 1341 cm^{-1} is characteristic of the wagging region of CH_2 in the PEO chain[24]. In the ATR-IR spectrum of paracetamol (**Figure 7-6**), bands in the region of 560 cm^{-1} are characteristic of the C-H out-of-plane bending of the p-substituted benzene ring, while the bands at 1651, 3108 and 3316 cm^{-1} represent C=O stretching, O-H stretching and N-H stretching respectively[25].

Table 7-3: Possible functional groups and wavenumbers of poloxamer 188

Possible functional group	Possible wavenumber (cm^{-1})	Notes
C-CH_3 (methyl group)	2970-2850 1383-1375	Single methyl group on C atom
C-O-C	1140-1110	strong
C-H (aliphatic)	2970-2850	(strong) stretch
O-H (deformation)	1640-1630	-
C-H (methyl ether)	2832-2815	medium

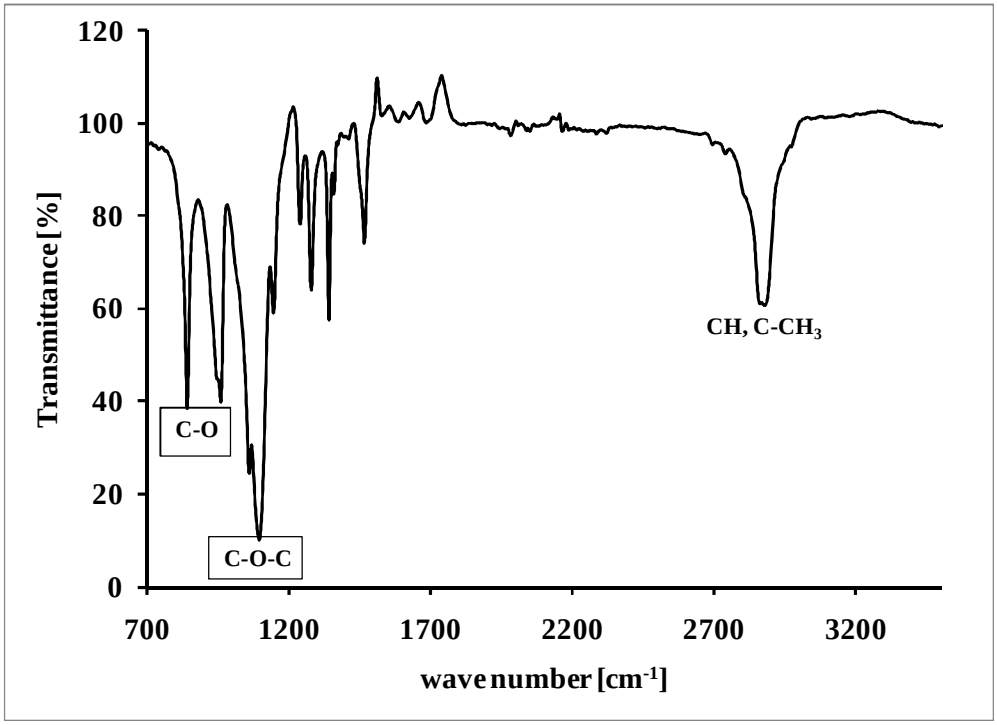

Figure 7-5: ATR-IR spectrum of pure poloxamer 188

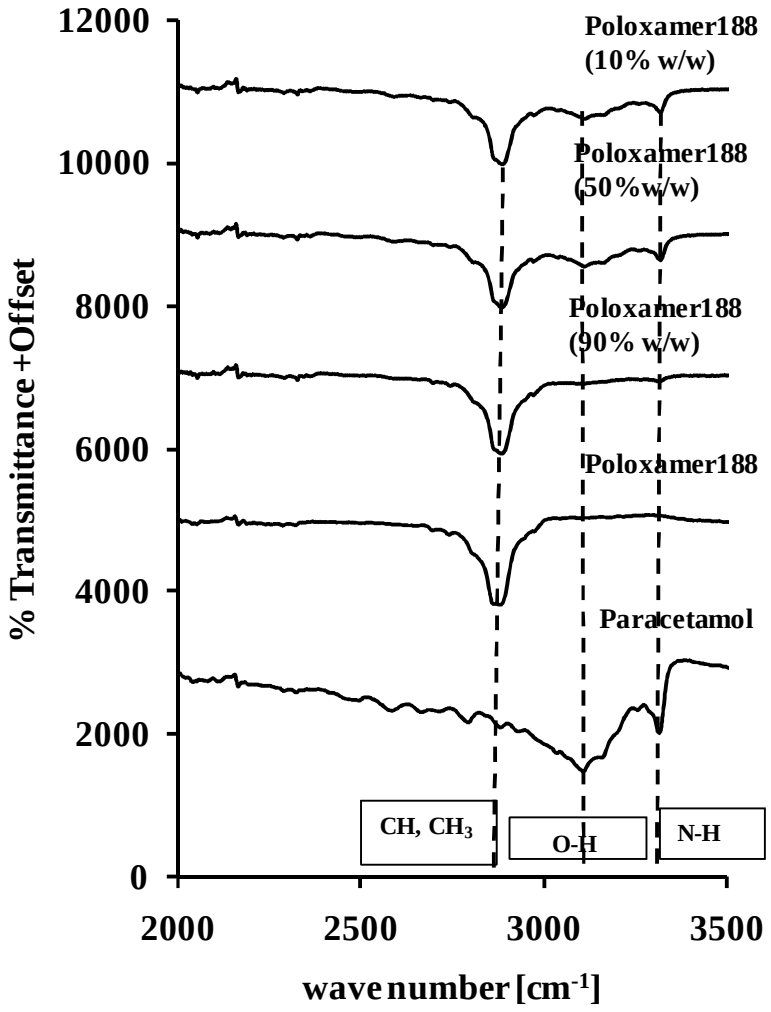

Figure 7-6: ATR-IR patterns of paracetamol and poloxamer 188 ground mixtures at wavenumbers 2000 cm^{-1} to 3500 cm^{-1}

The objective of ATR-IR analysis was to detect hydrogen bonds between paracetamol and poloxamer 188. It has been found that paracetamol molecules can have intermolecular hydrogen bonds in solid form through N-H...O and O-H...O bonds[26]. It is presumed that the O-H peak at 3108 cm^{-1} indicated a C-OH band. The existence of the peak in the blend indicated the formation of hydrogen bonds between paracetamol and poloxamer 188. At high poloxamer 188 concentrations, the absence of C-OH peaks indicated that poloxamer 188 did not form hydrogen bonds at the intermolecular level[27].

Table 7-4: Analysis of ATR-IR functional groups of paracetamol and poloxamer 188 mixtures

PEO % w/w	N-H (3500-3300) cm^{-1}	C-OH (3350-3250) (1080-1010) cm^{-1}	C-H (aliphatic) (2970-2850) cm^{-1}	C=O (1710-1670) 1665-1640) cm^{-1}	C-N or C-O (1340-1020) cm^{-1}	C-H or CH_3 (benzene) (870-675) cm^{-1}
(Paracetamol + poloxamer 188) ground						
90	3307.81 (very weak)	Not detected	2878.53	1649.77 (weak) 1610.05 (weak)	1097.61	839.44
50	3315.84	3108.56	2880.32	1649.38 1609.48	1105.10	836.82
10	3314.27	3108.47	Not detected	1648.70	1223.65	835.93
Poloxamer	Not detected	Not detected	2879.27	Not detected	1101.46	841.25
Paracetamol	3316.34	3108.67	Not detected	1648.98 1609.21	1223.01	835.67 681.45
(Paracetamol + poloxamer 188) milled						
90	3319.09 (very weak)	Not detected	2882.25	Not detected	1097.95	840.96
50	3317.40	3109.20	2883.54	1650.74 1610.28	1101.07	837.97
10	3317.01	3109.06	2882.85	1650.87 1610.30	1100.03	838.15 686.98

Table 7-4 shows the analysis of the functional groups of paracetamol and poloxamer 188 mixtures, ground and milled. At high concentrations of poloxamer 188 the N-H peak was found to be of very weak intensity and the C-OH peak was absent, while the benzene peak at 686 cm^{-1} (**Figure 7-7**) was observed at low poloxamer 188 concentrations for both types of blend. Only a little shift observed of the blending discerned to the pure paracetamol and poloxamer 188. Conversely, at a low concentration of ground blends (**Table 7-4**) poloxamer 188 the C-H peak disappeared.

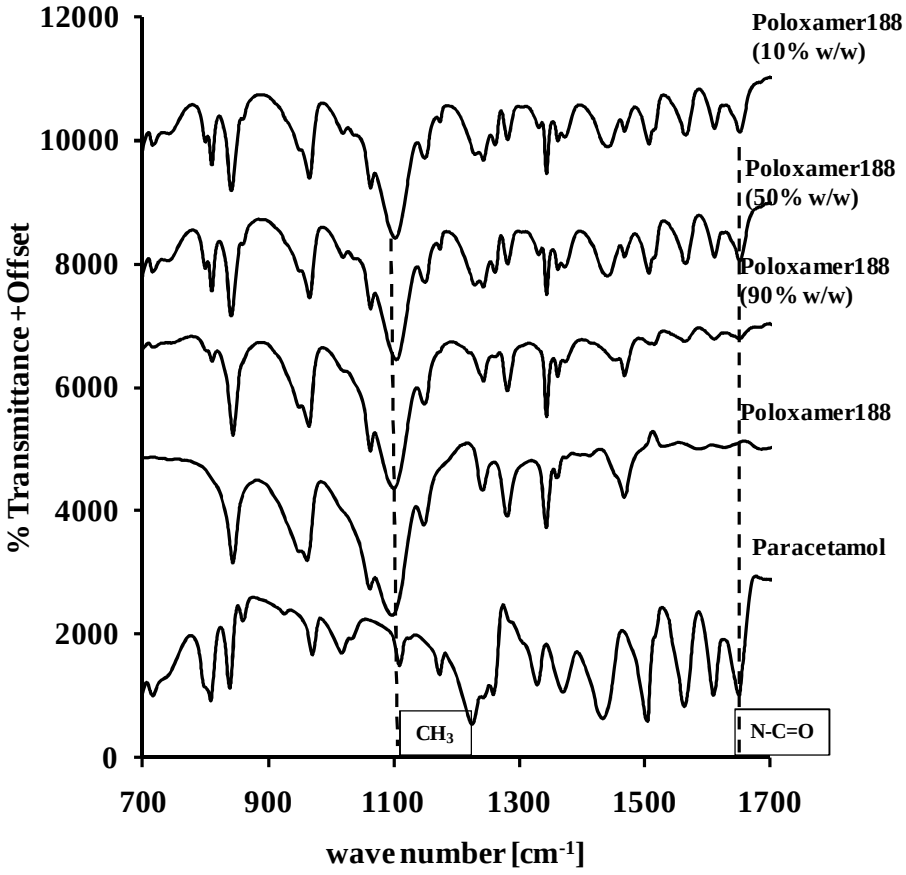

Figure 7-7 : ATR-IR spectra of paracetamol and poloxamer 188 ground mixture at wavenumbers 700 cm^{-1} to 1700 cm^{-1}

The difference between milled and ground samples was most obvious in the spectrum of the blend with 10% w/w poloxamer (**Table 7-4**). The spectrum of the milled mixture had higher intensity peaks for poloxamer 188 than paracetamol, particularly at 2800 cm^{-1} (**Table 7-4**), in the C-H aliphatic band. The ATR peak of 1100 cm^{-1} (**Figure 7-7**) of CH_3 was pointed as intensity of the band which did not change noticeably with the composition of the mixture. The 1648.9 cm^{-1} (**Figure 7-7**) peak was present only in the mixture of high crystallinity (low percentage of poloxamer 188). Therefore it was selected as intensity band.[22]

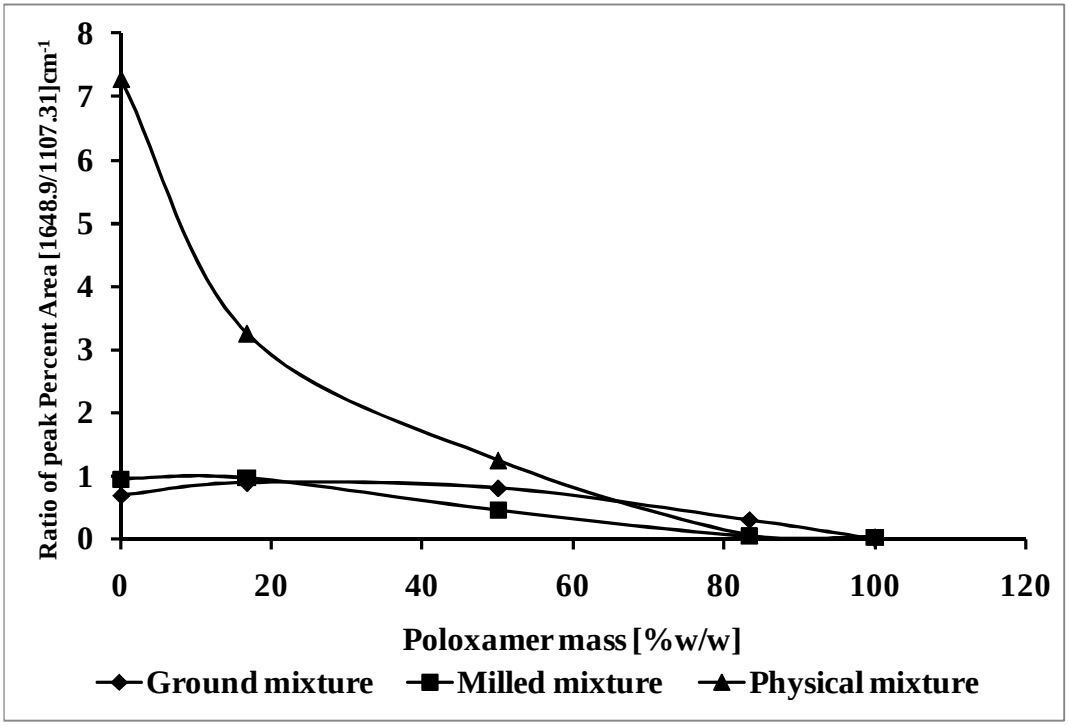

Figure 7-8: **Estimation of crystallinity of paracetamol and poloxamer 188 mixtures using the ATR-IR spectra as reference**

Figure 7-8 above shows the ATR-IR analysis of the crystallinity of different types of mixture. All the samples revealed the same pattern of crystallinity, where an increase in the proportion of poloxamer 188 reduced the crystallinity of the mixture, as indicated by the fact that all the lines on the graph have negative slopes. The milled mixture had the best correlation value, R, of 0.98, while the physical mixture was 0.82 and the ground mixture was 0.72. The crystallinity of the milled mixture varied only slightly as the concentration of poloxamer 188 was increased, indicating that the blending of paracetamol and poloxamer 188 did not affect the crystallinity of the molecular structure.

7.4.4. X-ray Photoelectron Spectroscopy (XPS)

Table 7-5: Moles of paracetamol and poloxamer 188 at different mass percentages

100%		**10% w/w Poloxamer 188**		**50% w/w Poloxamer 188**		**90% w/w Poloxamer 188**	
Mol paracetamol	Mol poloxamer 188	Mol paracetamol	Mol poloxamer 188	Mol paracetamol	Mol poloxamer 188	Mol paracetamol	Mol poloxamer 188
6.61×10^{-3}	1.19×10^{-4}	5.95×10^{-3}	1.06×10^{-5}	3.31×10^{-3}	5.32×10^{-5}	6.61×10^{-4}	9.57×10^{-5}

The XPS analysis technique was used to measure the composition of paracetamol and poloxamer 188 blends with surface sensitivity. **Table 7-5** shows the number of moles of each ingredient in three blends. Estimated calculations of paracetamol and Poloxamer 188 strength of interaction **(in Chapter 2**) predicted that paracetamol and poloxamer 188 interacted, from the harmonic mean equation, with an interaction parameter of 98.82. Poloxamer 188 was predicted to have the strongest interaction among all the poloxamers calculated.

7.4.5. Stoichiometry Analysis

The C, O and N binding energy, E_B, of all the samples was due to the C binding energy at 285.0 eV for the untreated powder, ground mixture and milled mixture. On the paracetamol and poloxamer 188 XPS fitting, the paracetamol C element was calibrated at 285.0 eV. **Table 7-6** below shows the elemental analysis of pure paracetamol and poloxamer 188 as well as ground and milled mixtures at three different ratios. **Figure 7-9** reveals that N emission intensity of pure paracetamol decreased as the poloxamer 188 concentration increased. However, the C and O elements were changeable between them.

Table 7-6 shows the theoretical and experimental elemental analysis values for the milled and ground mixtures, revealing similar trends: as the poloxamer 188 concentration increased, so did the C/N and O/N ratios. Since N is absent from the structure of poloxamer 188, the large differences in C/N and O/N ratios between experimental and calculated value reveals the loss of N concentration signal on the surface of the blends. However, for the C/O ratio, the experimental and calculated values show relatively little divergence at high milled poloxamer 188 concentrations. In addition, the ground mixture is characterised by a higher concentration of O than in the milled mixture. The high O concentration could be due either to surface oxidation [28] of paracetamol or poloxamer 188 during grinding or, more likely, the uptake of humidity by the more highly dispersed material with freshly created, and therefore more reactive, crystal surface areas.

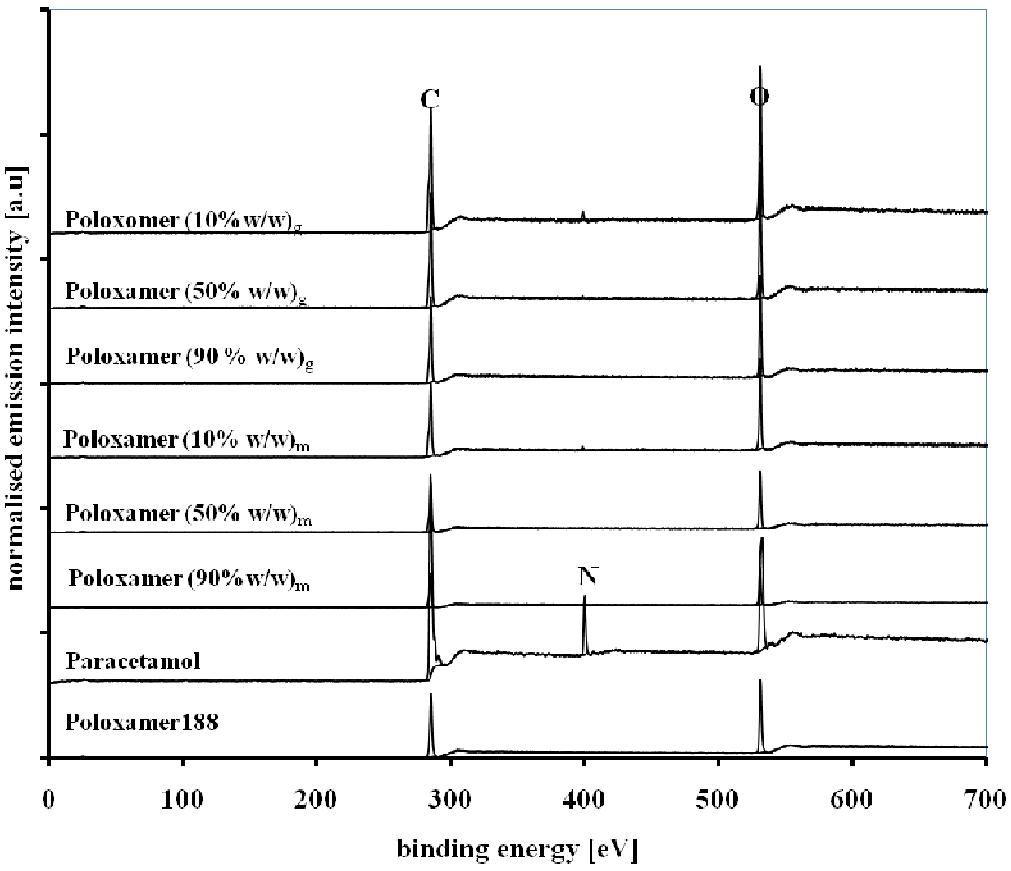

Figure 7-9: Survey spectra for pure paracetamol, poloxamer 188 and mixtures of various compositions, showing C, O and N elements

Table 7-6: Analysis of C, O and N elements, showing predicted elemental concentration and experimental data for pure paracetamol, poloxamer 188 and various mixtures of ground and milled compounds

	C (%)	O (%)	N (%)	C:O	C:N	O:N
Calculated						
Paracetamol	72.70	18.20	9.10	4.00	8.00	2.00
Poloxamer 188	68.42	31.58	-			
10% w/w Poloxamer 188	71.53	19.19	8.19	3.73	8.73	2.34
50% w/w Poloxamer 188	66.99	23.23	4.56	2.88	14.69	5.09
90% w/w Poloxamer 188	62.29	27.22	0.91	2.29	68.45	29.91
Experimental						
Paracetamol	76.55	15.69	7.76	4.88	9.86	2.02
Milled paracetamol	73.91	18.53	7.56	3.99	9.78	2.45
Poloxamer 188	71.63	28.37	-	2.52	-	-
(Paracetamol + poloxamer 188)$_{ground}$						
10% w/w Poloxamer 188	51.50	46.37	2.48	1.11	20.77	18.70
50% w/w Poloxamer 188	50.20	48.82	0.98	1.03	51.22	49.82
90% w/w Poloxamer 188	50.24	48.80	0.96	1.03	52.33	50.83
(Paracetamol + poloxamer 188)$_{milled}$						
10% w/w Poloxamer 188	72.19	26.54	1.27	2.72	56.84	20.89
50% w/w Poloxamer 188	71.47	28.04	0.50	2.55	142.94	56.08
90% w/w Poloxamer 188	72.15	27.41	0.43	2.63	167.79	63.74

7.4.6. High Resolution

C 1s

Photoemissions from the C 1s core level of paracetamol and poloxamers produced two different spectra. Obviously, two of three paracetamol poloxamer 188 spectra revealed the absence of shake-up peaks. The shake-up peak is the characteristic peak of C=C, which is aromatic in nature. C=C peak was set at 284.7 eV. Three difference shapes of paracetamol poloxamer 188 high resolution spectra were observed **(Figure 7-10).** Seven deconvoluted peaks were fitted according to the paracetamol and poloxamer 188

functional groups. The C 1s binding energy was calibrated through the aliphatic C-C peak at 285.0 eV, due to the loss of the shake-up peak from the blend spectra. The peak at high E_B is N-C=O (amide group of paracetamol) at a range of 287.9 to 288.3 eV. The high E_B (289 eV and above) emission from paracetamol is due to the π- π* shake up satellite peak arising from the aromatic ring [5, 29]. The adjacent high intensity peak was deconvoluted into three main peaks. The higher E_B with two different electronegative neighbours, set at a range between 285.7 and 285.9 eV and 286.3 and 286.1 eV respectively, was due to C-N and C-OH photoelectrons[5, 30]. The bare poloxamer 188 spectrum was deconvoluted into 2 peaks; the most electronegative neighbour of C-OH was assigned between 286.4 and 286.5 eV with FWHM different of 0.2. Next to the C-OH peak, the deconvoluted peak of the bulk concentration of poloxamer 188 was a C-C-O peak between 286.4 and 286.6 eV [30, 31]. The hydrophobic poloxamer 188 part, which is C-C, has been assigned at 285.0 eV. **Table 7-7** shows the estimated value of each deconvoluted peak on the XPS spectrum according to the real structures of paracetamol and poloxamer 188.

Table 7-7: Stoichiometrically numbers of C1s carbon environments for pure paracetamol, poloxamer 188 and mixture.

Compound/s	C-N/C-OH	N-C=O	C-C=O/C-C	C=C
Paracetamol	1/1 (12.50% + 12.50% = 25.00%)	1 (12.50%)	1/0 (12.50%)	4 (50.00%)
Poloxamer 188	0/1 (0.47)	0	0/30 (14.22)	C-C-O 180 (85.31%)
Paracetamol + poloxamer 188	1/2 (1.37%)	1 (0.46%)	1/30 (14.16%)	C=C (4 = 1.83%) C-C-O (180 = 82.19%)

The two components can be sdistinguished through the N-C=O and C=C emission from paracetamol, while the C-C-O and C-C peaks fitted was clearly part of the poloxamer 188 structure. Poloxamer 188 differs from other poloxamer types in the ratio of ethylene oxide (EO) and propylene oxide (PO) blocks. Poloxamer 188 has 140 chains of EO divided into blocks of EO, giving 70 blocks for each EO, while the PO block is sandwiched between EO blocks and has only 30 chains. Therefore, the C-C-O percentage was indicated as the highest in the composition of the poloxamer 188 structure. Due to the size of poloxamer 188 relative to paracetamol and its known high surface activity; it was expected that emission from the C-C-O groups would dominate at any mixture composition.

Figure 7-10 shows the spectra of three milled blends and of pure paracetamol and poloxamer 188. Interestingly, for the 50% w/w mixture the poloxamer 188 spectrum dominates, with paracetamol only evident as a weak low-binding energy component and its shake-up peak as an extremely weak tail at higher binding energy. This indicates that paracetamol is entirely covered by poloxamer in this mixture. In contrast, a much stronger shake up peak was observed for 10 % w/w poloxamer 188 content. The shoulder at low E_B and higher binding energy generally increased as the poloxamer 188 concentration decreased and the C=C feature of paracetamol at 284.7 eV emerges more visibly. The increasing N-C=O contribution of paracetamol also becomes visible as a small shoulder at higher E_B values.

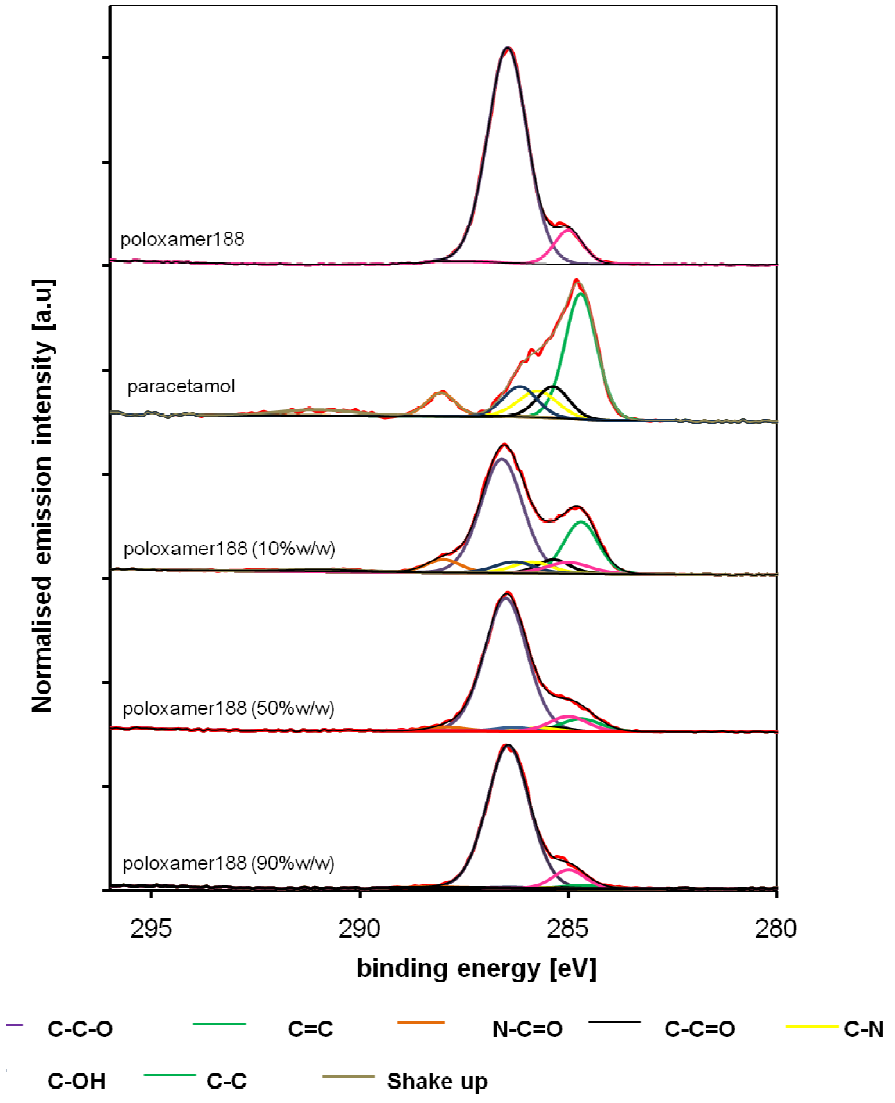

Figure 7-10: The C1s spectra of the three mixtures
All carbon environments are coloured as indicated in the legend.

Table 7-8: Calculated atomic concentrations of C 1s for blends of paracetamol and poloxamer 188 proportional to the calculated moles

	Mol paracetamol	**Mol poloxamer 188**
100% Paracetamol or Poloxamer 188	6.61×10^{-3}	1.19×10^{-4}
10% w/w Poloxamer 188	5.95×10^{-3}	1.06×10^{-5}
50% w/w Poloxamer 188	3.31×10^{-3}	5.32×10^{-5}
90% w/w Poloxamer 188	6.61×10^{-4}	9.57×10^{-5}
	[C-N]	[C-OH]
10% w/w Poloxamer 188	11.25	11.29
50% w/w Poloxamer 188	6.26	6.47
90% w/w Poloxamer 188	1.25	1.63
	[C=C]	
10% w/w Poloxamer 188	45.00	
50% w/w Poloxamer 188	25.04	
90% w/w Poloxamer 188	5.00	
	[C-C-O]	
10% w/w Poloxamer 188	0	7.60
50% w/w Poloxamer 188	0	38.17
90% w/w Poloxamer 188	0	68.61
	[C-C=O]	[C-C]
10% w/w Poloxamer 188	11.25	1.27
50% w/w Poloxamer 188	6.26	6.36
90% w/w Poloxamer 188	1.25	11.44
	[N-C=O]	
10% w/w Poloxamer 188	11.25	
50% w/w Poloxamer 188	6.26	
90% w/w Poloxamer 188	1.25	

Table 7-8 shows the atomic concentrations of each C 1s for blends of paracetamol and poloxamer 188 (calculated moles). For instance, in 6.61×10^{-3} mole of 100% w/w of paracetamol, the atomic concentration of C-N is 12.50%. Therefore, in 90% w/w of paracetamol (10% w/w of poloxamer 188) there is 5.95×10^{-3} mole of paracetamol and the atomic concentration of C-N is 11.25%.

Table 7-9: Photoemission of C 1s – data for ground and milled mixtures at different concentrations of poloxamer 188

	C-N	C-OH	N-C=O	C-C=O	C-C	C=C	C-C-O
(Paracetamol + poloxamer 188) ground							
10% w/w Poloxamer 188	6.00	6.00	6.00	6.00	2.97	24.01	48.28
50% w/w Poloxamer 188	2.51	2.51	2.51	2.51	6.35	10.04	73.52
90% w/w Poloxamer 188	1.11	1.11	1.11	1.11	7.29	4.43	83.87
(Paracetamol + Poloxamer) milled							
10% w/w Poloxamer 188	5.16	5.16	5.16	5.16	4.18	20.66	52.78
50% w/w Poloxamer 188	2.29	2.29	2.29	2.29	4.69	9.12	77.00
90% w/w Poloxamer 188	0.46	0.46	0.46	0.46	8.59	1.85	87.71
Pure powder							
Paracetamol	12.30	12.30	8.00	12.30		49.30	
Poloxamer 188		0.89			10.27		88.84
Milled paracetamol	12.16	12.15	9.37	12.16		48.64	

The C 1s concentrations (**Table 7-9**) indicate that all milled mixtures had high concentrations of C-C-O and C-C from poloxamer 188. As one would expect, the milled blend with the highest concentration of C-C-O at the surface was 90 % w/w of poloxamer 188. C=C aromatic, C-N, C-OH and N-C=O (**Table 7-9**) were observed to reduce as the poloxamer 188 concentration increased. For the ground mixture a higher concentration of paracetamol functional groups (C=C, C-C=O, C-N, C-OH and N-C=O) at the mixture surface relative to milled mixture was observed at all compositions. The results show that grinding the paracetamol/poloxamer 188 mixture was not sufficient to apply a complete coat of poloxamer 188 on the paracetamol surface. The highest concentration of poloxamer 188 coating was at 10 % and 50 % w/w due to the difference between calculated and experimental data. The value difference with regard to C-C-O and C-C of milled mixture. The difference value of calculated and experimental atomic concentration were 81% for 10 % w/w and of 50 % for 50% w/w mixture.

Table 7-10: C 1s binding energy and FWHM of ground and milled mixtures

Poloxamer 188 mass percent (% w/w)	C-N	C-OH	N-C=O	C-C=O	C-C	C=C	C-C-O
(Paracetamol + poloxamer 188) ground							
10% w/w Poloxamer 188	285.9	286.3	287.7	285.4	285.0	284.7	286.5
50% w/w Poloxamer 188	285.4	286.3	287.7	285.1	285.0	284.7	286.5
90% w/w Poloxamer 188	285.9	286.3	287.9	285.3	285.0	284.7	286.5
(Paracetamol + Poloxamer) milled							
10% w/w Poloxamer 188	285.8	286.2	288.0	285.4	285.0	284.7	286.6
50% w/w Poloxamer 188	285.7	286.3	287.9	285.4	285.0	284.7	286.5
90% w/w Poloxamer 188	285.9	286.3	288.2	285.3	285.0	284.7	286.5
Pure powder							
Paracetamol	285.7	286.2	288.1	285.4		284.7	
Poloxamer 188		286.8			285.0		286.4
Milled paracetamol	285.9	286.2	287.9	285.0		284.7	

O 1s

Table 7-1l summarises the results of the photoemission analysis of O 1s for all the ground and milled samples. Most significant differences between milled and ground mixtures were observed at 10 % w/w poloxamer 188, almost certainly as a result of poloxamer surface dispersion over the higher concentration of paracetamol after milling; in line with this, for the ground mixture the C-OH and N-C=O components were stronger and the lower concentration of poloxamer 188 was reflected by a lower C-C-O intensity. In the milled mixture the relative concentrations of these two O 1s environments were reversed. In contrast, for the mixtures with 50 % w/w and 90 % w/w poloxamer a higher concentration of paracetamol was evident in the milled mixture , indicating either that the milling process reduces the surface area of paracetamol so much that not all of it can be covered by the available poloxamer, or that poloxamer is not mobile enough to coat all paracetamol within the time scale of the experimental work.

Table 7-11: O 1s atomic concentration of paracetamol and poloxamer 188 blending.

Poloxamer 188 mass percent (% w/w)	**C-OH**	**N-C=O**	**C-C-O**
(Paracetamol + poloxamer 188) ground			
10% w/w Poloxamer 188	15.13	15.13	69.73
50% w/w Poloxamer 188	3.45	3.45	93.09
90% w/w Poloxamer 188	1.62	1.62	96.76
(Paracetamol + poloxamer) milled			
10% w/w Poloxamer 188	11.47	11.47	77.05
50% w/w Poloxamer 188	4.48	4.48	91.04
90% w/w Poloxamer 188	1.99	1.99	96.03
Pure powder			
Paracetamol	59.24	40.76	
Poloxamer 188	0.99		99.01
Milled paracetamol	54.01	45.99	

Table 7-12 lists the O 1s E_B values for all the samples. Paracetamol exhibits two photoemission peaks at 531.4 to 531.9 eV from its N-C=O and its C-OH was between 533.0 to 533.5 eV. The poloxamer 188 C-C-O was fixed between 532.0 to 532.9 eV. All O 1s data were fitted with a FWHM fixed at 0.9 to 1.1 eV. There were no significant shifts in E_B for the C-OH and C-C-O components. For the N-C=O emission there were slight variations as a function of composition by up to about 0.2 eV in the milled mixtures.

Table 7-12: O 1s binding energy of ground and milled samples

Poloxamer 188 mass percent (% w/w)	**C-OH [eV]**	**N-C=O [eV]**	**C-C-O [eV]**
(Paracetamol + poloxamer 188)ground			
10% w/w Poloxamer 188	533.3	531.4	532.8
50% w/w Poloxamer 188	533.6	531.2	532.8
90% w/w Poloxamer 188	533.6	531.2	532.8
(Paracetamol + poloxamer) milled			
10% w/w Poloxamer 188	533.5	531.1	532.8
50% w/w Poloxamer 188	533.6	531.2	532.8
90% w/w Poloxamer 188	533.7	531.4	532.6
Pure powder			
Paracetamol	533.0	531.5	
Poloxamer 188	533.2		532.5
Milled paracetamol	532.5	531.1	

N 1s

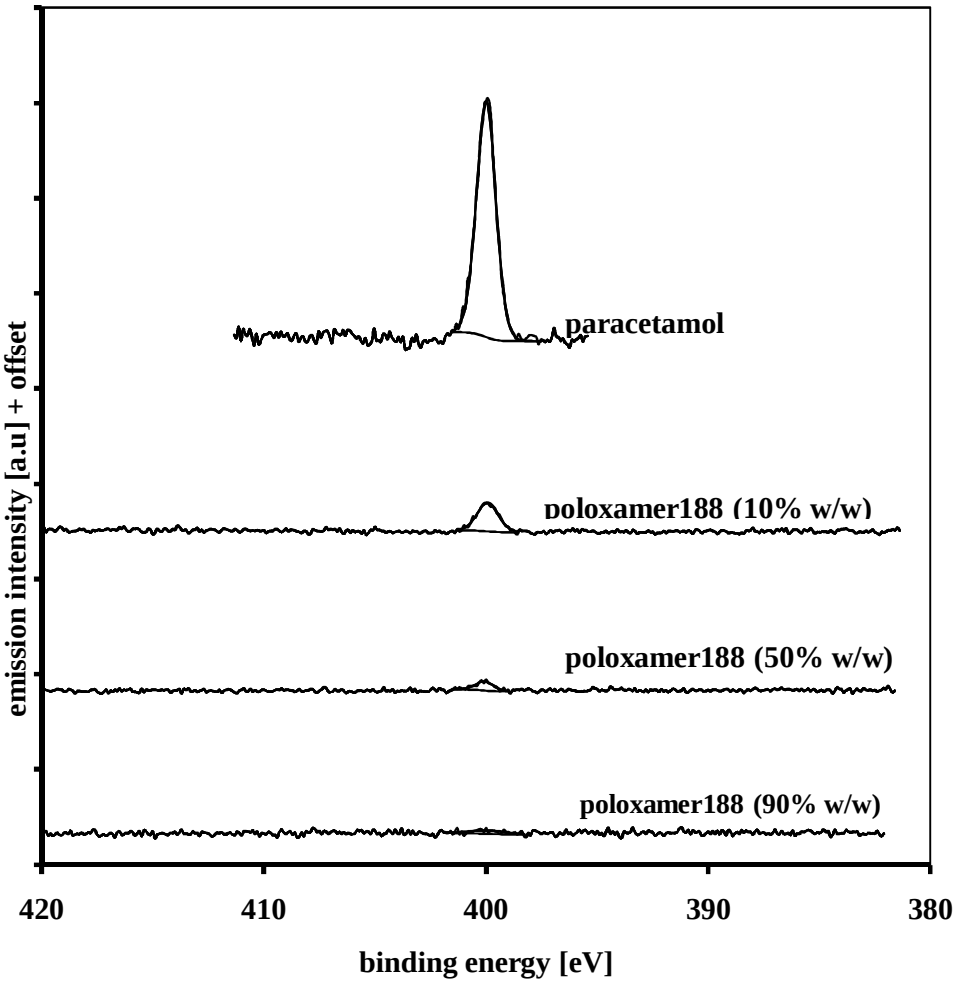

Figure 7-11: N 1s spectra for all the milled paracetaml and poloxamer 188 at different mass percent

The region of the N 1s emission is displayed in **Figure 7-11.** No N 1s feature is apparent in the mixture with a high mass percentage of Poloxamer 188 (90% w/w), in line with our above conclusion that poloxamer efficiently coats all paracetamol in this mixture. The N 1s emission from paracetamol is clearly evident for 10 % w/w Poloxamer 188 content. At 50% w/w poloxamer a small N 1s peak is visible as well.

7.4.7. Radiation Damage

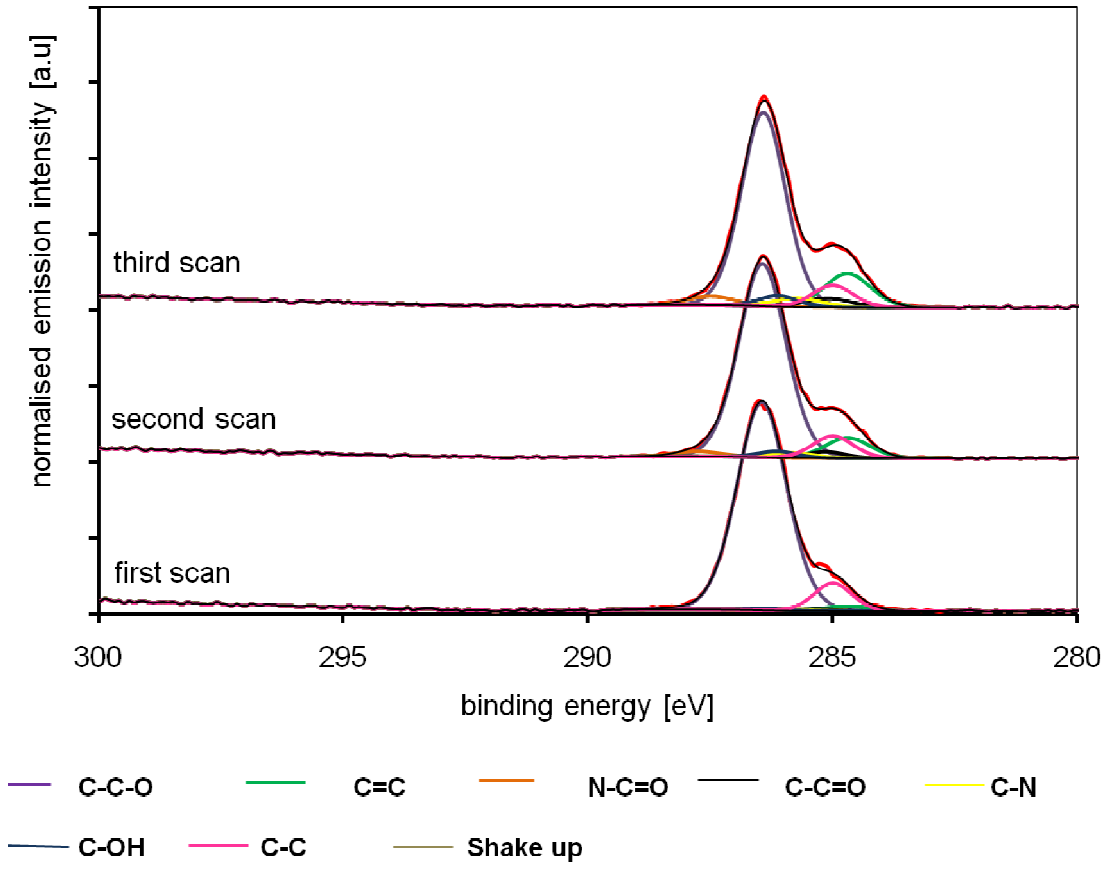

Figure 7-12: C 1s spectra of 90 % w/w of poloxamer 188 for three scans

Figure 7-12 shows three consecutive C 1s scans of the 90 % w/w poloxamer 188 mixture with paracetamol. The analysis of spectra composition was presented in barchart as in **Figure 7-15**. It can be seen that the shoulder at lower E_B broadens and becomes more intense on the second and third scans. The C-C-O peak was less intense on the second scan, while the C-N and C-OH peaks were of increased intensity. On the third scan the C-C=O and C-C peak broadened and became even less intense, while the intensity of the C=C and C-N and C-OH peaks increased.

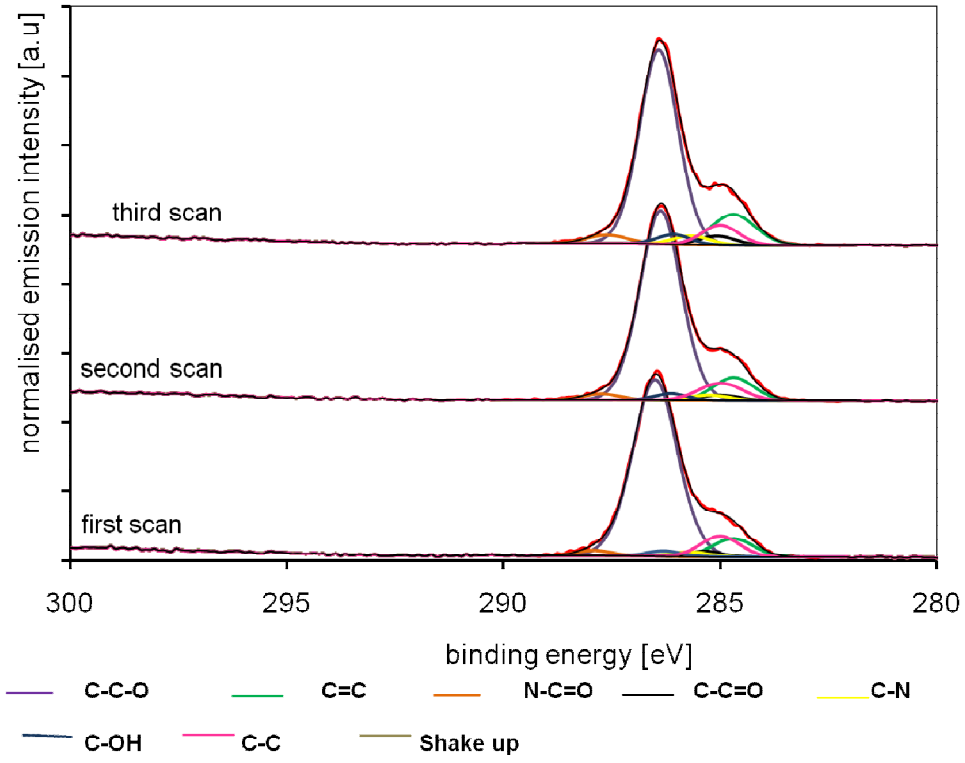

Figure 7-13: C 1s spectra of 50% w/w poloxamer 188 for three scans

Figure 7-13 shows three consecutively measured C 1s spectra of 50 % w/w poloxamer 188. The analysis of spectra composition was presented in barchart as in **Figure 7-16**.It is observed that the shoulder at lower E_B is increased in the third scan compared with the first and second scans. Also, the N-C=O peak was more intense on the third scan, while the C=C and C-C=O intensities increased with each successive scan.

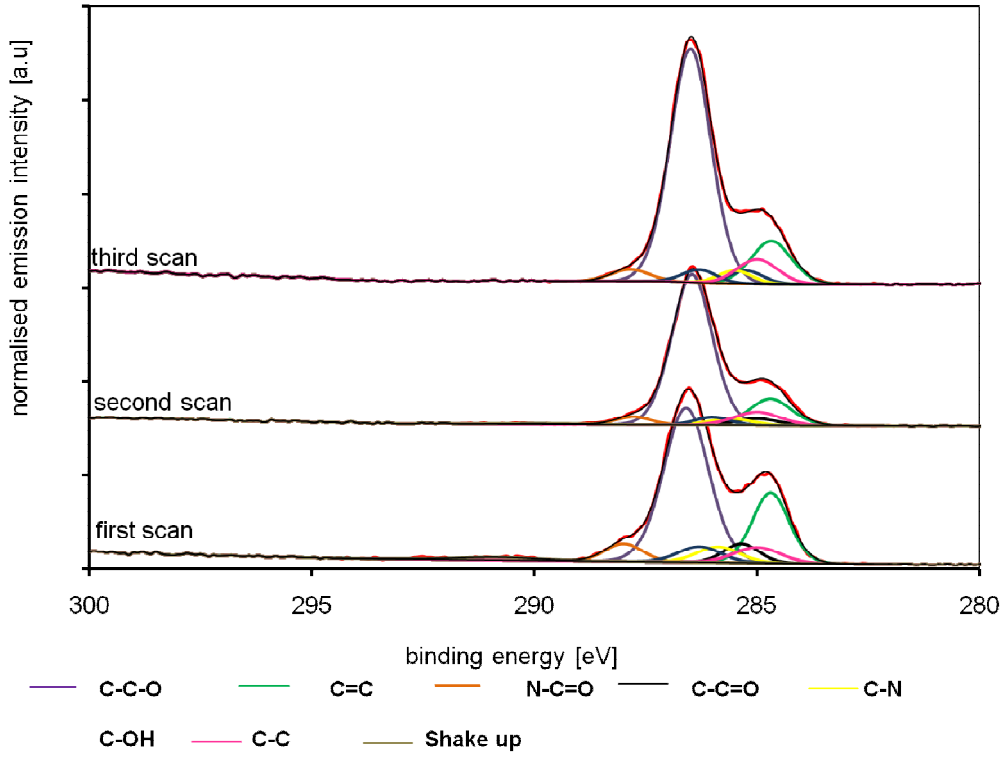

Figure 7-14: C 1s spectra of 10% w/w poloxamer 188 for three scans

Figure 7-14 shows three consecutively measured spectra of the 10 % w/w poloxamer 188 paracetamol mixture. The analysis of spectra composition was presented in barchart as in **Figure 7-17**. The shoulder peak intensity was reduced in the third scan. With each successive scan of the sample surface, there was an increase in C-C-O and C-C intensity, but a decrease in C-C=O, N-C=O, C=C, C-N and C-OH intensity. The shake-up peak is visible only in the first spectrum. It appears that increasing the X-ray dose leads to an increase of the concentration of poloxamer 188 on the surface, burying the emission from the paracetamol functional groups.

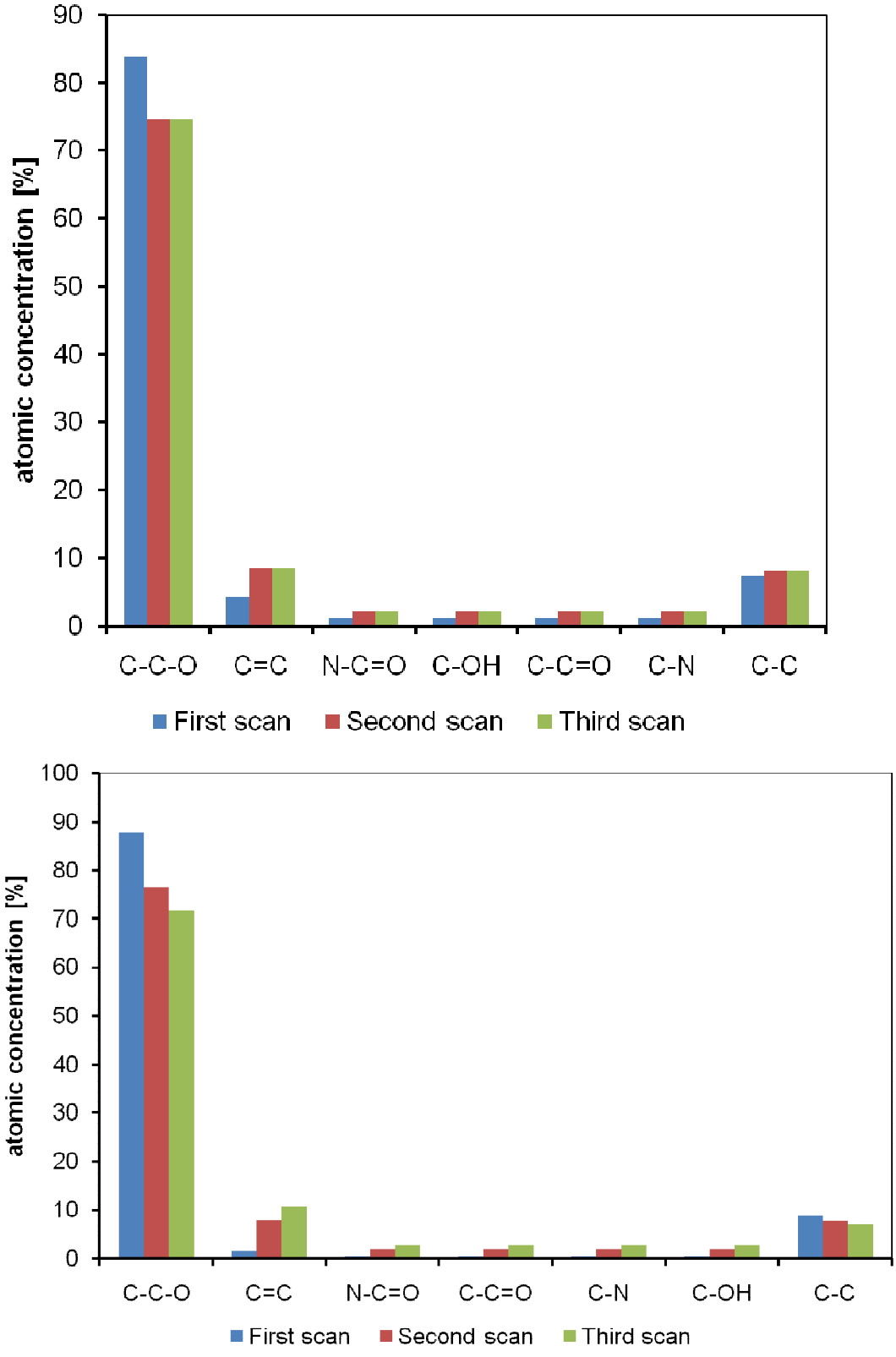

Figure 7-15: Carbon environments of milled (top) and ground (below) mixture of 90 % w/w poloxamer 188 for three scans.

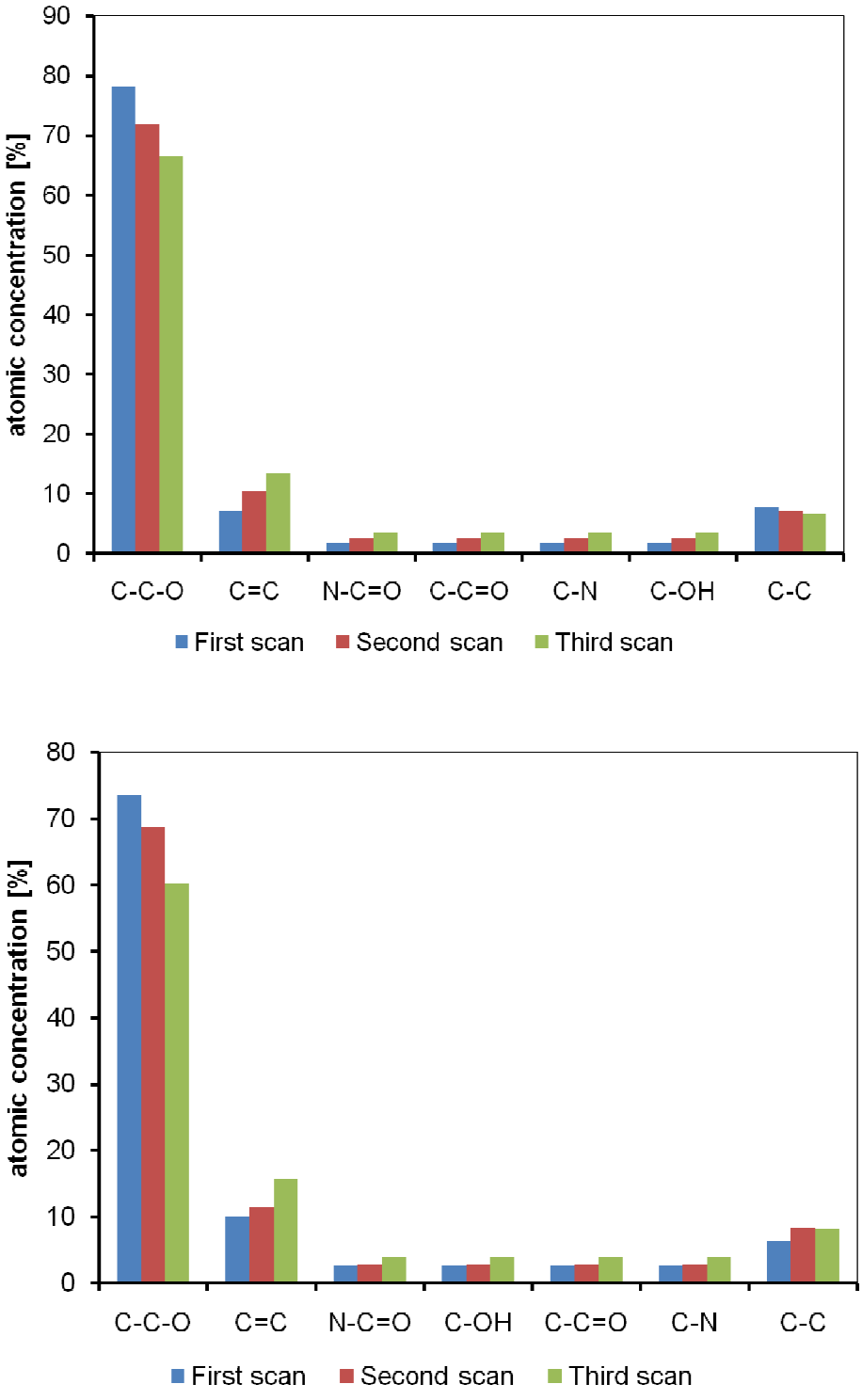

Figure 7-16: Carbon environments of milled (top) and ground (below) mixture of 50 % w/w poloxamer 188 for three scans

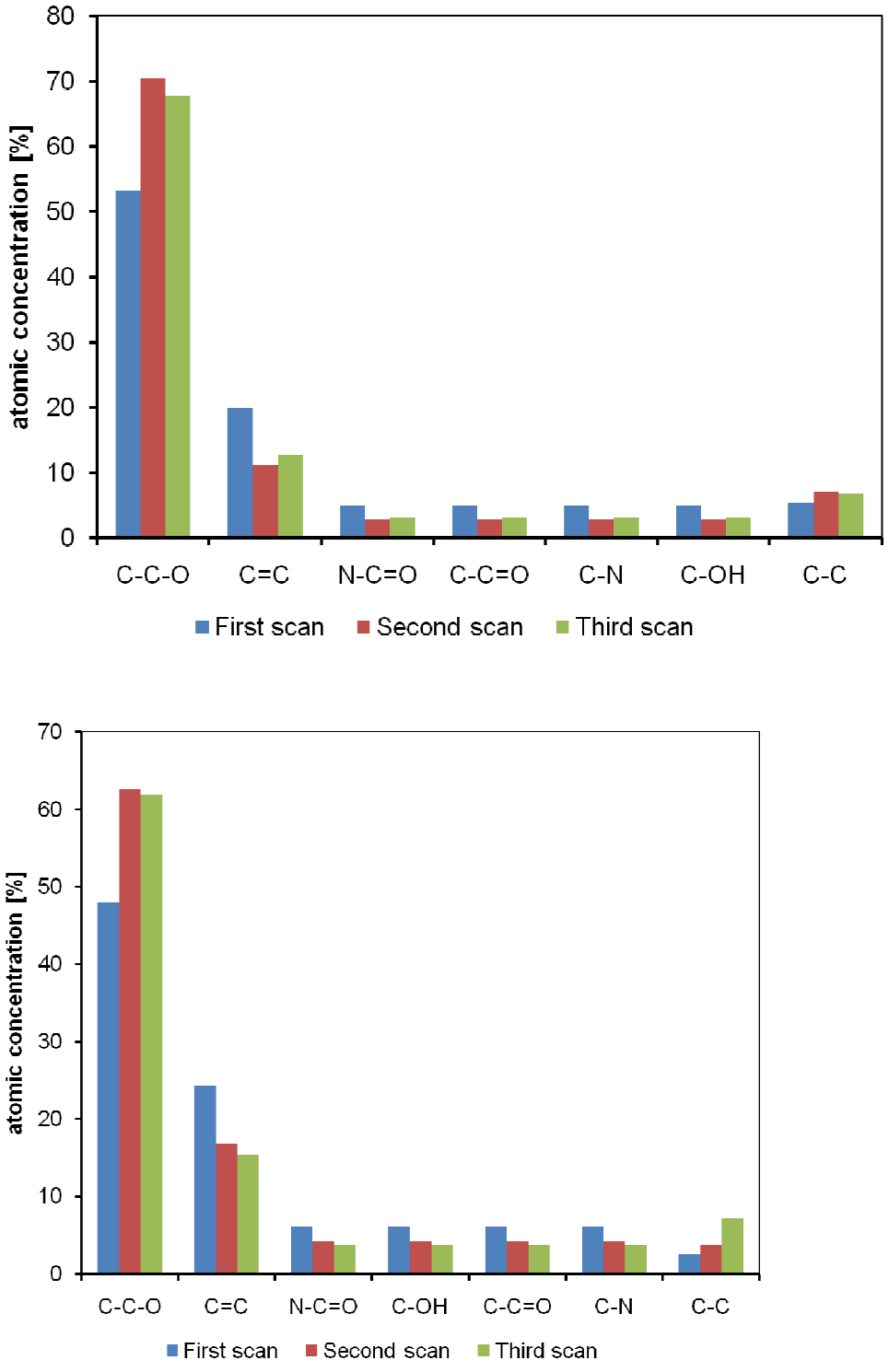

Figure 7-17: C 1s of milled (top) and ground (below) mixture of 10 % w/w poloxamer 188 for three successive scans

The three plots in **Figure 7-15 to 7-17** summarise the C 1s results monitoring of radiation damage for three scans of milled and ground samples. There was no significant difference in N-C=O, C-N, C-C=O, C-C and C-OH of 90 % w/w and 50 % w/w between milled and ground mixture, though the plots reveal that the C-C concentration was a little bit higher than N-C=O, C-N, C-C=O and C-OH. At 10 % w/w, C-C slightly decreases for the second and third scan. However, there was a sharp decrease in C-C-O, the predominant carbon environment of poloxamer 188, at 90 % w/w and 50 % w/w of mixture. The pattern of radiation-induced C-C-O formation at each mixture composition was also visible through a decrease in the C=C concentration. The same pattern of behaviour is evident for the ground mixtures. Interestingly, at 10 % w/w, the C-C concentration was significantly increased, while concentrations of other functional groups (N-C=O, C-N, C-C=O and C-OH) were decreased relative to the first scan. **Table 7-13** lists all of the E_B data. Generally, the C 1s chemical shifts were not significantly different for all milled and ground mixture, at any composition. The above observations are again summarised through plots shown in **Figures 7-18** and **7-20**.

Table 7-13: Induced radiation E_B for ground and milled paracetamol / poloxamer 188 for three scans.

	C-C-O	**C=C**	**N-C=O**	**C-C=O**	**C-N**	**C-OH**	**C-C**
90% w/w poloxamer 188							
First Scan (milled)	286.5	284.7	288.2	285.3	285.9	286.3	285.0
First Scan (ground)	286.5	284.7	287.9	285.3	285.9	286.3	285.0
Second Scan (milled)	286.4	284.7	287.9	285.1	285.9	286.3	285.0
Second Scan (ground)	286.5	284.7	287.9	285.3	285.9	286.3	285.0
Third Scan (milled)	286.5	284.7	288.0	285.3	285.6	286.4	285.0
Third Scan (ground)	286.5	284.7	287.9	285.3	285.9	286.3	285.0
50% w/w poloxamer 188							
First Scan (milled)	286.5	284.7	287.9	285.3	285.7	286.3	285.0
First Scan (ground)	286.5	284.7	287.7	285.1	285.4	286.3	285.0
Second Scan (milled)	286.4	284.7	287.7	285.3	285.7	286.2	285.0
Second Scan (ground)	286.4	284.7	287.7	285.1	285.5	286.2	285.0
Third Scan (milled)	286.4	284.7	287.6	285.2	285.9	286.2	285.0
Third Scan (ground)	286.4	284.7	287.7	285.4	285.9	286.2	285.0
10% w/w poloxamer 188							
First Scan (milled)	286.6	284.7	288.0	285.4	285.9	286.3	285.0
First Scan (ground)	286.5	284.7	287.7	285.4	285.9	286.3	285.0
Second Scan (milled)	286.6	284.7	287.9	285.3	285.5	286.1	285.0
Second Scan (ground)	286.5	284.7	287.7	285.3	285.5	286.3	285.0
Third Scan (milled)	286.5	284.7	287.8	285.4	285.7	286.3	285.0
Third Scan (ground)	286.5	284.7	287.7	285.3	285.9	286.3	285.0

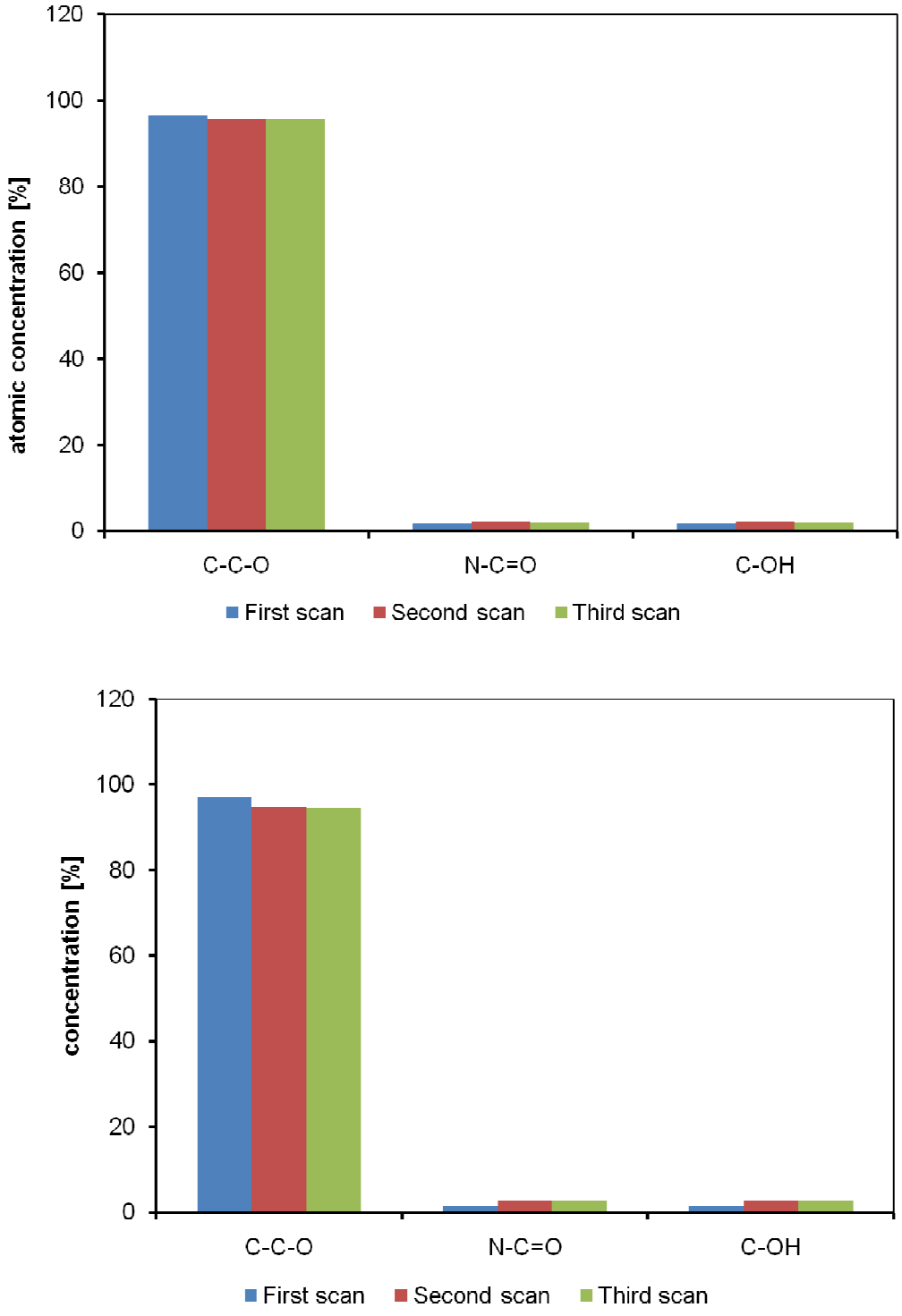

Figure 7-18: O1s of milled (top) and ground (below) mixture of 90 % w/w poloxamer 188 for three successive scans

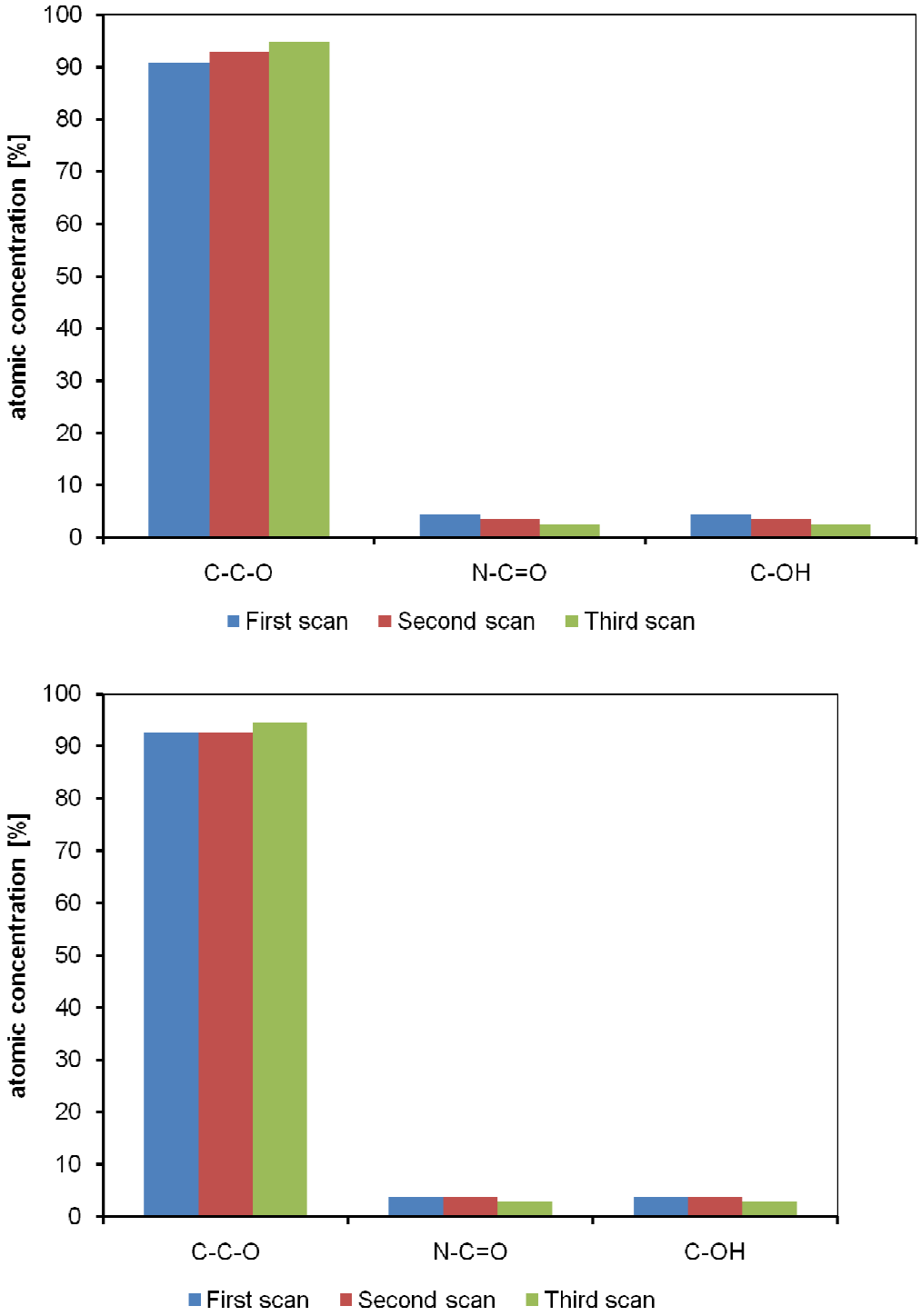

Figure 7-19: O1s of milled (top) and ground (below) mixture of 50 % w/w poloxamer 188 for three successive scans

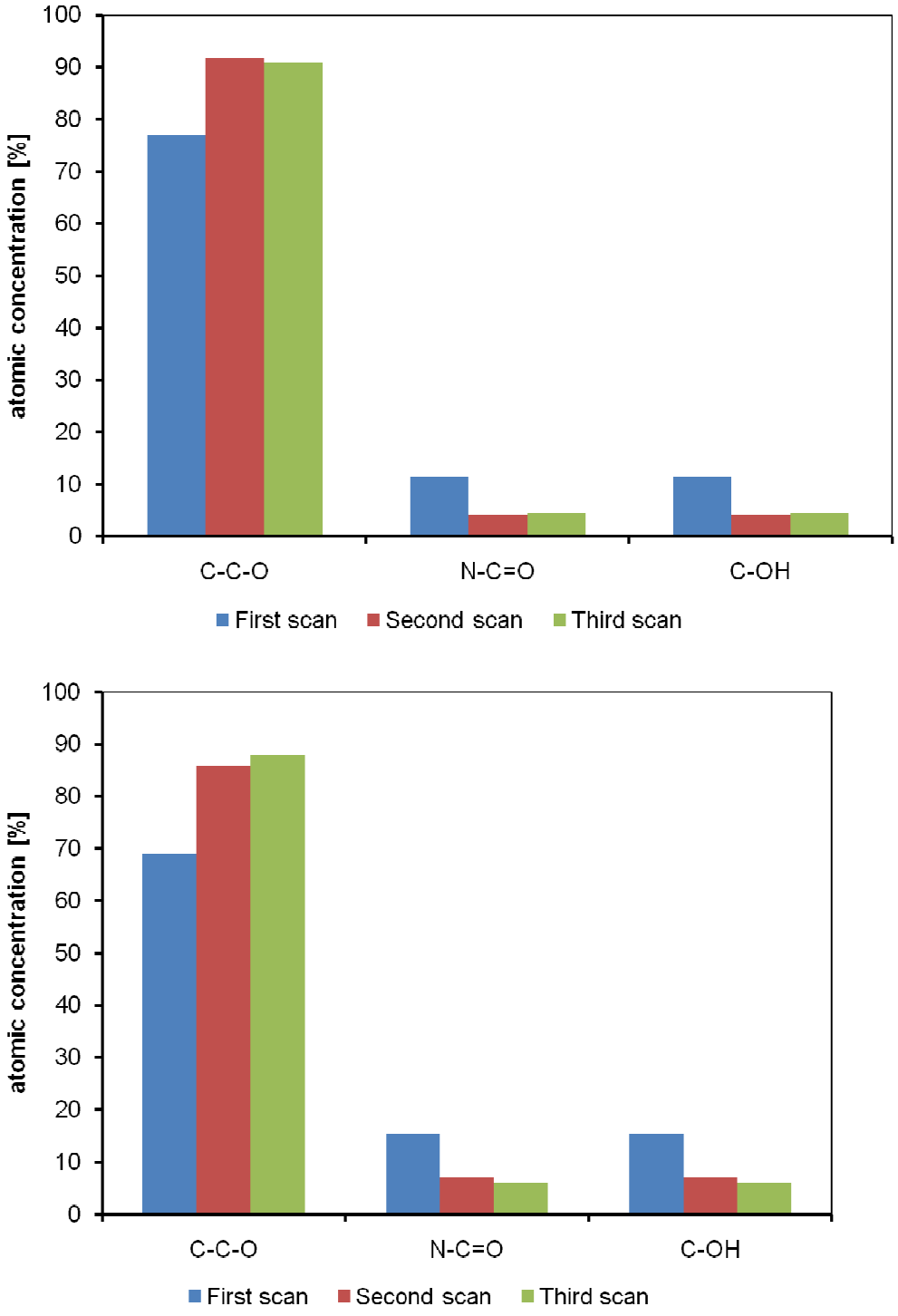

Figure 7-20: O1s of milled (top) and ground (below) mixture of 90 % w/w poloxamer 188 for three successive scans

7.5. Discussion

As stated in **Chapter 2** poloxamer 188 is expected to interact strongly with paracetamol compared to poloxamer 338 and poloxamer 407. Poloxamer 188 is known to contain a high proportion of hydrophilic chains rather than hydrophobic ones. Mechanical force applied to the ethyl p-hydroxybenzoate and poloxamer 188 during the crystallisation changes the crystalline habit and adsorption of poloxamer 188. The results showed that during crystallisation, the hydrophilic part of poloxamer 188 grew, but the hydrophobic part exhibited crystallisation[10, 11]. Ther have been only a few previous studies of paracetamol and poloxamer 188 mixture by solid dispersion and melt extrusion, due to the gelling effect of poloxamer 188 at low temperature (30 to 37 ^{o}C)[32]. The evaporation of solvent from the mixture is complicated by this gelling effect: solvent is trapped in the mixture, which remains a gel solution.

The results of the ATR-IR analysis of mixture crystallinity indicate that the poloxamer 188 concentration did not affect the bulk properties of paracetamol. Furthermore, PXRD results also show that the crystallinity in the mixtures was not significantly different. The crystallinity properties of paracetamol and poloxamer 188 mixtures are in agreement with reports that the composition of ibuprofen and poloxamer 188 solid dispersion mixtures[33] did not affect the crystallinity of the ibuprofen. Recently, it has been proposed that the hydrogen bonds of ibuprofen and poloxamer were at the head and tail of the poloxamer ends of OH and H groups[34].

Generally, ground and milled mixture results show that at high poloxamer 188 stoichiometry, the C 1s of C-C-O, which is characteristic of poloxamer 188, is increased, whereas at low poloxamer 188 concentrations, the C-C-O concentration is reduced. Conversely, structures characteristic of paracetamol, such as N-C=O, C=C and C-N and C-OH, are reduced as paracetamol concentration decreases. However, the photoemission from the characteristic C 1s environment (C=-C, C-C=O, N-C=O) of paracetamol in the milled mixture were less relatively intense than in the ground mixture, while poloxamer 188 characteristic groups (C-C-O and C-C) were more prominently evident on milled mixture surfaces. This indicates that the mechanical force associated with milling can be put to use for coating paracetamol by poloxamer 188 . Grinding appears to be much less efficient in dispersing poloxamer across the paracetamol surfaces.

The C 1s high resolution analysis is supported by the results of the O 1s analysis. It has been revealed at 10 % w/w milling mixture of poloxamer 188, N-C=O and C-OH; both paracetamol characteristic peaks, were lower in intensity in the milled than in the ground mixture. In addition, a chemical shift of the N-C=O group is observed for both C 1s and O 1s results, especially after milling the mixtures. The N-C=O C 1s E_B in the ground mixture at all compositions was between 287.7 and 287.9 eV. Milling increased it to approximately 288.0-288.2 eV. The significance different of 0.3 eV of milling relative to ground mixture; indicates a decrease of the N-C=O electron density due to the interaction of paracetamol and poloxamer 188. The absence of shake-up peaks and N 1s emission from the XPS spectra indicate a loss of aromaticity[8]. The low intensity of elemental N in the scan of 90% w/w poloxamer 188 indicated that the N signal was almost absent at the surface of the milled mixture.

For the 10 % w/w poloxamer 188 mixtures, the lowest concentration of poloxamer molecules at the mixture surface was observed (**Figure 7-14**). The above results indicate that the surface of the mixture was rich with poloxamer 188 molecules, while the low emission intensity from the paracetamol-specific groups (C=C, N-C=O, C-N and C-OH) supports the view that adsorption of poloxamer 188 onto the paracetamol structure takes place. It appears that only a small amount of poloxamer 188 is sufficient to coat the paracetamol molecules.

High concentrations of excipients in drug formulations will slow down drug disintegration, dissolution and/or bioavailability[35]. XPS has previously been used to study polymer conformation[31] from valence band data, but no significant valence band changes were detectable in the present case. The encapsulation of the drug surface by poloxamer is in agreement with previous results reported in the literature[35, 36].

The paracetamol-poloxamer mixtures, milled and ground, were investigated by scanning the surface with radiation. The results for the milled mixtures revealed that the C-C-O concentration increased with the amount of radiation of the surface. All paracetamol / poloxamer 188 compositions showed similar trends. At 50 % w/w and 90 % w/w of poloxamer 188, the shoulder peak of C=C increase but C-C-O intensity were decrease with successive scans, as shown in **Figure 7-19 and 7-20.** However, at this stoichiometry, the C-N, N-C=O and C-OH values showed no significant difference among all the scans, indicating that no peroxide was formed by the decomposition of ether of Poloxamer 188. The increase of C-C-O over successive XPS scans indicates that

the radiation changed the poloxamer 188 chain conformation[37], from compressed to loose (brush conformation), due to the electrostatic charge created by more C-C-O during the radiation process. Part of the polymer is expected to be adsorbed, contributing less to the XPS emission signals due to shielding by the free unadsorbed part. Such a morphology was apparent form the XPS results of the milled sample. The loose conformation thinned the layer of adsorbed poloxamer 188 and made space for exposing paracetamol, as suggested in **Figure 7.21** .

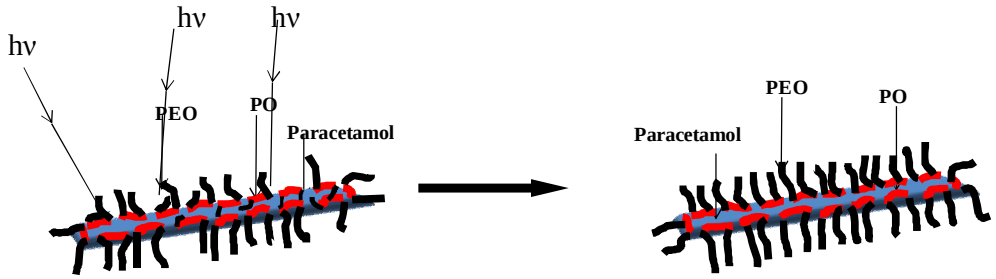

Figure 7-21: The electrostatic effect of XPS radiation on the C-C-O poloxamer 188 chain

A different phenomenon was evident for 10% w/w poloxamer 188. C 1s showed that the emission from C-C-O and C-C groups were high, but reduced concentrations of C=C, N-C=O, C-OH, C=O and C-N developed from first scan to second scan. The increased intensities stemmed from poloxamer 188, while the decreased ones came from paracetamol groups. No significant difference in chemical shift was observed for C 1s (C-C-O). As mentioned earlier, 10% w/w poloxamer perceived the highest coating on the mixture surface. It is showed most of the poloxamer 188 on the mixture is on the surface. Radiation induced damage increases the poloxamer 188 coverage, probably resulted in additional exposure of both PEO and PPO chains at the surface and closer packing of surface anchors of the poloxamer molecules on both ground and milled mixture.

7.6. Conclusion

XPS supported by ATR-IR, DSC and PXRD indicated that 10 % w/w poloxamer 188 mixtures in paracetamol, the poloxamer encapsulated paracetamol efficiently. For the milled mixture, weak signals were detected in respect of the main carbon environments of paracetamol, N-C=O and C-N/C-OH, but there was a high concentration of the main carbon environment of poloxamer 188.

Radiation-induced degradation of poloxamer 188 resulted in an increase in poloxamer 188 concentration, as detected by XPS scanning mainly via the C-C-O carbon environment. At higher poloxamer 188 concentration (50% w/w and 90% w/w) during XPS radiation, increased electrostatic charge at the surface probably stimulates the detachment of poloxamer 188 as well as conformational changes so that emission from the underlying paracetamol surface becomes more evident. The exception is the case of the lowest poloxamer 188 admixture, where radiation increased the poloxamer coverage of the mixture surface.

7.7. References

1. Schulz, M.; Fussnegger, B.; Bodmeier, R., Adsorption of carbamazepine onto crospovidone to prevent drug recrystallization. *Int. J. Pharm.* 391, 169-176.

2. Cassidy, O. E., Surface modification and electrostatic charge of polystyrene particles. *Int. J. Pharm.* **1999,** 182, 199-211.

3. Puri, V.; Dantuluri, A. K.; Kumar, M.; Karar, N.; Bansal, A. K., Wettability and surface chemistry of crystalline and amorphous forms of a poorly water soluble drug. *Eur. J.Pharm. Sci.* **2010,** 40, 84-93.

4. Goddard, J. M.; Hotchkiss, J. H., Polymer surface modification for the attachment of bioactive compounds. *Prog. Polym. Sci.* **2007,** 32, 698-725.

5. Rouxhet, P. G.; Doren, A.; Dewez, J. L.; Heuschling, O., Chemical composition and physico-chemical properties of polymer surfaces. *Prog.Org.Coat.* **1993,** 22, 327-344.

6. Duro, R.; Souto, C.; Gomez-Amoza, J.; Martenez-Pacheco, R.; Concheiro, A., Interfacial Adsorption of Polymers and Surfactants: Implications for the Properties of Disperse Systems of Pharmaceutical Interest. *Drug Dev. Ind.Pharm.* **1999,** 25, 817.

7. Law, S. L.; Kayes, J. B., Adsorption of non-ionic water-soluble cellulose polymers at the solid-water interface and their effect on suspension stability. *Int.J. Pharm.* **1983,** 15, 251-260.

8. Cao, X.; Coulter, S. K.; Ellison, M. D.; Liu, H.; Liu, J.; Hamers, R. J., Bonding of Nitrogen-Containing Organic Molecules to the Silicon(001) Surface: The Role of Aromaticity *J. Phys. Chem. B* **2001,** 105, 3759-3768.

9. Erbil, H. Y., *Surface chemistry of solid and liquid interfaces*. Blackwell Pub.: Malden, MA, 2006.

10. York, P., Solid-state properties of powders in the formulation and processing of solid dosage forms. *Int. J. Pharm.* **1983,** 14, 1-28.

11. Mackellar, A. J.; Buckton, G.; Newton, J. M.; Chowdhry, B. Z.; Orr, C. A., The controlled crystallisation of a model powder: 1. The effects of altering the stirring rate and the supersaturation profile, and the incorporation of a surfactant (poloxamer 188). *Int.J. Pharm.* **1994,** 112, (.), 65-78.

12. Wen, H.; Morris, K. R.; Park, K., Hydrogen bonding interactions between adsorbed polymer molecules and crystal surface of acetaminophen. *J.Colloid Interf. Sci.* **2005,** 290, 325-335.

13. Elamina, A. A.; Ahlneck, C.; Alderborna, G.; Nyström, C., Increased metastable solubility of milled griseofulvin, depending on the formation of a disordered surface structure. *Int. J. Pharm.* **1994,** 111, 159-170.

14. Zimmermann, A.; Millqvist-Fureby, A.; Elema, M. R.; Hansen, T.; Müllertz, A.; Hovgaard, L., Adsorption of pharmaceutical excipients onto microcrystals of siramesine hydrochloride: Effects on physicochemical properties. *Eur. J.Pharm. Biopharm.* **2009,** 71, 109-116.

15. Prashant, N. B.; Wai Kiong, N.; Reginald, B. H. T.; Sui Yung, C., Influence of excipients in comilling on mitigating milling-induced amorphization or structural disorder of crystalline pharmaceutical actives. *J.Pharmaceutic.Sci.* 99, 2462-2474.

16. Wischke, C.; Schwendeman, S. P., Principles of encapsulating hydrophobic drugs in PLA/PLGA microparticles. *Int. J. Pharm.* **2008,** 364, 298-327.

17. Santander-Ortega, M. J.; Jodar-Reyes, A. B.; Csaba, N.; Bastos-Gonzalez, D.; Ortega-Vinuesa, J. L., Colloidal stability of Pluronic F68-coated PLGA nanoparticles: A variety of stabilisation mechanisms. *J.Colloid Interf. Sci.* **2006**, 522-529.

18. Miyazaki, T.; Yoshioka, S.; Aso, Y., Physical stability of amorphous acetanilide derivatives improved by polymer excipients. *Chem.Pharmaceut.Bull.* **2006,** 54, 1207-1210.

19. Nair, R.; Nyamweya, N.; Gönen, S.; Martínez-Miranda, L. J.; Hoag, S. W., Influence of various drugs on the glass transition temperature of poly(vinylpyrrolidone): a thermodynamic and spectroscopic investigation. *Int. J. Pharm.* **2001,** 225, 83-96.

20. Brabander, C. d.; Mooter, G. v. d.; Vervaet, C.; Remon, J. P., Characterization of ibuprofen as a nontraditional plasticizer of ethyl cellulose. *J. Pharm. Sci.* **2002**, 1678-1685.

21. Changquan, S., A novel method for deriving true density of pharmaceutical solids including hydrates and water-containing powders. *J. Pharm.Sci.* **2004,** 93, 646-653.

22. Kamat, M. S.; Osawa, T.; DeAngelis, R. J.; Koyama, Y.; DeLuca, P. P., Estimation of the Degree of Crystallinity of Cefazolin Sodium by X-ray and Infrared Methods. *Pharm Res.* **1988,** 5, 426-429.

23. Shah, T.; Amin, A.; Parikh, J.; Parikh, R., Process optimization and characterization of poloxamer solid dispersions of a poorly water-soluble drug. *AAPS PharmSciTech* **2007,** 8, E18-E24.

24. Guo, C.; Liu, H.; Wang, J.; Chen, J., Conformational Structure of Triblock Copolymers by FT-Raman and FTIR Spectroscopy. *J.Colloid Interf.Sci.* **1999**, 368-373.

25. Misra, A. K., Thermoanalytical and microscopic investigation of interaction between paracetamol and fatty acid crystals. *J. Macromol. Sci. A Pure* **2007,** 44, 685-690.

26. Esrafili, M. D.; Behzadi, H.; Hadipour, N. L., Influence of N-H...O and O-H...O hydrogen bonds on the 17O, 15N and 13C chemical shielding tensors in crystalline acetaminophen: A density functional theory study. *Biophys. Chem.* **2007,** 128, 38-45.

27. He, Y.; Zhu, B.; Inoue, Y., Hydrogen bonds in polymer blends. *Prog. Polym. Sci.* **2004,** 29, 1021-1051.

28. Qiua, F.; Norwooda, D. L., Identification of pharmaceutical impurities. *J. Liq. Chromatogr.R. T* **2007,** 30, 877-935.

29. Kelemen, S. R.; Rose, K. D.; Kwiatek, P. J., Carbon aromaticity based on XPS II to II* signal intensity. *Appl. Surf.Sci.* **1993,** 64, 167-174.

30. Mozes, N., On the relations between the elemental surface composition of yeasts and bacteria and their charge and hydrophobicity. *Biochim. Biophys. Acta Biomembr.* **1988,** 945, 324-334.

31. Damodaran, V. B., Conformational studies of covalently grafted poly(ethylene glycol) on modified solid matrices using X-ray photoelectron spectroscopy. *Langmuir* 26, 7299-7306.

32. Choi, H. G., Development of in situ-gelling and mucoadhesive acetaminophen liquid suppository. *Int.J. Pharm.* **1998,** 165, 33-44.

33. Newa, M.; Bhandari, K. H.; Li, D. X.; Kwon, T.-H.; Kim, J. A.; Yoo, B. K.; Woo, J. S.; Lyoo, W. S.; Yong, C. S.; Choi, H. G., Preparation, characterization and in vivo evaluation of ibuprofen binary solid dispersions with poloxamer 188. *Int.J. Pharm.* **2007,** 343, 228-237.

34. Ali, W.; Williams, A. C.; Rawlinson, C. F., Stochiometrically governed molecular interactions in drug: Poloxamer solid dispersions. *Int.J. Pharm.* 391, 162-168.

35. Jackson, K.; Young, D.; Pant, S., Drug-excipient interactions and their affect on absorption. *Pharm. Sci. Technol. To.* **2000,** 3, 336-345.

36. Adams, M. L.; Lavasanifar, A.; Kwon, G. S., Amphiphilic block copolymers for drug delivery. *J. Pharm.Sci.* **2003**, 1343-1355.

37. Jia, L.; Guo, C.; Yang, L.; Xiang, J.; Tang, Y.; Liu, C.; Liu, H., Mechanism of PEO-PPO-PEO micellization in aqueous solutions studied by two-dimensional correlation FTIR spectroscopy. *J. Colloid . Interf. Sci.* 345, 332-337.

CHAPTER 8: CONCLUSION AND FUTURE WORK

8.1. Conclusions

The surface sensitive technique XPS complemented by other characterisation techniques has been used to investigate a broad range of paracetamol forms, including powders, partially amorphous milled powders and a number of single crystal facets obtained from different crystallisation media. Because of the high specificity of XPS measurements towards the amide group of paracetamol it was possible to distinguish, for the first time, the influence of surface contamination and adsorbed species on the paracetamol surface from intrinsic contributions from the paracetamol sample itself. While performing these analyses it had to be kept in mind that the surface sensitivity of laboratory XPS measurements with an Al K_α source is not sufficient to detect structural or compositional changes in the topmost molecular layer of organic materials. Analysis of polycrystalline powder samples, including two different polymorphs and various partially amorphous forms of paracetamol, indicated that the core-level shifts associated with varying intermolecular interactions do not perturb the local electronic structure variations in paracetamol enough to become detectable through chemical shifts in the core level photoemission spectra.

XPS investigations of single crystals indicated that the composition of paracetamol single crystal facets prepared from three different solvents was, averaged over the near-surface volume probed by XPS, identical within the accuracy of the measurements. Any variations in the observed spectra were compatible with the presence of adventitious of C and O contamination, or adsorbed surface active species that originated in the solvent media used for crystal preparations. Especially crystallisation from acetone appeared to be associated with the presence of significant contamination layers at the surfaces of the single crystal facets. Due to the ultra-high vacuum conditions applied during XPS measurements it was not possible to establish whether any co-adsorbed solvent molecules would influence the surface composition after preparation.

XPS data for three different aged and fresh poloxamer samples revealed that quantitative XPS analysis is sensitive to the PO/EO block stoichiometry of different poloxamers, through a a combination of survey and high resolution analysis. During aging, oxidative degradation leads to the formation of carbonyl functional groups. The

PO block only was actively degraded at the early stage of poloxamer degradation, while the EO block would later degrade more, especially in a poloxamer with high EO content.

Analysis of the milled and physical mixtures of Poloxamer188 and paracetamol revealed that poloxamers adsorb on the paracetamol surface, especially at a 10 % w/w composition of the poloxamer. Radiation damage during the XPS measurements induced significant degradation of Poloxamer188, detectable mainly via the C-C-O C1s environment.

8.2. Future Work

The aim of future work should be to deepen the understanding of surface interactions at paracetamol surfaces, to extend the application of core level spectroscopies to other molecular organic crystals and to consider other X-ray spectroscopies with sensitivity to local structure as techniques for organic solid state surface science.

More studies of paracetamol need to address issues whether the surface contamination can be reduced, or whether molecularly clean paracetamol surfaces be prepared, so that we can realistically hope to start investigating the surface properties (reconstructions, terminations) of molecular crystals. Particularly interesting, and a logical next step, would be synchrotron XPS studies of these systems to establish whether evidence for depth-dependent variations can be obtained by depth profiling with variable X-ray energies.

Before such work can be undertaken clean surfaces will have to be prepared. Given the prohibitive impurity levels in even the purest commercially available solvents and chemicals it seems unlikely that crystallisation from solution will ever produce sufficiently clean crystal facets to carry out such studies. One strategy could be to find techniques that permit cleaning of the facet surfaces in the vacuum chamber. Commonly used noble gas ion bombardment (‘sputtering’) techniques will not work for organic crystals because they induce too much radiation damage in these materials. Recently developed C_{60} or Au cluster ion sources may permit selective removal of the contamination layers observed in the present study, but their application will require systematic studies.

The alternative to cleaning, preparation of molecularly clean surfaces will require setting up a system for the controlled crystal growth under sufficiently clean conditions.

As a first step, evaporation under ultra-high vacuum conditions may be considered, but it may prove difficult to establish reliably the crystal structures of the evaporated samples. Spin coating of films on a suitable substrate may be another possibility. An advantage of these approaches would be that additional complications due to solvent inclusions could be avoided.

Many organic systems have sufficiently high vapour pressures that their investigation by XPS is complicated by the need to reduce their vapour pressure through constant cooling, which result in additional contamination by adsorption of molecules (especially water) from the residual gas in the vacuum chamber. Preparation protocols, e.g., cool-heat cycles, need to be established to deal with these adsorbed layers. By using high pressure XPS systems one may be able to side-step the vapour pressure issues, but high pressure XPS systems are expensive and mostly restricted to use at synchrotron radiation sources.

In contrast, soft X-ray absorption spectroscopy at high (= non-UHV) pressures is a relatively inexpensive technique that also produces more detailed information about local structure and composition than XPS. One drawback is that this technique also requires the use of a synchrotron radiation X-ray source.

APPENDIX

Appendix 1

AceSingle	C=C	C-C=O	C-N	C-OH	N-C=O	Shake-up
1	**0.9**	**0.9**	**1.1**	**1.1**	**0.8**	**2.2**
2	**0.9**	**0.9**	**1.0**	**1.0**	**0.9**	**2.5**
3	**1.0**	**1.1**	**0.8**	**1.1**	**1.1**	**2.5**
EtSingle	**C=C**	**C-C=O**	**C-N**	**C-OH**	**N-C=O**	**Shake-up**
1	**0.9**	**0.8**	**1.0**	**1.0**	**0.9**	**1.8**
2	**0.9**	**0.8**	**1.0**	**1.0**	**1.0**	**2.5**
3	**0.8**	**0.8**	**1.0**	**1.0**	**0.8**	**1.8**
4	**0.8**	**0.8**	**0.9**	**1.0**	**0.8**	**2.0**
5	**0.8**	**0.8**	**1.0**	**1.0**	**0.8**	**2.0**
6	**0.8**	**0.8**	**0.9**	**1.0**	**0.8**	**1.8**
7	**0.8**	**0.8**	**1.1**	**1.1**	**0.9**	**2.0**
8	**0.8**	**0.8**	**1.1**	**1.0**	**0.9**	**1.8**
9	**0.8**	**0.8**	**1.0**	**1.0**	**0.9**	**2.1**
10	**0.8**	**0.8**	**1.0**	**1.0**	**0.9**	**1.8**
11	**0.8**	**0.8**	**1.0**	**1.0**	**0.9**	**2.1**
12	**0.8**	**0.8**	**1.0**	**1.1**	**1.1**	**1.9**
13	**0.8**	**0.8**	**1.1**	**1.1**	**0.9**	**2.0**
14	**0.8**	**0.8**	**1.0**	**1.1**	**0.9**	**2.0**
15	**0.8**	**0.8**	**1.0**	**1.0**	**0.8**	**1.8**
16	**0.9**	**0.9**	**1.1**	**1.1**	**1.1**	**2.0**
17	**0.8**	**0.8**	**1.0**	**1.1**	**1.0**	**1.9**
18	**0.8**	**0.9**	**1.1**	**1.1**	**0.9**	**1.8**
19	**0.8**	**0.8**	**1.1**	**1.1**	**0.8**	**1.8**
20	**0.8**	**0.8**	**1.1**	**1.1**	**0.9**	**1.7**
21	**0.8**	**0.8**	**1.0**	**1.1**	**0.9**	**2.0**
22	**0.8**	**0.8**	**1.1**	**1.1**	**0.9**	**2.0**
23	**0.8**	**0.8**	**1.0**	**1.1**	**0.8**	**1.9**
MeSingle1	**C=C**	**C-C=O**	**C-N**	**C-OH**	**N-C=O**	**Shake-up**
	0.9	**0.9**	**0.9**	**1.1**	**0.9**	**2.1**
	0.9	**0.8**	**0.9**	**1.0**	**0.8**	**1.9**
	0.9	**0.8**	**0.8**	**0.9**	**0.8**	**1.9**
	0.9	**0.8**	**0.8**	**0.9**	**0.9**	**2.3**
	1.1	**0.8**	**0.8**	**1.1**	**1.1**	**2.5**
	0.9	**0.8**	**0.9**	**0.9**	**0.9**	**2.5**
	0.9	**0.8**	**1.0**	**1.0**	**0.9**	**1.9**
MeSingle2	**C=C**	**C-C=O**	**C-N**	**C-OH**	**N-C=O**	**Shake-up**
	0.9	**0.9**	**1.1**	**1.0**	**0.9**	**2.0**
	0.9	**0.9**	**1.0**	**1.0**	**0.9**	**2.0**
	0.9	**0.9**	**0.9**	**1.0**	**0.9**	**2.0**
	0.9	**0.9**	**1.1**	**1.1**	**0.9**	**2.1**
	0.9	**0.9**	**1.1**	**1.1**	**0.9**	**2.3**
	0.9	**0.9**	**1.0**	**0.9**	**0.9**	**2.5**
	1.1	**1.1**	**0.8**	**1.1**	**1.0**	**2.3**
	1.0	**1.0**	**0.8**	**1.0**	**0.9**	**2.1**
Powder	**C=C**	**C-C=O**	**C-N**	**C-OH**	**N-C=O**	**Shake-up**
	0.9	**0.9**	**1.1**	**0.9**	**0.8**	**2.2**

Appendix 2

AceSingle	C=C	C-C=O	C-N	C-OH	N-C=O	Shake-up
	284.7	285.3	285.7	286.1	288.1	291.0
	284.7	285.4	285.7	286.3	288.1	290.9
	284.7	285.2	285.9	286.3	288.1	291.0
EtSingle	**C=C**	**C-C=O**	**C-N**	**C-OH**	**N-C=O**	**Shake-up**
1	284.7	285.3	285.8	286.3	288.1	290.1
2	284.7	285.1	285.8	286.4	288.1	290.6
3	284.7	285.3	285.9	286.2	288.1	291.0
4	284.7	285.3	285.8	286.3	288.1	291.0
5	284.7	285.2	285.7	286.3	288.1	291.1
6	284.7	285.3	285.9	286.3	288.1	290.9
7	284.7	285.1	285.6	286.3	288.2	291.2
8	284.7	285.2	285.6	286.3	288.2	291.2
9	284.7	285.1	285.6	286.3	288.2	291.1
10	284.7	285.1	285.7	286.3	288.2	291.2
11	284.7	285.1	285.6	286.3	288.2	291.2
12	284.7	285.2	285.7	286.4	288.3	291.3
13	284.7	285.2	285.6	286.4	288.3	291.3
14	284.7	285.0	285.6	286.3	288.3	291.2
15	284.7	285.0	285.5	286.3	288.2	291.2
16	284.7	285.1	285.6	286.3	288.3	291.3
17	284.7	285.1	285.6	286.3	288.3	291.2
18	284.7	285.0	285.5	286.3	288.2	291.2
19	284.7	285.0	285.5	286.3	288.2	291.1
20	284.7	285.1	285.6	286.3	288.3	291.2

21	284.7	285.0	285.5	286.3	288.2	291.3
22	284.7	285.0	285.6	286.3	288.2	291.2
23	284.7	285.2	285.8	286.3	288.1	291.0
MeSingle1	**C=C**	**C-C=O**	**C-N**	**C-OH**	**N-C=O**	**Shake-up**
	284.7	285.1	285.7	286.3	288.1	291.1
	284.7	285.3	285.8	286.2	288.1	290.91
	284.7	285.3	285.8	286.3	288.0	290.91
	284.7	285.3	285.8	286.3	288.1	291.0
	284.7	285.3	285.8	286.4	288.1	291.0
	284.7	285.3	285.9	286.4	288.1	290.9
	284.7	285.3	285.7	286.2	288.1	291.1
MeSingle2	**C=C**	**C-C=O**	**C-N**	**C-OH**	**N-C=O**	**Shake-up**
	284.7	285.3	285.8	286.2	288.1	291.0
	284.7	285.3	285.8	286.2	288.1	291.1
	284.7	285.4	285.8	286.2	288.0	291.0
	284.7	285.4	285.8	286.3	288.1	291.0
	284.7	285.4	285.8	286.3	288.1	291.0
	284.7	285.4	285.8	286.2	288.1	290.8
	284.7	285.2	285.8	286.3	288.0	291.0
	284.7	285.0	285.8	286.2	288.0	290.6
Powder	**C=C**	**C-C=O**	**C-N**	**C-OH**	**N-C=O**	**Shake-up**
	284.7	285.4	285.7	286.2	288.1	291.1

Appendix 3

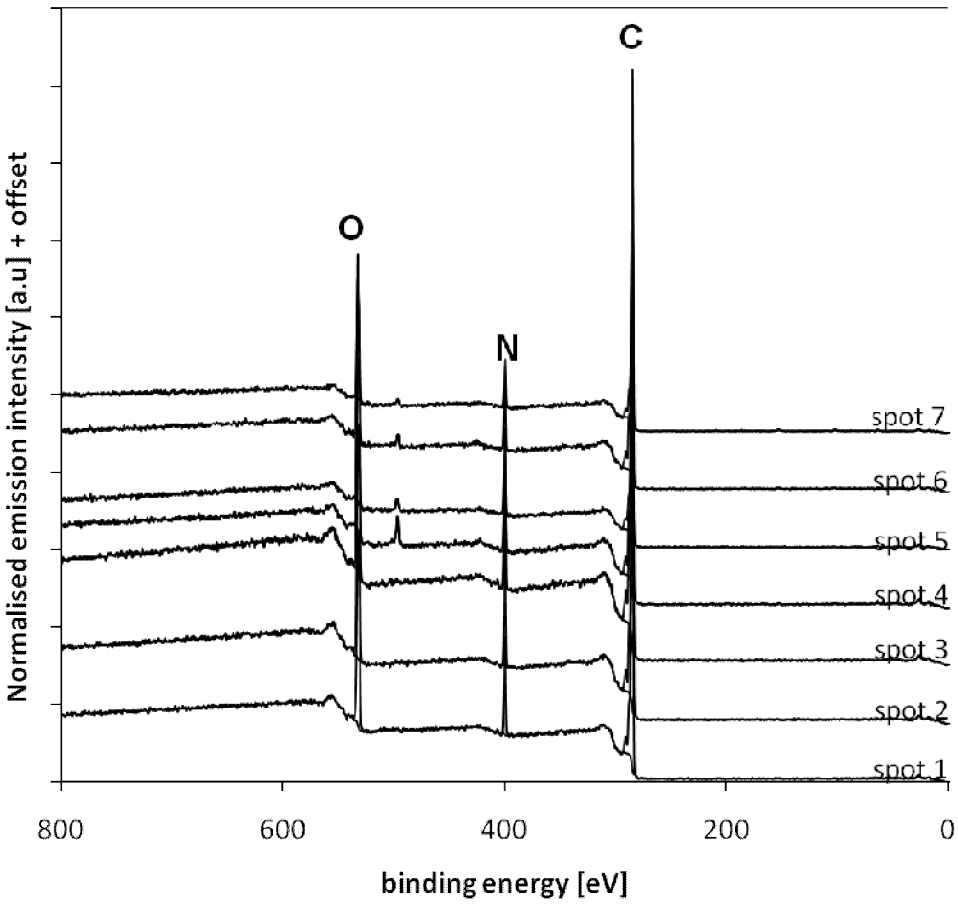

MeSingle1 survey analysis at different spots

Appendix 4

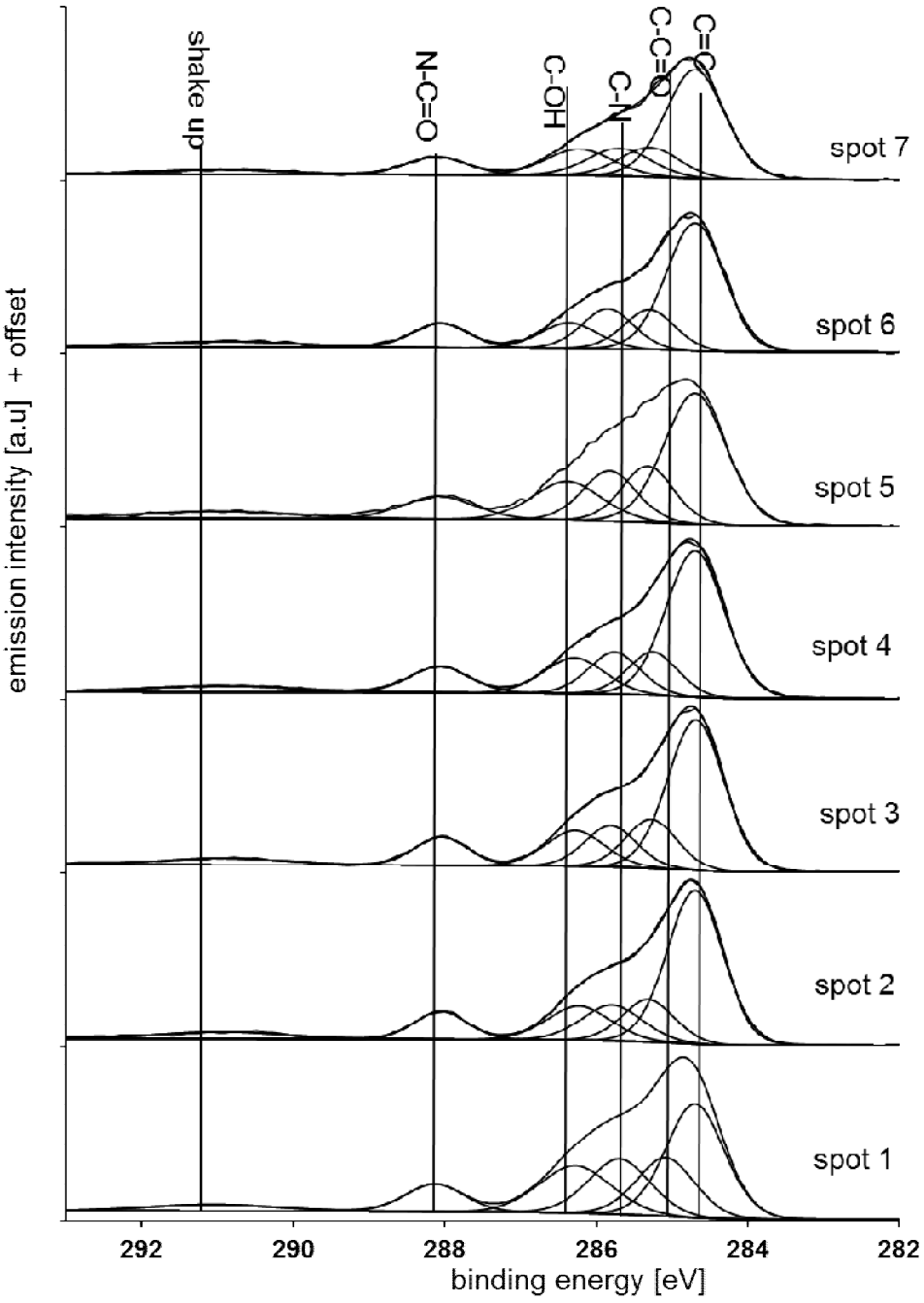

MeSingle1 C1s fitting at different spots analysis

Appendix 5

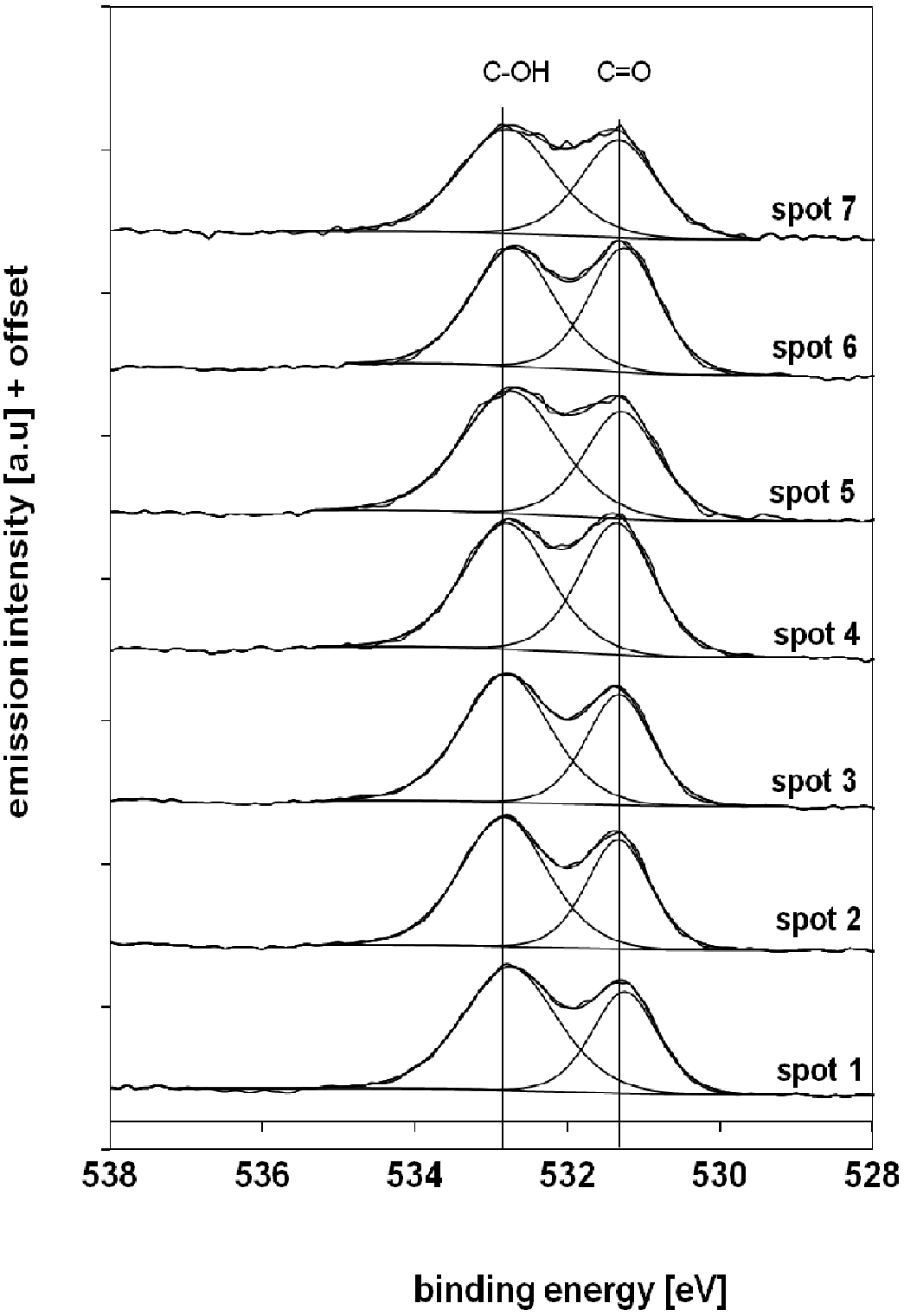

MeSingle1 O1s fitting at different spots analysis

Appendix 6

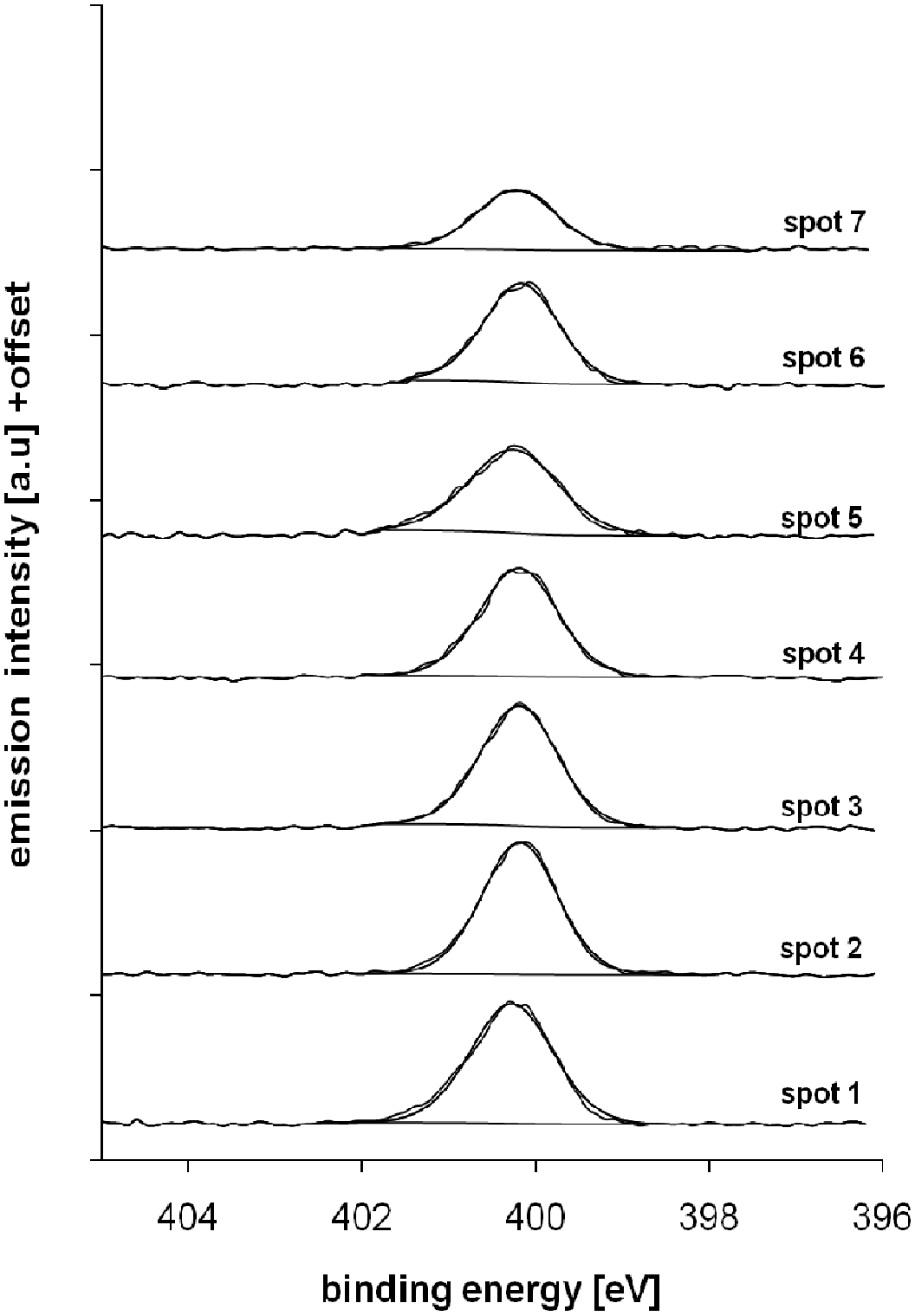

MeSingle1 N1s fitting at different spots analysis

Appendix 7

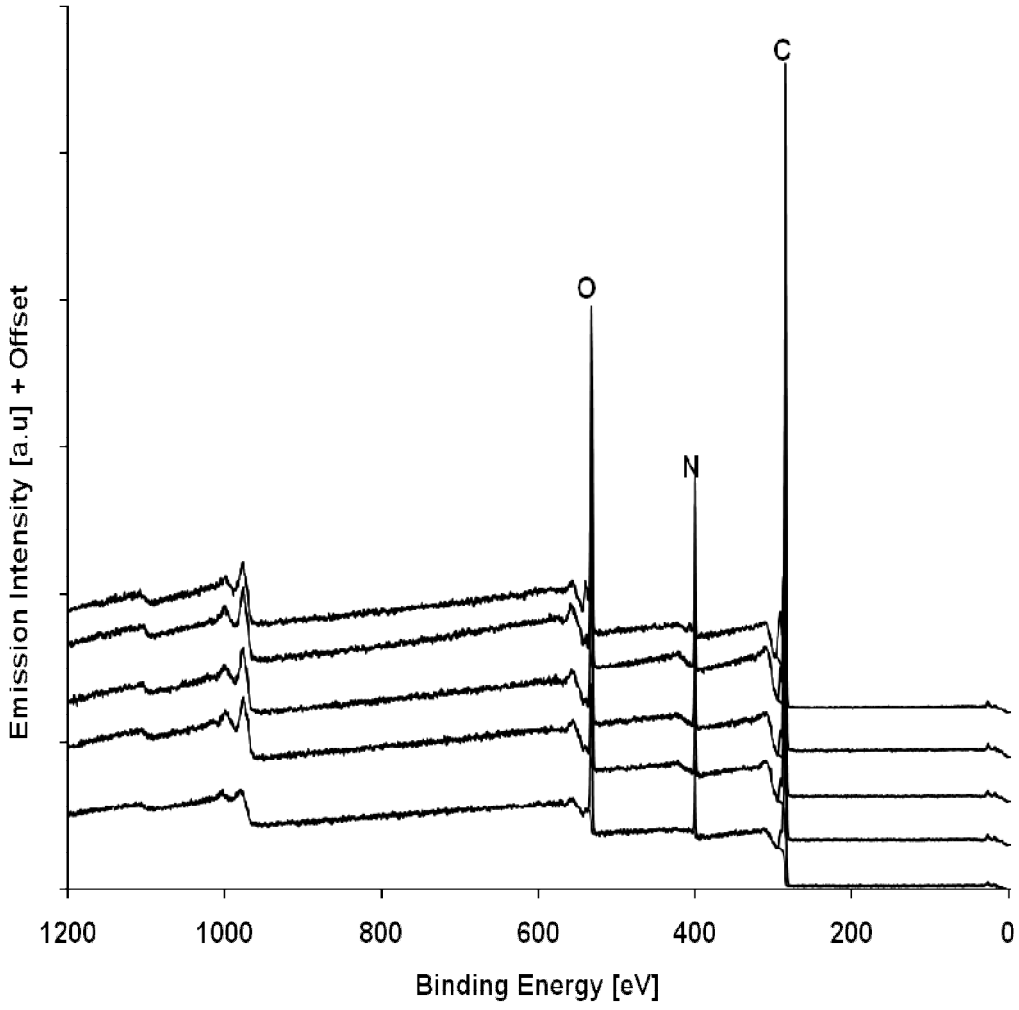

MeSingle2 survey analysis at different spots

Appendix 8

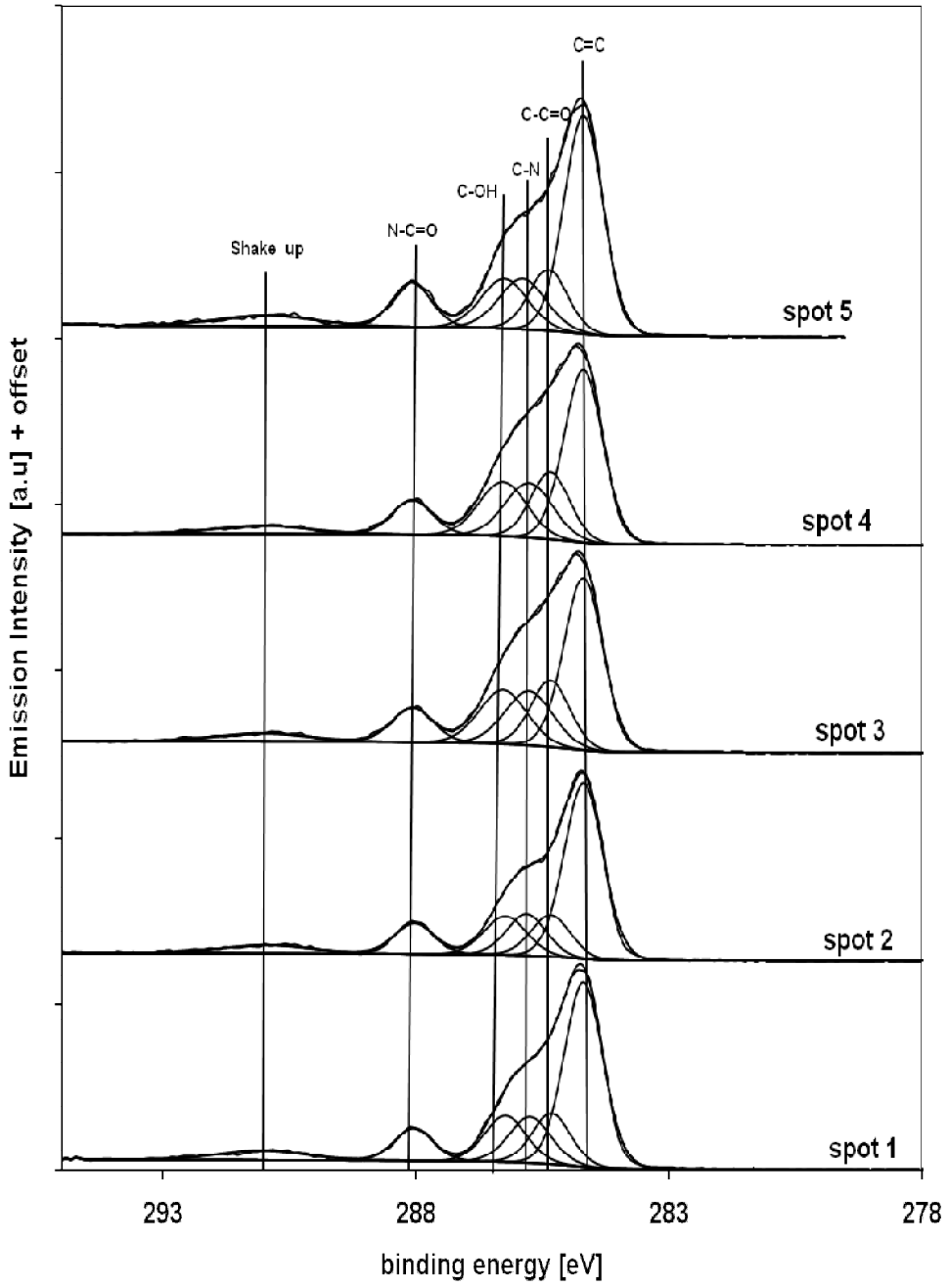

MeSingle2 C1s fitting at different spots analysis

Appendix 9

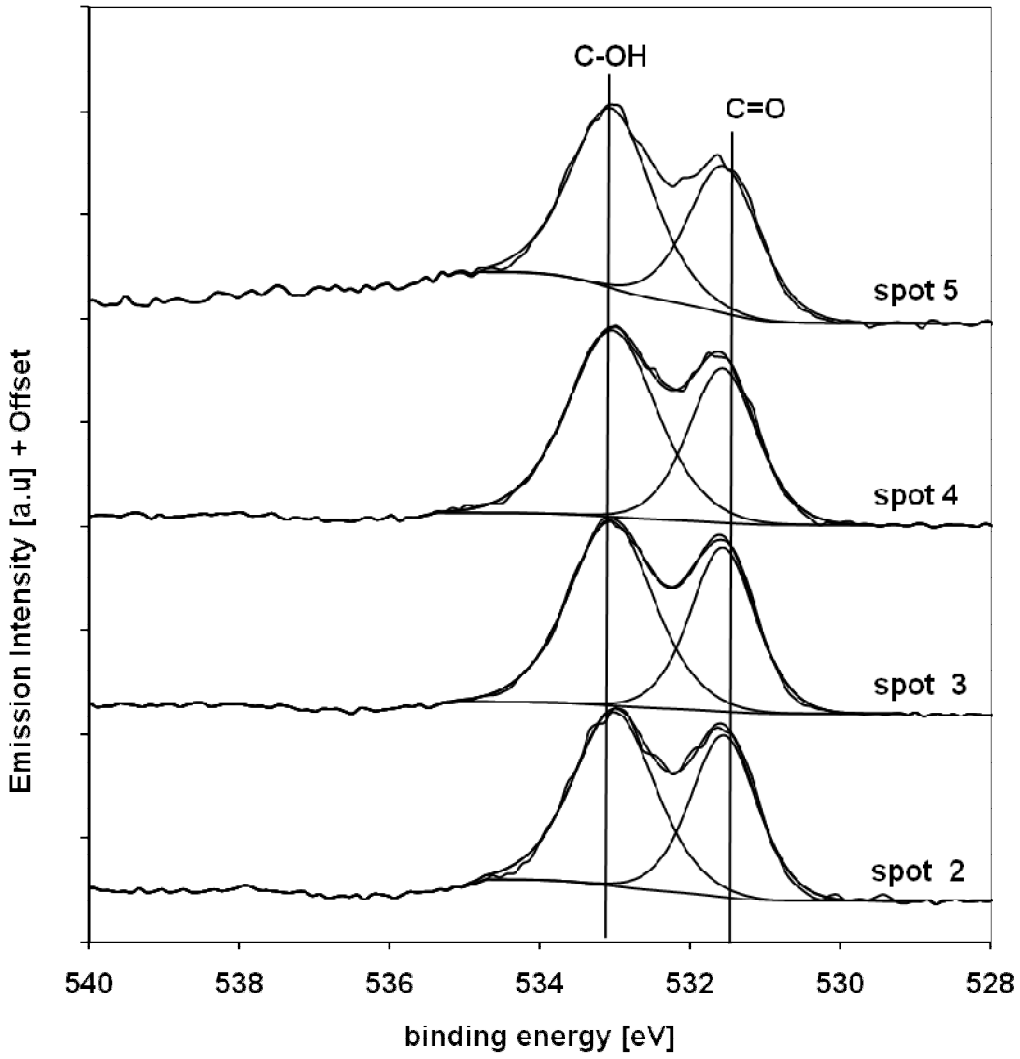

MeSingle2 O1s fitting at different spots analysis

Appendix 10

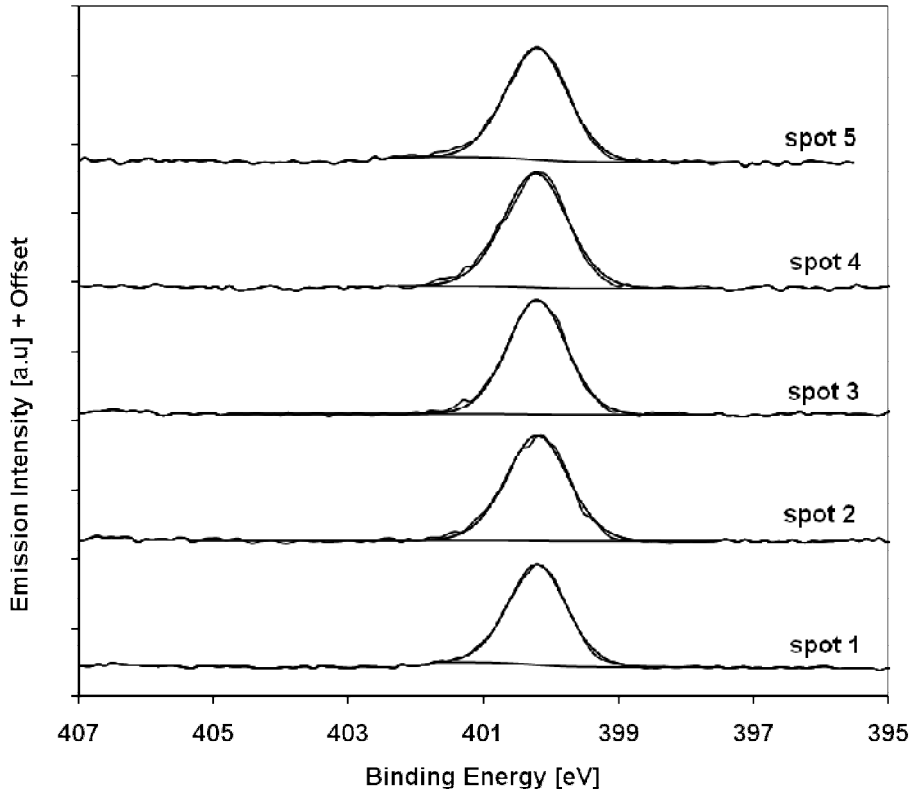

MeSingle2 N1s fitting at different spots analysis

Appendix 11

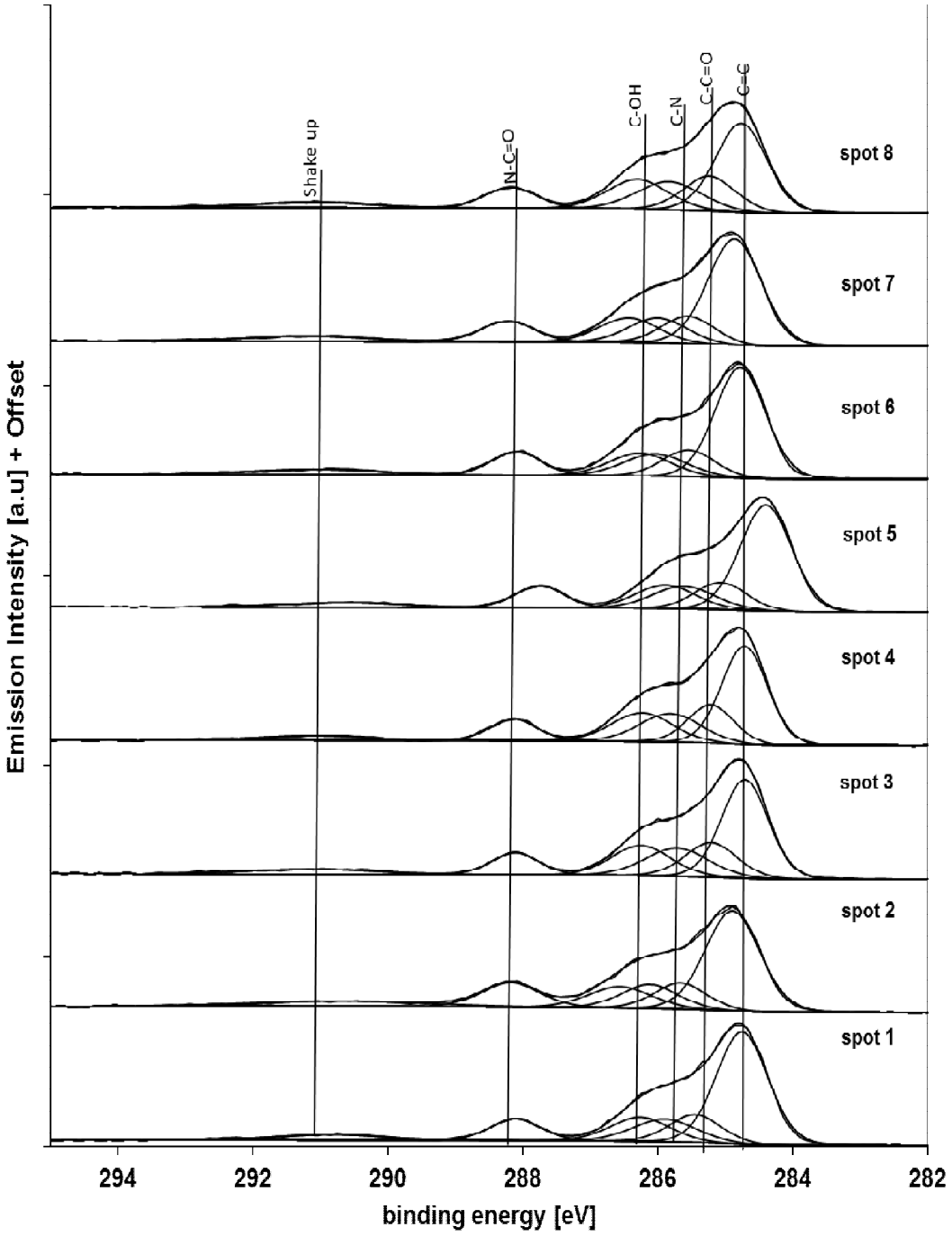

EtSingle C1s fitting at different spots (1-8) analysis

Appendix 12

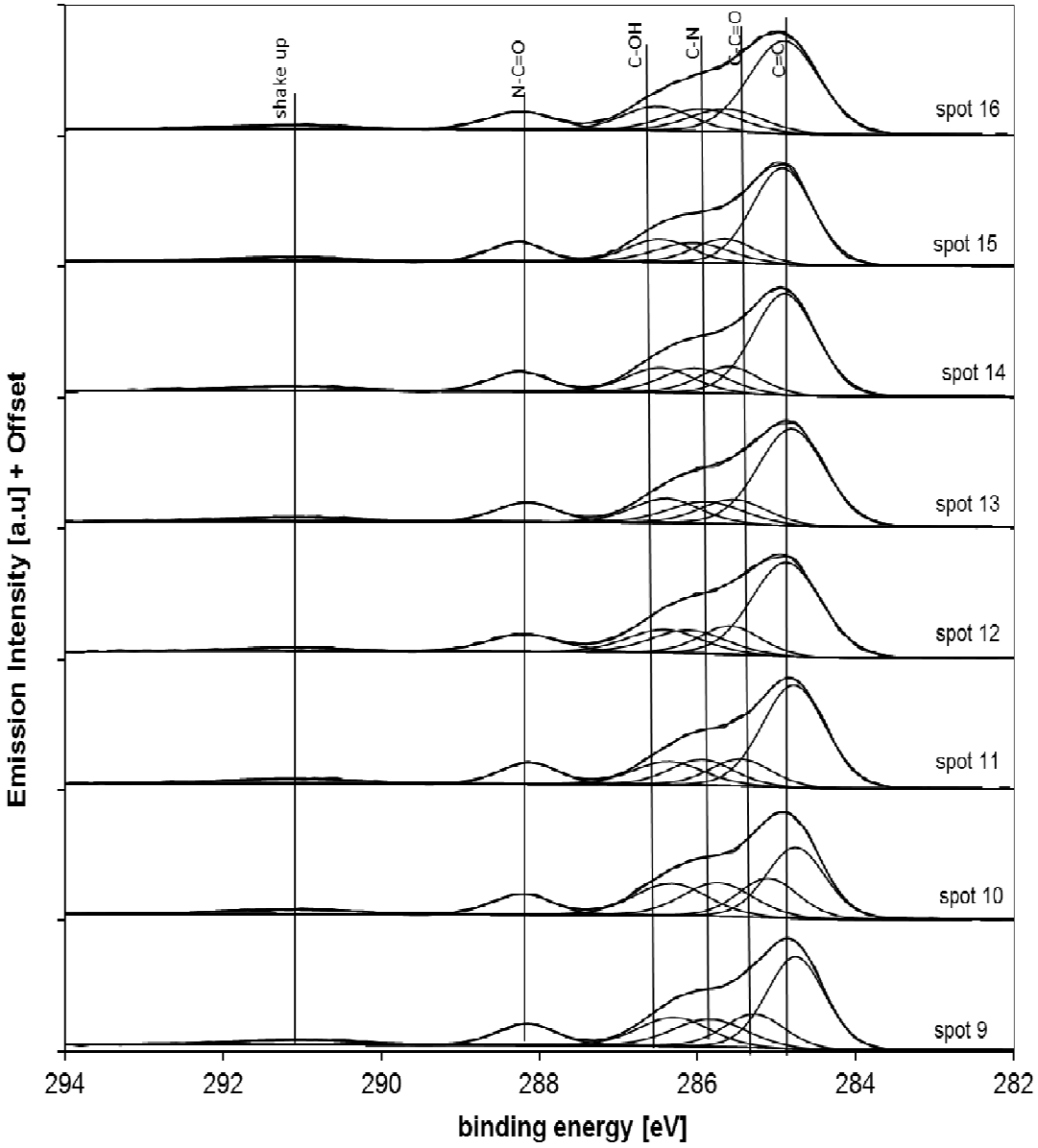

EtSingle C1s fitting at different spots (9-16) analysis

Appendix 13

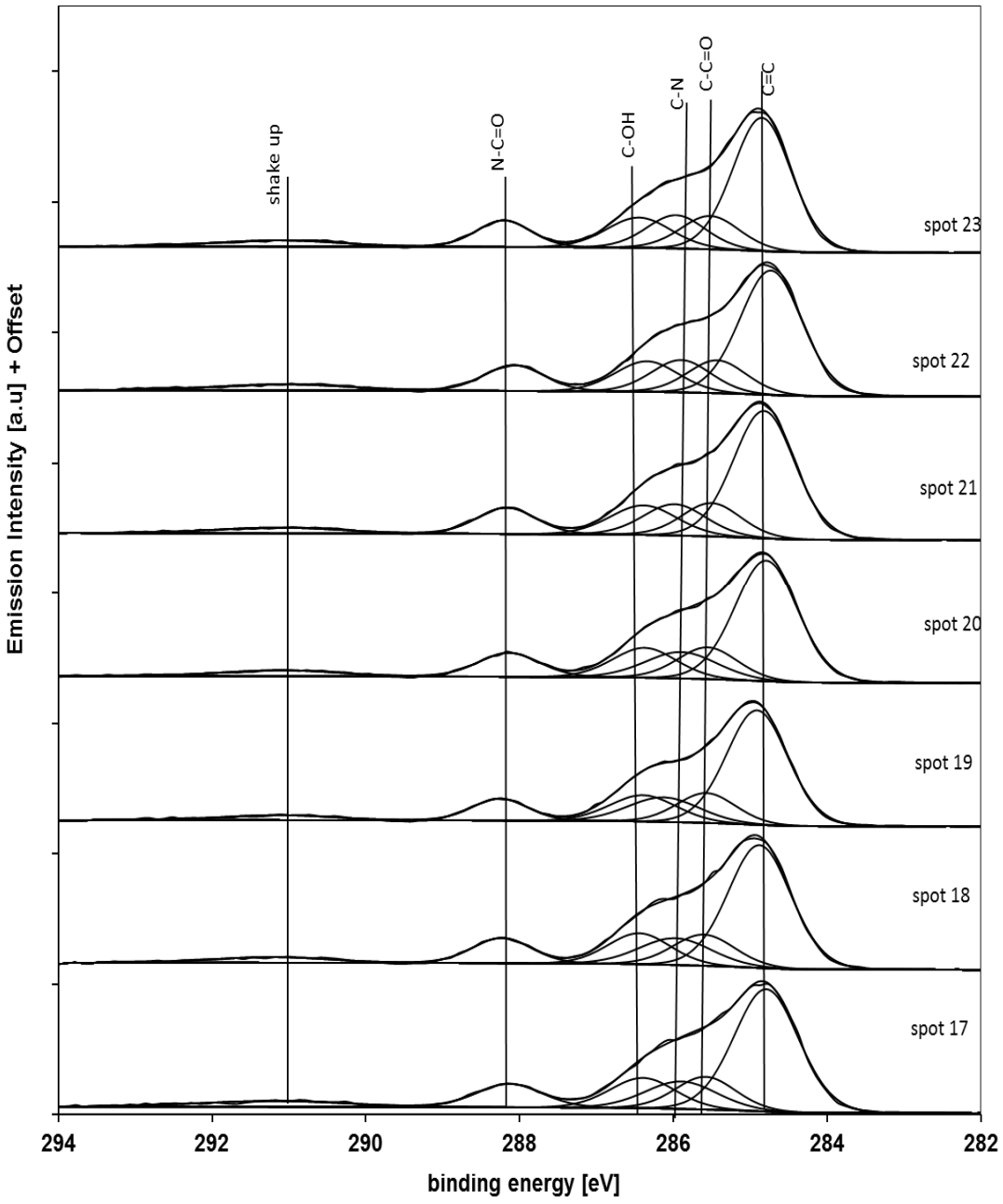

EtSingle C1s fitting at different spots (17-23) analysis

Appendix 14

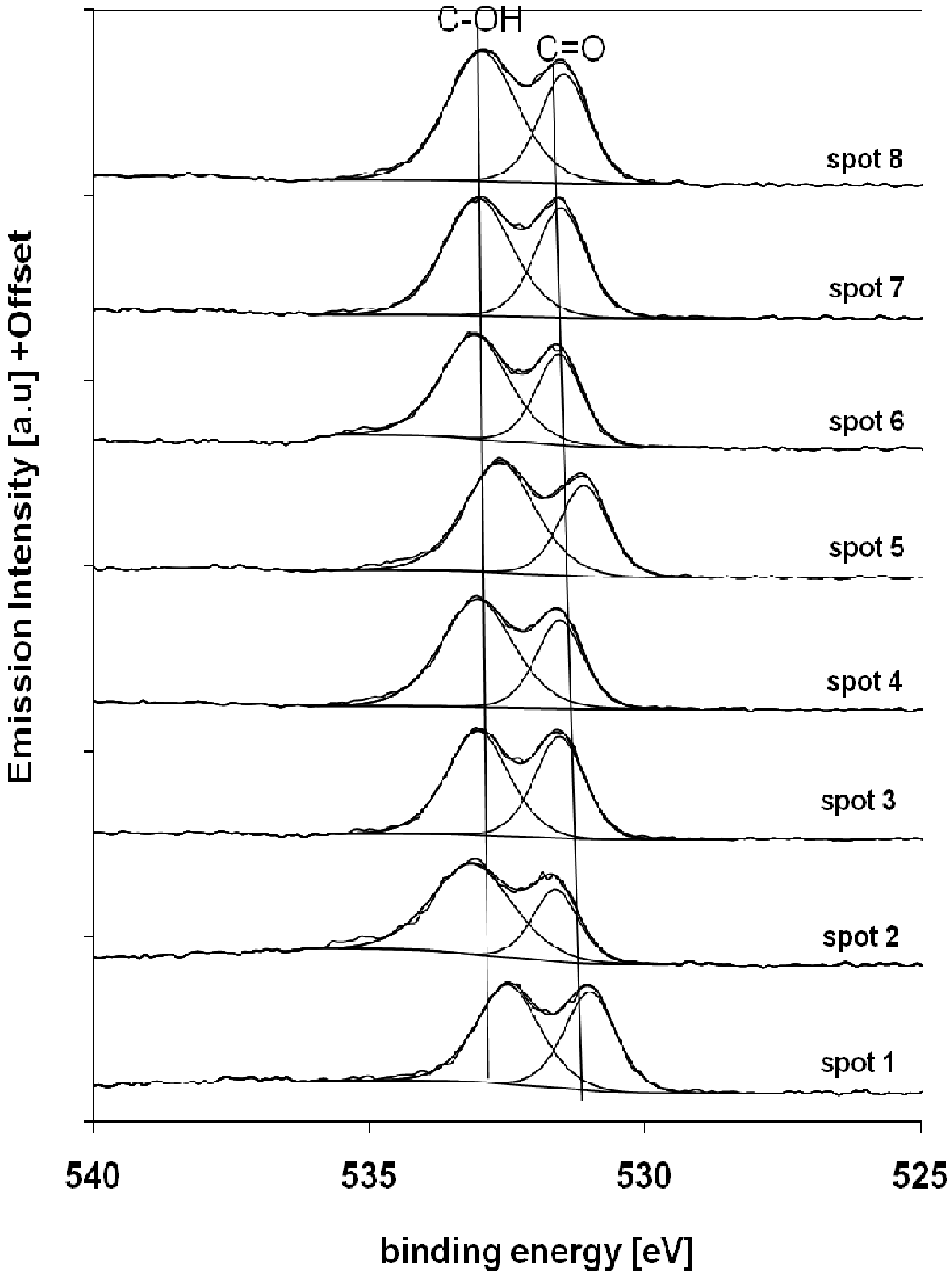

EtSingle O1s fitting at different spots (1-8) analysis

Appendix 15

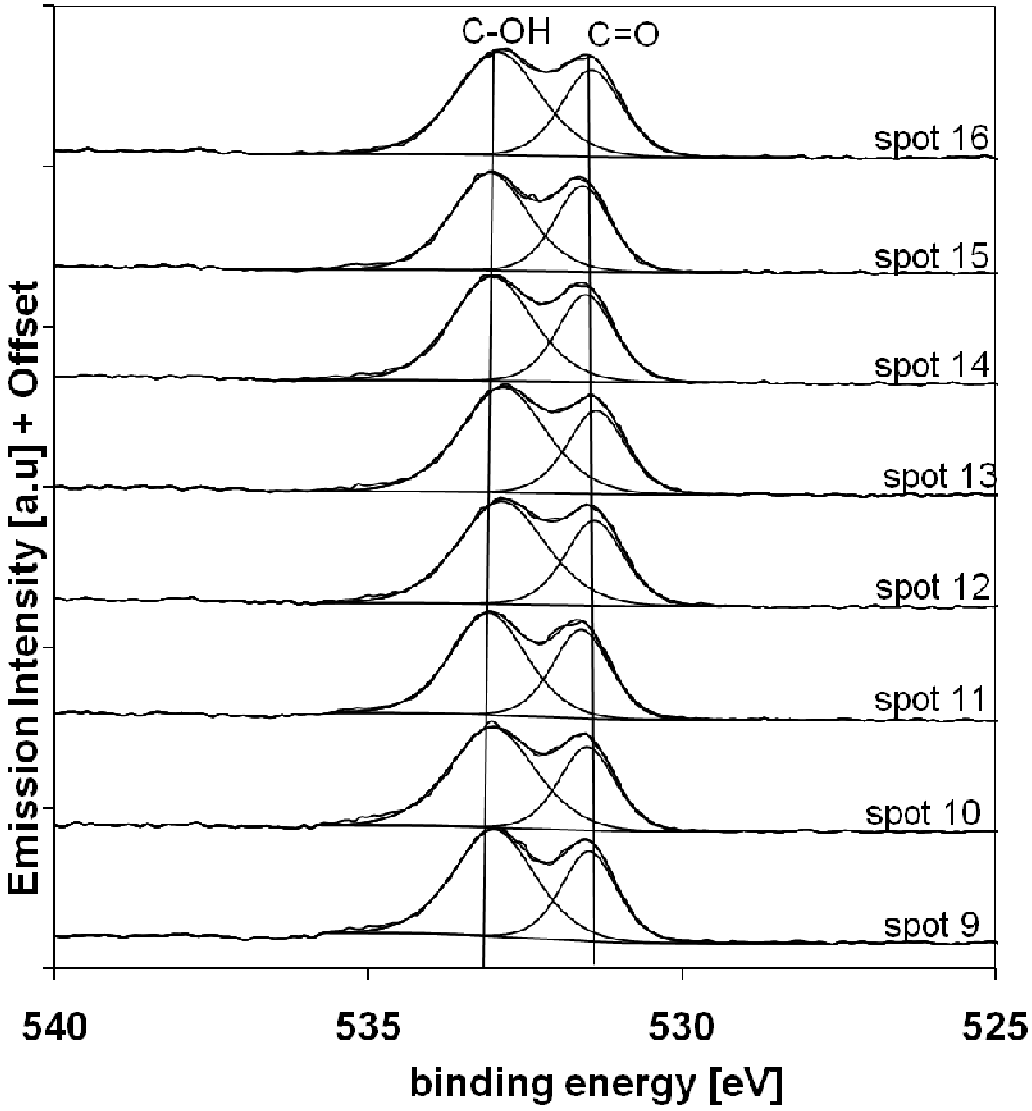

EtSingle O1s fitting at different spots (9-16) analysis

Appendix 16

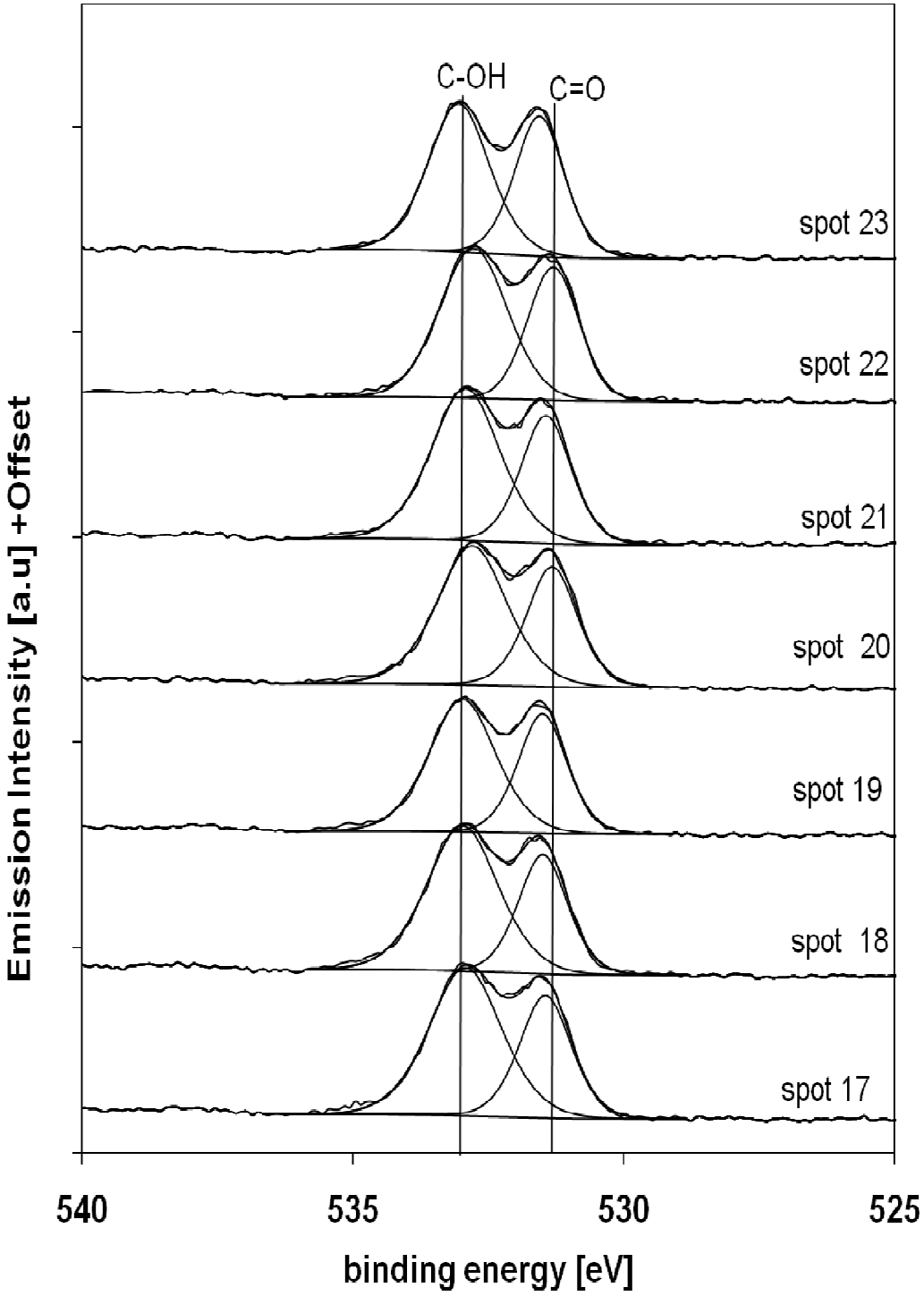

EtSingle O1s fitting at different spots (17-23) analysis

Appendix 17

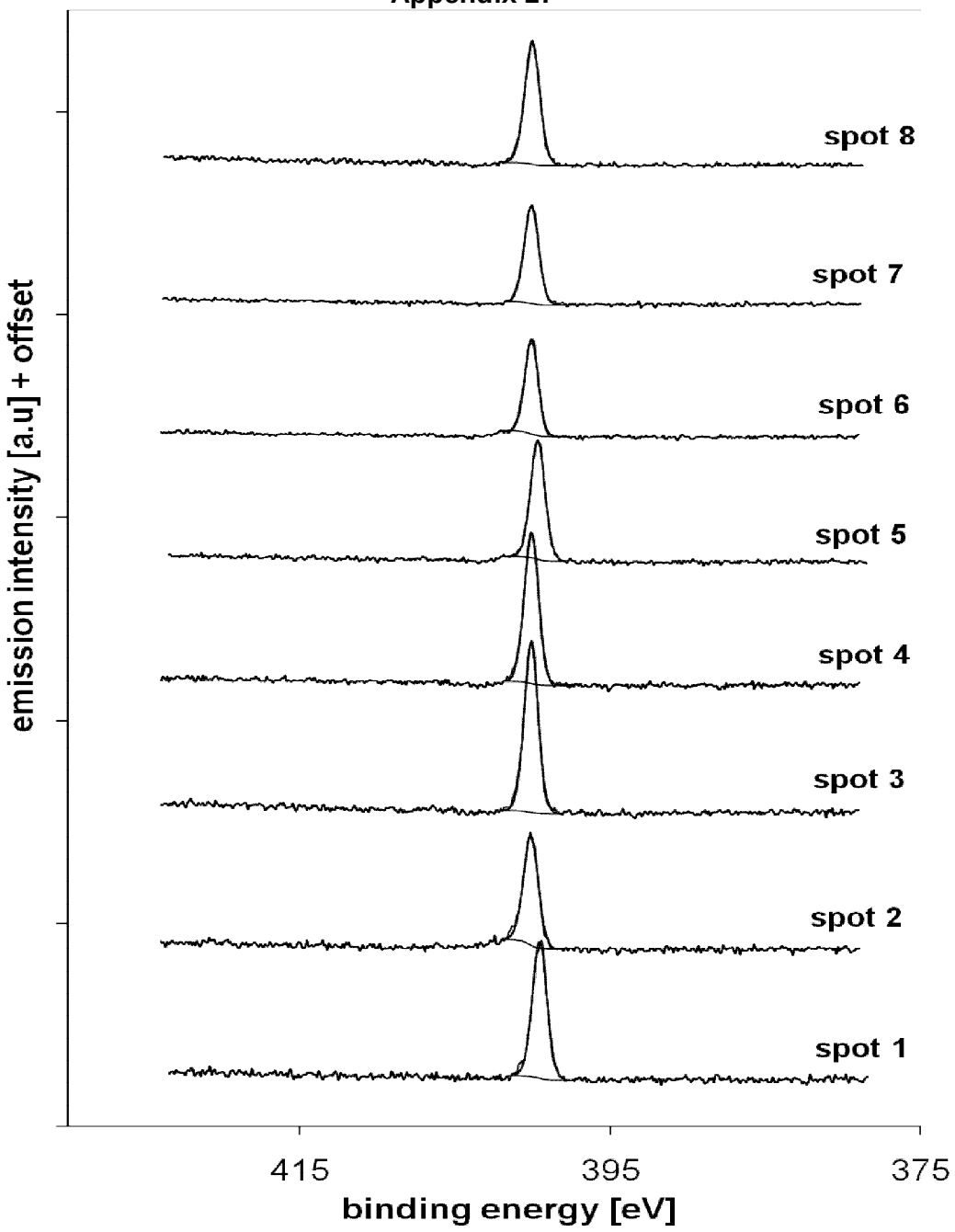

EtSingle N1s fitting at different spots (1-9) analysis

Appendix 18

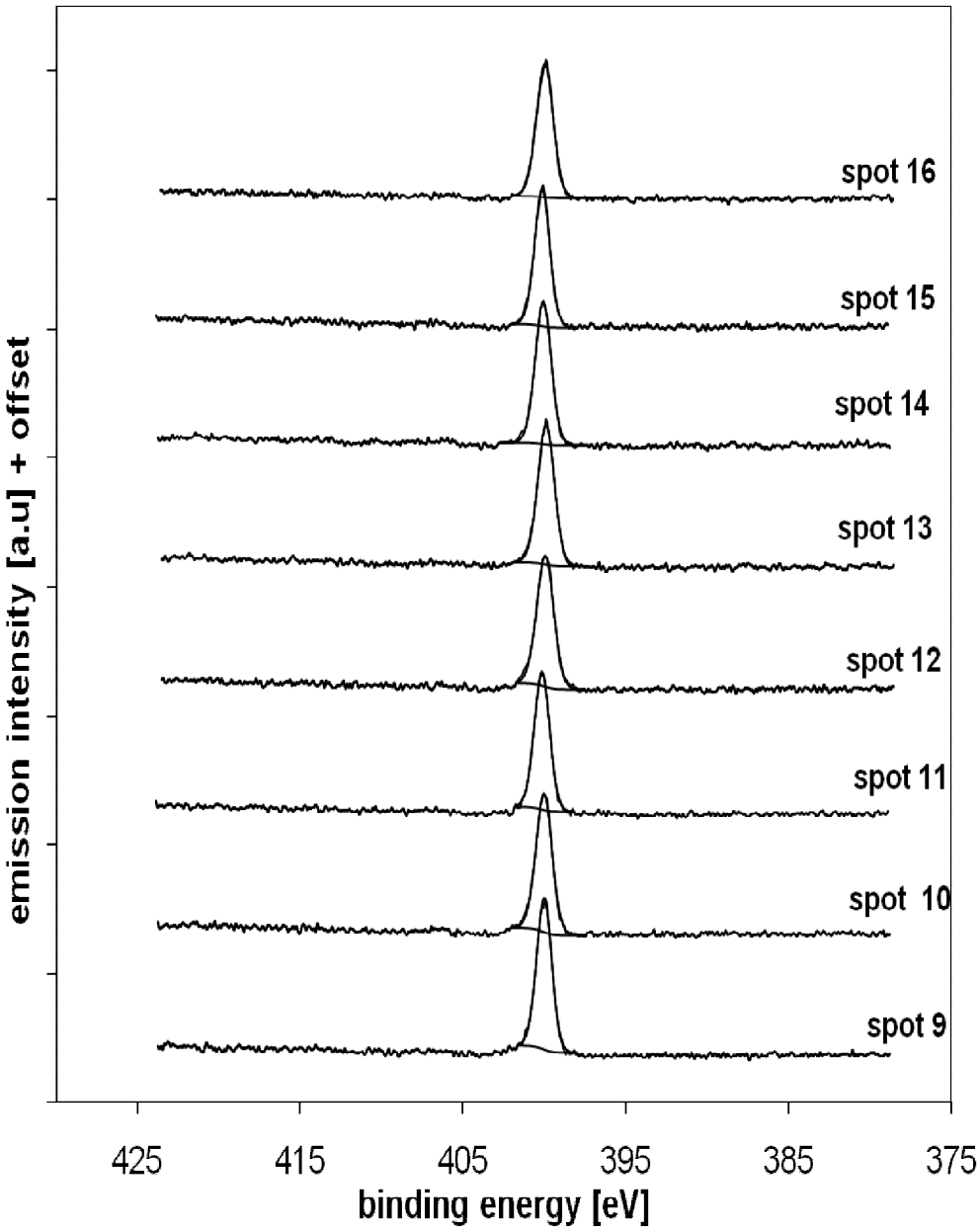

EtSingle N1s fitting at different spots (9-16) analysis

Appendix 19

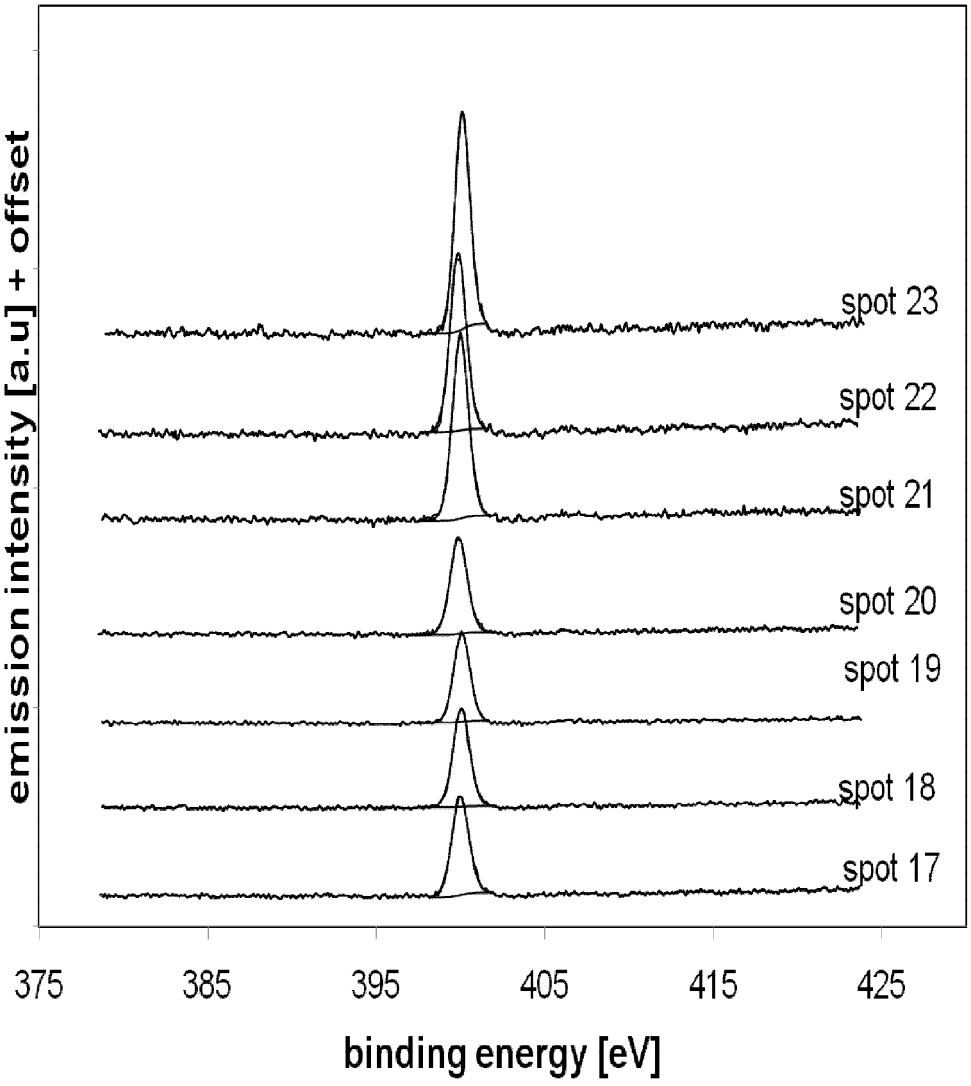

EtSingle N1s fitting at different spots (17-23) analysis

Appendix 20

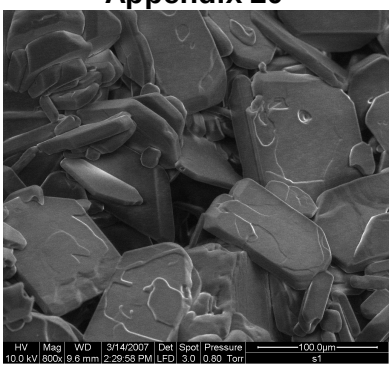

Vapour diffusion crystallisation of ibuprofen

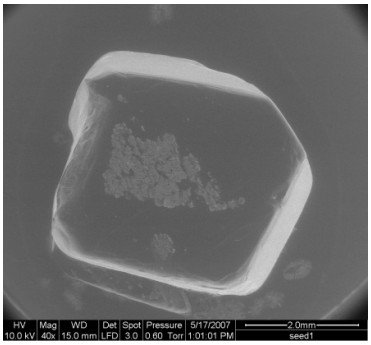

(a)

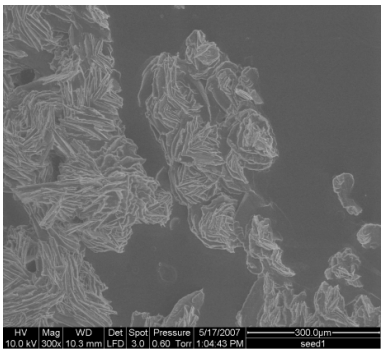

(b)

SEM results of ibuprofen crystallisation. (a) Ibuprofen crystal (b) 'trapped' impurities

(No further analysis to Ibuprofen crystal due to the sublimation in XPS chamber and broken the XPS pump, major fixing of XPS instrument. No Ibuprofen analysis had been allowed by XPS officer.)

Appendix 21

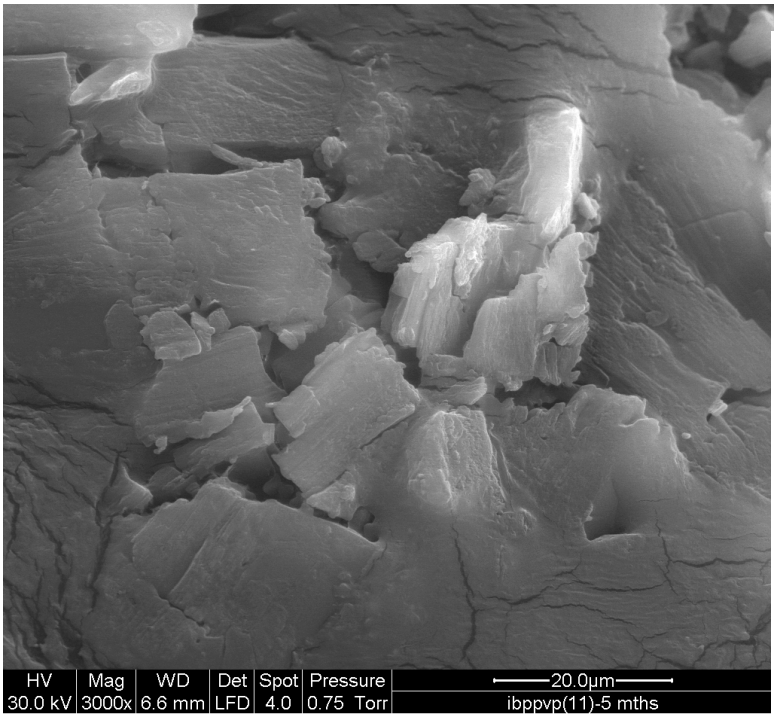

Physical Mixture Ibuprofen/PVP (50% PVP w/w) at 5 months. No further analysis can be done due to the very hard samples (sample was like a rock). Sample was stick at the bootom of container. No further analysis can be done. No Ibuprofen particles has been observed at this mass percent. (refer to Appendix 24 for ibuprofen particles.)

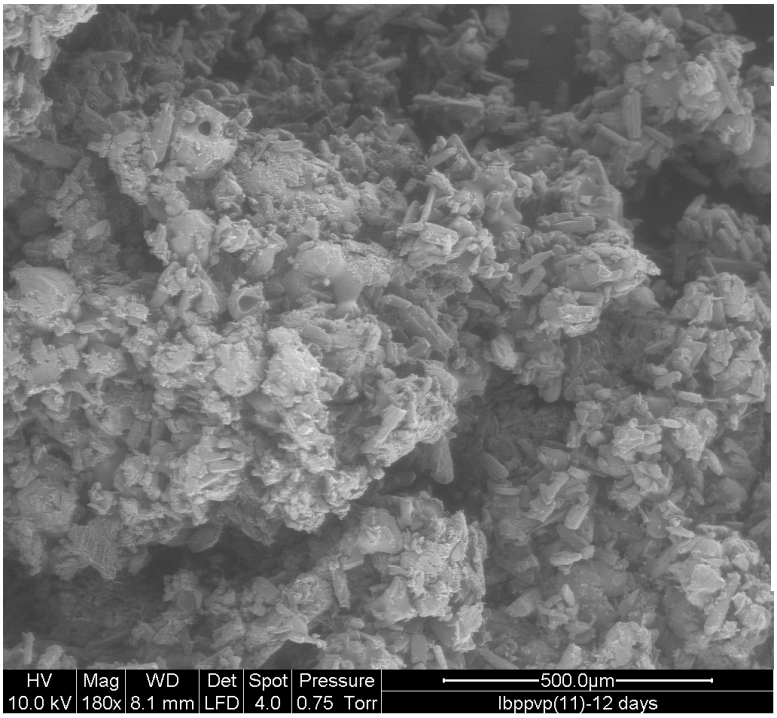

Physical Mixture Ibuprofen/PVP (50% PVP w/w) 12 days. Rubbery samples stick at the bottom of containers. No further analysis can be done. Ibuprofen and PVP particles were agglomerate together.

Appendix 22

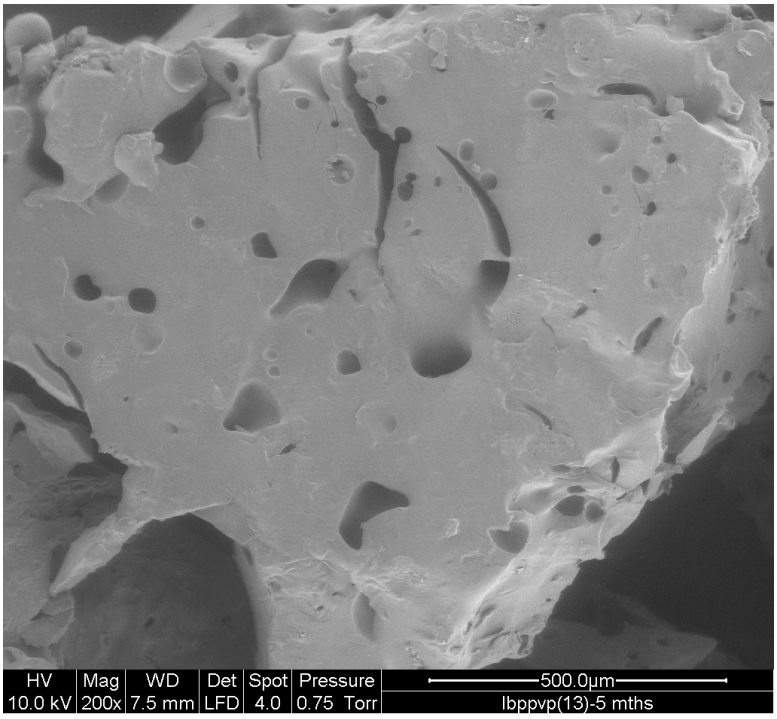

Physical Mixture Ibuprofen/PVP (25% PVP w/w) at 5 months. Very hard samples, no further analysis can be done. No certain shape of particles (neither Ibuprofen nor PVP can be observed).

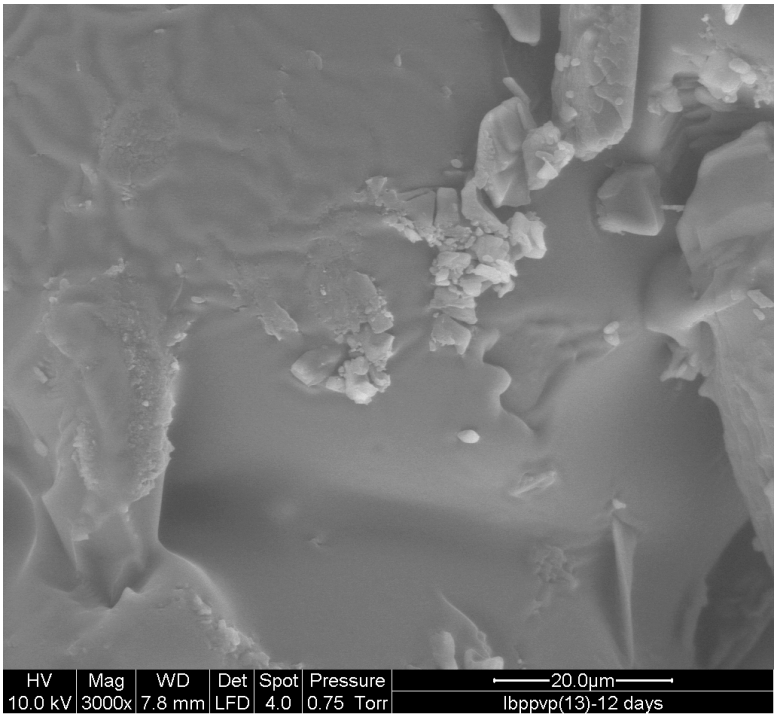

Physical Mixture Ibuprofen/PVP (25% PVP w/w) at 12 days. Rubbery and hard samples, no further analysis can be done.

Appendix 23

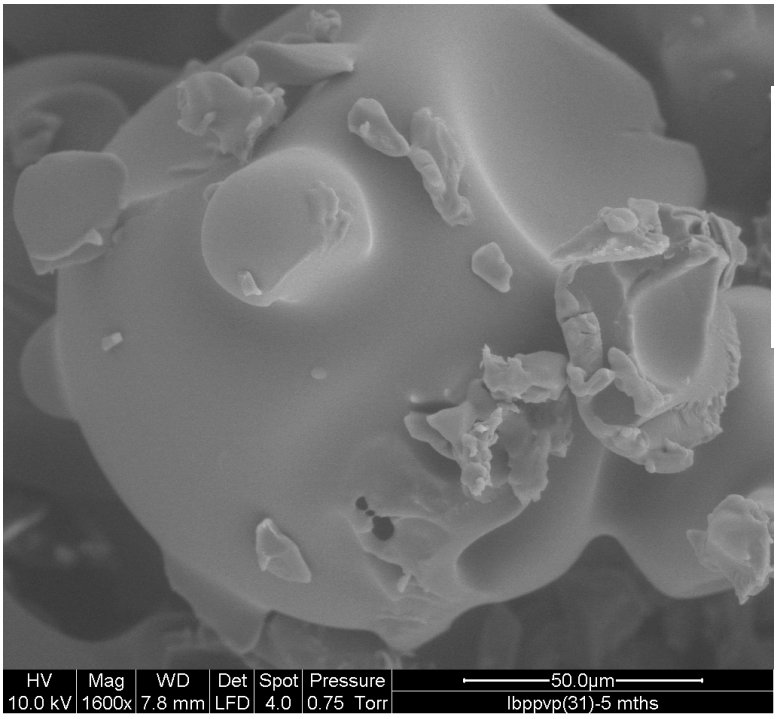

Physical Mixture Ibuprofen/PVP (67.7% PVP w/w) at 5 months. Samples was very hard like a rock.No further analysis can be done.

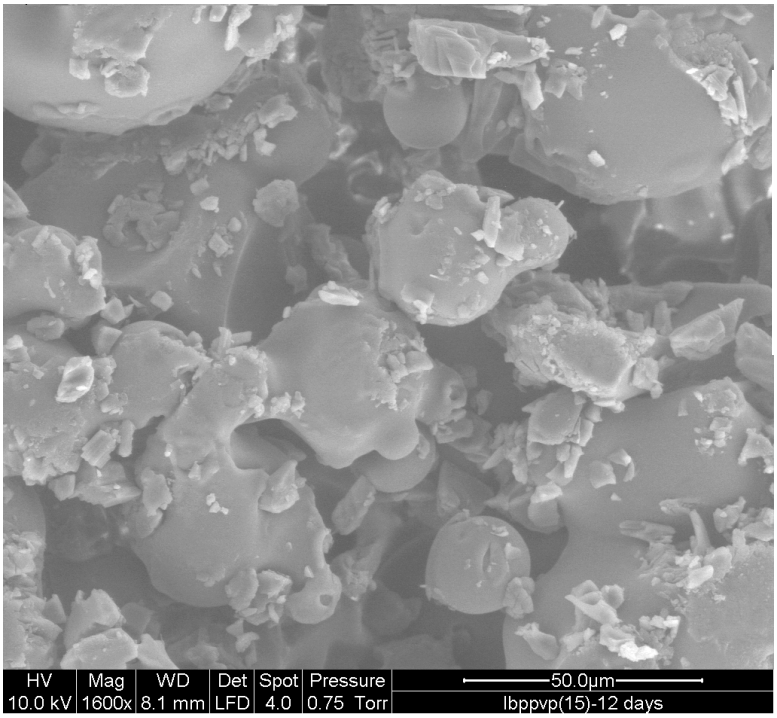

Physical Mixture Ibuprofen/PVP (67.7% PVP w/w) at 12 days. Rubbery sample, stick at the bottom of container. No further analysis can be done.

Appendix 24

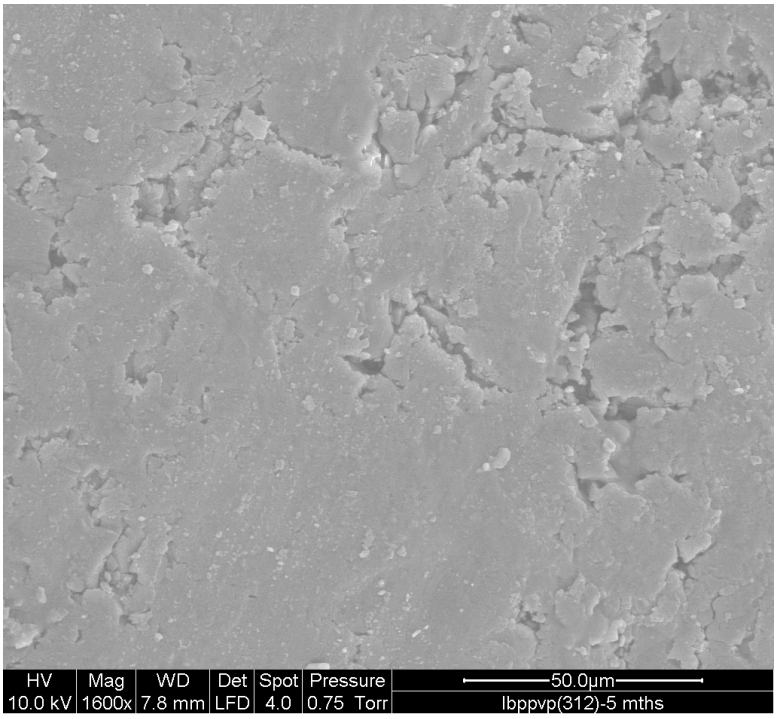

Physical Mixture Ibuprofen/PVP (25% PVP w/w) at 5 months. Very hard samples. No further analysis can be done.

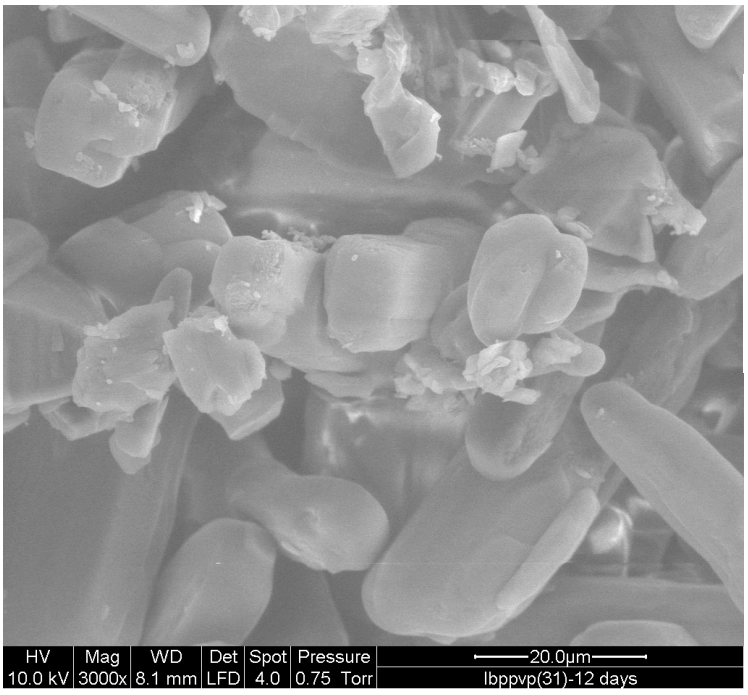

Physical Mixture Ibuprofen/PVP (25% PVP w/w) at 12 days. Rubbery samples, stick at the bottom of the containers. No further analysis can be done.

Appendix 25

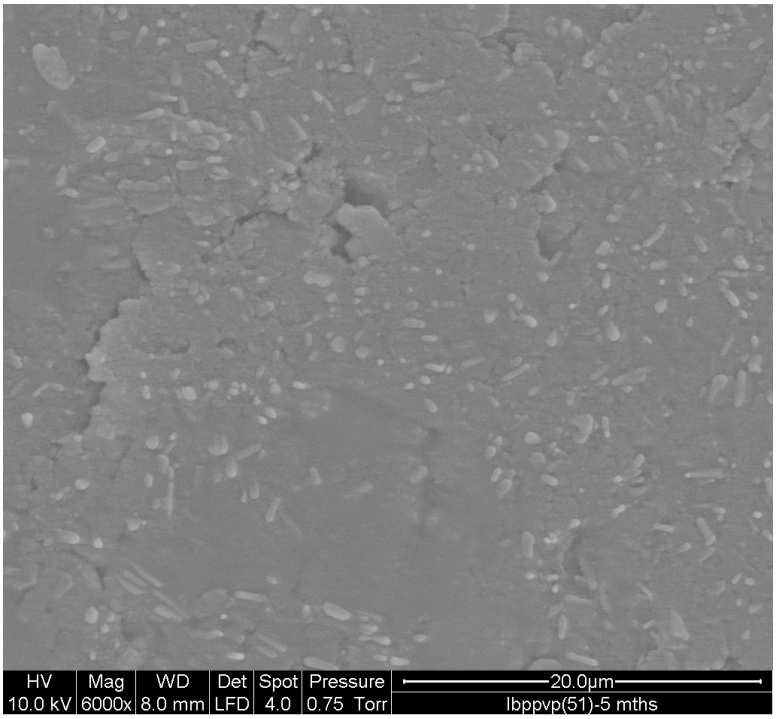

Physical Mixture Ibuprofen/PVP (75% PVP w/w) at 5 months. Sample has been changed to very hard (like rock) and no further analysis can be done.

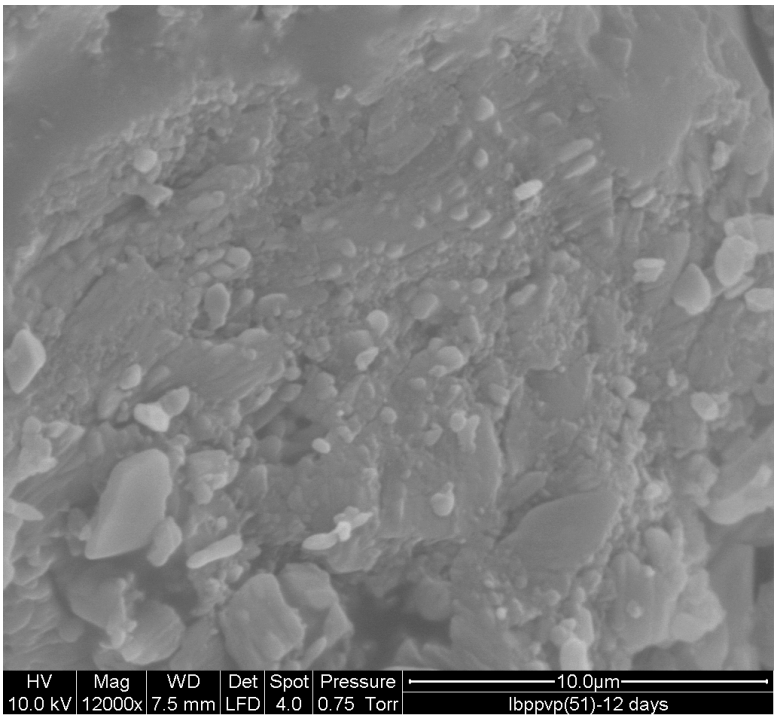

Physical Mixture Ibuprofen/PVP (75% PVP w/w) at 12 days. Very rubbery and samples cannot take out from the container. No further analysis can be done.

Appendix 26

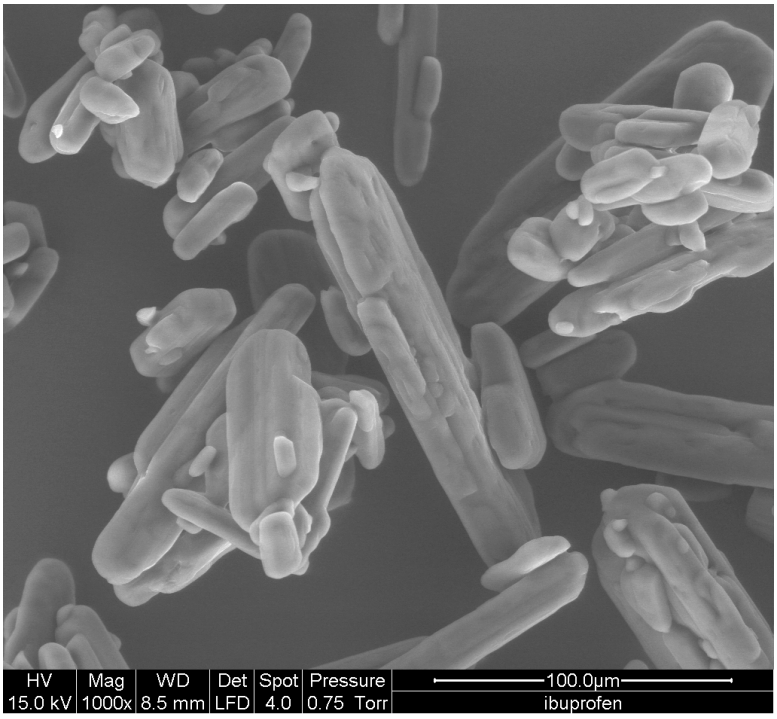

Ibuprofen. Scanning Electron Microscope micrograph of Ibuprofen powder.